Polarized radiative transfer in solar atmosphere

Jiri Stepan

OBSERVATOIRE DE PARIS

ECOLE DOCTORALE
ASTRONOMIE ET ASTROPHYSIQUE D'ILE-DE-FRANCE

Doctorat
ASTRONOMIE ET ASTROPHYSIQUE

par

Jiří ŠTĚPÁN

Etude du transfert du rayonnement polarisé dans l'atmosphère solaire

Thèse en cotutelle internationale dirigée par

Petr HEINZEL
Sylvie SAHAL-BRÉCHOT

Soutenue le 23 septembre 2008 à l'Observatoire de Paris à Meudon
devant la commission d'examen constituée par:

Mme	Marianne FAUROBERT	Président
M.	Petr HEINZEL	Directeur
Mme	Sylvie SAHAL-BRÉCHOT	Directeur
M.	Egidio LANDI DEGL'INNOCENTI	Rapporteur
M.	Javier TRUJILLO BUENO	Rapporteur
M.	Jiří HORÁČEK	Examinateur
M.	Marian KARLICKÝ	Examinateur
M.	Frédéric PALETOU	Examinateur

CHARLES UNIVERSITY IN PRAGUE
FACULTY OF MATHEMATICS AND PHYSICS

A dissertation presented in partial fulfillment of the requirements for the degree of
DOCTOR OF PHILOSOPHY

in the subject of
THEORETICAL PHYSICS, ASTRONOMY AND ASTROPHYSICS

by
Jiří ŠTĚPÁN

Polarized radiative transfer in solar atmosphere

Thesis in the frame of cotutelle supervised by

Petr HEINZEL
Sylvie SAHAL-BRÉCHOT

The defense held on September 23, 2008 at the Paris Observatory in Meudon
Committee:

Ms.	Marianne FAUROBERT	Committee chair
Mr.	Petr HEINZEL	Thesis co-supervisor
Ms.	Sylvie SAHAL-BRÉCHOT	Thesis co-supervisor
Mr.	Egidio LANDI DEGL'INNOCENTI	Referee
Mr.	Javier TRUJILLO BUENO	Referee
Mr.	Jiří HORÁČEK	Examiner
Mr.	Marian KARLICKÝ	Examiner
Mr.	Frédéric PALETOU	Examiner

Dedicated to my parents,
Irena and Josef Štěpán.

This thesis has been prepared in the frame of cotutelle at the following laboratories:

Astronomical Institute
Academy of Sciences of the Czech Republic, v.v.i.

Fričova 298
251 65 Ondřejov
CZECH REPUBLIC

Laboratoire d'Étude du Rayonnement et de la Matière en Astrophysique
Observatoire de Paris – Meudon
CNRS UMR 8112

5 place Jules Janssen
92195 Meudon Cedex
FRANCE

Thèse directeur
Petr HEINZEL and Sylvie SAHAL-BRÉCHOT

Auteur
Jiří ŠTĚPÁN

Etude du transfert du rayonnement polarisé dans l'atmosphère solaire

Résumé

L'interprétation des spectres compliqués de l'atmosphère solaire magnétisée requiert des modèles théoriques adéquats de transfert radiatif hors ETL. Dans la première partie, la théorie quantique de la polarisation est revue ainsi que celle du transfert radiatif hors ETL de 2^{e} espèce. Une notation générale est introduite pour traiter numériquement la matrice densité atomique. Une technique de "lambda-operator splitting" est présentée et utilisée pour développer une méthode originale de préconditionnement analogue à l'algorithme itératif de Jacobi. De nombreux processus sont pris en compte: l'effet Zeeman, l'effet Paschen-Back, l'effet Hanle, la polarisation atomique, les croisements de niveaux, le pompage optique, la (dé)polarisation par collisions. Une technique multigrille non linéaire est développée dans le cadre du transfert de rayonnement polarisé et l'efficacité de la méthode est discutée. Les possibilités de ce nouveau solveur sont démontrées sur l'exemple d'une raie optiquement épaisse d'un atome multiterme dans le régime de l'effet Paschen-Back. Dans la deuxième partie, la polarisation par impact de la raie H-alpha de l'hydrogène est étudiée. Les modèles semi-empiriques de la chromosphère éruptive sont utilisés pour déterminer les effets différentiels du faisceau de protons sur les profils d'intensité et de polarisation. Il est montré qu'il est improbable que les faisceaux de protons soient la source de la polarisation linéaire observée. Dans le dernier chapitre, il est montré que les courants électriques de retour sont un ingrédient significatif de la formation des raies et ils sont proposés comme une source possible de la polarisation observée.

Mots clés: polarisation, transfert radiatif, raie: formation, champs magnétiques, méthodes: numerique

Thesis advisors
Petr HEINZEL and Sylvie SAHAL-BRÉCHOT

Author
Jiří ŠTĚPÁN

Polarized radiative transfer in solar atmosphere

Abstract

The adequate theoretical models of the NLTE radiative transfer are needed for interpretation of the complicated spectra emerging from the magnetized solar atmosphere. In the first part of the thesis, the quantum theory of polarization is reviewed along with the problem of NLTE radiative transfer of the 2nd kind. A general notation for a numerical treatment of the atomic density matrix is introduced. A lambda-operator splitting technique is presented and used for development of a novel preconditioning method analogous to the Jacobi iteration algorithm. Number of processes is taken into account: atomic polarization, level-crossings, Paschen-Back effect, Hanle and Zeeman effects, optical pumping, collisional (de)polarization. A nonlinear multigrid technique is developed in the framework of polarized radiative transfer theory and the efficiency of the method is discussed. The potential of this new solver is demonstrated on an example of transfer of the optically thick line of a multiterm atom in the Paschen-Back effect regime. In the second part of the thesis, the particular problem of impact polarization of the hydrogen H-alpha line in solar flares is considered. The semi-empirical models of the flaring chromosphere are used to find the differential effects of the proton beam on the line intensity and linear polarization profiles. Proton beams are shown to be an unlikely source of the observed linear polarization. In the last chapter, it is shown that the electric return currents are significant ingredient of the line formation and they are proposed as being a possible source of the observed linear polarization.

Key words: polarization, radiative transfer, line: formation, magnetic fields, methods: numerical

Contents

List of Figures

List of Tables

List of Algorithms

Acknowledgments

I am grateful to many people who helped me along the way, explained many things to me and to those that have shared their friendship and love and have been source of my inspiration. For example, I am grateful to Jean Aboudarham, Christian Balança, Marie and Gilbert Beringer, Moncef Derouich, Jaroslav Dudík, Stanislav Gunár, Petr Hašlar, Alois Havelka, Jean-Claude Hénoux, Jiří Horáček, Iveta Horáčková, Jana Kabourková, Marián Karlický, Jana Kašparová, Tomáš Kundrát, Marian Martinez Gonzalez, Danielle Michoud, Mourad Roudain, Štěpán Štverák, Aleš Táborský, Sonja Vidojevic, Etienne Vogt, Zhi Xu and many others. I am especially grateful to Nicole Feautrier for her help with administration in the beginning of my stay in France and for stimulating scientific discussions. I am also thankful to Brigitte Schmieder for her help with lodging after my first arrival to France. A particular acknowledgment goes to Vèronique Bommier for number of motivating discussions concerning atomic polarization.

I have been lucky to have the opportunity to study under the supervision of two extraordinary advisors. A lot of thanks go to my Czech supervisor, Petr Heinzel, who initiated my interest in the exciting field of radiative transfer and helped me to understand many parts of this difficult subject. A lot of thanks go to my French supervisor, Sylvie Sahal-Bréchot, who has not only taught me a lot of things about atomic physics but who has also been an exceptional source of my support in France. Both of my supervisors have always been willing to discuss the scientific problems and have been constantly encouraging my steps forward.

My work has been supported by the Solar Department of the Astronomical Institute of Academy of Sciences of the Czech Republic, v.v.i. and by the Laboratoire d'Etudes du Rayonnement et de la Matière en Astrophysique of Observatoire de Paris – Meudon. Both of these laboratories provided me a pleasant environment for my work.

Last but not least I highly appreciate an encouragement from my family during the long years. It would be impossible for me to finish this work without their continuous support.

This work has been partially supported by the grants 205/06/P135 and 205/08/H005 of the Grant Agency of the Czech Republic, A3003203 and A300030701 of the Grant Agency of the Academy of Sciences of the Czech Republic and partially by the project LC06014 of the Center for Theoretical Astrophysics. My stay in France in the frame of cotutelle has been funded by the fellowship n°20052646 of the French government.

Chapter 1

Introduction and summary

The rapid progress in the instrumentation for solar spectropolarimetry rises new demands for theoretical interpretation of the data. The complicated polarized spectra of different atoms and ions in the solar atmosphere often result from multiple scattering of the photons. The lack of tools suitable for NLTE modeling of the 2nd kind for a wide variety of multilevel atomic models and magnetic field regimes makes it difficult to understand the physical conditions leading to the observed polarization signature of the emergent radiation. The aim of the thesis is twofold: Firstly, it concerns a problem of synthesis of the line Stokes profiles in the one-dimensional optically thick magnetized atmospheres taking into account a number of ingredients of the spectral line formation (atomic polarization, level crossing coherences, Paschen-Back effect, Hanle and Zeeman effects, optical pumping, collisional (de)polarization). Secondly, the thesis concerns the problem of impact polarization of the hydrogen Hα line in solar flares.

The outline of the thesis is as follows. In Chapter 2 the problem of interaction between an atomic system and a bath of radiation and perturbers in external magnetic field is briefly reviewed within the framework of non-relativistic quantum electrodynamics. The theory of master equation for the density operator is recalled and a particular emphasis is paid on the problems of different models of atomic levels (multilevel, multiterm, and multilevel picture with hyperfine structure), level-crossing coherences, joint action of Hanle and Zeeman effects, and the NLTE equations. The interaction of radiation and atoms is treated in the so-called complete frequency redistribution approximation. Although a solution of the NLTE problem in a closed form is not possible in general, an idealized two-level problem can be solved analytically to a certain extent. A simple generalization of the so-called $\sqrt{\epsilon}$-law to the case of non-thermal collisional rates is presented in the end of Chapter 2. In Chapter 3, a unified notation for the NLTE equations is established. This simple notation is useful for development of the numerical solvers and is used throughout this thesis. Hereafter a modification of the so-called lambda-operator splitting technique with the short-characteristics formal solver is used for construction of the generalized accelerated lambda iteration (ALI) numerical scheme. An advanced non-linear multigrid (MG) technique is introduced into the field of polarized radiative transfer (RT) in Chapter 4. After a brief introduction of the philosophy of the method, the specific properties of the MG strategy in the density matrix framework are pointed out. An implementation of the so-called Standard MG and Nested MG methods is described. The convergence properties of the MG method are analyzed using an example of RT in the ^{3}S–^{3}P multiplet in a magnetized semi-infinite model atmosphere. The second part of the thesis is based upon a particular application of the methods described so far. The problem of interest is a modeling of the impact polarization of chromospheric hydrogen in solar flares. There is an overview of the problem of proton beam bombardment contained in Chapter 5. Proton beams are often considered as being responsible for the linear polarization of Balmer lines observed from time to time close to the limb during

the impulsive or gradual phase of the flares. The emergent linear polarization signal could be used for diagnostics of the 100 keV proton beams. After a brief review of the recent works on this subject, a closer reinvestigation of the beam propagation through the chromospheric plasmas is made. The semi-empirical models of the flaring chromosphere are used to find the differential effects of the proton beam on the line intensity and linear polarization profiles. The detailed NLTE calculations using the three-principal-level plus continuum hydrogen model shows that resonance scattering polarization dominates over the effect of impact polarization in the emergent linear polarization profiles of the Hα line. This result contradicts some of the recent theoretical investigations which did not take properly into account the deceleration effect of the chromospheric plasmas, underestimated the effect of RT, and the depolarizing effect of the background electrons and protons. In conclusion, proton beams are shown to be an unlikely source of the observed linear polarization of the Hα line. Another phenomenon possibly leading to the Balmer line impact polarization is discussed in Chapter 6. It is the effect of an electric beam injected into the solar chromosphere and accompanied by a neutralizing return current (RC) formed of the ambient electrons. The effect of RC on the first three Balmer line intensity profiles is studied. Using a simple monoenergetic model of RC it is shown that RC plays an important role in the line formation process. A discussion of the possible impact polarization effect of RC is presented.

The numerical methods for solution of the NLTE problem of the 2nd kind described in this thesis have been implemented in the code called Monopost. The architecture of the code and some of the algorithms are described in Appendix A. Appendix B contains a brief review of the representation of the irreducible spherical tensors for the atomic density matrix and radiation field. Finally, the remaining appendices C to G contain some papers that have resulted from my thesis.

Convention, notation, and units

The bold italic font (eg., $\boldsymbol{x}$) is used for the vectors and matrices. The symbol $\mathbf{1}$ denotes the identity matrix,

$$\mathbf{1} \equiv \begin{pmatrix} 1 & 0 & \cdots & 0 \\ 0 & 1 & \cdots & 0 \\ \vdots & \vdots & \ddots & \vdots \\ 0 & 0 & \cdots & 1 \end{pmatrix} . \tag{1.1}$$

Complex conjugation, adjoint, and transpose are, respectively, denoted by $\boldsymbol{A}^*$, $\boldsymbol{A}^\dagger$, and $\boldsymbol{A}^T$. The trace operator is denoted by Tr, the partial trace over the subspace X is denoted by Tr_X.

The symbol "+" in superscript indicates the quantities calculated in the previous iteration step.

I prefer the compact notation

$$[X] \equiv 2X+1, \quad [XY\cdots] \equiv (2X+1)(2Y+1)\cdots . \tag{1.2}$$

I often use the number of grid nodes, the number of independent density matrix elements of a given atomic model, the number of transitions, the number of discrete frequencies, and the number of discrete rays used in the numerical model. These quantities are denoted by $\mathbb{N}$ ($\mathbb{N}_\ell$ in the case of grid G_ℓ), N, $\mathsf{N}_{\mathfrak{tr}}$, F, and $\mathsf{N}_{\boldsymbol{\Omega}}$. The volume density of the atoms is denoted by $\mathcal{N}$.

Density matrix is denoted by ρ. The density matrix of radiation field is denoted by ρ_R. Atomic density matrix is denoted by ρ_A or just by ρ if there is no risk of confusion. If the density matrix is printed in the bold font ($\boldsymbol{\rho}$) it refers to the formal vector composed of the density matrix elements of the discretized atmosphere.

Einstein coefficients for spontaneous emission, absorption, and stimulated emission are, respectively, denoted by $A_{u\to\ell}$, $B_{\ell\to u}$, and $B_{u\to\ell}$. I use $\boldsymbol{k}$ for the wave vector and $\boldsymbol{\Omega}$ for the unit vector in the direction of wave propagation.

The operators in the interaction representation have a tilde above them ($\tilde{\rho}$).

The time variable is always denoted by t (or t', t'', etc.). The same symbol is sometimes also used for an optical path which is usually denoted by τ. If there is no risk of misunderstanding then the explicit time dependencies are often dropped.

The quantum theory of polarization used in this thesis has been recently developed in the extensive monograph of Landi Degl'Innocenti & Landolfi (2004). I tried to follow the conventions used in this book where possible. However, I decided to use slightly different convention in some cases. For instance, I prefer to use the angular frequency ω instead of frequency ν. The Planck constant $\hbar$ is used instead of h. The CGS system of the physical units is consistently used throughout the thesis.

Chapter 2

Elements of NLTE polarized radiative transfer

2.1 Introduction

In this chapter, I briefly review some of the most important physical ideas standing behind the contemporary theory of multilevel polarized radiative transfer as they were developed in the previous years. The discussion is made with a particular emphasis on the conceptual constraints and numerical issues of the NLTE solutions.

The aim of this chapter is to briefly review the basic concepts of the radiative transfer theory of the 2nd kind and to build a basis the subsequent chapters. All the calculations in this thesis are based upon the non-relativistic limit of quantum electrodynamic (QED). The velocities of particles are supposed to be small compared with the light speed c. Within this approximation, particles (except photons) cannot be created nor destroyed.

Outline of this chapter is as follows. In Section 2.2, I recall the framework of the density matrix formalism which is used throughout this thesis. Section 2.3 contains a quantum-mechanical description of the atomic states affected by an external magnetic field. In that section, there is a brief discussion of angular momenta coupling, Zeeman, and Paschen-Back effects. In the subsequent Section 2.4, I review the definition of Stokes parameters, the common procedure of quantization of free electromagnetic field, I mention the definition and properties of the density operator for an incoherent ensembles of photons. After that, the master equation theory is sketched in Section 2.5. I begin by formulation of a non-relativistic QED Hamiltonian. The interaction of radiation and matter is then treated in the lowest order perturbation of the interaction potential. As a result, the equations of statistical equilibrium and the radiative transfer equations are derived in the so-called impact approximation. In the end, the effect of collisions with particle perturbers is briefly recalled. The role of the so-called flat-spectrum approximation on the resonance scattering problem is also addressed along with the discussion of simplified models of atomic levels suitable for polarized radiative transfer studies. The results obtained in Section 2.5 are used in Section 2.6 where a closer attention is paid on the formulation of the NLTE problem. In the last Section 2.7 an example of partial analytical solution of a simple NLTE problem is shown.

With the small exception of Section 2.7, which contains a few original ideas, the chapter is entirely an overview of well established physical concepts. It is partly based on the non-relativistic quantum mechanics of atomic systems whose description is contained in the classical books of Landau & Lifshitz (1977) and Messiah (1961). The density matrix theory is well covered by Blum (1981). In the section on quantization of the electromagnetic field, the chapter draws mainly from the texts of Mandl (1960), Greiner (1998b), and Cohen-Tannoudji et al.

(1997). The section on the master equation theory follows the works of Cohen-Tannoudji (1977), Bommier & Sahal-Bréchot (1991), Bommier (1991), and Cohen-Tannoudji et al. (1998). The work of Landi Degl'Innocenti (1983), in which the equations of statistical equilibrium and the radiative transfer equation have been derived in a unified manner, influenced significantly the later parts of the chapter which deal with phenomenological line profiles and the NLTE equations in general. Most of the material contained in this chapter, though sometimes derived using a slightly different approach or in a bit different notation, is covered in very much detail in the monography of Landi Degl'Innocenti & Landolfi (2004). The amount of material addressed in this chapter is enormous. It was thus impossible (and even not worth) to present all the details that can be found in the literature. Most of the derivations – especially in Section 2.5 – are only outlined. The detailed discussion can be found in the works listed above.

2.2 Density matrix

Density matrix formalism originally introduced by von Neumann (1927) is a natural ingredient of the astrophysical line-polarization problem. Density matrix approach can be advantageously used for a description of the sate of weakly coupled incoherent ensembles of atoms and photons; and it is the problem we meet in the physics of stellar atmospheres.

The approach used in this thesis is based on the works of Fano (1957), Cohen-Tannoudji (1977), Omont (1977), and Blum (1981).

Definition and properties

An isolated quantum mechanical system in the Hilbert space $\mathcal{H}$ with the orthonormal basis $\{|m\rangle\}$ is, in pure state, described by the *state vector*

$$|\psi(t)\rangle = \sum_m c_m(t)\,|m\rangle \ , \tag{2.1}$$

where $c_m(t)$ are the time-dependent amplitudes. An equivalent description of such a pure state is in terms of the *pure-state density operator* (or *density matrix*),

$$\rho(t) = |\psi(t)\rangle\,\langle\psi(t)| = \sum_{mn} c_m(t)c_n^*(t)\,|m\rangle\,\langle n| = \sum_{mn}\rho_{mn}(t)\,|m\rangle\,\langle n| \ . \tag{2.2}$$

In the following, I will suppress the explicit time dependencies. The diagonal density matrix elements, $\rho_{mm} = c_m c_m^*$, can be interpreted as being the probabilities of the system to be in the pure state $|m\rangle$ or, in other words, populations of states $|m\rangle$. The off-diagonal elements ($m \neq n$) are the so-called quantum coherences between the states $|m\rangle$ and $|n\rangle$. The distinction between populations and coherences obviously depends on the particular choice of basis. For instance, one can always choose $\{|m\rangle\}$ to be eigenvectors of the density operator in which ρ is diagonal.

Let us now consider an *incoherent ensemble* of N particles of the same kind whose *mutual interaction can be neglected* so that collective effects are negligible. A good example of such a system is a statistical ensemble of atoms or photons in solar atmosphere where typical distances among atoms are rather large compared to typical size of the atoms and the successive interactions of photons can be supposed to be uncorrelated to a high degree of confidence. The density operator of such a statistical ensemble is defined as the ensemble-averaged density operator,

$$\rho = \sum_{i=1}^{N}\rho^{(i)} = \sum_{i=1}^{N}\left|\psi^{(i)}\right\rangle\left\langle\psi^{(i)}\right| = \sum_{mn}\rho_{mn}\,|m\rangle\,\langle n| \ , \tag{2.3}$$

where

$$\rho_{mn} = \langle m \left| \rho \right| n \rangle = \sum_{ij} c_m^{(i)} c_n^{(j)*} \,, \tag{2.4}$$

are the average density matrix elements. The important properties of the density matrix following directly from its definition are Hermiticity,

$$\rho^\dagger = \rho \,, \tag{2.5}$$

and the normalization condition,

$$\mathrm{Tr}\, \rho = \sum_m \rho_{mm} = 1 \,. \tag{2.6}$$

Density matrices contain all the measurable information about the system. The expectation value of any quantity with the associated operator G can be obtained from ρ as

$$\langle G \rangle = \mathrm{Tr}\, G\rho \,, \tag{2.7}$$

where Tr denotes the trace operator. The density operator is a solution of the Schrödinger (or Liouville) equation,

$$\frac{\mathrm{d}}{\mathrm{d}t}\rho = \frac{1}{i\hbar}[H, \rho] \,, \tag{2.8}$$

where H is a Hamiltonian of the system.

Density matrix of a subsystem

Let us consider a system that consists of two subsystems, X and Y. Let $\{|i\rangle\}$ be the orthonormal basis of X indexed by the Latin letters and let $\{|\alpha\rangle\}$ be the orthonormal basis of Y indexed by the Greek letters. The orthonormal basis of the state space is $\{|i, \alpha\rangle \equiv |i\rangle\,|\alpha\rangle\}$.

If we are interested only in the variables of X then we can define the *reduced density operator* of X as

$$\rho_X = \mathrm{Tr}_Y\, \rho \,, \tag{2.9}$$

with the elements

$$\langle i \left| \rho_X \right| j \rangle = \sum_\alpha \langle i, \alpha \left| \rho \right| j, \alpha \rangle \,. \tag{2.10}$$

The partial trace over the Y degrees of freedom, Tr_Y, allows one to deal only with the X variables: The expectation value of the quantity G_X *acting only on* X variables is given by

$$\langle G_X \rangle = \mathrm{Tr}_X\, G_X \rho_X \,. \tag{2.11}$$

For derivation of Eq. (2.11) see Cohen-Tannoudji (1977)

An important case to be investigated is if the systems X and Y can be decoupled, i.e., the *correlation between the systems is negligible*. Then the total density matrix can be decoupled as

$$\rho = \rho_X \otimes \rho_Y \,. \tag{2.12}$$

If G_X and G_Y are, respectively, the operators acting only on the variables of X and Y then Eq. (2.12) implies

$$\mathrm{Tr}\, G_X G_Y \rho = \mathrm{Tr}_X\, G_X \rho_X\, \mathrm{Tr}_Y\, G_Y \rho_Y \,, \tag{2.13}$$

i.e., the expectation value of the product is equal to the product of the expectation values. This condition obviously holds for any number of non-correlated subsystems and it has deep consequences for the development of the NLTE equations.

2.3 Atom in an external magnetic field

Atomic electrons follow the laws of quantum mechanics. Depending on approximations used in the description of the atomic state, possible presence of nuclear spin, and strength of external magnetic fields, one can distinguish several models of atomic levels that require slightly different treatment. This section deals with a set of models of increasing complexity which can be usually encountered in solar atmospheric applications.

If external fields are switched off then the rotational invariance of the atomic system implies that the common eigenvectors of the square of the total angular momentum operator, J^2, of its projection to the z-axis, J_z, and of the total Hamiltonian ,H, make up an orthogonal basis of states. This basis can obviously be used even if the symmetry is broken by external fields. However, in such a case, the energy eigenvectors are, in general, no-longer coincident with the angular momentum eigenvectors.

2.3.1 Spinless atom

Unperturbed Hamiltonian

We start by considering an atom with *spinless* electrons in an electrostatic potential field of the spinless nucleus.[1] Coulomb interaction among the atomic electrons and the nucleus is given by the *unperturbed Hamiltonian*,

$$H_0 = \sum_i \frac{\boldsymbol{p}_i^2}{2m_\mathrm{e}} + \sum_{i<j} V^{\mathrm{el.}}_{\mathrm{Coul.}}(|\boldsymbol{r}_i - \boldsymbol{r}_j|) + \sum_i V^{\mathrm{nucl.}}_{\mathrm{Coul.}}(r_i)\,, \tag{2.14}$$

where $\boldsymbol{p}_i$ is the momentum of i-th electron, and $V^{\mathrm{el.}}_{\mathrm{Coul.}}$ is the mutual Coulomb potential of electrons. The last term stands for the Coulomb potential of electrons in the nuclear field. The electron mass is denoted by m_e.

In this model, the total angular momentum of electrons equals to the total orbital momentum, $\boldsymbol{L}$. The commuting operators are thus H_0, L^2, and L_z, with a common set of eigenvectors denoted by $|\alpha L M_L\rangle$ and satisfying

$$H_0\,|\alpha L M_L\rangle = E_{\alpha L}\,|\alpha L M_L\rangle\,, \tag{2.15}$$
$$L^2\,|\alpha L M_L\rangle = L(L+1)\,|\alpha L M_L\rangle\,, \tag{2.16}$$
$$L_z\,|\alpha L M_L\rangle = M_L\,|\alpha L M_L\rangle\,. \tag{2.17}$$

From now on, α denotes a set of quantum numbers describing the electron configuration.

Spinless atom in a uniform magnetic field

Let us turn a uniform magnetostatic field $\boldsymbol{B}$ on.[2] In order to investigate the effect of the field, one has to define a position operator, $\boldsymbol{r} = \sum_i \boldsymbol{r}_i$, as a sum of the position operators of atomic electrons. The total Hamiltonian is thus given by the expression

$$H = H_0 + \mu_0 \boldsymbol{B}\cdot\boldsymbol{L} + \frac{e^2}{2m_\mathrm{e}c^2}|\boldsymbol{B}\times\boldsymbol{r}|^2\,, \tag{2.18}$$

[1] The problem is formulated in the atomic rest frame and the nuclear mass is supposed to be infinite compared to the electron mass.

[2] We use the following gauge conditions for the scalar and vector potentials: $\varphi(\boldsymbol{r},t) = 0$ and $\boldsymbol{A}(\boldsymbol{r},t) = \frac{1}{2}\boldsymbol{B}\times\boldsymbol{r}$.

where e is the absolute value of electron charge and

$$\mu_0 = \frac{e\hbar}{2m_\mathrm{e}c} \approx 9.27 \times 10^{-21}\,\mathrm{erg\,G^{-1}}\,, \tag{2.19}$$

is the so-called *Bohr magneton*. The quantity $\mu_0 \boldsymbol{L}$ represents the operator of magnetic moment related to the orbital motion of the electrons. The third term in Eq. (2.18) is called the *diamagnetic term*. It is negligible when compared to the other terms in all the solar-physics applications. In the following, it will always be neglected.

From now on, I will use the coordinate system with the z-axis oriented in the direction of magnetic field. This choice, though physically arbitrary, makes many calculations more effortless.

It is easy to find the energy spectrum of the spinless atom in magnetic field: It follows from Eqs. (2.18) and (2.17) that

$$H\,|\alpha L M_L\rangle = (E_{\alpha L} + \mu_0 B M_L)\,|\alpha L M_L\rangle\ . \tag{2.20}$$

We see that the unperturbed $(2L+1)$-fold degenerated levels $E_{\alpha L}$ are equidistantly split by magnetic field (the so-called *Zeeman effect*) as

$$E_{\alpha L M_L} = E_{\alpha L} + \mu_0 B M_L\,. \tag{2.21}$$

2.3.2 Fine structure of levels

Unperturbed Hamiltonian

Since real electrons possess the spin $s = 1/2$, there is an associated magnetic moment

$$\boldsymbol{\mu} = \mu_\mathrm{e}\frac{\boldsymbol{s}}{s} = 2\mu_\mathrm{e}\boldsymbol{s}\,, \tag{2.22}$$

with each of the electrons. The quantity μ_e follows from the Dirac's relativistic theory:[3]

$$\mu_\mathrm{e} = \frac{e\hbar}{2m_\mathrm{e}c} = \mu_0\,. \tag{2.23}$$

Since electrons move in the electrostatic field, there is an additional interaction of their spin magnetic momentum and the electrostatic field: the so-called *spin-orbit interaction*. The precise form of the interaction can be deduced from the correspondence principle and, in general, follows from the relativistic quantum mechanics. It can be shown that the interaction potential is proportional to the operator $\boldsymbol{L}\cdot\boldsymbol{S}$, where $\boldsymbol{S} = \sum_i \boldsymbol{s}_i$ is the total spin of atomic electrons. The operator $\boldsymbol{L}\cdot\boldsymbol{S}$ commutes with the total angular momentum, $\boldsymbol{J} = \boldsymbol{L}+\boldsymbol{S}$, and with L^2. However, it does not commute with $\boldsymbol{L}$. The same is true for $H_0 + H_\mathrm{so}$. Thus the orbital momentum is no longer conserved. A suitable basis of states is now $|\alpha J M\rangle$ with M being a quantum number associated with the J_z operator. We have

$$\begin{aligned}
(H_0 + H_\mathrm{so})\,|\alpha J M\rangle &= E_{\alpha J}\,|\alpha J M\rangle\ , &(2.24)\\
J^2\,|\alpha J M\rangle &= J(J+1)\,|\alpha J M\rangle\ , &(2.25)\\
J_z\,|\alpha J M\rangle &= M\,|\alpha J M\rangle\ . &(2.26)
\end{aligned}$$

[3]The more precise investigations lead to the expression $\boldsymbol{\mu} = g_\mathrm{e}\frac{e\hbar}{2m_\mathrm{e}c}\boldsymbol{s}$ with $g_\mathrm{e} \approx 2.0023$, where g_e is the so-called g-factor of electron. In this work I will always use $g_\mathrm{e} = 2$.

One can often approximate S and L as being good quantum numbers (the so-called *Russel-Saunders* or *LS coupling*). In the LS-coupling scheme, the spin-orbit Hamiltonian is often given by (Condon & Shortley 1935)

$$H_{\rm so} = \zeta(\alpha LS)\boldsymbol{L}\cdot\boldsymbol{S}\,, \tag{2.27}$$

where $\zeta(\alpha LS)$ has the dimension of energy and determines a degree of splitting of the αLS term into the fine-structure levels with the angular momenta,

$$J = |L-S|, |L-S|+1, \ldots, L+S-1, L+S\,. \tag{2.28}$$

The eigenvectors of H_0 can be found in the $|\alpha LSJM\rangle$ representation. Using the fact that $\boldsymbol{L}\cdot\boldsymbol{S} = (J^2-L^2-S^2)/2$, the eigenenergies of $H_{\rm so}$ are given by

$$E_{\alpha LS}(J) = \frac{1}{2}\zeta(\alpha LS)\left[J(J+1)-L(L+1)-S(S+1)\right]\,, \tag{2.29}$$

whenever Eq. (2.27) holds. In some cases (such as in the case of helium atoms) this simple relation cannot be applied. Even though the analysis described below can be applied with the use of experimental values for $E_{\alpha LS}(J)$.

Uniform magnetic field

A new term $2\mu_0\boldsymbol{B}\cdot\boldsymbol{S}$ has to be added into the atomic Hamiltonian to take into account the interaction between the external magnetic field and atomic spin. The total Hamiltonian becomes

$$H = H_0 + H_{\rm so} + \mu_0\boldsymbol{B}\cdot(\boldsymbol{L}+2\boldsymbol{S}) = H_0 + H_{\rm so} + H_B\,. \tag{2.30}$$

One can find a new energy spectrum by diagonalization of the operator $H_{\rm so}+H_B$. After some algebra (for details see Landi Degl'Innocenti & Landolfi 2004) one arrives at

$$\begin{aligned}\langle \alpha LSJM\,|H_{\rm so}+H_B|\,\alpha' L'S'J'M'\rangle = \\ \delta_{\alpha\alpha'}\delta_{LL'}\delta_{SS'}\delta_{MM'}\,\langle \alpha LSJM\,|H_{\rm so}+H_B|\,\alpha LSJ'M\rangle\,.\end{aligned} \tag{2.31}$$

The matrix to be diagonalized is block-diagonal with one square block per each degenerated level $(\alpha LS, M)$. J is no longer a good quantum number.

2.3.3 Paschen-Back effect

In the LS-coupling scheme, the only non-zero matrix elements we get from Eq. (2.31) are the diagonal ones,

$$\langle \alpha LSJM\,|H_{\rm so}+H_B|\,\alpha LSJM\rangle = E_{\alpha LS}(J) + \mu_0 B g_{LS}(J) M\,, \tag{2.32}$$

where

$$g_{LS}(J) = 1 + \frac{1}{2}\frac{J(J+1)+S(S+1)-L(L+1)}{J(J+1)}\,, \tag{2.33}$$

is the so-called Landé factor, and the off-diagonal ones,

$$\begin{aligned}\langle \alpha LS\,J-1\,M\,|H_{\rm so}+H_B|\,\alpha LSJM\rangle = \langle \alpha LSJ\,M\,|H_{\rm so}+H_B|\,\alpha LS\,J-1\,M\rangle \\ = -\frac{\mu_0 B}{2J}\sqrt{\frac{(J+S+L+1)(J-S+L)(J+S-L)(-J+S+L+1)(J^2-M^2)}{(2J+1)(2J-1)}}\,.\end{aligned} \tag{2.34}$$

The unknown energy eigenvectors can be expressed as linear combinations of the $|\alpha LSJM\rangle$ basis,

$$|\alpha LSjM\rangle = \sum_J C_J^j(\alpha LS, M)\,|\alpha LSJM\rangle\ , \tag{2.35}$$

where transformation coefficients $C_J^j(\alpha LS, M)$ are found by diagonalization of the $H_{\rm so} + H_B$ submatrices for every particular every degenerated level $(\alpha LS, M)$. Since the matrix with elements (2.32) and (2.34) is tridiagonal, real, and symmetric, the $C_J^j(\alpha LS, M)$ coefficients can be chosen to be real. In a common notation, the energy eigenvalues of $H_{\rm so} + H_B$ are denoted by $\lambda_j(\alpha LS, M)$. Finally, we have

$$H\,|\alpha LSjM\rangle = [E_{\alpha LS} + \lambda_j(\alpha LS, M)]\,|\alpha LSjM\rangle\ . \tag{2.36}$$

If the magnetic field is so strong that the H_B becomes comparable to $H_{\rm so}$ then we say that the levels are in the so-called *Paschen-Back effect regime*. The ratio of magnetic and spin-orbit interactions can be naturally quantified by the dimensionless quantity

$$\gamma = \frac{\mu_0 B}{\zeta(\alpha LS)}\,. \tag{2.37}$$

The levels $(\alpha LS, M)$ are degenerated and in the presence magnetic field strength of about $\gamma \approx 1$ some of them cross. This so-called *level-crossing effect* gives rise to an interesting phenomena in a polarization state of scattered quasi-resonant radiation (Bommier 1980, see also Chapter 4).

2.3.4 Limiting case of weak and strong magnetic field

The general case studied in the preceding subsection is rather complicated. This procedure can be avoided in two extremal cases in which perturbation theory can be advantageously applied:

Zeeman effect regime

If the magnetic field is weak enough so that H_B can be considered as perturbation to the spin-orbit interaction, i.e., $\gamma \ll 1$, (the so-called *Zeeman effect regime*) then

$$C_J^j(\alpha LS, M) \to \delta_{jJ}\,, \tag{2.38}$$

and the first-order correction to $E_{\alpha LS}(J)$ is just

$$E_{\alpha LS}^{(1)}(J) = \mu_0 B g_{LS}(J) M\,. \tag{2.39}$$

In this approximation, the angular momentum eigenvectors $|\alpha LSJM\rangle$ remain coincident with the energy eigenvectors and no Hamiltonian diagonalization is necessary.

Complete Paschen-Back effect regime

An opposite case to the preceding is the limit of strong magnetic field, $\gamma \gg 1$. In that case, orbital and spin momenta precess independently around the quantization axis (i.e., around the magnetic field direction) since they are strongly coupled to the external magnetic field rather than to each other. Both L and S are good quantum numbers and the suitable basis is the one composed of the vectors $|\alpha LSM_L M_S\rangle$, where M_S denotes the projection of the spin moment. The eigenvalues of the magnetic Hamiltonian spread linearly with the magnetic field intensity as $\mu_0 B(M_L + 2M_S)$. This strong-field limit is called the *complete Paschen-Back effect regime*.

2.3.5 Hyperfine structure of levels

Unperturbed Hamiltonian

If the nuclear spin, $\boldsymbol{I}$, of a given isotope is non-zero then the interaction between magnetic moment of the nucleus and the electron shell leads to the so-called *hyperfine splitting of the levels*. Since the hyperfine interaction is some three orders of magnitude weaker than is the fine structure energy, the hyperfine splitting is often directly unobservable in the astrophysical lines whose width is dominated by the Doppler broadening. In spite of this fact, the existence of hyperfine splitting has important consequences for formation of the line polarization.

The nuclear spin and the total electron angular momentum $\boldsymbol{J}$ get coupled and the total angular momentum of the atom (including the nucleus) is usually denoted by $\boldsymbol{F} = \boldsymbol{J} + \boldsymbol{I}$. The fine-structure level J is now splitted into the hyperfine components with the angular momenta

$$F = |J - I|, |J - I| + 1, \ldots, J + I - 1, J + I \,. \tag{2.40}$$

A suitable basis is composed of the common eigenvectors of total angular momentum and the Hamiltonian, $|\alpha JIFf\rangle$, where f denotes the quantum number associated with the F_z operator.

The most important role in the hyperfine interaction is played by the *magnetic dipole* and *electric quadrupole* moments of the nucleus. Higher moments can usually be neglected because the dimension of the nucleus is much smaller than is the dimension of electron cloud. The magnetic dipole contribution reads

$$E^{(1)}_{\rm hfs} = \frac{a(\alpha JI)}{2} K \,, \tag{2.41}$$

and the electric quadrupole contribution is given by

$$E^{(2)}_{\rm hfs} = b(\alpha JI) \left[K(K+1) - \frac{4}{3} J(J+1) I(I+1) \right] , \tag{2.42}$$

where

$$K = F(F+1) - J(J+1) - I(I+1) \,. \tag{2.43}$$

Experimental values for $a(\alpha JI)$ and $b(\alpha JI)$ can be found in tables.

Uniform magnetic field

If the external magnetic field is turned on then one has to diagonalize the magnetic and hyperfine-structure Hamiltonians in a way analogous to Subsection 2.3.3. The appropriate replacements

$$L \to J,\, S \to I,\, j \to i,\, M \to f \,,$$

have to be done, where i denotes the quantum number of the states of the degenerated subspace corresponding to the level $(\alpha JI, f)$. The same approximations concerning a strength of the magnetic field can be done as long as Zeeman splitting of the hyperfine levels is smaller than is the fine-structure splitting of the levels. If this condition is not satisfied (as it is usually the case for atomic hydrogen) then more general picture is necessary (see for instance Casini & Manso Sainz 2005).

2.4 Radiation field

2.4.1 Stokes parameters classically

Suppose we have a right-handed coordinate system and the monochromatic electromagnetic wave with the angular frequency ω propagating in the direction of the unit vector $\boldsymbol{\Omega}$. We can define two real orthonormal vectors, $\boldsymbol{e}_a(\boldsymbol{\Omega})$ and $\boldsymbol{e}_b(\boldsymbol{\Omega})$, for every direction $\boldsymbol{\Omega}$, which are perpendicular to $\boldsymbol{\Omega}$. The vector $\boldsymbol{e}_a$ is called the *reference direction vector* and $\boldsymbol{e}_b$ is the so-called *associated vector*. One can also define a set of two complex vectors $\boldsymbol{e}_\pm(\boldsymbol{\Omega})$ by

$$\boldsymbol{e}_\pm(\boldsymbol{\Omega}) = \frac{1}{\sqrt{2}} \left[\mp \boldsymbol{e}_a(\boldsymbol{\Omega}) + \mathrm{i}\boldsymbol{e}_b(\boldsymbol{\Omega}) \right] . \tag{2.44}$$

These vectors do satisfy the following relations:

$$\begin{aligned} \boldsymbol{e}_\lambda(\boldsymbol{\Omega}) \cdot \boldsymbol{e}^*_{\lambda'}(\boldsymbol{\Omega}) &= \delta_{\lambda\lambda'} , \quad \text{where} \quad \lambda, \lambda' \equiv \pm , \\ \boldsymbol{e}_\lambda(\boldsymbol{\Omega}) \cdot \boldsymbol{\Omega} &= 0 , \\ \boldsymbol{e}^*_\pm(\boldsymbol{\Omega}) &= -\boldsymbol{e}_\mp(\boldsymbol{\Omega}) , \end{aligned} \tag{2.45}$$

and since they have simple spherical components, they are preferably used in theoretical derivations.

It is shown in the classical theory of electromagnetism (Greiner 1998a) that the electric vector[4] of a *monochromatic transverse wave* is, in the plane perpendicular to $\boldsymbol{\Omega}$, described by the plane waves

$$\boldsymbol{E}(t) = \frac{1}{\sqrt{2}} \left[\boldsymbol{\mathcal{E}} \mathrm{e}^{\mathrm{i}\omega t} + \boldsymbol{\mathcal{E}}^* \mathrm{e}^{-\mathrm{i}\omega t} \right] , \tag{2.46}$$

where $\boldsymbol{\mathcal{E}}$ is a complex amplitude of the wave. The trajectory of the tip of the electric vector of the wave is, in general, elliptic. The so-called *polarization ellipse* can be described in terms of "size", shape, orientation, and the sense of the electric vector precession (Chandrasekhar 1960). An equivalent and more useful description is in terms of the so-called polarization tensor (Stenflo 1994),

$$\boldsymbol{J} = \boldsymbol{\mathcal{E}}^* \boldsymbol{\mathcal{E}} . \tag{2.47}$$

One can relate $\boldsymbol{J}$ with the so-called Stokes parameters (Stokes 1852; Born & Wolf 1999) which, in the basis $\{\boldsymbol{e}_a, \boldsymbol{e}_b\}$, read

$$\begin{aligned} I &= b(J_{aa} + J_{bb}) , \\ Q &= b(J_{aa} - J_{bb}) , \\ U &= b(J_{ab} + J_{ba}) , \\ V &= \mathrm{i}b(J_{ab} - J_{ba}) , \end{aligned} \tag{2.48}$$

or, equivalently, in the basis $\{\boldsymbol{e}_+, \boldsymbol{e}_-\}$,

$$\begin{aligned} I &= b(J_{++} + J_{--}) , \\ Q &= -b(J_{+-} + J_{-+}) , \\ U &= -\mathrm{i}b(J_{+-} - J_{-+}) , \\ V &= b(J_{++} - J_{--}) . \end{aligned} \tag{2.49}$$

The constant b is a dimensionality constant making Stokes parameters of dimension of specific intensity. An elegant relation between the polarization tensor and Stokes parameters can be

[4] Magnetic component of the wave is, up to a convention concerning the pseudovector direction, uniquely determined by the electric vector. However, magnetic interactions of electromagnetic waves will be ignored in this work because of their little physical importance for the problems under consideration.

found by use of the 2×2 Pauli matrices (Stenflo 1994; Landi Degl'Innocenti & Landolfi 2004). It is often useful to construct a formal vector of Stokes parameters

$$\boldsymbol{I} = \begin{pmatrix} I_0 \\ I_1 \\ I_2 \\ I_3 \end{pmatrix} \equiv \begin{pmatrix} I \\ Q \\ U \\ V \end{pmatrix} . \tag{2.50}$$

This indexing notation is especially useful in the theory of polarized radiative transfer. The convention for definition of Stokes parameters differs slightly from author to author. Here I adopt the convention consistent with Landi Degl'Innocenti & Landolfi (2004).

Monochromatic waves are just a mathematical abstraction. Real electromagnetic beams always consist of a superposition of different wave modes. In this work I only consider the *incoherent superposition* of waves. For such a radiation, one can use the so-called *addition theorem* for Stokes parameters which states that Stokes parameters of the incoherent beams of radiation add together. This approximation seems to be well justified in the conditions of solar atmosphere. A close relation of this approximation with the additivity of radiation density matrices (cf. Section 2.2) will be pointed out in Subsection 2.4.3. In the case of quasi-monochromatic beams, the quantities of interest in measurements are the time-average values of Stokes parameters,

$$\boldsymbol{I} \to \langle \boldsymbol{I} \rangle_{\text{time}} . \tag{2.51}$$

We say that radiation beam is *polarized* if $(Q, U, V) \neq (0, 0, 0)$. If the only nonzero Stokes parameter is I then there is no mean coherence between different polarization modes of the ensemble of electromagnetic waves and the beam is said to be *unpolarized*. If the radiation is monochromatic, it is $I^2 = Q^2 + U^2 + V^2$. From the quantum-mechanical point of view, this situation arises for an ensemble of photons in a pure state. In a more realistic case of quasi-monochromatic beam, one always has $I^2 > Q^2 + U^2 + V^2$ and usually even $I^2 \gg Q^2 + U^2 + V^2$ because the so-called *polarization degree*,

$$p = \frac{\sqrt{Q^2 + U^2 + V^2}}{I} , \tag{2.52}$$

is typically small in the conditions of the solar atmosphere.

2.4.2 Quantization of the electromagnetic field

One can easily construct the Hamiltonian of free electromagnetic field, H_R, from the correspondence principle (Mandl 1960; Greiner 1998b),

$$H_R = \sum_{\boldsymbol{k}\lambda} \hbar\omega a^\dagger(\boldsymbol{k}, \lambda) a(\boldsymbol{k}, \lambda) , \tag{2.53}$$

where

$$\boldsymbol{k} = \frac{\omega}{c} \boldsymbol{\Omega} , \tag{2.54}$$

is the wave vector and λ is the given polarization state defined by Eq. (2.45). $a(\boldsymbol{k}, \lambda)$ and $a^\dagger(\boldsymbol{k}, \lambda)$ denote, respectively, the annihilation and creation operators of the mode $(\boldsymbol{k}, \lambda)$. Note that the vacuum energy, $\hbar\omega/2$, has been removed from the definition of H_R.

An operator of electric field can also be expressed in terms of creation and annihilation operators,

$$\boldsymbol{E}_{\boldsymbol{k}\lambda} = \mathrm{i} \sqrt{\frac{2\pi\hbar\omega}{\mathcal{V}}} \left[a(\boldsymbol{k}, \lambda) \boldsymbol{e}_\lambda(\boldsymbol{\Omega}) \mathrm{e}^{\mathrm{i}\boldsymbol{k}\cdot\boldsymbol{r}} - a^\dagger(\boldsymbol{k}, \lambda) \boldsymbol{e}^*_\lambda(\boldsymbol{\Omega}) \mathrm{e}^{-\mathrm{i}\boldsymbol{k}\cdot\boldsymbol{r}} \right] , \tag{2.55}$$

where $\mathcal{V}$ is the volume of normalization box (Cohen-Tannoudji et al. 1997). The quantum counterpart of the polarization tensor (2.47) or, more precisely, of the quantity $b\boldsymbol{J}$, is the operator (Landi Degl'Innocenti 1983)

$$I_{\alpha\beta}(\boldsymbol{k}) = \frac{1}{4\pi^2}\frac{\hbar\omega^3}{c^2}a^\dagger(\boldsymbol{k},\alpha)a(\boldsymbol{k},\beta)\,. \tag{2.56}$$

The operators of Stokes parameters can be constructed in a way analogous to Eqs. (2.49). For explicit expressions see, for instance, Landi Degl'Innocenti (1987).

2.4.3 Density matrix of radiation

One can describe the one-photon radiation field on the basis of state vectors for polarized plane waves, $|\boldsymbol{k}\lambda\rangle$ (Omont 1977). A statistical ensemble of *partially polarized* monochromatic plane waves is thus well described by the density operator (cf. Section 2.2)

$$\rho(\boldsymbol{k}) = \sum_{\lambda\lambda'}\rho_{\lambda\lambda'}(\boldsymbol{k})\,|\boldsymbol{k}\lambda\rangle\,\langle\boldsymbol{k}\lambda'|\,, \tag{2.57}$$

where $\rho_{\lambda\lambda'}(\boldsymbol{k})$ is the 2×2 monochromatic density matrix. This density matrix is easily generalized to the case of multi-wavelength field by summation over the different wave vectors $\boldsymbol{k}$. This density matrix will be denoted by ρ_R. Calculation of the expectation value of the operator G_R acting on the radiation field is calculated from

$$\langle G_R\rangle = \mathrm{Tr}\,G_R\rho_R\,. \tag{2.58}$$

The expectation value of the operator (2.56) is – up to the factor b – the classical polarization matrix. In fact, there is a simple relation between the density matrix of radiation and the polarization matrix (Bommier & Sahal-Bréchot 1978),

$$\rho_{\alpha\beta} = \frac{J_{\alpha\beta}}{\mathrm{Tr}\,\boldsymbol{J}}\,. \tag{2.59}$$

Approximation concerning radiation field

Radiation incoherency means that the expectation value of any quantity which is linear in electric field is zero. One also expects that there is no correlation between states of different occupying numbers with different energy. In the language of annihilation and creation operators these conditions read (Landi Degl'Innocenti 1983):

$$\mathrm{Tr}\,a(\boldsymbol{k},\lambda)\rho_R = \mathrm{Tr}\,a^\dagger(\boldsymbol{k},\lambda)\rho_R = \mathrm{Tr}\,a(\boldsymbol{k},\lambda)a(\boldsymbol{k}',\lambda')\rho_R = \mathrm{Tr}\,a^\dagger(\boldsymbol{k},\lambda)a^\dagger(\boldsymbol{k}',\lambda')\rho_R = 0. \tag{2.60}$$

Also, there is no correlation between modes of different $\boldsymbol{k}$. The only permitted correlation is the one between different polarization modes,

$$\mathrm{Tr}\,\left[a^\dagger(\boldsymbol{k},\lambda)a(\boldsymbol{k}',\lambda')\rho_R\right] = 0, \quad \text{unless} \quad \boldsymbol{k}=\boldsymbol{k}'\,. \tag{2.61}$$

2.5 Master equation

Dynamics of the system of charged particles and electromagnetic field in the Coulomb gauge is fully described by the Hamiltonian (Cohen-Tannoudji et al. 1998)

$$H = \sum_i \frac{1}{2m_i}\left[\boldsymbol{p}_i - q_i\boldsymbol{A}(\boldsymbol{r}_i)\right]^2 + \sum_i\left(-\frac{g_iq_i}{2m_i}\right)\boldsymbol{s}_i\cdot\boldsymbol{B}(\boldsymbol{r}_i) + V_{\mathrm{Coul.}} + H_R\,. \tag{2.62}$$

The first term represents the kinetic energy of the particles indexed by i. $\boldsymbol{A}$ is the vector potential of electromagnetic field. The second term stands for the interaction of spins $\boldsymbol{s}_i$ with the magnetic field $\boldsymbol{B}$, and the third term is the potential energy due to longitudinal electrostatic interaction (the Coulomb energy). q_i and g_i denote, respectively, the charge and the g-factor of the particles (see the footnote on page 32). The last term is the free-field Hamiltonian.

2.5.1 Atom-photon interactions

For the purposes of the studies of the interaction among the atomic system in magnetic field, radiation, and other perturbers, it is useful to reorganize the Hamiltonian (2.62) as follows

$$H = H_A + H_R + H_{AR} + H_P + H_{AP} + H_{RP}\,, \tag{2.63}$$

where H_A is the atomic Hamiltonian including the effect of magnetic field, is the Hamiltonian of the atom of interest, H_{AR} is the atom-radiation interaction potential, H_P is the Hamiltonian of the particle colliders (electrons, ions, ...), and H_{AP} and H_{RP} are, respectively, the atom-perturbers and radiation-perturbers interaction potentials.

In this work, I do not take consistently into account the external degrees of freedom of atoms. Only internal state is considered (see also Section 2.6). The interaction of the atom with particle colliders will be discussed Subsection 2.5.7. The interaction term H_{RP} will not be discussed (it describes the effects like Thomson scattering or absorption by different atomic species).

In solar-physics applications, one can suppose that the radiation field is weak. In other words, the Rabi frequency is very small compared to the inverse of the life-time of the levels (Blum 1981). Thus the perturbation theory is sufficient for description of the atom-radiation interaction.

The state of the global system "atom + radiation" is described by the density matrix $\rho(t)$. Moreover, both radiation and atoms are supposed to be incoherent statistical ensembles as stated above. We can express the problem in the *interaction picture* in which the operators have the form

$$\tilde{\rho}(t) = \mathrm{e}^{\mathrm{i}(H_A+H_R)t/\hbar}\rho(t)\mathrm{e}^{-\mathrm{i}(H_A+H_R)t/\hbar} \tag{2.64}$$

$$\tilde{\rho}_A(t) = \mathrm{e}^{\mathrm{i}H_At/\hbar}\rho_A(t)\mathrm{e}^{-\mathrm{i}H_At/\hbar} \tag{2.65}$$

$$\tilde{H}_{AR}(t) = \mathrm{e}^{\mathrm{i}(H_A+H_R)t/\hbar}H_{AR}\mathrm{e}^{-\mathrm{i}(H_A+H_R)t/\hbar}\,, \tag{2.66}$$

where $\tilde{\rho}_A(t) = \mathrm{Tr}_R\,\tilde{\rho}(t)$ denotes the reduced density matrix of the atomic system A. Similarly one can define $\tilde{\rho}_R(t) = \mathrm{Tr}_A\,\tilde{\rho}(t)$ for the density matrix of the radiation R (cf. Eq. 2.9). The Schrödinger equation (2.8) becomes

$$\frac{\mathrm{d}}{\mathrm{d}t}\tilde{\rho}(t) = \frac{1}{\mathrm{i}\hbar}\left[\tilde{H}_{AR}(t), \tilde{\rho}(t)\right]\,. \tag{2.67}$$

In the forthcoming perturbative development, we will need a formal solution of Eq. (2.67), which is given by

$$\tilde{\rho}(t+\Delta t) - \tilde{\rho}(t) = \Delta\tilde{\rho}(t) = \frac{1}{\mathrm{i}\hbar}\int_t^{t+\Delta t}\mathrm{d}t'\left[\tilde{H}_{AR}(t'), \tilde{\rho}(t')\right]\,, \tag{2.68}$$

and can be rewritten after one iteration as

$$\begin{aligned}\Delta\tilde{\rho}(t) &= \frac{1}{\mathrm{i}\hbar}\int_t^{t+\Delta t}\mathrm{d}t'\left[\tilde{H}_{AR}(t'), \tilde{\rho}(t)\right] \\ &+ \left(\frac{1}{i\hbar}\right)^2\int_t^{t+\Delta t}\mathrm{d}t'\int_t^{t'}\mathrm{d}t''\left[\tilde{H}_{AR}(t'), \left[\tilde{H}_{AR}(t''), \tilde{\rho}(t'')\right]\right]\,.\end{aligned} \tag{2.69}$$

Our aim in this section is to find the so-called *master equation* for $\mathrm{d}\rho_A(t)/\mathrm{d}t$ and $\mathrm{d}\rho_R(t)/\mathrm{d}t$, and, consequently, the NLTE equations of the polarized problem. In contrast to time evolution of $\tilde{\rho}(t)$, time evolution of A, which is not isolated, reads

$$\frac{\mathrm{d}}{\mathrm{d}t}\tilde{\rho}_A(t) = \mathrm{Tr}_R \frac{\mathrm{d}}{\mathrm{d}t}\tilde{\rho}(t) = \frac{1}{i\hbar}\frac{\mathrm{d}}{\mathrm{d}t}\mathrm{Tr}_R \left[\tilde{H}_{AR}(t), \tilde{\rho}(t)\right] . \tag{2.70}$$

It is not driven by a Hamiltonian operator – there is, in general, no Hermitian operator equivalent to H that would determine the evolution of ρ_A in a way analogous to Eq. (2.8). This fact has deep consequences for the evolution of ρ_A: Due to the complicated term $\mathrm{Tr}_R \left[\tilde{H}_{AR}, \tilde{\rho}\right]$ that couples A to R, the evolution of A is basically a dissipative processes that makes the evolution of A irreversible. The same conclusions can be made for evolution of R. To make the problem trackable, we suppose the radiation field to be uncorrelated with the atomic state,

$$\tilde{\rho}(t) = \tilde{\rho}_A(t) \otimes \tilde{\rho}_R(t) , \quad \text{for} \quad t \geq 0 . \tag{2.71}$$

Since we want to study the *interaction* between the radiation field and matter, the decomposition (2.71) is obviously somewhat inadequate. However, it is justified in the lowest-order approximation. One can consider distinct time scales of the scattering process: The interaction time, τ_c, with an incident wave whose spectral width $\Delta\omega$ is sufficiently large is, due to the Heisenberg uncertainty principle, of the order of $\Delta\omega^{-1}$. This time is typically very short when compared to the typical evolution time of the atom, T, which is comparable to the lifetime of the level, Γ^{-1}. If we are interested in the processes on the time scale $\tau_\mathrm{c} \ll \Delta t \ll T$ the perturbations exerted by radiation on A (and vice versa) can be averaged over the time. The system can be studied on the so-called *coarse-grained* time scale Δt. It can be shown (see Section IV.D.4 of Cohen-Tannoudji et al. 1998) that the relative error due to decomposition (2.71) is of the order of $\tau_\mathrm{c}/\Delta t$. For $\Delta t \gg \tau_\mathrm{c}$ the approximation is well justified.

Interaction potential, dipolar approximation

In the *dipolar approximation*, the interaction potential H_{AR} can be deduced from Eq. (2.62),

$$H_{AR} = -\boldsymbol{D} \cdot \boldsymbol{E} , \tag{2.72}$$

where $\boldsymbol{D} = e\boldsymbol{r}$ is the operator of atomic electric dipolar moment, and $\boldsymbol{E}$ is the electric intensity of the field (Eq. 2.55, or, more precisely a superposition of possible field modes) at the position of the nucleus.

2.5.2 Evolution of the atomic system

State of the radiation

Let us focus our attention on evolution of the atomic system A. Since there are no coherences between radiation modes of different $\boldsymbol{k}$, the radiation density matrix commutes with H_R and we have

$$\tilde{\rho}_R(t) = \rho_R(t) . \tag{2.73}$$

Following Cohen-Tannoudji et al. (1998) we can consider A as being surrounded by the *reservoir* of radiation R with a huge "heat capacity" so that there is no macroscopic modification of R due to its interaction with A (this is the so-called *no back-reaction approximation*). We may also assume that R is in a stationary state, $\mathrm{d}\rho_R/\mathrm{d}t = 0$, hence

$$\tilde{\rho}_R(t) = \tilde{\rho}_R(0) = \rho_R , \tag{2.74}$$

and one can write

$$\tilde{\rho}(t) = \tilde{\rho}_A(t) \otimes \rho_R \,. \tag{2.75}$$

Moreover, it follows from Eqs. (2.72) using Eq. (2.60) that

$$\mathrm{Tr}_R \, \tilde{H}_{AR}(t)\tilde{\rho}_R = \sum_{\mu=1}^{3} \tilde{D}_\mu \mathrm{Tr} \, \tilde{E}_\mu \tilde{\rho}_R = 0 \,. \tag{2.76}$$

Coarse grained rate of evolution

Evolution on the coarse grained scale can be obtained from Eq. (2.69) by applying the partial trace operator over the radiation degrees of freedom. Using Eq. (2.75), we get

$$\frac{\Delta\tilde{\rho}_A(t)}{\Delta t} = \frac{1}{\Delta t}\left(\frac{1}{i\hbar}\right)^2 \int_t^{t+\Delta t} \mathrm{d}t' \int_t^{t'} \mathrm{d}t'' \mathrm{Tr}_R \left[\tilde{H}_{AR}(t'), \left[\tilde{H}_{AR}(t''), \tilde{\rho}_A(t) \otimes \rho_R\right]\right] . \tag{2.77}$$

We have replaced $\tilde{\rho}_A(t'') \to \tilde{\rho}_A(t)$ which allows us to get the lowest-order approximation to the solution. Note that the first term on the r.h.s. of Eq. (2.69) vanished due to Eq. (2.76) and only the second order term remained.

$\Delta\tilde{\rho}_A/\Delta t$ is the so-called coarse-grained rate of variation of $\tilde{\rho}_A$. By averaging over the short (τ_c) interactions during the coarse-grained time Δt we lose the chance to study the history of the system. The evolution of the state is, in this approximation, determined by the instantaneous state $\tilde{\rho}_A(t)$ and not by the past evolution: We have the *Markov process*.

Atomic master equation

Without going into technical details,[5] it is worth to note the following: The quantities that appear in the commutators in Eq. (2.77) are bilinear in the electric field, i.e., either of the form $\rho_R\tilde{E}(t')\tilde{E}(t'')$ or $\rho_R\tilde{E}(t'')\tilde{E}(t')$. Traces of such quantities over the radiation degrees of freedom leads naturally to the definition of the so-called two-time average functions $g(\tau)$ dependent only on the time difference $\tau = t' - t''$ and having a narrow peak about $\tau = 0$. For $|\tau| > \tau_\mathrm{c}$ the two-time average functions drop rapidly to zero due to destructive interferences of the complex exponentials of different modes of the field. The integrations in Eq. (2.77) can be replaced by

$$\int_t^{t+\Delta t} \mathrm{d}t' \int_t^{t'} \mathrm{d}t'' \to \int_0^{\Delta t} \mathrm{d}\tau \int_{t+\tau}^{t+\Delta t} \mathrm{d}t' \tag{2.78}$$

and the upper limits of the integration over τ can safely be extended to infinity. The lower bound of the integration over t' can be extended to t. In fact, the transition $\Delta t \to \infty$ must be understood as follows: The condition $\Delta t \gg \tau_\mathrm{c}$ allows to extend formally the integration to infinity because there is always a negligible contribution to the integral from the $(\Delta t, \infty)$ interval if $\Delta t \gg \tau_\mathrm{c}$. In the same time, the condition $\Delta t \ll T$ has to be satisfied as stated above. This condition allows us to approximate the coarse time derivatives by differences.

Let us now consider the basis $\{|a\rangle\}$ of H_A eigenstates, $H_A\,|a\rangle = E_a\,|a\rangle$. Expansion of the commutators in Eq. (2.77) leads to the equation (omitting the index A in $\tilde{\rho}_A$)

$$\frac{\Delta\tilde{\rho}_{ab}(t)}{\Delta t} = \sum_{cd} \gamma_{ab\leftarrow cd}(t)\tilde{\rho}_{cd}(t) \,, \tag{2.79}$$

[5] For the derivations and discussion of all the expressions see Cohen-Tannoudji et al. (1998).

where $\gamma_{ab\leftarrow cd}(t)$ is the double time integral of the combination of the two-time average functions of τ and the bilinear terms in the atomic dipole operator $\boldsymbol{D}$ (cf. Eq. 2.72); all divided by Δt. The integral over t' can be easily evaluated: The atomic terms are proportional to $\mathrm{e}^{\mathrm{i}(\omega_{ab}-\omega_{cd})t'}$, where

$$\omega_{ij} = \frac{E_i - E_j}{\hbar}\,, \tag{2.80}$$

is the Bohr frequency between the states $|i\rangle$ and $|j\rangle$. The integral over t' is thus

$$\lim_{\Delta t\to\infty} \int_t^{\Delta t} \mathrm{d}t'\, \mathrm{e}^{\mathrm{i}(\omega_{ab}-\omega_{cd})t'} = \pi\delta(\omega_{ab}-\omega_{cd}) + \mathrm{i}\mathscr{P}\frac{1}{\omega_{ab}-\omega_{cd}}\,, \tag{2.81}$$

where δ is the Dirac delta-function and $\mathscr{P}$ is the Cauchy principal value. Finally, $\int_0^{\Delta t}\mathrm{d}\tau = \Delta t$, which cancels out with the difference Δt in the denominator.

Replacement $\Delta/\Delta t \to \mathrm{d}/\mathrm{d}t$ and transition from the interaction picture to the Schrödinger picture gives the master equation for atomic system in the form

$$\frac{\mathrm{d}\rho_{ab}(t)}{\mathrm{d}t} = -\mathrm{i}\omega_{ab}\rho_{ab}(t) + \sum_{cd}\mathcal{R}_{ab\leftarrow cd}\rho_{cd}(t)\,, \tag{2.82}$$

where $\mathcal{R}_{ab\leftarrow cd}$ are the time-independent coefficients. The first term on r.h.s. of Eq. (2.82) represents a free evolution of ρ_{ab}. This term is responsible for modification of the coherences due to magnetic field and gives rise to the so-called *Hanle effect*, i.e., modification of atomic coherences and, consequently, modification of the polarization state of the emitted radiation (Hanle 1924). Obviously, this term is zero if levels $|a\rangle$ and $|b\rangle$ have the same energy. The coefficients $\mathcal{R}_{ab\leftarrow cd}$ describe the rates of electric dipolar transitions of the atom due to its interaction with real and virtual photons. All the non-vanishing rates are proportional to a square of the reduced dipolar moments, $|\langle m\|\boldsymbol{D}\|n\rangle|^2$, i.e., to the line strengths or Einstein coefficients A, B. Magnitude of these rates is of the order of the inverse lifetime of the levels, i.e., $\Gamma \sim T^{-1}$.

Some of the coefficients $\mathcal{R}_{ab\leftarrow cd}$ vanish due to the so-called *secular approximation*: Taking into account a finite width of the levels (which cannot be directly revealed by the lowest-order perturbation theory), coupling of the coherences ρ_{ab} and ρ_{cd} with $|\omega_{ab}-\omega_{cd}| \gg \Delta t^{-1}$ disappears in the integral over t' due to the destructive coherence of the complex exponentials. Moreover, if $|\omega_{ab}-\omega_{cd}| \gg T^{-1}$, the coupling is also negligibly weak because $|\mathcal{R}_{ab\leftarrow cd}| \sim T^{-1}$. Since $T \gg \Delta\tau$, the coupling will also vanish if $|\omega_{ab}-\omega_{cd}| \sim \Delta t^{-1}$. The secular approximation can be understood as a consequence of the Heisenberg uncertainty relation between time and energy as pointed out by Bommier & Sahal-Bréchot (1991).

2.5.3 Equations of statistical equilibrium

It is useful to rewrite Eq. (2.82) in the form highlighting a physical content of the coefficients. To this end, one usually introduces the rates T_A, T_E, T_S and R_A, R_E, R_S for coherence transfer and coherence relaxation respectively (Landi Degl'Innocenti 1983). The indices A, E, and S denote, in this order, *absorption*, *emission*, and *stimulated emission* processes. Dropping the explicit time dependencies, Eq. (2.82) becomes

$$\begin{aligned}\frac{\mathrm{d}\rho_{ab}}{\mathrm{d}t} = -\mathrm{i}\omega_{ab}\rho_{ab} &+ \sum_{\ell,\ell'} T_A(a,b;\ell,\ell')\rho_{\ell\ell'} + \sum_{u,u'}\left[T_S(a,b;u,u') + T_E(a,b;u,u')\right]\rho_{uu'} \\ &- \sum_{n,n'}\left[R_A(a,b;n',n'') + R_S(a,b;n',n'') + R_E(a,b;n',n'')\right]\rho_{nn'}\,.\end{aligned} \tag{2.83}$$

As indicated by the indices ℓ and u, the first and the second summation is performed only over lower and upper levels respectively relative to ρ_{ab}. On the other hand, in the relaxation sums, the coherences $\rho_{nn'}$ and ρ_{ab} pertain to the same manifold of levels with possibly non-negligible coherences. The relaxation rates are themselves defined as a summation over the optical transitions to the lower and upper levels relative to ρ_{ab} ($\rho_{nn'}$). Eqs. (2.83) are the so-called *statistical equilibrium equations* (ESE). The equations of statistical equilibrium have been previously formulated by Bommier & Sahal-Bréchot (1978) in order to study the Hanle effect

Explicit expressions for $T_{A,E,S}$ and $R_{A,E,S}$ can be found in Landi Degl'Innocenti (1983). For some particular cases they will be given and analyzed in the following chapter. Here we limit our discussion to the qualitative analysis of their dependence on the radiation field.

The rates for spontaneous emission, T_E and R_E, do not depend on the incident radiation. The rates for absorption and stimulated emission, on the other hand, are proportional to the angle- and frequency-averaged polarization matrix,[6]

$$I_{\alpha\beta} = \int \frac{\mathrm{d}\boldsymbol{\Omega}}{4\pi} \int \mathrm{d}\omega \, I_{\alpha\beta}(\boldsymbol{k}) \Phi(\omega_0 - \omega) \,, \tag{2.84}$$

where $\Phi(\omega_0 - \omega)$ is a phenomenological complex profile introduced by Landi Degl'Innocenti (1983) and used in the lowest-order theory instead of the profiles (2.81) in order to overcome the impossibility of the theory to deal with the natural broadening of the levels. The real part of the profiles is determined by the lifetime of the levels. The imaginary part contains an information on the Lamb shifts of the levels. However, this information can be formally included into the atomic Hamiltonian, H_A. The frequency ω_0 denotes a particular Bohr frequency of the transition.

2.5.4 Flat-spectrum approximation

It is important to highlight the inconsistency of the 2nd order perturbation method described so far. The problem of finite width of the levels can be solved by introduction of the phenomenological profiles $\Phi(\omega_0 - \omega)$. In fact, there are often different Bohr frequencies for transitions between different coherences making up the upper and lower manifolds of a given spectral line. These differences cannot be properly taken into account in our approximation of the matter-radiation interaction if the radiation is not spectrally flat across the frequency interval $\Delta\omega$ much broader than the frequency separation of the levels in coherence. In such a case the oscillations of atomic coherences known as *quantum beats* appear (Blum 1981). This phenomenon cannot be correctly described by the present theory.

The *flat-spectrum approximation* states that the incident radiation has to be spectrally flat across the frequency interval larger than the Bohr frequency between the non-degenerated levels involved in a coherence. Moreover, it must be spectrally flat over the frequency interval much larger than the natural width of the levels.

In the NLTE problem, one has to deal with subsequent scatterings of the photons in a given spectral line. Since the medium is not optically thin, the line formation process itself leads to a non-flat character of the spectrum. The flat-spectrum approximation can be fully satisfied in the case that the upper and lower levels of the line are degenerated. In fact, this situation is rarely met in the magnetized solar atmosphere. Another possibility is that there are no coherences at all. Such a situation can be found in the problems with cylindrical symmetry (cf. Chapter 5) and in the situations in which the magnetic field or collisional depolarization are

[6]The factor $(\omega_0/\omega)^2$ in the integrand has been approximated by 1.

strong enough to destroy the coherences. However, coherences between non-degenerated levels often appear both for Zeeman sublevels of given J-level and for the crossing fine- and hyperfine structure levels. Fortunately, the Doppler width of typical lines in the solar atmosphere is much larger than their natural width, hence the thermal motion leads to redistribution of the line-core photons and the spectrum can be often considered to be flat across the frequency interval comparable to natural width of the line.

An important property arising out of Eqs. (2.83) is the fact that the larger is a separation of the levels, the smaller is their mutual coherence. For example, if the magnetic field is so strong that Zeeman splitting of the level is larger than its natural width – so that it could be potentially comparable to the Doppler width – the Zeeman coherences vanish due to the secular approximation. The same rule applies to the well separated fine structure levels. If the coherence between the levels is negligible, the flat-spectrum approximation is automatically satisfied. That is the reason why it is useful to define different approximations depending on the complexity of the manifolds of the coherences (see Subsection 2.5.6). Attention must be paid to case of "intermediate splitting" and to some special multiplets in which coherences play a significant role despite a large separation of the levels (such as in the case of sodium).

The flat spectrum approximation is analogous to the *complete frequency redistribution approximation* (CRD) of the unpolarized radiative transfer theory. The present multilevel theory cannot give correct results for the lines for which the effects of *partial frequency redistribution* (PRD) are important. This can be especially the case of strong resonance lines with well developed wings. While the radiation is incoherently redistributed in the Doppler core, coherent scattering may actually be important in the wings. There are attempts to incorporate the PRD effects into the polarized radiative transfer theory. The models restricted to the case of two-level atoms and based on the master equation theory have been developed in the past (Bommier 1997a,b). A heuristic approach to a multilevel solution of the PRD problem has been presented by Landi Degl'Innocenti et al. (1997). There is also a multilevel approach based on the master equation theory by Bommier (1999), but a consistent and useful framework is still missing.

2.5.5 Radiative transfer equation

The derivation of master equation for the density matrix of radiation or *radiative transfer equation* (RTE) can be done in a way analogous to the derivation of ESE. In the case of RTE, one considers a radiation mode R as a small system weakly coupled to an ensemble of atoms A. Now the atoms play the role of a reservoir with huge heat capacity, unaffected by interaction with R. The quantity of interest is indeed the operator $I_{\alpha\beta}(\boldsymbol{k})$.

The density matrix of radiation is still supposed to have no coherences between the modes of different energy, $[\rho_R(t), H_R] = 0$, so that $\rho_R(t) = \tilde{\rho}_R(t)$. But now $\mathrm{d}\rho_R(t)/\mathrm{d}t \neq 0$. On the other hand, the atoms are now assumed to be in a stationary state, $\mathrm{d}\rho_A(t)/\mathrm{d}t = 0$, hence $\rho_A(t) = \rho_A$. The decoupling condition for the density matrices,

$$\rho(t) = \rho_A \otimes \rho_R(t)\,, \tag{2.85}$$

now holds.

The transfer equation for radiation gives a variation of the mean polarization tensor,

$$\frac{\mathrm{d}\langle I_{\alpha\beta}(\boldsymbol{k})\rangle}{\mathrm{d}s}\,, \tag{2.86}$$

(or, equivalently, the Stokes parameters) along the ray path parametrized by the geometrical

length s. Since the radiation propagates with the velocity c, we have[7]

$$\frac{\mathrm{d}}{\mathrm{d}s}\langle I_{\alpha\beta}(\boldsymbol{k})\rangle = \frac{1}{c}\frac{\mathrm{d}}{\mathrm{d}t}\langle I_{\alpha\beta}(\boldsymbol{k})\rangle = \frac{1}{c}\frac{\mathrm{d}}{\mathrm{d}t}\mathrm{Tr}_B\,[I_{\alpha\beta}(\boldsymbol{k})\rho_R(t)] = \frac{1}{c}\mathrm{Tr}_B\,\left[I_{\alpha\beta}(\boldsymbol{k})\frac{\mathrm{d}}{\mathrm{d}t}\rho_R(t)\right]\,. \tag{2.87}$$

The master equation for radiation, $\mathrm{d}\rho_R(t)/\mathrm{d}t$, can be derived in a way similar to the derivation of $\mathrm{d}\rho_A(t)/\mathrm{d}t$. The first derivation of the general polarized RTE was presented by Landi Degl'Innocenti (1983). A detailed derivation of the equations using the master equation formalism can be found in Bommier (1991). We will not go into technical details and we only write down the resulting transfer equation for polarization tensor expressed in the basis $\{\boldsymbol{e}_\pm\}$ for a pencil of radiation propagating with a wave vector $\boldsymbol{k}$,

$$\begin{aligned}\frac{\mathrm{d}}{\mathrm{d}s}\langle I_{\alpha\beta}(\boldsymbol{k})\rangle = &- \sum_\gamma \left[g_{\alpha\gamma}\langle I_{\gamma\beta}(\boldsymbol{k})\rangle + g^*_{\beta\gamma}\langle I_{\alpha\gamma}(\boldsymbol{k})\rangle\right] \\ &+ \sum_\gamma \left[h_{\alpha\gamma}\langle I_{\gamma\beta}(\boldsymbol{k})\rangle + h^*_{\beta\gamma}\langle I_{\alpha\gamma}(\boldsymbol{k})\rangle\right] + \frac{1}{2}(f_{\alpha\beta} + f^*_{\alpha\beta})\,,\end{aligned} \tag{2.88}$$

where

$$g_{\alpha\beta} = \frac{\pi\omega}{c\hbar}\mathcal{N}\sum_{mnn'}(\boldsymbol{D}\cdot\boldsymbol{e}_\alpha)_{mn}(\boldsymbol{D}\cdot\boldsymbol{e}^*_\beta)_{n'm}\rho_{nn'}\Phi(\omega_{mn}-\omega)\,, \tag{2.89}$$

$$h_{\alpha\beta} = \frac{\pi\omega}{c\hbar}\mathcal{N}\sum_{mm'n}(\boldsymbol{D}\cdot\boldsymbol{e}_\alpha)_{mn}(\boldsymbol{D}\cdot\boldsymbol{e}^*_\beta)_{mn}\rho_{m'm}\Phi(\omega_{mn}-\omega)\,, \tag{2.90}$$

$$f_{\alpha\beta} = \frac{\hbar\omega^3}{2\pi^2c^2}h_{\alpha\beta}\,. \tag{2.91}$$

As in ESE the delta-function profiles have been replaced by the the phenomenological complex profiles Φ. The quantity $\mathcal{N}$ denotes the *volume density of atoms* and it appears in the equations in order to take into account a number of atoms in the normalization box $\mathcal{V}$ of the radiation field.

The physical meaning of the individual terms in Eq. (2.88) is as follows: The first term represents an *absorption* of the photons by excitation from the coherence $\rho_{nn'}$ to the upper level $|m\rangle$. The second term represents the process of *stimulated emission* from the coherence $\rho_{m'm}$ to the lower level $|n\rangle$. The last term represents the creation of photons due to *spontaneous emission*.

The Bohr frequencies ω_{mn} in Eqs. (2.89–2.91) are modified by the Zeeman effect. Shifts of the individual profiles are especially important for development of the antisymmetric Stokes-V signal. If the external magnetic field is weak enough so that Zeeman coherences can survive (Hanle effect) and, in the same time, Zeeman splitting is strong enough for emergence of the Stokes-V signal, we speak about the *Hanle-Zeeman regime*. It is worth to say that while Zeeman effect leads to shifts of the transition profiles, Hanle effect is a dynamical mechanism related to time evolution of the levels. The joint action of these two effects provides a very general tool for analysis of the physical conditions in the solar atmosphere.

Eq. (2.88) can be easily transformed into the transfer equation for the set of Stokes parameters (Landi Degl'Innocenti 1983). In such a form one can identify several physically important phenomena that will be addressed in Section 2.6.

[7]Note that we consider only stationary models. In the general case, one would use $\mathrm{d}/\mathrm{d}t \to \partial/\partial t + c\,\mathrm{d}/\mathrm{d}s$.

2.5.6 Particular models, spherical statistical tensors

An incoherent ensemble of identical atoms in solar plasmas can be described in terms of mean density matrices (cf. Section 2.2),

$$\rho_A = \sum_{mn} \rho_{A\,mn} \left|m\right\rangle \left\langle n\right| \,, \tag{2.92}$$

where $|m\rangle$ is the vector of a particular basis associated with a model of levels introduced above (for example $|\alpha LSJM\rangle$ in the case of multiterm atom in LS coupling). We say that atom is *polarized* if there is an imbalance of population of the Zeeman sublevels and/or there are coherences among them. It follows from Eqs. (2.83) and (2.88) that atomic polarization is intimately related to the polarization of absorbed/emitted radiation.

The so-called *standard representation* of atomic density matrix in the dyadic basis of operators $|\alpha JM\rangle \langle \alpha J'M'|$ is usually replaced by the the so-called basis of *spherical statistical tensors* or the basis of *irreducible tensorial operators* (ITO) (see Appendix B for details). In this basis, the transformation rules under rotation are significantly simpler than in the standard basis, and the physical interpretation of the density matrix components is more straightforward.

Following Landi Degl'Innocenti & Landolfi (2004), it is useful to define several models depending on whether there are coherences between fine structure levels or not, whether there is a hyperfine splitting of the levels, and depending on the intensity of external magnetic field:

1. *Multilevel atom in the Zeeman effect regime.* This model can be used if $\boldsymbol{I} = 0$ and if all the coherences between different J-levels can be neglected due to secular approximation. Magnetic field is supposed to be weak, $\gamma \ll 1$, so that the first-order perturbative Zeeman splitting can be used. The effect of profiles separation can be often neglected. If there is no illumination by circularly polarized light, such a model can be relatively easily implemented for only the subset (I, Q, U) of Stokes parameters and be used for studies of many lines in the Hanle effect regime. The natural basis for construction of the multilevel density matrix is $|\alpha JM\rangle$. The density matrix elements taken into account in the multilevel model read in the standard representation

$$\rho(\alpha JM, \alpha JM') \,. \tag{2.93}$$

   The multipole moments of ρ are

$$\rho^K_Q(\alpha J) \,. \tag{2.94}$$

2. *Multiterm atom.* It is more complicated model than the multilevel one in which one takes into account possible interferences between the different J-levels of the same term. Again, $\boldsymbol{I} = 0$. Any limitation on magnetic field intensity is removed[8] and the atomic Hamiltonian has to be diagonalized in order to find new energy spectrum and the transition coefficients C^j_J. Separation of the absorption/emission profiles is generally taken into account so that this model is suitable for modeling of the joint action of Hanle and Zeeman effects in the full set of Stokes parameters. The density matrix elements read in the standard representation

$$\rho(\alpha LSJM, \alpha LSJ'M') \,, \tag{2.95}$$

   and in the representation of spherical tensors,

$$\rho^K_Q(\alpha LSJ, \alpha LSJ') \,. \tag{2.96}$$

[8]However, different atomic terms have to remain well separated.

3. *Multilevel atom with hyperfine structure.* Coherences between different J-levels are negligible but there is a nonzero nuclear spin, $\boldsymbol{I} \neq 0$, leading to the hyperfine splitting of the levels. The situation is formally analogous to the multiterm case. The role of the αLS terms is now played by levels αJ, the role of total angular momentum, $\boldsymbol{J} = \boldsymbol{L} + \boldsymbol{S}$, is now played by $\boldsymbol{F} = \boldsymbol{J} + \boldsymbol{I}$. Diagonalization of the Hamiltonian has to be performed in order to take into account the effect of mixture of different hyperfine levels. The density matrix elements taken into account in this picture read in the standard representation

$$\rho(\alpha JIFf, \alpha JIF'f') \,. \tag{2.97}$$

The multipole moments of ρ then read

$$\rho^K_Q(\alpha JIF, \alpha JIF') \,. \tag{2.98}$$

All the models listed above can be treated in a unified formalism that will be developed in the following chapter. Even more general models can be considered (such as the multiterm atom with hyperfine structure, see Casini & Manso Sainz 2005).

2.5.7 Collisions

So far, we have ignored the effect of collisions of the atom with other atmospheric particles except photons. In fact, collisions with neutral or charged perturbers are known to play a significant role in the formation of spectral lines. Moreover, in polarization studies, a new problem of collisional (de)polarization arises. The theory of collisions and collisional broadening is quite complex and here it is only possible to point out some of the most important results for the line polarization.

We suppose that all collisions are very short in time in the sense that one can apply the impact approximation. Hence collisions can be decoupled from the interactions with the radiation field. The radiative and collisional rates can be simply added together in the equations of statistical equilibrium. This approximation is usually well satisfied in the solar atmosphere (see the discussion of Bommier & Sahal-Bréchot 1991). Similarly, the profiles of transitions should be modified in order to take take into account the shortened lifetime of the levels due to collisions. However, more complicated line broadening effects (such as in the case of hydrogen) cannot be correctly described within the impact approximation. We usually do not take into account the effect of external magnetic fields on the collisional rates (Landi Degl'Innocenti & Landolfi 2004).

Collisional transitions do not obey as strong selection rules as the optical transitions do. One often needs to take into account not only collisions with thermal electrons but also the collisions with other complex species, especially with neutral hydrogen. On the other hand, there are usually strong geometrical constraints limiting the collisional processes that make the problem tractable: The velocity distribution of particles is often isotropic and can even be, to a high degree of confidence, approximated by the Maxwell-Boltzmann distribution (Jefferies 1968; Mihalas 1970). The rotational symmetry then imposes strong limitations on the collisional rates between different multipoles of the atomic density matrix. A general rule states that isotropic processes lead to decrease of atomic polarization. This indeed applies to the case of isotropic collisions, hence the term *collisional depolarization*. However, there are also examples of processes in stellar atmospheres in which anisotropic velocity distributions of colliders play a role. Such anisotropic collisions can result in creation of atomic polarization (see below).

We can basically distinguish the two kinds of collisions:

Inelastic collisions

which involve transfer of energy between the collider and the atom. Depending on whether atom is left in a state with higher or lower energy after the collision, we can distinguish between *exciting* and *deexciting* collisions respectively (or *inelastic* and *superelastic* collisions). Inelastic collisions play a significant role in the NLTE line transfer since they couple the density matrix to the local thermodynamical properties of the medium. The weaker the inelastic collisions the stronger the NLTE effects. Physically this is due to reduction of the information transfer through the medium by radiation: If the radiatively excited state is deexcited by a collision, the information transfered from the non-local sources is dissipated into the local thermal energy of the medium. On the other hand, if scattering terms are dominating, collisional destruction of the photon is unlikely and the information can spread out through the extended regions of the atmosphere giving rise to the NLTE effects. Departures from the Saha-Boltzmann equilibrium populations can be rather significant. The main contribution to the collisional (de)excitation rates in the solar atmosphere comes from collisions with the thermal electrons.

Elastic collisions

do not involve transfer of energy between the perturber and the atom and do not lead to complete destruction of the information transferred from different parts of the atmosphere. However, the state of the atom is modified by the elastic collision since it involves transfer of coherences between different Zeeman sublevels. Elastic collisions are highly responsible for collisional depolarization of the lines. In this sense, elastic collisions also couple the density matrix to the local plasma conditions which leads to a reduction of the information transferred by radiation from point to point. In some cases, elastic collisions can significantly affect populations of the levels (see Section 10.7 of Landi Degl'Innocenti & Landolfi 2004) Typically, the main contribution to the collisional depolarization rates comes from the collisions with atomic hydrogen (in the case of the lines of the second solar spectrum) and with electrons and protons (in the case of ion forbidden lines of the corona and hydrogen lines of solar prominences and flares).

Particular case of hydrogen

Neutral hydrogen atom is the main constituent of the solar atmosphere. It has somewhat exclusive status in the polarization studies, since its levels show high degree of accidental (quasi)degeneration. The fine-structure levels of the given Bohr level n (i.e., the levels nlj and $nl'j'$ in common notation) are very close to each other; not mentioning the hyperfine splitting. A typical separation of the fine-structure levels is of the order of 10^{-7} to 10^{-5} eV for small n. Radiative transition between such levels is of negligible importance but it can be shown that collisional transitions induced by electrons and especially by protons play a significant role in the depolarization process (Bommier et al. 1986). Since the thermal energy of the perturbers is orders of magnitude above the transition threshold, the most efficient transitions are the dipolar ones, $nlj \rightarrow n\,l \pm 1\,j'$. Strictly speaking, these transitions are inelastic but they have a depolarizing effect in first place. As such, they are also called the depolarizing collisions.

Isotropic collisional rates

As for the radiative interactions, there are both coherence transfer and relaxation rates for collisions that enter ESE. These rates can be derived using the master equation theory by considering an appropriate interaction potential H_{AP} in Eq. (2.63). Example of such calculations

in the semiclassical approximation can be found in Bommier et al. (1986); Sahal-Bréchot et al. (1996); Derouich et al. (2005).

Let us now assume the Maxwellian velocity distribution of multilevel atoms and colliders. Ignoring the radiative transitions, one can write for the evolution of the atomic density matrix due to collisional processes,

$$\begin{aligned}\frac{\mathrm{d}}{\mathrm{d}t}\rho^K_Q(\alpha J) &= \sum_{\alpha_\ell J_\ell}\sqrt{\frac{[J_\ell]}{[J]}}C_I^{(K)}(\alpha J \leftarrow \alpha_\ell J_\ell)\rho^K_Q(\alpha_\ell J_\ell)\\ &+ \sum_{\alpha_u J_u}\sqrt{\frac{[J_u]}{[J]}}C_S^{(K)}(\alpha J \leftarrow \alpha_u J_u)\rho^K_Q(\alpha_u J_u) \qquad (2.99)\\ &- \left(\sum_{\alpha_u J_u} C_I^{(0)}(\alpha_u J_u \leftarrow \alpha J) + \sum_{\alpha_u J_u} C_S^{(0)}(\alpha_\ell J_\ell \leftarrow \alpha J) + D^{(K)}(\alpha J)\right)\rho^K_Q(\alpha J)\,,\end{aligned}$$

where $C_I^{(K)}$ and $C_S^{(K)}$ denote, respectively, the inelastic and superelastic contributions to coherence transfer from lower $(\alpha_\ell J_\ell)$ and upper $(\alpha_u J_u)$ levels. Similarly, the rates $C_I^{(0)}(\alpha_u J_u \leftarrow \alpha J)$ and $C_S^{(0)}(\alpha_\ell J_\ell \leftarrow \alpha J)$ denote, respectively, the relaxation rates of the coherence $\rho^K_Q(\alpha J)$ to the upper and lower levels. The coefficient $D^{(K)}(\alpha J)$ denotes the collisional depolarization rate of $\rho^K_Q(\alpha J)$ due to elastic collisions. Obviously $D^{(0)}(\alpha J) = 0$.

The multipole expansion of the density operator has been used in Eq. (2.99) because the collisional part of ESE has so extremely symmetric form independent of rotation of the reference frame: Due to symmetry of the interaction, only the multipoles of the density matrix with the same KQ are coupled by collisions and the same collisional rate applies to all the Q-coherences of given rank K. The structure of collisional part of ESE is thus very simple.

There is a general relation connecting the inelastic and the inverse superelastic rates that comes from very principle of detailed balance (Derouich et al. 2007),

$$C_S^{(K)}(\alpha_\ell J_\ell \leftarrow \alpha_u J_u) = \frac{[J_\ell]}{[J_u]}\mathrm{e}^{\frac{E_{\alpha_u J_u} - E_{\alpha_\ell J_\ell}}{k_\mathrm{B} T}} C_I^{(K)}(\alpha_u J_u \leftarrow \alpha_\ell J_\ell)\,. \qquad (2.100)$$

Calculation of the inelastic rates requires an integration of the cross-sections $\sigma(\alpha_u J_u \leftarrow \alpha_\ell J_\ell, \boldsymbol{v})$ over the relative velocity distribution $f(v)$ of the colliders and atoms (i.e., the Maxwell-Boltzmann distribution in our case). The zero-rank multipole of the rate due to electron collisions can be obtained as easily as

$$C_I^{(0)}(\alpha_u J_u \leftarrow \alpha_\ell J_\ell) = N_\mathrm{e}\int \sigma(\alpha_u J_u \leftarrow \alpha_\ell J_\ell, v) v f(v)\,\mathrm{d}v\,, \qquad (2.101)$$

where N_e is the electron volume density. Calculation of the rates of higher ranks is less straightforward. In some case, however, relatively simple estimates for $C_I^{(K)}$ can be made (see Appendix 4 of Landi Degl'Innocenti & Landolfi 2004).

Anisotropic collisions and impact polarization

If the velocity distribution of particles is anisotropic, the symmetry of the interaction appearing in Eq. (2.99) is broken. Different ranks of levels can be coupled by collisions and these interactions can even lead to creation of atomic polarization. This effect is known as the so-called *impact polarization*.

The problem of impact polarization will be studied in more detail in Chapter 5 in the particular case of impact polarization of hydrogen levels in solar flares. Here, we only point

out that creation of level polarization by inelastic collision is simply due to velocity-vector dependence of transition cross-sections $\sigma(\alpha' J' M' \leftarrow \alpha J M, \boldsymbol{v})$ leading to an uneven population of the Zeeman sublevels.

In order to account for general velocity distributions, one has to introduce te more general collisional rates of the form

$$C^{K' \leftarrow K}_{Q' \leftarrow Q}(\alpha' J' \leftarrow \alpha J)\,, \tag{2.102}$$

for both coherence transfer and relaxation.

2.6 NLTE problem of the 2nd kind

In the impact approximation, radiative and collisional rates can be simply added together. The statistical equilibrium equations in the most compact form thus become

$$\frac{\mathrm{d}}{\mathrm{d}t}\rho_{ab} = \sum_{pq} \Pi_{ab \leftarrow pq}\rho_{pq}\,, \tag{2.103}$$

where

$$\Pi_{ab \leftarrow pq} = \mathrm{i}\delta_{ap}\delta_{bq}\omega_{ab}\rho_{ab} + \mathcal{R}_{ab \leftarrow pq} + \mathcal{C}_{ab \leftarrow pq}\,. \tag{2.104}$$

is the total transition rate. The symbols $\mathcal{R}_{ab \leftarrow pq}$ and $\mathcal{C}_{ab \leftarrow pq}$ denote, respectively, the total radiative and collisional rates of the $ab \leftarrow pq$ transition.

In this work, I only suppose the steady-state models. Thus the condition

$$\frac{\mathrm{d}}{\mathrm{d}t}\rho_{ab} = 0\,, \tag{2.105}$$

is satisfied and the system of differential equations (2.103) is reduced to the system of linear algebraic equations,

$$\sum_{pq} \Pi_{ab \leftarrow pq}\rho_{pq} = 0\,. \tag{2.106}$$

Since $\det \Pi = 0$, one has to close the system by replacing one of the equations by the normalization condition (2.6).

The radiative transfer equation for Stokes parameters can be deduced from Eq. (2.88) and written in the compact form

$$\frac{\mathrm{d}}{\mathrm{d}s}\boldsymbol{I}(\boldsymbol{k}) = \boldsymbol{J}(\boldsymbol{k}) - \boldsymbol{K}(\boldsymbol{k})\boldsymbol{I}(\boldsymbol{k})\,, \tag{2.107}$$

where (dropping the dependence on the wave vector)

$$\boldsymbol{J} = \begin{pmatrix} \epsilon_I \\ \epsilon_Q \\ \epsilon_U \\ \epsilon_V \end{pmatrix}\,, \tag{2.108}$$

is the formal vector of spontaneous emission, and

$$\boldsymbol{K} = \boldsymbol{K}^A - \boldsymbol{K}^S\,, \tag{2.109}$$

is the so-called 4×4 propagation matrix. It consists of the absorption part, $\boldsymbol{K}^A$, and the stimulated-emission part, $\boldsymbol{K}^S$. The general form of the propagation matrix is

$$\boldsymbol{K} = \begin{pmatrix} \eta_I & \eta_Q & \eta_U & \eta_V \\ \eta_Q & \eta_I & \rho_V & -\rho_U \\ \eta_U & -\rho_V & \eta_I & \rho_Q \\ \eta_V & \rho_U & -\rho_Q & \eta_I \end{pmatrix} , \tag{2.110}$$

where $\eta_i = \eta_i^A - \eta_i^S$, $\rho_i = \rho_i^A - \rho_i^S$. Explicit expressions for ϵ_i, η_i^A and η_i^S can be deduced from Eqs. (2.89–2.91) and can be found in Landi Degl'Innocenti (1983). Their form in the particular models of atomic levels and magnetic field strength will be discussed in the following chapter.

One can identify several interesting features in the propagation matrix: (1) The coefficient η_I is equivalent to the absorption coefficient of the standard theory of 1st kind, i.e., the NLTE problem with polarization neglected. The diagonal part of $\boldsymbol{K}$ is thus referred to as the *absorption matrix*. (2) The part of $\boldsymbol{K}$ involving only first row and first column (excluding η_I coefficient) is the so-called *dichroism matrix*. It is responsible for selective absorption of different polarization states. (3) The antisymmetric submatrix of ρ's is the so-called *dispersion matrix* and is responsible for dephasing of the different polarization states.

Eqs. (2.106) and (2.107) form a system of coupled equations defining, along with the boundary conditions, the so-called *NLTE problem of the 2nd kind* (Landi Degl'Innocenti 1987), i.e., the NLTE problem including the line polarization phenomena. One has to find the atomic density matrix throughout the atmosphere which is consistent with the solution of RTE and given boundary conditions. The system is basically *nonlinear* and *nonlocal* (Trujillo Bueno 1999, 2003). The density matrix in every point is determined by the local radiation field which itself is determined by the density matrix in every point of the medium through the radiative transfer equation. One has to take into account proper collisional rates and the magnetic field vector which is spatially dependent. It follows that one needs, in general, to diagonalize the Hamiltonian in every point of the atmosphere and to take into account different orientation of the magnetic field vector which complicates the choice of the local reference frame (the effect of turbulent fields is not discussed in this work). Solution of such a system is nontrivial task that requires advanced numerical techniques such as those developed by Trujillo Bueno & Manso Sainz (1999); Manso Sainz & Trujillo Bueno (2003a). For a simple analytical analysis see the next section. In realistic applications, one usually has to extend the problem by taking into account the bound-free radiative and collisional transitions and the effect of continuum opacity. These processes can be easily incorporated into the present theory but they are left apart here to keep the formalism simple. The problem here was even more reduced by ignoring all the magnetohydrodynamical contexts which define the atmospheric model.

Doppler broadening

The radiative transfer coefficients and the coefficients of the radiative rates have been derived in the rest frame of the atom. As indicated in Subsection 2.5.4, in real atmospheres there is always a thermal motion of the atoms leading to redistribution of the radiation in the line Doppler core. In general, one needs to take into account a dependency of the density matrix on the atomic velocity (cf. Sahal-Bréchot et al. 1998, and references therein). However, it is often possible to suppose that the external and internal degrees of freedom of the atom are decoupled in the way that one only needs to consider one density matrix for internal degrees of freedom of the whole ensemble. Since we do not consider any macroscopic motions of the medium and velocity distribution of the atoms is supposed to be Maxwellian, we have to replace the

complex profiles Φ in Eqs. (2.107) by the convolution with the local Gaussian profile. Resulting absorption/emission profile is thus the Voigt and Faraday-Voigt profile for real and imaginary part of Φ, respectively (Mihalas 1970; Landi Degl'Innocenti 1983).

2.7 A generalized $\sqrt{\epsilon}$-law

This short section is an extract of the paper by Štěpán & Bommier (2007), from now on referred to as Paper I. The entire paper can be found in Appendix C. Here, I only point out the key ideas that can demonstrate a partial analytical solution of a simple NLTE problem.

The NLTE problem can be solved analytically to some extent. The well-known $\sqrt{\epsilon}$-law for a two-level atom is one of the rare examples of such solution (Avrett & Hummer 1965; Mihalas 1970). It connects a surface value of the line source function, $S = \epsilon/\eta$, to the common photon destruction probability ϵ (Mihalas 1970). The law was generalized for the case of polarized radiation by Ivanov (1990) who found a relation in a closed form between the destruction probability and the surface value of the source function tensor. The model considered was the non-magnetic, plan-parallel, semi-infinite, and homogenous atmosphere. The lower atomic level with angular momentum j was supposed to be unpolarized and stimulated emission from the upper level j' was neglected. These approximations simplify the NLTE problem significantly. In particular, the problem becomes *linear*. A further generalization of the $\sqrt{\epsilon}$-law accounting for a homogenous magnetic field was found by Landi Degl'Innocenti & Bommier (1994).

In our work, we have used the idea of unphysical terms (cf. Frisch 1999), ϵ^K_Q, introduced into ESE in order to derive the simple analytical formulas for the surface value of the source function tensor,

$$S^K_Q = \frac{2h\nu_0^3}{c^2}\frac{2j+1}{\sqrt{2j'+1}}\rho^K_Q\,. \tag{2.111}$$

The *unphysical collisional terms* we add into ESE are analogous to the *nonthermal collisional rates* in realistic situations. Note however that generalization to a realistic case would involve collisional coupling of different multipoles of the upper level; such a problem would no longer be linear. However, such a generalization can be, in addition to the academic interest, useful for testing of the accuracy of the radiative transfer codes intended for solution of the NLTE problems with the presence of non-thermal collisional processes (for instance in the impact polarization studies of solar flares). The interest of our approach in contrast to the approach of (Frisch 1999) is not only to provide the handy closed-form formulas but also to connect the unphysical collisional terms to the realistic problems of impact polarization. An example of application can be the nonthermal excitation of $1s$–$2p$ transition of hydrogen by anisotropic electrons. In this case, elastic collisions are negligible and the collisional coupling of the level $2p$ with the metastable level $2s$ can be formally treated as the depolarization term (for a motivation see Vogt et al. 1997).

The numerical interest arises from fact that in the realistic atmosphere models, it is usually $|S^0_0| \gg |S^K_Q|$, while the unphysical terms can be used to amplify the higher-rank components of the source tensor.

One can introduce the dimensionless parameter of depolarization rate,

$$\delta^{(K)} = \frac{D^{(K)}}{A_{j'j}}\,, \tag{2.112}$$

and the irreducible tensor which plays the role of generalized photon destruction probability,

$$\epsilon^K_Q = \frac{(C^{\mathrm{R}}_{j'j})^K_Q}{A_{j'j'}}\,, \tag{2.113}$$

where $(C^{\rm R}_{j'j})^K_Q$ is the de-excitation rate of the upper multipole $\rho^K_Q(j')$. In the case of thermal collisional rates ($\epsilon^K_Q = \delta_{K0}\delta_{Q0}$), negligible depolarization ($\delta^{(K)} = 0$), and zero magnetic field, one recovers the $\sqrt{\epsilon}$-law in the form

$$\sqrt{[S^0_0(0)]^2 + [S^2_0(0)]^2} = \sqrt{\frac{\epsilon}{1+\epsilon}} B_{\rm P} = \sqrt{\epsilon'} B_{\rm P}, \tag{2.114}$$

which is the result derived in different notation by Ivanov (1990). Here $B_{\rm P}$ is the Planck function. If collisional depolarization is strong enough to destroy upper level polarization, one obtains

$$S^0_0(0) = \sqrt{\frac{\epsilon}{1+\epsilon}} B_{\rm P} = \sqrt{\epsilon'} B_{\rm P}\,, \tag{2.115}$$

which is the common $\sqrt{\epsilon}$-law of the unpolarized theory. A general result is expressed by Eq. (23) of Paper I.

In the following, I will neglect the effect of magnetic field; it is not necessary, but the expressions would become too complicated. In particular, let us assume an example corresponding to the relative velocity distribution of particles axially symmetric with the axis of symmetry parallel to the vertical of the atmosphere. The process can thus be described by only the first two even multipole moments. Setting $\epsilon^0_0 = \epsilon^2_0 = \epsilon$ leads to

$$\sqrt{[S^0_0(0)]^2 + [S^2_0(0)]^2} = \frac{\epsilon'}{\sqrt{1 - \frac{7}{10} W_2 (1-\epsilon')}} B_{\rm P}\,, \tag{2.116}$$

where $W_2 = [w^{(2)}_{j'j}]^2$ is the coefficient defined by Landi Degl'Innocenti (1984).

Chapter 3

Iterative methods for the NLTE problems of the second kind

3.1 Introduction

This chapter deals with the iterative methods for a solution of the NLTE problems of the 2nd kind. The polarized NLTE models – being a generalization of the 1st kind problems – share many characteristics with the standard unpolarized case: The problems rely on ESE and RTE. The structure of equations is formally similar in both cases even though the polarized equations are generally much more complicated. A computation complexity is certainly higher in the polarized case but the convergence rate is driven by the same physical principles behind the propagation of photons in optically thick media. In contrast to the unpolarized case, the polarized NLTE equations usually contain complex quantities. Instead of just level populations, a state of the polarized multilevel atoms has to be described in terms of quantum mechanical density matrix. From a numerical point of view, lot of attention has to be paid to a particular model of the atomic levels. Different equations are employed for different pictures of levels and different strength of the external magnetic field. (Hyper)fine-structure interferences can play a significant role along with the Zeeman coherences. The new degree of freedom of radiation – polarization – gives rise to the vector RTE (2.107) for the set of four Stokes parameters. Coupling of different Stokes parameters due to dichroism and dispersion requires a special treatment in formal solvers.

This chapter extends the previous multilevel methods developed by Trujillo Bueno (1999) and Manso Sainz & Trujillo Bueno (2003a) by inclusion of level-crossing coherences within a quite general picture of atomic levels.

The aim of this chapter is to develop a simple notation for the 2nd kind problems suitable for a derivation of the iterative scheme and useful for a numerical implementation in the same time. In a later part of the chapter, I introduce a modification of the so-called operator-splitting technique that can be used for the development of a general Jacobi iteration scheme suitable for solution of the transfer problems involving atoms in the Paschen-Back effect regime. The methods described in this chapter have been partially presented at the Solar Polarization Workshop 5 (Štěpán 2008). The paper can also be found in Appendix D.

Outline of this chapter is as follows: Section 3.2 introduces some of the general aspects of numerical iterative solution of the NLTE problems. The basics of the preconditioning strategy of numerical linear algebra is recalled and it is connected to the radiative transfer problem in the optically thick medium. Discretization of the continuous models and the question of choice of a suitable reference frame is presented. In Section 3.2, I introduce the notation suitable for a numerical solution of the NLTE problem of the 2nd kind disregarding a particular atomic

picture. I expand the radiative rates of ESE in terms of the average profile tensors of radiation. The radiative transfer coefficients of RTE are also decoupled with respect to atomic multipoles. The definition of the "decoupling matrices" in Subsection 3.3.3 opens a convenient way for efficient implementation of the formal solvers. The last Section 3.4 begins with a review of the formal solver DELOPAR (Trujillo Bueno 2003) which is used for calculating the formal solution of RTE. The section continues by an introduction of the new lambda-operator splitting technique based on the simple analogy with the unpolarized radiative transfer solutions. In the end of the section, a generalization of the iterative scheme is presented. This scheme can be understood as a generalization of the present iterative schemes based on the Jacobi iteration method.

3.2 Iterative approach to the NLTE problem

3.2.1 Discretization of the model

This work deals with the one-dimensional plan-parallel geometry of the medium. Variation of the properties of the medium can thus be parametrized by a single spatial coordinate z. In the radiation transfer theory, it is natural to define the so-called *optical path* in addition to the usual geometrical path s. The optical path can be introduced by the differential relation

$$\mathrm{d}\tau(\boldsymbol{k}) = \eta_I(\boldsymbol{k})\,\mathrm{d}s\,. \tag{3.1}$$

Optical path is a dimensionless quantity whose physical interpretation is the number of photon mean free paths in a given direction and frequency. Moreover, one usually defines the *optical depth scale* of the one-dimensional atmosphere by the relation $\mathrm{d}\tau(z,\omega) = -\eta_I(z,\omega)\,\mathrm{d}z$, where the absorption coefficient is measured in the direction of z axis (cf. §2-2 of Mihalas 1970).

The NLTE problem as it was formulated in the preceding chapter can be expressed in rather general form

$$\mathcal{L}[\rho(z)] = 0\,, \tag{3.2}$$

where $\mathcal{L}$ is a functional acting on the density matrix. The problem is well defined if the boundary illumination conditions of the atmospheric slab are defined. Explicit expressions for the nonlinear operator $\mathcal{L}$ can be found by expressing all the radiative rates in terms of integrals over the density matrix multipoles of the medium.[1] The resulting expressions would be quite complicated and useless for practical purposes: It is not possible to find a full analytical solution of the NLTE problem in a closed form even for the simplest models. Numerical solutions have thus to be implemented.

The problem needs to be discretized on a grid G with $\mathbb{N}$ nodes. The atomic density matrices in the individual grid nodes can be organized in the formal column vector with total number of $\mathsf{N} \times \mathbb{N}$ complex elements. In the self-evident notation we can write

$$\boldsymbol{\rho} = (\rho_1(1), \rho_2(1), \cdots, \rho_{\mathsf{N}}(1), \rho_1(2), \rho_2(2), \cdots, \rho_{\mathsf{N}}(2), \cdots, \rho_1(\mathbb{N}), \rho_2(\mathbb{N}), \cdots, \rho_{\mathsf{N}}(\mathbb{N}))^T. \tag{3.3}$$

The operator $\mathcal{L}$ can now be replaced by the block-diagonal matrix with $\boldsymbol{\Pi}$-matrices on the diagonal. As noticed in the preceding chapter, the normalization condition, Eq. (2.6), has to be used to close the system. This is reflected by a nontrivial right-hand side $\boldsymbol{f}$ of the discretized problem,

$$\boldsymbol{\mathcal{L}\rho} = \boldsymbol{f}\,. \tag{3.4}$$

[1] Note that in the problems of the 1st kind the density matrix can be replaced by only populations of the levels.

It is obvious that the problem is only quasi-linear and quasi-local: The non-linearity and non-locality due to resonance scattering is hidden in the radiative rates. Next discretization concerns the wave vector $\boldsymbol{k}$.

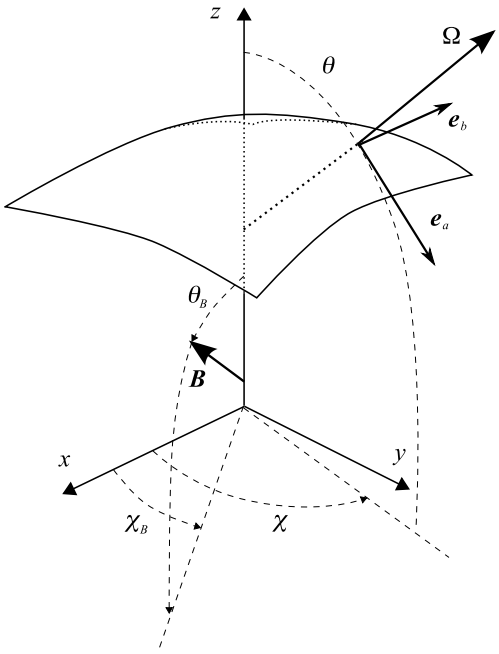

Figure 3.1: A laboratory reference frame of the NLTE problem. For each ray direction $\boldsymbol{\Omega}$, described by the polar angle θ and the azimuthal angle χ, the reference direction vector $\boldsymbol{e}_a$ and the associated vector $\boldsymbol{e}_b$ are defined according to the figure: $\{\boldsymbol{e}_a, \boldsymbol{e}_b, \boldsymbol{\Omega}\}$ make up a right-handed coordinate system with $\boldsymbol{e}_a$ lying in the meridian plane. Note that $\{-\boldsymbol{e}_a, -\boldsymbol{e}_b, \boldsymbol{\Omega}\}$ basis leads to the equivalent equations. The direction of the magnetic field $\boldsymbol{B}$ is described by the polar and azimuthal angles, θ_B and χ_B respectively.

The integrations of the radiation field over the ray directions, $\oint \mathrm{d}\boldsymbol{\Omega}/4\pi$, become quadratures in the discretized model. In the particular implementation described in Appendix A, I use the Gaussian quadrature in the polar angle $0 \leq \theta \leq \pi$ (i.e., $-1 \leq \mu \leq 1$ for $\mu = \cos\theta$) and the trapezoidal rule for the azimuthal angle $0 \leq \chi < 2\pi$.

After all, discretization in the radiation frequencies is implemented. In this work, I use the trapezoidal rule for the integration over the spectral line frequencies.

Solution of the discrete problem is always affected by the so-called *truncation error*. Generally, the finer is the model discretization, the smaller is the truncation error. This problem will be discussed in more detail in Chapter 4.

3.2.2 Preconditioning technique

There are basically two possible approaches to the solution of the NLTE problem: *direct* and *iterative*. Since the direct methods involve inversions of large matrices and are only applicable to the *linear* models, they are not very suitable for solution of the complex multilevel problems. As in the modern numerical linear algebra, the method of choice is the iterative solution.

As indicated by Eq. (3.4), the iterative solutions of the multilevel NLTE problem of both 1st and 2nd kind involves application of the methods of numerical linear algebra to the linearized transfer problem. In this subsection I briefly review the basics of the preconditioning technique which are essential for development of efficient NLTE solvers.

Preconditioning of the linear system

Let us consider the system of linear algebraic equations,

$$\boldsymbol{A}\boldsymbol{x} = \boldsymbol{b}\,, \tag{3.5}$$

where $\boldsymbol{A}$ is a square matrix, $\boldsymbol{b}$ is a known vector and $\boldsymbol{x}$ is an unknown vector. The number of operations needed for a direct solution of Eq. (3.5) by inversion of the matrix $\boldsymbol{A}$ is proportional to N^3, where N denotes the dimension of $\boldsymbol{A}$. It is thus difficult to find the solution for high N. To overcome this difficulty one can use an iterative preconditioning method. The initial guess of the solution $\boldsymbol{x}$ will be denoted by $\boldsymbol{x}^{(0)}$. In the k-th iteration step we have an approximate solution of the system denoted by $\boldsymbol{x}^{(k)}$. By iterative solution of the system (3.5) one means the process

$$\boldsymbol{x}^{(0)} \to \boldsymbol{x}^{(1)} \to \cdots \to \boldsymbol{x}^{(k)} \to \boldsymbol{x}^{(k+1)} \to \cdots \tag{3.6}$$

of successive approximations of the exact solution generated by the linear mapping

$$\boldsymbol{x}^{(k+1)} = \boldsymbol{M}\boldsymbol{x}^{(k)} + \boldsymbol{N}\boldsymbol{b}\,, \tag{3.7}$$

where $\boldsymbol{M}$ is the so-called *iteration matrix* which is constant during the iteration and $\boldsymbol{N}$ is a constant matrix. The process is said to be convergent if $\lim_{k\to\infty} \|\boldsymbol{x} - \boldsymbol{x}^{(k)}\| = 0$, where $\|\cdot\|$ is an arbitrary norm.

One defines the so-called *residual vector* or *residuum* of the k-th iteration (Press et al. 1994; Trujillo Bueno & Fabiani Bendicho 1995) by

$$\boldsymbol{r}^{(k)} = \boldsymbol{b} - \boldsymbol{A}\boldsymbol{x}^{(k)}\,. \tag{3.8}$$

Note that some authors define the residuum with an opposite sign (cf. Hackbush 1985). The *error vector* is defined as a difference of the exact solution and its current estimation,

$$\boldsymbol{e}^{(k)} = \boldsymbol{x} - \boldsymbol{x}^{(k)}\,. \tag{3.9}$$

Using the previous definitions it becomes clear that

$$\boldsymbol{r}^{(k)} = \boldsymbol{A}(\boldsymbol{x} - \boldsymbol{x}^{(k)}) = \boldsymbol{A}\boldsymbol{e}^{(k)}\,, \tag{3.10}$$

while for the error vector we get

$$\boldsymbol{e}^{(k)} = \boldsymbol{A}^{-1}\boldsymbol{r}^{(k)}\,. \tag{3.11}$$

From Eq. (3.9) it follows that

$$\boldsymbol{x} = \boldsymbol{x}^{(k)} + \boldsymbol{A}^{-1}\boldsymbol{r}^{(k)}\,. \tag{3.12}$$

The second term on the right-hand side is as difficult to evaluate as the original problem (3.5). On the other hand, Eq. (3.12) is a good point from which to start an iteration process: We can replace the matrix $\boldsymbol{A}$ in Eq. (3.12) by an *approximate matrix* $\boldsymbol{A}^*$ in order to get the *approximate error* $\boldsymbol{e}^{*(k)}$. The iterative scheme then becomes

$$\boldsymbol{x}^{(k+1)} = \boldsymbol{x}^{(k)} + \boldsymbol{A}^{*-1}\boldsymbol{r}^{(k)} = \boldsymbol{x}^{(k)} + \boldsymbol{e}^{*(k)}\,. \tag{3.13}$$

The form of the approximate matrix is not unique. From a practical point of view, $\boldsymbol{A}^*$ has to be efficiently invertible, i.e., it should be possible to find the inverse within $O(N)$ operations. The second condition concerns convergence properties of the iteration process. From Eq. (3.13) we obtain for the new estimation of the solution:

$$\boldsymbol{x}^{(k+1)} = \boldsymbol{x}^{(k)} + \boldsymbol{A}^{*-1}(\boldsymbol{b} - \boldsymbol{A}\boldsymbol{x}^{(k)}) = \boldsymbol{G}\boldsymbol{x}^{(k)} + \boldsymbol{A}^{*-1}\boldsymbol{b}\,, \tag{3.14}$$

where

$$\boldsymbol{G} = \boldsymbol{1} - \boldsymbol{A}^{*-1}\boldsymbol{A} \tag{3.15}$$

is the so-called *amplification matrix*.

From the definition (3.9) one gets

$$\boldsymbol{e}^{(k+1)} = \boldsymbol{x} - \boldsymbol{x}^{(k+1)} = \boldsymbol{x} - \boldsymbol{G}\boldsymbol{x}^{(k)} - \boldsymbol{A}^{*-1}\boldsymbol{b}\,. \tag{3.16}$$

Multiplying Eq. (3.9) from left by $\boldsymbol{G}$ and subtracting the result from Eq. (3.16) leads to the important result

$$\boldsymbol{e}^{(k+1)} = \boldsymbol{G}\boldsymbol{e}^{(k)}\,. \tag{3.17}$$

In other words, the error in the $(k+1)$-th iteration is obtained from the one of the k-th iteration by applying the amplification matrix. Let us suppose that the matrix $\boldsymbol{G}$ has a set of N orthonormal eigenvectors $\{\boldsymbol{u}_i\}$ with a set of associated eigenvalues $\{\lambda_i\}$,

$$\boldsymbol{G}\boldsymbol{u}_i = \lambda_i \boldsymbol{u}_i\,. \tag{3.18}$$

We can express the error vectors in the basis of these eigenvectors,

$$\boldsymbol{e}^{(k)} = \sum_{i=1}^{N} \epsilon_i^{(k)} \boldsymbol{u}_i, \qquad \boldsymbol{e}^{(k+1)} = \sum_{i=1}^{N} \epsilon_i^{(k+1)} \boldsymbol{u}_i, \tag{3.19}$$

where $\epsilon_i^{(k)}$ is the i-th coordinate of the error vector in the k-th iteration step. From Eq. (3.17) we arrive at

$$\sum_{i=1}^{N} \epsilon_i^{(k+1)} \boldsymbol{u}_i = \boldsymbol{G} \sum_{i=1}^{N} \epsilon_i^{(k)} \boldsymbol{u}_i = \sum_{i=1}^{N} \epsilon_i^{(k)} \lambda_i \boldsymbol{u}_i\,. \tag{3.20}$$

The dot product of this equation with $\boldsymbol{u}_j$ leads to

$$\epsilon_j^{k+1} = \lambda_j \epsilon_j^k. \tag{3.21}$$

It is thus clear that the convergence of the iterative process is achieved if all the eigenvalues of the amplification matrix are (in absolute value) smaller than 1. Independently of a particular definition of the norm, the iterative process is asymptotically governed by the largest eigenvalue,

$$\|\boldsymbol{e}^{(k)}\| \underset{\text{assympt.}}{\propto} \max|\lambda_j|^k\,. \tag{3.22}$$

The number of iterations required to decrease the error by a given factor is proportional to

$$-1/\log\varrho\,, \tag{3.23}$$

where one usually defines the so-called *spectral radius* $\varrho \equiv \max|\lambda_j|$ of the amplification matrix. From the definition of $\boldsymbol{G}$ it becomes clear that ϱ is small if $\boldsymbol{A}^*$ is "close" to $\boldsymbol{A}$ in some sense.

A motivating example: Two-level unpolarized problem, Λ-iteration

Application of the iterative methods in the NLTE line transfer can be clearly demonstrated on the example of the two-level unpolarized transfer in the spectral line with complete redistribution in a homogenous isothermal atmosphere (Olson et al. 1986).

The formal solution (FS) of the NLTE problem can be expressed in the form of the so-called Λ-*operator* (see §2-2 of Mihalas 1970). The angle- and profile-averaged radiation intensity in

every point of the grid is given by a formal vector $\boldsymbol{J}$ (do not mismatch with the Stokes emission vector). It can be expressed as a function of the source function vector, $\boldsymbol{S}$ (Mihalas 1970),[2]

$$\boldsymbol{J} = \boldsymbol{\Lambda}[\boldsymbol{S}]\,, \tag{3.24}$$

where $\boldsymbol{\Lambda}$ is the Λ-operator matrix. Since the selected problem is *linear* with respect to atomic populations (or source function), the intensity is related to the source function by the simple relation

$$\boldsymbol{S} = (1-\epsilon)\boldsymbol{J} + \epsilon\boldsymbol{B}_{\rm P}\,, \tag{3.25}$$

where ϵ denotes the collisional destruction probability (cf. Section 2.7) and $\boldsymbol{B}_{\rm P}$ is the vector of the Planck function. Combination of Eq. (3.24) and Eq. (3.25) leads to the equation

$$[\mathbf{1} - (1-\epsilon)\boldsymbol{\Lambda}]\boldsymbol{S} = \epsilon\boldsymbol{B}_{\rm P} \tag{3.26}$$

for the unknown vector $\boldsymbol{S}$. Using the analogy with Eq. (3.5), one can identify $\boldsymbol{A} = [\mathbf{1} - (1-\epsilon)\boldsymbol{\Lambda}]$ and $\boldsymbol{b} = \epsilon\boldsymbol{B}_{\rm P}$ and use the approximate matrix $\boldsymbol{\Lambda}^*$ to define $\boldsymbol{A}^* = [\mathbf{1} - (1-\epsilon)\boldsymbol{\Lambda}^*]$. The iterative scheme then reads

$$\begin{aligned}\boldsymbol{S}^{(k+1)} &= \boldsymbol{S}^{(k)} + [\mathbf{1} - (1-\epsilon)\boldsymbol{\Lambda}^*]^{-1}\left\{-[\mathbf{1} - (1-\epsilon)\boldsymbol{\Lambda}]\boldsymbol{S}^{(k)} + \epsilon\boldsymbol{B}_{\rm P}\right\} \\ &= \boldsymbol{S}^{(k)} + [\mathbf{1} - (1-\epsilon)\boldsymbol{\Lambda}^*]^{-1}[(1-\epsilon)\boldsymbol{J}^{(k)} + \epsilon\boldsymbol{B}_{\rm P} - \boldsymbol{S}^{(k)}]\,. \end{aligned} \tag{3.27}$$

It is worth to say that the $\boldsymbol{\Lambda}$-matrix does not have to be constructed physically in the computer memory. The intensities $\boldsymbol{J}^{(k)}$ are obtained via FS of RTE from known $\boldsymbol{S}^{(k)}$. On the other hand the elements of the approximate operator $[\mathbf{1} - (1-\epsilon)\boldsymbol{\Lambda}^*]$ have to be found. However, it is usually a straightforward task since $\boldsymbol{\Lambda}^*$ can be chosen to have a rather simple form.

The well known Λ-iteration method (or Piccard iteration, see §5-3 of Mihalas 1970) is recovered from Eq. (3.27) by setting $\boldsymbol{\Lambda}^* = 0$, i.e., $\boldsymbol{A}^* = \mathbf{1}$. The amplification matrix then reads $\boldsymbol{G} = 1 - \boldsymbol{A}$ and its spectral radius is $\varrho \approx (1-\epsilon)(1-T^{-1})$, where T is the total profile-integrated optical thickness of the slab (Olson et al. 1986). It is clear that $\varrho \approx 1$ if T is large and $\epsilon \ll 1$. That is the reason why Λ-iteration is useless in practical applications to optically thick atmospheres where one typically has $\epsilon \approx 10^{-4}$ or lower. Physically, this is due to a slow propagation of information at large optical depths.

3.2.3 Accelerated lambda iteration

Cannon (1973) has introduced the idea of approximate lambda operators into the field of radiative transfer. Different choices of Λ^* were proposed by different authors (e.g. Scharmer 1984). It was pointed out by Olson et al. (1986) that a suitable choice of the approximate Λ^*-operator is the *diagonal part* of Λ. This choice corresponds to a separation of *local* sources of the radiation in a given grid node from the radiation transmitted from other parts of the atmosphere. This technique is numerically analogous to the *Jacobi iteration* algorithm of linear algebra and is now known as the so-called *accelerated lambda iteration* (ALI) technique. In the following, this approach will be applied to the solution of a multilevel polarized radiative transfer problem.

It is worth to say that different choices of Λ^* can be made. The local operator can be replaced by a finite-band operator leading to even better convergence properties with the cost of inversion of matrices connecting the successive grid nodes. Trujillo Bueno & Fabiani Bendicho (1995) introduced a set of quite efficient numerical techniques based on the Gauss-Seidel iteration (GS)

[2] I assume zero illumination at boundaries to keep the notation simple.

and the successive overrelaxation (SOR). To achieve the same accuracy as the Jacobi method, these techniques can be factor of 4 faster (in the GS case) or even need only $O(\mathbb{N}\log\mathbb{N})$ iterations in the case of optimal SOR (see also Trujillo Bueno & Fabiani Bendicho 1995; Paletou & Léger 2007). The Jacobi iteration is naturally a $O(\mathbb{N}^2)$ algorithm and its usefulness decreases with increasing number $\mathbb{N}$ of grid nodes. However, it is a useful method for numerical radiative transfer especially in connection with the multigrid methods (cf. Chapter 4).

Although the first NLTE models of polarized radiative transfer were developed some decades ago (for example Rees & Saliba 1982, and references therein), the progress in this field was substantially slower in comparison to the models of the 1st kind. In the following paragraphs I quickly go through the history of development of the NLTE techniques. However, the list of the significant contributions is far from being complete.

Polarized linear problems

The simplest NLTE model of the 2nd kind is the two-level atom with unpolarized lower level. The privilege status of this problem lies in the fact that it is *linear* and thus not as difficult as the general case. The matrix $\boldsymbol{\mathcal{L}}$ can be found as independent on $\boldsymbol{\rho}$ and, from a numerical point of view, one recovers the linear problem formulated in the preceding subsection.

The direct methods of solution involving inversions of the large matrices can be used for solution of both unpolarized and polarized linear problems (Mihalas et al. 1978; Faurobert-Scholl 1991; Bommier & Landi Degl'Innocenti 1991, 1996). However, the time required for construction of the Λ-matrix and especially the time demands on inversion of the matrices makes the direct methods limited in practical use.

Thus the iterative methods for the linear problems of resonance polarization and Hanle effect have been extensively developed in the previous decade (Faurobert-Scholl et al. 1997; Nagendra et al. 1998; Trujillo Bueno & Manso Sainz 1999). For a generalization to the multidimensional geometries and for a review of the iterative methods see Manso Sainz & Trujillo Bueno (1999).

Unpolarized multilevel problems

The use of multilevel ALI models for unpolarized radiation transfer has been initiated by the works of Werner (1986); Scharmer & Carlsson (1985) and further stimulated by Rybicki & Hummer (1991, 1992, 1994) whose multilevel ALI (or MALI) technique attracted lot of attention and has been used in both one- and multi-dimensional geometries (Heinzel 1995; Auer & Paletou 1994; Paletou 1995; Auer et al. 1994). This method uses the Λ-operator splitting technique for derivation of the preconditioned ESE. The fact that the radiative rates depend on the atomic populations through the RTE leads to a natural nonlinearity of the multilevel problem. The equations need a straightforward linearization with respect to atomic populations. In contrast to the linear problems, matrix $\boldsymbol{\mathcal{L}}$ is no longer constant during the iterations. The successive approximations of the *preconditioned* matrices $\boldsymbol{\mathcal{L}}'^{(k)}$ are found in each iteration step following the scheme[3]

$$\boldsymbol{\rho}^{(0)} \rightarrow \boldsymbol{\mathcal{L}}'^{(0)} \rightarrow \boldsymbol{\rho}^{(1)} \rightarrow \boldsymbol{\mathcal{L}}'^{(1)} \rightarrow \cdots \boldsymbol{\rho}^{(k)} \rightarrow \boldsymbol{\mathcal{L}}'^{(k)} \rightarrow \cdots . \tag{3.28}$$

The new populations (density matrices) are found in each iteration from the equation

$$\boldsymbol{\mathcal{L}}'^{(k)}\boldsymbol{\rho}^{(k+1)} = \boldsymbol{f} . \tag{3.29}$$

[3]Although the use of density matrix formalism is not necessary for the unpolarized problem, I prefer to keep the formalism consistent.

The MALI technique is not the only method available for solution of the multilevel transfer. The *complete linearization method* of Auer & Mihalas (1969) is another possibility. For a detailed comparison of the MALI and linearization methods see Socas-Navarro & Trujillo Bueno (1997). Implementation of even more rapidly convergent GS and multigrid techniques was done by Fabiani Bendicho et al. (1997) who extended the previous works on the two-level GS technique (Trujillo Bueno & Fabiani Bendicho 1995) and the linear multigrid method (Steiner 1991) to the full multilevel NLTE problem.

Polarized nonlinear problems

The most general problem involves both nonlinearity and light polarization. Approximate solutions based on the so-called *field-free approximation* (Rees 1969) and the *polarization-free approximation* (Trujillo Bueno & Landi Degl'Innocenti 1996) have been developed to make the problem trackable. For other approximate solutions see, for instance, Faurobert-Scholl (1996), Sánchez Almeida & Trujillo Bueno (1999). However, a general self-consistent solution was missing for a long time.

A generalization of the linear two-level problem to the *non-linear* two-level problem with a polarized lower level was proposed by Trujillo Bueno (1999). Later on, a full multilevel solution based on the ideas of the work just cited has been presented by Manso Sainz & Trujillo Bueno (2003a). The authors presented a self-consistent solution of the transfer in the Ca II infrared triplet in a weakly magnetized solar chromosphere. They generalized the standard Λ-operator to the case of 36 operators $\mathbf{\Lambda}'_{ij}$, $i,j = 0,\ldots,5$, acting on the multipoles ρ^0_0, ρ^2_0, ρ^2_{-1}, ρ^2_1 ρ^2_{-2}, and ρ^2_2 of the aligned upper level of a given line. Application of these operators leads to the averaged line radiation tensors, J^0_0, J^2_0, J^2_{-1}, J^2_1, J^2_{-2}, and J^2_2. The authors successfully implemented the iteration scheme based on the $\mathbf{\Lambda}'_{00}$-operator splitting and the DELOPAR formal solver of Trujillo Bueno (2003). They used the method for a study of the Hanle effect and zero-field dichroism in the transfer of Ca II infrared triplet (Manso Sainz & Trujillo Bueno 2003b).

3.2.4 Choice of the reference frame

In contrast to the problems of the 1st kind, geometry plays a much more important role in the polarization scattering case. Both ESE and RTE have different coefficients in different coordinate systems. The attention must be paid to the choice of the reference frame in which the equations are formulated.

The reference frame fixed in the atmosphere (the xyz system in Figure 3.1) shall be called the *observer's frame* whereas the coordinate system in which ESE are expressed will be called the *atomic frame*. In general, there are two possibilities for choice of the atomic frame: (1) the observer's frame is identical to the atomic frame, or (2) it is not. Each choice has its advantages and disadvantages. In the first case, one has to formulate the equations in the frame independently of orientation of the local magnetic field vector. The expressions are then more complicated than in the case 2 in which one can choose quantization axis to be parallel to $\boldsymbol{B}$. The disadvantage of the case 2 is that one needs to transform the quantities from one frame to another. The case 2 is implemented in Monopost (see Appendix A). In particular, calculation of the radiation transfer is done in the observer's frame whereas ESE are solved in the atomic frame (see Appendix A for details). In general, the case 1 is a better choice. For instance, one can easily incorporate the effect of other symmetry-breaking phenomena such as the effect of external electric fields.

3.3 Unified notation for the NLTE equations

3.3.1 Structure of the atomic manifolds

One may consider the atomic levels to be organized in the well separated manifolds $\mathcal{M}_\alpha$, $\mathcal{M}_\beta$, etc. (see Fig. 3.2). Each manifold $\mathcal{M}_\alpha$ consists of a group of the discrete levels $|\alpha m\rangle$. I use the Latin indices to denote the quantum numbers distinguishing the individual states of the manifold. Quantum numbers distinguishing different manifolds are identified by the Greek indices. We can always choose the $|\alpha m\rangle$ states to be eigenvectors of the atomic Hamiltonian,

$$H_A\,|\alpha m\rangle = E_{\alpha m}\,|\alpha m\rangle\ , \tag{3.30}$$

where $E_{\alpha m}$ is the energy of the given level. The levels of the manifold are supposed to be close to each other in comparison to the separation of the different manifolds,

$$|E_{\alpha m} - E_{\beta n}| \gg |E_{\alpha p} - E_{\alpha q}| \quad \text{if} \quad \alpha \neq \beta\,. \tag{3.31}$$

On the other hand, a separation of the manifolds is supposed to be much larger than their natural width,

$$|E_{\alpha m} - E_{\beta n}| \gg \max(\Gamma_\alpha, \Gamma_\beta) \quad \text{if} \quad \alpha \neq \beta\,. \tag{3.32}$$

As a consequence of the secular approximation, quantum coherences between the manifolds can be neglected. In the same time, separation of the manifold's sublevels is supposed to be small enough so that their natural width is comparable or smaller than their separation,

$$|E_{\alpha m} - E_{\alpha n}| \lesssim \Gamma_m,\, \Gamma_n\,, \tag{3.33}$$

and the mutual coherences can be taken into account. The condition (3.33) can be weaken to take into account the case $|E_{\alpha m} - E_{\alpha n}|$ larger than Γ_m and Γ_n *if* the flat spectrum approximation holds for the manifold $\mathcal{M}_\alpha$. The manifold $\mathcal{M}_\alpha$ can represent a single quasi-degenerated J-level, a LS-term, a group of hyperfine-structured levels, or even a more general group of close levels.

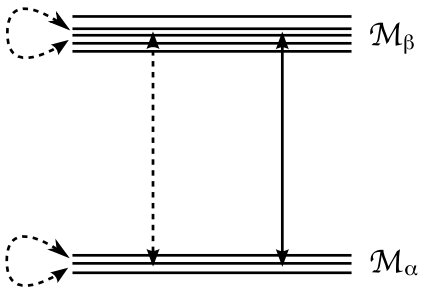

Figure 3.2: Manifolds of the atomic Hamiltonian H_A. The horizontal lines represent different sublevels of the manifolds. The radiative transitions (the solid vertical line) couple the coherences of different manifolds whereas collisions (the dashed lines) couple between different manifolds (inelastic collisions; the vertical line) and different levels of the same manifold (depolarizing collisions; the curved lines).

The coherences taken into account in the atomic density matrix have thus the general form

$$\rho_{\alpha m,\beta n} = \langle \alpha m\,|\rho|\,\beta n\rangle = \delta_{\alpha\beta}\,\langle \alpha m\,|\rho|\,\alpha n\rangle\ . \tag{3.34}$$

In the following, I will systematically use the basis of ITO. This basis has several benefits over the standard basis as summarized in Appendix B. In order to simply the expressions, I shall use the notation

$$\{\rho_{\alpha m,\alpha n}\}_{\text{standard representation}} \rightarrow \{\rho_i\}_{\text{irreducible representation}} , \tag{3.35}$$

i.e., there is only *one Latin index for each coherence of the density matrix* in the irreducible representation. There is no risk of confusion between the standard representation and the ITO basis since the number of indices clearly distinguishes these two representations. The manifold index of a given coherence will still be indicated by a Greek index. In spite of the "one-index per coherence" notation can make a direct physical interpretation of the equations more difficult, it is especially useful for a numerical treatment of the problem.In the particular pictures described in Subsection 2.5.6 one can construct the indices as in the Table 3.1.

It is useful to extend the notation and to define some relations among the coherences and manifolds:

- α_i denotes the manifold $\mathcal{M}_\alpha$ that contains the multipole ρ_i
- X_i is any quantum number associated with the density matrix coherence i (for instance, J_m would denote the total angular momentum of the multilevel atom). Similarly for L_α, J_α, etc., if such quantities are well defined for given manifold.
- $\alpha\beta$ denotes a multiplet between the manifolds $\mathcal{M}_\alpha$ and $\mathcal{M}_\beta$ (for instance, $J^K_Q(\alpha\beta)$ is the profile-averaged radiation multipole).
- $A_{\alpha\rightarrow\beta}$ denotes the Einstein coefficient for spontaneous emission for given transition. Similarly for other Einstein coefficients.
- $m = n$: multipoles m and n are identical.
- $m \sim n$: m belongs to the same manifold as n.
- $\alpha \succ \beta$ ($\alpha \prec \beta$): the manifold $\mathcal{M}_\alpha$ has higher (lower) energy than $\mathcal{M}_\beta$ (similarly for $m \succ n$, $i \succ \alpha$, etc.).

Picture	Manifold	Coherence ρ_i
Multilevel	αJ	$\rho(\alpha J)^K_Q$
Multiterm	αLSJ	${}^{\alpha LS}\rho^K_Q(J, J')$
Multilevel with hyperfine splitting	αJI	${}^{\alpha JI}\rho^K_Q(F, F')$

Table 3.1: Indexing notation for different atomic pictures. The second column contains a set of quantum numbers defining a given manifold. The third column stands for a description of a multipole i representing a particular atomic coherence.

For notational convenience it will be useful to use the single symbols representing *transitions* between different Zeeman sublevels or between whole manifolds (depending on whether the Zeeman splitting is negligible or not). In order to distinguish the transitions from other indices, I shall use the Fraktur font face, $\mathfrak{t}$, etc. The transition's lower and upper levels description differ for different pictures. These are summarized in Table 3.2 (cf. Landi Degl'Innocenti & Landolfi 2004).

The density matrix elements driving the convergence of the NLTE problem are *populations*, i.e., the density matrix multipoles of zero rank (see Trujillo Bueno & Manso Sainz 1999;

Manso Sainz & Trujillo Bueno 1999). These elements require a special treatment in the iterative solvers, hence they need to be clearly distinguished from the higher-rank components. I use the notation of $\bar{i}$ to indicate that ρ_i is a population multipole.

Picture	Lower – upper level of the transition $\mathtt{t}$
Multilevel	$\alpha_\ell J_\ell - \alpha_u J_u$
Multiterm	$\alpha_\ell L_\ell S_\ell j_\ell M_\ell - \alpha_u L_u S_u j_u M_u$
Multilevel with hyperfine splitting	$\alpha_\ell J_\ell I_\ell i_\ell f_\ell - \alpha_u J_u I_u i_u f_u$

Table 3.2: Indexing notation for the transition index $\mathtt{t}$ in different pictures. The multilevel picture is only considered in the Hanle effect regime in which Zeeman splitting of the profiles can be neglected.

3.3.2 Equations of statistical equilibrium

Eq. (2.106) reads, in the notation introduced in the previous subsection,

$$\sum_j \Pi_{ij}\rho_j = 0\,, \tag{3.36}$$

with the additional normalization condition which, in the basis of ITO, reads

$$\sum_{\overline{m}} \sqrt{[J_{\overline{m}}]}\rho_{\overline{m}} = 1\,, \tag{3.37}$$

where $J_{\overline{m}}$ denotes the total angular momentum of given level (Landi Degl'Innocenti 1984).

The total number of *independent* atomic multipoles taken into account in the particular model will be donoted by N throughout the rest of this thesis. The density matrix obeys the conjugation relations reducing the number of independent quantities required for the full description of the state. Obviously the rate matrix $\mathbf{\Pi}$ also obeys some symmetries. There is a discussion of possible reduction of ESE in Appendix A.

Let us now ignore the collisional part of $\mathbf{\Pi}$. For reasons that will become clear later it is advantageous to express the elements of $\mathbf{\Pi}$ as a linear combination of the mean radiation field tensors.Due to the flat-spectrum approximation, the precise position of the profiles is not crucial for the rates if ESE and only one line profile can be for calculation of the line mean radiation tensor which, in the ITO basis, can be defined as

$$J^K_Q(\alpha\beta) = \int \mathrm{d}\omega\, J^K_Q(\omega)\varphi(\omega_{\alpha\beta} - \omega)\,, \tag{3.38}$$

where $\varphi(\omega_{\alpha\beta} - \omega)$ is the real part of the line absorption/emission profile centered at the line frequency $\omega_{\alpha\beta}$. The monochromatic multipole components $J^K_Q(\omega)$ can be calculated from the Stokes parameters via Eq. (B.8). Note that, in the CRD approximation, one has $J^K_Q(\alpha\beta) = J^K_Q(\beta\alpha)$. The $\mathbf{\Pi}$-matrix elements can be expanded as follows:

$$\Pi_{ij} = -\mathrm{i}N_{ij} + \sum_{\alpha KQ} s_{ij}(\alpha KQ)J^K_Q(\alpha\alpha_i) + s^{\mathrm{E}}_{ij}\,, \tag{3.39}$$

where N_{ij} is the magnetic kernel (cf. Landi Degl'Innocenti 1985) and the coefficients $s_{ij}(\alpha KQ)$ and s^{E}_{ij} arise from a particular model of the levels. In general, N_{ij} only couples coherences within a given manifold and it is uniquely determined by the external magnetic field. Its

explicit expression is given below. The coefficients $s_{ij}(\alpha KQ)$ describe the transition rates due to absorption and stimulated emission of radiation. Finally, $s^{\rm E}_{ij}$ denotes the spontaneous emission rates.

The important property of $s_{ij}(\alpha KQ)$ and $s^{\rm E}_{ij}$ is that they do not depend on local physical conditions of the atmosphere and they can be pre-calculated only once in the model and used in every point and every iteration of the model. The time demands of such approach are thus negligible. On the other hand, the magnetic kernel has to be calculated and stored in every point of the atmosphere.

The most difficult coefficient in Eq. (3.39) is $s_{ij}(\alpha KQ)$. It must be, in general, calculated not only for every combination of atomic coherences but also for every multipole of radiation field. In fact, most of these coefficients vanish due to selection rules. The explicit expressions for this and the other coefficients can be derived from the expressions for $T_{A,E,S}$ and $R_{A,E,S}$ used in Eq. (2.83). In order to follow the compact notation, replacements like $T_A(a,b;\ell,\ell') \rightarrow T^A_{ij}$ (and analogously for the other rates) have to be performed. The coherence ρ_{ab} is replaced by ρ_i and $\rho_{\ell\ell'}$ by ρ_j. Matrix element of the system (2.83) can thus be rewritten in the form

$$\begin{aligned}\Pi_{ij} &= -{\rm i}(j\sim i)N_{ij} + (j\prec i)T^A_{ij} + (j\succ i)(T^S_{ij}+T^E_{ij}) \\ &\quad -(j\sim i)(R^A_{ij}+R^S_{ij}+R^E_{ij})\,, \end{aligned} \tag{3.40}$$

where

$$(j\sim i) = \delta_{\alpha_j\alpha_i}\,, \tag{3.41}$$

$$(j\prec i) = \begin{cases} 1 & \text{if} \quad j\prec i \\ 0 & \text{otherwise} \end{cases}\,. \tag{3.42}$$

The radiative rates can be expanded in terms of radiation multipoles, i.e.,

$$T^A_{ij} = \sum_{KQ} t^A_{ij}(KQ) J^K_Q(\alpha_j\alpha_i)\,, \tag{3.43}$$

$$T^S_{ij} = \sum_{KQ} t^S_{ij}(KQ) J^K_Q(\alpha_j\alpha_i)\,, \tag{3.44}$$

$$T^E_{ij} = t^E_{ij}\,, \tag{3.45}$$

$$R^A_{ij} = \sum_{KQ}\sum_{\alpha\succ\alpha_i} r^A_{ij}(\alpha KQ) J^K_Q(\alpha\alpha_i)\,, \tag{3.46}$$

$$R^S_{ij} = \sum_{KQ}\sum_{\alpha\prec\alpha_i} r^S_{ij}(\alpha KQ) J^K_Q(\alpha\alpha_i)\,, \tag{3.47}$$

$$R^E_{ij} = r^E_{ij}\,, \tag{3.48}$$

where the coefficients $t^{A,E,S}_{ij}$ and $r^{A,E,S}_{ij}$ are to be derived for each particular picture of levels.[4] It follows from a comparison of Eq. (3.39) and Eqs. (3.43–3.48) that

$$\begin{aligned} s_{ij}(\alpha KQ) &= (j\prec i)\delta_{\alpha\alpha_j} t^A_{ij}(KQ) + (j\succ i)\delta_{\alpha\alpha_j} t^S_{ij}(KQ) \\ &\quad -(j\sim i)\left[r^A_{ij}(\alpha KQ) + r^S_{ij}(\alpha KQ)\right]\,, \end{aligned} \tag{3.49}$$

$$s^{\rm E}_{ij} = (j\succ i)t^E_{ij} - (j\sim i)r^E_{ij}\,. \tag{3.50}$$

Explicit expressions for the t, r, and N in the particular level models can be extracted from expressions for T, R, and N given by Landi Degl'Innocenti & Landolfi (2004). These coefficients read:

[4] Do not confuse the symbols $t^{A,E,S}_{ij}$ and $r^{A,E,S}_{ij}$ with the quantities $t_{A,E,S}$ and $r_{A,E,S}$ of Landi Degl'Innocenti & Landolfi (2004) defined by their Eqs. (7.20a)–(7.20f).

Multilevel atom

$$t_{ij}^{A}(KQ) = [J_j]B_{\alpha_j\to\alpha_i}\sqrt{3[K_i;K_j;K]}(-1)^{K_j+Q_j} \times \left\{ \begin{array}{ccc} J_i & J_j & 1 \\ J_i & J_j & 1 \\ K_i & K_j & K \end{array} \right\} \left(\begin{array}{ccc} K_i & K_j & K \\ -Q_i & Q_j & -Q \end{array} \right), \tag{3.51}$$

$$t_{ij}^{S}(KQ) = [J_j]B_{\alpha_j\to\alpha_i}\sqrt{3[K_i;K_j;K]}(-1)^{K+K_j+Q_j} \times \left\{ \begin{array}{ccc} J_i & J_j & 1 \\ J_i & J_j & 1 \\ K_i & K_j & K \end{array} \right\} \left(\begin{array}{ccc} K_i & K_j & K \\ -Q_i & Q_j & -Q \end{array} \right), \tag{3.52}$$

$$t_{ij}^{E} = \delta_{K_iK_j}\delta_{Q_iQ_j}[J_j]A_{\alpha_j\to\alpha_i}(-1)^{1+J_i+J_j+K_i} \left\{ \begin{array}{ccc} J_j & J_j & K_i \\ J_i & J_i & 1 \end{array} \right\}, \tag{3.53}$$

$$r_{ij}^{A}(\alpha KQ) = [J_i]B_{\alpha_i\to\alpha}\sqrt{3[K_i;K_j;K]}(-1)^{1+J_\alpha-J_i+K+Q_j} \left\{ \begin{array}{ccc} K_i & K_j & K \\ J_i & J_i & J_i \end{array} \right\} \times \frac{1}{2}\left\{ \begin{array}{ccc} 1 & 1 & K \\ J_i & J_i & J_\alpha \end{array} \right\} \left(\begin{array}{ccc} K_i & K_j & K \\ Q_i & -Q_j & Q \end{array} \right) \left[1+(-1)^{K_i+K_j+K}\right], \tag{3.54}$$

$$r_{ij}^{S}(\alpha KQ) = [J_i]B_{\alpha_i\to\alpha}\sqrt{3[K_i;K_j;K]}(-1)^{1+J_\alpha-J_i+Q_j} \left\{ \begin{array}{ccc} K_i & K_j & K \\ J_i & J_i & J_i \end{array} \right\} \times \frac{1}{2}\left\{ \begin{array}{ccc} 1 & 1 & K \\ J_i & J_i & J_\alpha \end{array} \right\} \left(\begin{array}{ccc} K_i & K_j & K \\ Q_i & -Q_j & Q \end{array} \right) \left[1+(-1)^{K_i+K_j+K}\right], \tag{3.55}$$

$$r_{ij}^{E} = \delta_{ij}\sum_{\mu\prec\alpha_i} A_{\alpha_i\to\mu}, \tag{3.56}$$

$$N_{ij} = \delta_{ij}\omega_L g_{\alpha_iJ_i}Q_i, \tag{3.57}$$

where

$$\omega_L = \frac{\mu_0 B}{\hbar}, \tag{3.58}$$

is the so-called Larmor frequency.

Multiterm atom

$$t_{ij}^{A}(KQ) = [L_j]B_{\alpha_j\to\alpha_i}\sqrt{3[J_i;J_i';J_j;J_j';K_i;K_j;K]}(-1)^{K_j+Q_j+J_j'-J_j} \left\{ \begin{array}{ccc} J_i & J_j & 1 \\ J_i' & J_j' & 1 \\ K_i & K_j & K \end{array} \right\} \times \left\{ \begin{array}{ccc} L_i & L_j & 1 \\ J_j & J_i & S \end{array} \right\} \left\{ \begin{array}{ccc} L_i & L_j & 1 \\ J_j' & J_i' & S \end{array} \right\} \left(\begin{array}{ccc} K_i & K_j & K \\ -Q_i & Q_j & -Q \end{array} \right), \tag{3.59}$$

$$t_{ij}^S(KQ) = [L_j]B_{\alpha_j\to\alpha_i}\sqrt{3[J_i;J_i';J_j;J_j';K_i;K_j;K]}(-1)^{K+K_j+Q_j+J_j'-J_j}\left\{\begin{array}{ccc} J_i & J_j & 1\\ J_i' & J_j' & 1\\ K_i & K_j & K\end{array}\right\}$$
$$\times \left\{\begin{array}{ccc} L_j & L_i & 1\\ J_i & J_j & S\end{array}\right\}\left\{\begin{array}{ccc} L_j & L_i & 1\\ J_i' & J_j' & I\end{array}\right\}\left(\begin{array}{ccc} K_i & K_j & K\\ -Q_i & Q_j & -Q\end{array}\right), \quad (3.60)$$

$$t_{ij}^E = \delta_{K_iK_j}\delta_{Q_iQ_j}[L_j]A_{\alpha_j\to\alpha_i}\sqrt{[J_i;J_i';J_j;J_j;J_j']}(-1)^{1+K_i+J_i'+J_j'}\left\{\begin{array}{ccc} J_i & J_i' & K_i\\ J_j' & J_j & 1\end{array}\right\}$$
$$\times \left\{\begin{array}{ccc} J_i & J_i' & K_i\\ J_j' & J_j & 1\end{array}\right\}\left\{\begin{array}{ccc} L_j & L_i & 1\\ J_i & J_j & S\end{array}\right\}\left\{\begin{array}{ccc} L_j & L_i & 1\\ J_i' & J_j' & S\end{array}\right\}, \quad (3.61)$$

$$r_{ij}^A(\alpha KQ) = [L_i]B_{\alpha_i\to\alpha}\sqrt{\frac{3}{2}[K_i;K_j;K]}(-1)^{1+L_\alpha-S+J_i+Q_j}\left\{\begin{array}{ccc} L_i & L_i & K\\ 1 & 1 & L_\alpha\end{array}\right\}$$
$$\times \left(\begin{array}{ccc} K_i & K_j & K\\ Q_i & -Q_j & Q\end{array}\right)\left[\delta_{J_iJ_j}\sqrt{[J_i';J_j']}\left\{\begin{array}{ccc} L_i & L_i & K\\ J_j' & J_i' & I\end{array}\right\}\left\{\begin{array}{ccc} K_i & K_j & K\\ J_j' & J_i' & J_i\end{array}\right\}\right.$$
$$\left. + \delta_{J_i'J_j'}\sqrt{[J_i;J_j]}(-1)^{J_j-J_i'+K_i+K_j+K}\left\{\begin{array}{ccc} L_i & L_i & K\\ J_j & J_i & S\end{array}\right\}\left\{\begin{array}{ccc} K_i & K_j & K\\ J_j & J_i & J_i'\end{array}\right\}\right], \quad (3.62)$$

$$r_{ij}^S(\alpha KQ) = [L_i]B_{\alpha_i\to\alpha}\sqrt{\frac{3}{2}[K_i;K_j;K]}(-1)^{1+L_\alpha-S+J_i+K+Q_j}\left\{\begin{array}{ccc} L_i & L_i & K\\ 1 & 1 & L_\alpha\end{array}\right\}$$
$$\times \left(\begin{array}{ccc} K_i & K_j & K\\ Q_i & -Q_j & Q\end{array}\right)\left[\delta_{J_iJ_j}\sqrt{[J_i';J_j']}\left\{\begin{array}{ccc} L_i & L_i & K\\ J_j' & J_i' & S\end{array}\right\}\left\{\begin{array}{ccc} K_i & K_j & K\\ J_j' & J_i' & J_i\end{array}\right\}\right.$$
$$\left. + \delta_{J_i'J_j'}\sqrt{[J_i;J_j]}(-1)^{J_j-J_i'+K_i+K_j+K}\left\{\begin{array}{ccc} L_i & L_i & K\\ J_j & J_i & S\end{array}\right\}\left\{\begin{array}{ccc} K_i & K_j & K\\ J_j & J_i & F_i'\end{array}\right\}\right], \quad (3.63)$$

$$r_{ij}^E = \delta_{ij}\sum_{\mu\prec\alpha_i} A_{\alpha_i\to\mu}\,, \quad (3.64)$$

$$N_{ij} = \delta_{ij}\omega_{J_iJ_i'} + \delta_{Q_iQ_j}\omega_L g_{\alpha_iL_i}(-1)^{J_i'+J_j+Q_i}\sqrt{[K_i;K_j]}\left(\begin{array}{ccc} K_i & K_j & 1\\ -Q_i & Q_i & 0\end{array}\right)\left[\delta_{J_i'J_j'}\Gamma_{L_iI}(J_i,J_j)\right.$$
$$\left.\times \left\{\begin{array}{ccc} K_i & K_j & 1\\ J_j & J_i & J_i'\end{array}\right\} + \delta_{J_iJ_j}(-1)^{K_i-K_j}\Gamma_{L_iS}(J_i',J_j')\left\{\begin{array}{ccc} K_i & K_j & 1\\ J_j' & J_i' & F_i\end{array}\right\}\right], \quad (3.65)$$

where

$$\omega_{J_iJ_i'} = \frac{E_{\alpha LS}(J_i) - E_{\alpha LS}(J_i')}{\hbar}\,. \quad (3.66)$$

Multilevel atom with hyperfine structure

The coefficients for a multilevel atom with hyperfine splitting are formally identical to the multiterm case with substitutions

$$L \to J,\; S \to I,\; J \to F\,. \quad (3.67)$$

3.3.3 Radiative transfer equation

The slowest part of the numerical calculation of the NLTE model is typically the formal solution of the radiative transfer equation Eq. (2.107). In a general model, it is necessary to solve the equation for every discrete frequency ω and every direction $\mathbf{\Omega}$ of the ray. I will denote the *total number of the discrete frequencies* of radiation by F, and a number of the discrete ray directions by $\mathsf{N}_{\mathbf{\Omega}}$.

The transfer coefficients ϵ_p, η_p, and ρ_p for the individual Stokes components p ($p = 0, \ldots, 3$) can be expressed in terms of atomic density matrix elements (Landi Degl'Innocenti & Landolfi 2004). Their form which is very general and very useful for iterative solvers at the same time, is

$$\eta_p^A(\boldsymbol{k}) = \mathrm{Re}\left[\sum_i a_i(p,\boldsymbol{k})\rho_i\right], \tag{3.68}$$

$$\eta_p^S(\boldsymbol{k}) = \mathrm{Re}\left[\sum_i b_i(p,\boldsymbol{k})\rho_i\right], \tag{3.69}$$

$$\rho_p^A(\boldsymbol{k}) = \eta_p^A(\boldsymbol{k})\{\mathrm{Re} \rightarrow \mathrm{Im}\}, \tag{3.70}$$

$$\rho_p^S(\boldsymbol{k}) = \eta_p^S(\boldsymbol{k})\{\mathrm{Re} \rightarrow \mathrm{Im}\}, \tag{3.71}$$

$$\epsilon_p(\boldsymbol{k}) = \frac{\hbar\omega^3}{2\pi^2c^2}\eta_p^S(\boldsymbol{k}), \tag{3.72}$$

where "$\{\mathrm{Re} \rightarrow \mathrm{Im}\}$" denotes a replacement of "Re" by "Im" in the last expression.

In the discrete model, coefficients $a_i(p,\boldsymbol{k})$ and $b_i(p,\boldsymbol{k})$ become $\mathsf{F}\times\mathsf{N}$ matrices. When applied to a *formal* N*-vector of atomic multipoles*, $\boldsymbol{\rho}$, it results in *formal vector of transfer coefficients* ($\boldsymbol{\eta}_p^{A,S}$, $\boldsymbol{\rho}_p^{A,S}$, or $\boldsymbol{\epsilon}_p$) *with one frequency per row*. In the matrix notation, this can be expressed by

$$\boldsymbol{\eta}_p^A(\mathbf{\Omega}) = \mathrm{Re}\left[\boldsymbol{a}(p,\mathbf{\Omega})\boldsymbol{\rho}\right], \tag{3.73}$$

$$\boldsymbol{\eta}_p^S(\mathbf{\Omega}) = \mathrm{Re}\left[\boldsymbol{b}(p,\mathbf{\Omega})\boldsymbol{\rho}\right], \tag{3.74}$$

$$\boldsymbol{\rho}_p^A(\mathbf{\Omega}) = \boldsymbol{\eta}_p^A(\mathbf{\Omega})\{\mathrm{Re} \rightarrow \mathrm{Im}\}, \tag{3.75}$$

$$\boldsymbol{\rho}_p^S(\mathbf{\Omega}) = \boldsymbol{\eta}_p^S(\mathbf{\Omega})\{\mathrm{Re} \rightarrow \mathrm{Im}\}, \tag{3.76}$$

$$\boldsymbol{\epsilon}_p(\mathbf{\Omega}) = \frac{\hbar\omega^3}{2\pi^2c^2}\boldsymbol{\eta}_p^S(\mathbf{\Omega}). \tag{3.77}$$

It is worth to say that the matrices $\boldsymbol{a}$ and $\boldsymbol{b}$ have to be calculated in every point and every direction $\mathbf{\Omega}$ of the ray. In the following, I will call them the *decoupling matrices*. Memory demands of using the decoupling matrices are negligible even for complex atomic models: Only one instance of the matrices has to be created and it is used over and over again during the formal solution.

Calculation of the decoupling matrices

Calculation of the transfer coefficients can be rather time consuming. Number of transitions necessary to take explicitly into account increases significantly if Zeeman splitting of the levels cannot be neglected in the emission and absorption profiles. A further complication arises in the Paschen-Back effect regime in which one needs to take into account a coupling of different J- or F-levels. The symmetry of the equations is thus lost and one has to deal with an enormous number of terms.

In general, the absorption profiles between separate Zeeman levels $|\alpha JM\rangle$, $|\alpha LSjM\rangle$, etc., have to be explicitly taken into account. The Bohr frequencies between the the shifted levels can be calculated from Eq. (2.39), Eq. (2.36), etc. The individual transitions $\mathfrak{t}$ and profiles can be indexed according to Table 3.2. In the following, the expression $\ell_\mathfrak{t}$ ($u_\mathfrak{t}$) denotes the lower (upper) manifold of the given transition $\mathfrak{t}$. Similarly, $M_{\ell_\mathfrak{t}}$ denotes the magnetic quantum number associated with the lower level of $\mathfrak{t}$, and analogously for another quantum numbers. The total number of transition profiles to be taken into account in the model will be denoted by $\mathsf{N}_{\mathfrak{tr}}$.

It is worth to find an efficient way of calculation of the decoupling matrices. In the NLTE models, it is necessary to take into account a non-homogenous magnetic field across the medium and the fact that transfer coefficients in every point have to be calculated repeatedly (typically thousand-times in every point: 100 directions, 10 iterations). A suitable decomposition of the decoupling matrices elements is thus desirable. The computational time demands can be preferred above the memory demands in the contemporary computers. It is thus possible to calculate all the spatially-dependent parts of the $\boldsymbol{a}$ and $\boldsymbol{b}$ matrices and store them in the computer memory. This approach can lead to an increase of the calculation speed of the transfer coefficients by *orders of magnitude* in comparison to the straightforward calculation directly from the definition. The cost is an increase of memory demands but still easily tractable by contemporary workstations. A more detailed discussion of the optimal implementation of pre-calculations can be found in Appendix A. Here, I only give a general recipe.

The local part of the decoupling matrices is to be stored in a suitable grid. Taking into account the general structure of transfer coefficients, we can decompose the complex matrices $\boldsymbol{a}$ and $\boldsymbol{b}$ as follows,

$$a_{\omega i}(p,\boldsymbol{\Omega}) = \mathcal{N}\omega \sum_{KQ}\sum_{\mathfrak{t}} \mathcal{T}^K_Q(p,\boldsymbol{\Omega})\Phi_\mathfrak{t}(\omega)\xi_{i\mathfrak{t}}(p,K,Q)\,, \tag{3.78}$$

$$b_{\omega i}(p,\boldsymbol{\Omega}) = \mathcal{N}\omega \sum_{KQ}\sum_{\mathfrak{t}} \mathcal{T}^K_Q(p,\boldsymbol{\Omega})\Phi_\mathfrak{t}(\omega)\chi_{i\mathfrak{t}}(p,K,Q)\,, \tag{3.79}$$

where $\mathcal{T}^K_Q(p,\boldsymbol{\Omega})$ is the geometrical tensor defined in Table B.1, $\Phi_\mathfrak{t}(\omega) \equiv \Phi_\mathfrak{t}(\omega_\mathfrak{t}-\omega)$ is the profile of transition $\mathfrak{t}$, and ξ and χ are the coefficients depending on a given picture and transition. Note that the index ω in $a_{\omega i}$ and $b_{\omega i}$ denotes a given discrete frequency. The coefficients ξ and χ are calculated from the Einstein coefficients for absorption and stimulated and spontaneous emission, and, eventually, from the Hamiltonian diagonalizing coefficients C^j_J.

It is important to point out that the summation over the transitions $\mathfrak{t}$ only involves those with ρ_i in the lower (upper) manifold. This fact is reflected by the definition of ξ and χ coefficients including corresponding Kronecker δ's: $\delta_{\alpha_i\ell_\mathfrak{t}}$ ($\delta_{\alpha_i u_\mathfrak{t}}$). The $\mathsf{N}\times\mathsf{N}_{\mathfrak{tr}}$ matrices $\boldsymbol{\xi}$ and $\boldsymbol{\chi}$ obviously contain a large number of zero elements. In a practical implementation it is thus not useful (and practical with respect to memory demands – note that $\boldsymbol{\xi}$ and $\boldsymbol{\chi}$ data have to be stored separately for each grid node) to store the whole matrices. The better idea is to generate a *list of transitions* for each atomic multipole (see Figure A.3).

The decomposition (3.78–3.79) into the geometrical part ($\mathcal{T}^K_Q$), the frequency part ($\Phi_\mathfrak{t}$), and the "atomic part" has to be slightly modified if one considers the systematic motions in the atmospheric plasmas by taking the $\boldsymbol{\Omega}$-dependence of the profiles into account.

The explicit expressions for $\xi_{i\mathfrak{t}}(p,K,Q)$ and $\chi_{i\mathfrak{t}}(p,K,Q)$ are as follows:

Multilevel atom in the Hanle effect regime

$$\xi_{i\mathfrak{t}}(p,K,Q) = \frac{\hbar}{4\pi}\delta_{K_iK}\delta_{Q_iQ}\delta_{\alpha_i\ell_\mathfrak{t}}[J_{\ell_\mathfrak{t}}]B_{\ell_\mathfrak{t}\to u_\mathfrak{t}}\sqrt{3}(-1)^{1+J_{\ell_\mathfrak{t}}+J_{u_\mathfrak{t}}+K}\left\{\begin{array}{ccc}1 & 1 & K\\ J_{\ell_\mathfrak{t}} & J_{\ell_\mathfrak{t}} & J_{u_\mathfrak{t}}\end{array}\right\} \tag{3.80}$$

$$\chi_{i\mathfrak{t}}(p,K,Q) = \frac{\hbar}{4\pi}\delta_{K_iK}\delta_{Q_iQ}\delta_{\alpha_iu_\mathfrak{t}}[J_{u_\mathfrak{t}}]B_{u_\mathfrak{t}\to\ell_\mathfrak{t}}\sqrt{3}(-1)^{1+J_{\ell_\mathfrak{t}}+J_{u_\mathfrak{t}}}\left\{\begin{array}{ccc}1 & 1 & K\\ J_{u_\mathfrak{t}} & J_{u_\mathfrak{t}} & J_{\ell_\mathfrak{t}}\end{array}\right\} \tag{3.81}$$

Multiterm atom

$$\begin{aligned}\xi_{i\mathfrak{t}}(p,K,Q) = \frac{\hbar}{4\pi}\delta_{\alpha_i\ell_\mathfrak{t}}\sum_{J_\ell J_u J'_u}\sum_{M'_\ell qq'}[L_{\ell_\mathfrak{t}}]B_{\ell_\mathfrak{t}\to u_\mathfrak{t}}\sqrt{3[K;K_i]}(-1)^{1+J_i-M_{\ell_\mathfrak{t}}+q'}\\ C^{j_{\ell_\mathfrak{t}}}_{J_\ell}(\ell_\mathfrak{t})C^{j_{\ell_\mathfrak{t}}}_{J_i}(\ell_\mathfrak{t})C^{j_{u_\mathfrak{t}}}_{J_u}(u_\mathfrak{t})C^{j_{u_\mathfrak{t}}}_{J'_u}(u_\mathfrak{t})\sqrt{[J_\ell J'_i J_u J'_u]}\left(\begin{array}{ccc}J_u & J_\ell & 1\\ -M_{u_\mathfrak{t}} & M_{\ell_\mathfrak{t}} & -q\end{array}\right)\\ \left(\begin{array}{ccc}J'_u & J'_\ell & 1\\ -M_{u_\mathfrak{t}} & M'_\ell & -q'\end{array}\right)\left(\begin{array}{ccc}1 & 1 & K\\ q & -q' & -Q\end{array}\right)\left(\begin{array}{ccc}J_i & J'_i & K_i\\ M_{\ell_\mathfrak{t}} & -M'_\ell & -Q_i\end{array}\right)\\ \left\{\begin{array}{ccc}L_{u_\mathfrak{t}} & L_{\ell_\mathfrak{t}} & 1\\ J_\ell & J_u & S\end{array}\right\}\left\{\begin{array}{ccc}L_{u_\mathfrak{t}} & L_{\ell_\mathfrak{t}} & 1\\ J'_i & J'_u & S\end{array}\right\}\end{aligned} \tag{3.82}$$

$$\begin{aligned}\chi_{i\mathfrak{t}}(p,K,Q) = \frac{\hbar}{4\pi}\delta_{\alpha_iu_\mathfrak{t}}\sum_{J_u J_\ell J'_\ell}\sum_{M'_u qq'}[L_{u_\mathfrak{t}}]B_{u_\mathfrak{t}\to\ell_\mathfrak{t}}\sqrt{3[KK_i]}(-1)^{1+J_i-M_{u_\mathfrak{t}}+q'}\\ C^{j_{\ell_\mathfrak{t}}}_{J_\ell}(\ell_\mathfrak{t})C^{j_{\ell_\mathfrak{t}}}_{J'_\ell}(\ell_\mathfrak{t})C^{j_{u_\mathfrak{t}}}_{J_u}(u_\mathfrak{t})C^{j_{u_\mathfrak{t}}}_{J'_i}(u_\mathfrak{t})\sqrt{[J_\ell J'_\ell J_u J_i]}\left(\begin{array}{ccc}J_u & J_\ell & 1\\ -M_{u_\mathfrak{t}} & M_{\ell_\mathfrak{t}} & -q\end{array}\right)\\ \left(\begin{array}{ccc}J_i & J'_\ell & 1\\ -M'_u & M_{\ell_\mathfrak{t}} & -q'\end{array}\right)\left(\begin{array}{ccc}1 & 1 & K\\ q & -q' & -Q\end{array}\right)\left(\begin{array}{ccc}J_i & J'_i & K_i\\ M'_u & -M_{u_\mathfrak{t}} & -Q_i\end{array}\right)\\ \left\{\begin{array}{ccc}L_{u_\mathfrak{t}} & L_{\ell_\mathfrak{t}} & 1\\ J_\ell & J_u & S\end{array}\right\}\left\{\begin{array}{ccc}L_{u_\mathfrak{t}} & L_{\ell_\mathfrak{t}} & 1\\ J'_\ell & J_i & S\end{array}\right\}\end{aligned} \tag{3.83}$$

Multilevel atom with hyperfine structure

The coefficients for a multilevel atom with hyperfine splitting are formally identical to the ones of the multiterm case if one uses the following substitutions for the quantum numbers:

$$L \to J,\ S \to I,\ J \to F,\ j \to i\,. \tag{3.84}$$

3.4 The iterative scheme

3.4.1 Formal solution

Let us recall a formal solution (FS) of the radiative transfer equation along the ray in the direction $\boldsymbol{\Omega}$. Rewriting RTE using the optical path (3.1) it is easy to verify (Rees et al. 1989) that FS of Eq. (2.107) is given by the integral equation

$$\boldsymbol{I}(\tau_2) = \boldsymbol{I}(\tau_1)\mathrm{e}^{-(\tau_2-\tau_1)} + \int_{\tau_1}^{\tau_2}\mathrm{d}t\ [\boldsymbol{S}(t) - \boldsymbol{K}'(t)\boldsymbol{I}(t)]\,\mathrm{e}^{-(\tau_2-t)}\,, \tag{3.85}$$

where we assume $\tau_2 > \tau_1$. $\boldsymbol{K}'$ denotes the so-called *modified propagation matrix*,

$$\boldsymbol{K}' = \frac{\boldsymbol{K}}{\eta_I} - \mathbf{1}\,, \tag{3.86}$$

and

$$\boldsymbol{S} = \frac{\boldsymbol{J}}{\eta_I}\,, \tag{3.87}$$

is the formal *source function vector*. The symbol $\mathbf{1}$ represents the 4×4 identity matrix. Consider three successive points of the grid, M, O, and P. Then Eq. (3.85) becomes

$$\boldsymbol{I}(O) = \boldsymbol{I}(M)e^{-\Delta\tau_{MO}} + \int_{\tau_M}^{\tau_O} \mathrm{d}\tau\,[\boldsymbol{S}(\tau) - \boldsymbol{K}'(\tau)\boldsymbol{I}(\tau)]\,e^{-(\tau_O-\tau)}\,, \tag{3.88}$$

where $\Delta\tau_{MO} = \tau_O - \tau_M$. FS in the *discretized atmosphere* can be calculated by different numerical methods. In this work, I adopt the approach based on the so-called *short characteristics method* (Olson & Kunasz 1987). In this method, one integrates FS over the range of few successive grid nodes between which the integrand in Eq. (3.85) is interpolated by polynomials. Rees et al. (1989) generalized the method for a treatment of the full Stokes vector transfer using the *linear* interpolation of the integrand. Their DELO method has been further improved by Trujillo Bueno (2003) in his DELOPAR technique with a *parabolic* interpolation of the source vector among the points MOP whereas the $\boldsymbol{K}'(\tau)\boldsymbol{I}(\tau)$ term is interpolated by a linear function between M and O. This approach leads to a method of higher accuracy with only little computational time penalty. The DELOPAR formal solver is the method of choice in the present work.

The interpolation coefficients are easily obtained from the grid spacing, $\boldsymbol{\Omega}$, and the absorption coefficients. After the integration, one has for the Stokes vector at point O:

$$\begin{aligned}\boldsymbol{I}(O) = \boldsymbol{I}(M)\mathrm{e}^{-\Delta\tau_{MO}} + \psi_M\boldsymbol{S}(M) + \psi_O\boldsymbol{S}(O) + \psi_P\boldsymbol{S}(P)\\ -\psi'_M\boldsymbol{K}'(M)\boldsymbol{I}(M) - \psi'_O\boldsymbol{K}'(O)\boldsymbol{I}(O)\,,\end{aligned} \tag{3.89}$$

where $\psi_{M,O,P}$ and $\psi'_{M,O}$ are, respectively, the quadratic and linear interpolation coefficients. To extract $\boldsymbol{I}(O)$ from Eq. (3.89) one can define the matrix

$$\boldsymbol{\kappa} = \left[\mathbf{1} + \psi'_O\boldsymbol{K}'(O)\right]^{-1}\,, \tag{3.90}$$

and finally get (cf. Trujillo Bueno 2003)

$$\boldsymbol{I}(O) = \boldsymbol{T}_{MO} + \boldsymbol{\kappa}\left[\psi_M\boldsymbol{S}(M) + \psi_O\boldsymbol{S}(O) + \psi_P\boldsymbol{S}(P)\right]\,, \tag{3.91}$$

where

$$\boldsymbol{T}_{MO} = \boldsymbol{\kappa}\left[\mathbf{1}\mathrm{e}^{-\Delta\tau_{MO}} - \psi'_M\boldsymbol{K}'(M)\right]\boldsymbol{I}(M)\,. \tag{3.92}$$

Since the formal solution proceeds along the ray starting at the boundary of the integration domain (where the illumination is known *a priori*), the Stokes vector in each successive node is computed from the current guess of the source function and the fraction of radiation transmitted from the preceding point.

The coefficients $\psi_{M,O,P}$ and ψ'_{MO} can be found in Olson et al. (1986)

$$\psi_M = e_0 + \frac{e_2 - (\Delta\tau_{OP} + 2\Delta\tau_{MO})e_1}{\Delta\tau_{MO}(\Delta\tau_{MO} + \Delta\tau_{OP})}\,, \tag{3.93}$$

$$\psi_O = \frac{(\Delta\tau_{MO} + \Delta\tau_{OP})e_1 - e_2}{\Delta\tau_{MO}\Delta\tau_{OP}}\,, \tag{3.94}$$

$$\psi_P = \frac{e_2 - \Delta\tau_{MO}e_1}{\Delta\tau_{OP}(\Delta\tau_{MO} + \Delta\tau_{OP})}\,, \tag{3.95}$$

and

$$\psi'_M = e_0 - \frac{e_1}{\Delta\tau_{MO}}\,, \tag{3.96}$$

$$\psi'_O = \frac{e_1}{\Delta\tau_{MO}}\,, \tag{3.97}$$

where

$$e_0 = 1 - e^{-\Delta\tau_{MO}}\,, \tag{3.98}$$

$$e_1 = \Delta\tau_{MO} - e_0\,, \tag{3.99}$$

$$e_2 = \Delta\tau^2_{MO} - 2e_1\,. \tag{3.100}$$

3.4.2 Operator splitting

In order to find the approximate solution of the polarized NLTE problem we need to reformulate the operator splitting technique and find a suitable preconditioning strategy in the formalism of atomic density matrix. In this subsection, I use an analogy with the unpolarized ALI solution to build a new iterative scheme for the polarized problem (see also Paper II in Appendix D).

Unpolarized operator splitting

If polarization of radiation can be neglected then only the specific intensity component, I, needs to be taken into account. The vector equation (2.107) is reduced to the scalar equation with $\boldsymbol{K}$ reduced to η_I. Obviously $\boldsymbol{K}' = 0$ in Eq. (3.85) and FS becomes

$$I(\tau_2) = I(\tau_1)\mathrm{e}^{-(\tau_2-\tau_1)} + \int_{\tau_1}^{\tau_2} \mathrm{d}t\, S(t)\mathrm{e}^{-(\tau_2-t)}\,. \tag{3.101}$$

This can be expressed in the compact form

$$I(\tau_2) = \Lambda(\tau_2,\tau_1)[S(t)] + T(\tau_2,\tau_1)\,, \tag{3.102}$$

where

$$\Lambda(\tau_2,\tau_1)[S(t)] = \int_{\tau_1}^{\tau_2} \mathrm{d}t\, \mathrm{e}^{-(\tau_2-t)} S(t) \tag{3.103}$$

is the *monochromatic lambda operator* (cf. Rybicki & Hummer 1991) and

$$T(\tau_2,\tau_1) = I(\tau_1)\mathrm{e}^{-(\tau_2-\tau_1)}\,, \tag{3.104}$$

is the fraction of radiation transmitted from τ_1 to τ_2.

The operator (3.103) can be rewritten as (dropping the $\tau_{1,2}$ dependencies for the sake of notational convenience)

$$\Lambda = \Lambda^* + (\Lambda - \Lambda^*)\,, \tag{3.105}$$

where Λ^* is the *approximate monochromatic lambda operator*. As stated in Section 3.2, Λ^* can be constructed as the diagonal of Λ. The iterative scheme can thus be developed as

$$\begin{aligned} \Lambda[S] &= \Lambda^*[S] + (\Lambda - \Lambda^*)[S] \\ &\rightarrow \Lambda^*[S] + (\Lambda - \Lambda^*)[S^+] = \Lambda[S^+] + \Lambda^*[S - S^+]\,, \end{aligned} \tag{3.106}$$

where "+" denotes the quantities calculated in the *previous iteration*, i.e., the *known* quantities (the terms "old" and "new" will be also occasionally used). Note that the Λ-operator (and Λ^*) is always calculated using *old* level populations. Substitution of the scheme (3.106) into ESE and linearization of the equations with respect to atomic populations leads to the standard ALI iteration scheme. For a detailed discussion see Rybicki & Hummer (1992) and Socas-Navarro & Trujillo Bueno (1997).

Polarized operator splitting

In a general polarized model, the upper manifold of the transition consist of number of coherences of multiple levels whose decay contributes to the line emission. In analogy with the unpolarized transfer of overlapping lines (Rybicki & Hummer 1992) one expects that the desired iterative scheme will require an additional summation over the levels of the upper manifold.

We begin by rewriting the formal solution (3.85) using the common lambda operator defined by Eq. (3.103)

$$\boldsymbol{I}(\tau_2) = \Lambda(\tau_2,\tau_1)\left[\boldsymbol{S}(t)\right] - \Lambda(\tau_2,\tau_1)\left[\boldsymbol{K}'(t)\boldsymbol{I}(t)\right] + \boldsymbol{T}(\tau_2,\tau_1)\,. \tag{3.107}$$

Radiative transfer in the dispersive and dichroic medium leads to a coupling of the different Stokes parameters (the second term in Eq. (3.107)). To avoid the complications caused by this coupling, we apply the operator splitting procedure (3.106) only in the first term of Eq. (3.107), i.e.,

$$\Lambda[\boldsymbol{S}] \to \Lambda[\boldsymbol{S}^+] + \Lambda^*[\boldsymbol{S} - \boldsymbol{S}^+]\,. \tag{3.108}$$

From this we get a new guess for the Stokes vector,

$$\begin{aligned}\boldsymbol{I}(\tau_2) &= \Lambda(\tau_2,\tau_1)\left[\boldsymbol{S}^+(t)\right] + \Lambda^*(\tau_2,\tau_1)\left[\boldsymbol{S}(t) - \boldsymbol{S}^+(t)\right] \\ &\quad -\Lambda(\tau_2,\tau_1)\left[\boldsymbol{K}'(t)\boldsymbol{I}(t)\right] + \boldsymbol{T}(\tau_2,\tau_1)\,.\end{aligned} \tag{3.109}$$

To complete the iterative scheme, I use the substitutions

$$\boldsymbol{K}' \to \boldsymbol{K}'^{+}\,, \quad \boldsymbol{I} \to \boldsymbol{I}^+\,, \quad \boldsymbol{T} \to \boldsymbol{T}^+\,, \tag{3.110}$$

in the last two terms of Eq. (3.107) to get

$$\begin{aligned}\boldsymbol{I}(\tau_2) &= \Lambda(\tau_2,\tau_1)\left[\boldsymbol{S}(t)^+\right] + \Lambda^*(\tau_2,\tau_1)\left[\boldsymbol{S}(t) - \boldsymbol{S}(t)^+\right] \\ &\quad -\Lambda(\tau_2,\tau_1)\left[\boldsymbol{K}'(t)^+\boldsymbol{I}(t)^+\right] + \boldsymbol{T}(\tau_2,\tau_1)^+\,.\end{aligned} \tag{3.111}$$

We see that the first, third, and fourth term in the right-hand side make up the Stokes vector calculated in the previous iteration. Thus we arrive at

$$\boldsymbol{I}(\tau_2) = \boldsymbol{I}(\tau_2)^+ + \Lambda^*(\tau_2,\tau_1)\left[\boldsymbol{S}(t) - \boldsymbol{S}(t)^+\right]\,. \tag{3.112}$$

This iterative scheme is analogous to the one of the unpolarized theory. The unpolarized limit is easily obtained by ignoring the Q, U, and V components of $\boldsymbol{I}$.

In the discrete grid model, taking into account that Λ^* is the *local* operator, Eq. (3.112) is simplified to

$$\boldsymbol{I}(m) = \boldsymbol{I}(m)^+ + \Lambda^*(m,m)\left[\boldsymbol{S}(m) - \boldsymbol{S}(m)^+\right]\,, \tag{3.113}$$

where m identifies a given grid node of interest and $\Lambda^*(m,m)$ denotes the diagonal element of the $\mathbb{N}\times\mathbb{N}$ matrix $\boldsymbol{\Lambda}^*$. In the following, the index m will be ignored without any risk of confusion.

Preconditioning of $\boldsymbol{\mathcal{L}}$

The spherical components of the radiation tensor can be calculated from the Stokes parameters using Eq. (B.8). From Eq. (3.113) it follows that

$$J^K_Q(\omega) = J^K_Q(\omega)^+ + \sum_{p=0}^{3} \oint \frac{\mathrm{d}\Omega}{4\pi}\Big\{\mathcal{T}^K_Q(p,\boldsymbol{\Omega})\Lambda^*(\boldsymbol{k})[S_p(\boldsymbol{k}) - S_p(\boldsymbol{k})^+]\Big\}\,, \tag{3.114}$$

where all the quantities correspond to the same node of the grid. The explicit dependence of Λ^* on $\boldsymbol{k}$ needs to be emphasized in the integrations. Radiation field enters ESE through the averaged line radiation tensors $J^K_Q(\alpha\beta)$ defined by Eq. (3.38). Substitution of the iteration scheme (3.114) into Eq. (3.38) leads to

$$J^K_Q(\alpha\beta) = J^K_Q(\alpha\beta)^+ + \sum_{p=0}^{3} \int \mathrm{d}\omega\, \varphi_{\alpha\beta}(\omega) \oint \frac{\mathrm{d}\boldsymbol{\Omega}}{4\pi} \mathcal{T}^K_Q(p,\boldsymbol{\Omega}) \Lambda^*(\boldsymbol{k}) [S_p(\boldsymbol{k}) - S_p(\boldsymbol{k})^+] \,, \quad (3.115)$$

where I have used $\varphi_{\alpha\beta}(\omega) \equiv \varphi(\omega_{\alpha\beta} - \omega)$.

For the use in the preconditioning of ESE, it is worth to express the source function vector in terms of the density matrix multipoles of the *upper manifold* of the given line. This procedure is analogous to the one of Rybicki & Hummer (1992) intended for their unpolarized MALI method. For the source function vectors in the new and the old iteration step we can write respectively:

$$S_p(\boldsymbol{k}) = \frac{J_p(\boldsymbol{k})}{\eta_I(\boldsymbol{k})^+} \,, \quad (3.116)$$

$$S_p(\boldsymbol{k})^+ = \frac{J_p(\boldsymbol{k})^+}{\eta_I(\boldsymbol{k})^+} \,. \quad (3.117)$$

The absorption coefficient η_I is always calculated using the old density matrix. It is an essential property of the technique that only the density matrix elements contributing to emission (i.e., those of the *upper* manifold) are explicitly used in the preconditioning scheme because the emission vector is a linear combination of these elements. The nonlinear dependence on the *lower* manifold elements is advantageously hidden by the formal solver. Note that Rybicki & Hummer (1992) use the name Ψ instead of Λ for their analogous operator. An expansion of $\boldsymbol{S}$ in terms of ρ_i follows from Eqs. (3.69) and (3.72),

$$S_p(\boldsymbol{k}) = \frac{\hbar\omega^3}{2\pi^2 c^2} \frac{1}{\eta_I(\boldsymbol{k})^+} \mathrm{Re} \left[\sum_i b_i(p,\boldsymbol{k}) \rho_i \right] . \quad (3.118)$$

Substitution of this expression into Eq. (3.115) gives

$$\begin{aligned} J^K_Q(\alpha\beta) &= J^K_Q(\alpha\beta)^+ + \sum_{p=0}^{3} \int \mathrm{d}\omega\, \frac{\hbar\omega^3}{2\pi^2 c^2} \varphi_{\alpha\beta}(\omega) \oint \frac{\mathrm{d}\boldsymbol{\Omega}}{4\pi} \\ &\quad \times \mathcal{T}^K_Q(p,\boldsymbol{\Omega}) \frac{\Lambda^*(\boldsymbol{k})}{\eta_I(\boldsymbol{k})^+} \mathrm{Re} \left[\sum_i b_i(p,\boldsymbol{k}) (\rho_i - \rho_i^+) \right] . \end{aligned} \quad (3.119)$$

Following Rybicki & Hummer (1991, 1992) and the polarized generalization of Trujillo Bueno (1999) and Manso Sainz & Trujillo Bueno (2003a), we can apply the operator splitting *only* to the mean intensity component of radiation J^0_0 that is a convergence-driving component (see also the discussion of Trujillo Bueno & Manso Sainz 1999). Furthermore, only the real population multipoles, $\rho^{\bar{i}}$, shall be preconditioned. After all, one arrives at

$$J^0_0(\alpha\beta) = J^0_0(\alpha\beta)^+ + \sum_{\bar{i}} L_{\alpha\beta\bar{i}} (\rho^{\bar{i}} - \rho^+_{\bar{i}}) \,, \quad (3.120)$$

$$J^K_Q(\alpha\beta) = J^K_Q(\alpha\beta)^+ \quad \text{if} \quad K > 0 \,. \quad (3.121)$$

Note that $\rho^{\bar{i}}$ are populations of the upper levels of the $\alpha\beta$ transition. Using the fact that $\mathcal{T}^0_0(p,\boldsymbol{\Omega}) = \delta_{p0}$ (see Table B.1) the real quantity $L_{\alpha\beta\bar{i}}$ introduced in Eq. (3.120) reads

$$L_{\alpha\beta\bar{i}} = \int \mathrm{d}\omega\, \frac{\hbar\omega^3}{2\pi^2 c^2}\varphi_{\alpha\beta}(\omega) \oint \frac{\mathrm{d}\boldsymbol{\Omega}}{4\pi}\frac{\Lambda^*(\boldsymbol{k})}{\eta_I(\boldsymbol{k})^+}\mathrm{Re}\left[b_i(0,\boldsymbol{k})\right]. \tag{3.122}$$

Putting (3.120) and (3.121) into the radiative rates (3.39) of $\boldsymbol{\mathcal{L}}$, one obtains a nonlinear system of equations since the quantities bilinear with respect to the density matrix appear,

$$J^0_0(\alpha\beta)\rho_j = J^0_0(\alpha\beta)^+\rho_j + \sum_{\bar{i}} L_{\alpha\beta\bar{i}}(\rho^{\bar{i}}\rho_j - \rho^+_{\bar{i}}\rho_j), \tag{3.123}$$

where ρ_j is a *lower* multipole of the $\alpha\beta$ transition. The term $\rho^{\bar{i}}\rho_j$ is a source of nonlinearity. Following Rybicki & Hummer (1992) and Trujillo Bueno (1999), we can linearize the equations by setting $\rho^{\bar{i}}\rho_j \to \rho^{\bar{i}}\rho^+_j$. The desired iterative scheme thus reads

$$J^0_0(\alpha\beta)\rho_j = J^0_0(\alpha\beta)^+\rho_j + \sum_{\bar{i}} L_{\alpha\beta\bar{i}}(\rho^{\bar{i}}\rho^+_j - \rho^+_{\bar{i}}\rho_j), \tag{3.124}$$

$$J^K_Q(\alpha\beta)\rho_j = J^K_Q(\alpha\beta)^+\rho_j \quad \text{if} \quad K > 0\,. \tag{3.125}$$

This scheme leads to a new guess for the density matrix multipoles from the old ones in rather general picture of atomic levels. The coefficients $L_{\alpha\beta\bar{i}}$ can be easily calculated from the known Λ^*-operator. The integrands of Eq. (3.122) are accumulated and integrated along the way of the formal solution for different $\boldsymbol{k}$'s. It is worth to say that the iterative scheme (3.124)–(3.125) is, in the limiting case of weak magnetic fields and in the multilevel picture of levels, numerically equivalent to the technique of Manso Sainz & Trujillo Bueno (2003a). In the case of negligible polarization it is equivalent to the full-preconditioning strategy of Rybicki & Hummer (1992) which is more general than the method for non-overlapping transitions discussed in Rybicki & Hummer (1991). Our scheme is more general than the previous works in the sense that it can also be used in the case of overlapping lines (such as in the case of fine structure of hydrogen) and for more general pictures of atomic levels (multiterm, multilevel with hyperfine splitting, or more general ones).

Calculation of $\Lambda^*(\boldsymbol{k})$

The advantage of using the diagonal approximate operator is that ESE remain local and it is easy to evaluate the expressions for $L_{\alpha\beta\bar{i}}$. This approach is especially advantageous for the multidimensional problems. Although other choices of Λ^* (such as a tridiagonal operator) can lead to improvement of the convergence rate, the use of multigrid methods makes these differences of secondary interest (Chapter 4).

The $\boldsymbol{\Lambda}$-matrix elements can be obtained during the formal solution of RTE. Since the Λ-operator used in our development is exactly the one used in the 1st kind theory, we can just use the expressions of Olson & Kunasz (1987) for $\Lambda^*(m,m) = \Lambda(m,m)$ which is the only element explicitly required in the solution. In our notation for FS at the point O, the diagonal element reads

$$\Lambda^*(m,m) = \psi_M \mathrm{e}^{-\Delta\tau_{MO}} + \psi_O\,. \tag{3.126}$$

Chapter 4

Nonlinear multigrid techniques for radiative transfer

4.1 Introduction

The Jacobi iteration developed in the preceding chapter is quite useful since it overcomes the main disadvantage of the lambda iteration algorithm, i.e., extremely slow propagation of the information throughout the optically thick atmosphere. However, efficiency of this approach declines rapidly with the increasing number of grid nodes. This problem becomes especially weighty in multi-dimensional applications but it is also of interest to study the more advanced techniques in the one-dimensional case (especially in the complicated models of the 2nd kind). This chapter describes a significant improvement of the convergence time by the use of the so-called *multigrid methods* (MG). This approach was applied in the previous decades in a wide range of applications of numerical linear algebra. Since it is straightforwardly applicable to the nonlinear problems it is also of great importance for the radiative transfer modeling. The numerical polarized radiative transfer in spectral lines achieved a great progress in recent years Steiner (1991); Auer et al. (1994); Fabiani Bendicho et al. (1997). However, the superior MG methods have not yet been systematically used in solar physics research. This chapter contains an extension of the unpolarized MG techniques developed in the past years to the general NLTE problem of the 2nd kind that was discussed in the previous chapter. This work has been partly published in Štěpán (2006) (from now on referred to as Paper III). This paper can also be found in Appendix E.

Outline of this chapter is as follows: In Section 4.2, I define a reference model problem which is used in the subsequent sections for the convergence analysis and demonstration of the NLTE effects on the emergent radiation. I recall a definition of the Euclidean norm that is used for measurement of the length of the formal vectors constructed from the density matrix components. The suitable quantities for an analysis of the error of the approximate solutions are then defined. It is demonstrated quantitatively that the Jacobi iteration process slows down significantly if the grid refinement increases. In the subsequent Section 4.3 a philosophy of the MG approach is presented along with a review of the existing applications in the field of unpolarized RT. A general description of the essential element of every MG method, the so-called coarse-grid correction, is presented in the later part of the section. Finally, the so-called restriction and prolongation operators are introduced into the density matrix framework. In Section 4.4, I describe a robust MG algorithm called Standard MG method. Furthermore, there is Section 4.5 containing a description of a superior MG method, the so-called Nested MG, saving approximately a half of the CPU time when compared to Standard MG. In the last Section 4.6, examples of the particular solutions of the NLTE problem are shown.

4.2 Measurement of convergence

4.2.1 The reference problem

For the studies of the convergence properties of the iterative methods, it is useful to introduce a *reference problem*. In this work, I consider a simple model of the *two-term atom* devoid of hyperfine structure (see Chapter 2). In the same time, this problem is complex enough for demonstration of interesting physical phenomena and requires implementation of all the numerical methods developed in this thesis. The lower atomic term will be ^{3}S and the upper term will be ^{3}P. Thus the lower term consists of one level with total angular momentum $J_\ell = 1$ and the upper term consists of the three fine-structure levels with the respective angular momenta $J_u = 0$, 1, and 2. Let us suppose that the fine structure of the upper term obeys the Landé interval rule with ζ_u defined in Eq. (2.27). The total number of density matrix multipoles is 90 (taking into account the Zeeman and level-crossing coherences). Both lower and upper terms can be polarized. The fine-structure splitting of the upper term can be related to the natural width of the levels by a dimensionless quantity (cf. Eq. (10.142) of Landi Degl'Innocenti & Landolfi 2004)

$$x = \frac{\zeta_u}{2\hbar A_{u\to\ell}}\,, \tag{4.1}$$

where $A_{u\to\ell}$ is an Einstein coefficient for spontaneous emission from the upper to the lower term. In the particular model used in this chapter it is $x = 0.5$. This means that fine-structure splitting of the upper term is comparable to the level widths.

The flat-spectrum approximation (see Subsection 2.5.4) is satisfied in all the following calculations due to sufficient Doppler broadening: The Doppler width

$$\Delta\lambda_\mathrm{D} = \lambda_\mathrm{line}\sqrt{\frac{2k_\mathrm{B}T}{m_\mathrm{atom}c^2}} \tag{4.2}$$

is set to be approximately 300-times the natural level width. Even in the case of maximum Zeeman splitting considered in this chapter, $\gamma = 6$ (cf. Eq. 2.37), the flat-spectrum approximation holds. In the present numerical solution, I only assume Doppler broadening of the line – natural broadening is ignored. The range of the magnetic field strength is chosen so that the upper term is mostly in the incomplete Paschen-Back effect regime. Magnetic field is supposed to be uniform in the atmosphere and *horizontal*, i.e., $\theta_B = 90°$ (see Figure 3.1). Even though the lower-level Hanle effect is naturally taken into account, the field strength is always strong enough to destroy the lower-level coherences in the examples below. In the assumed range of field strengths ($\gamma = 0.01$ to 6) the lower-level coherences are well relaxed since the lower-level relaxation time is much longer due to weak irradiation (see below). However, there is non-negligible amount of polarization contained in the lower term due to imbalance of the Zeeman sublevel populations (in the atomic frame; cf. the effect of depopulation pumping, Trujillo Bueno 2001).

The plan-parallel atmosphere considered in the reference problem is *semi-infinite* with zero illumination on the surface. The atmosphere is *isothermal* and the photon destruction probability (generalized to the two-term atom) is set to

$$\epsilon = \frac{C_S^{(0)}(J_\ell \leftarrow J_u)}{A_{u\to\ell}} = 10^{-4}\,. \tag{4.3}$$

This value is constant for the whole atmosphere. No depolarization collisions are assumed. Density of the atmosphere increases exponentially with z.

Radiation in the atmosphere is very weak. In the deep parts of the atmosphere the average number of photons per mode at the line central frequency (cf. definition (10.62) of Landi Degl'Innocenti & Landolfi 2004) is of the order of 10^{-4}. In the parts of the atmosphere close to the surface it is still smaller. Even though the stimulated emission effects are negligible, they are incorporated in the NLTE equations.

There is no background continuum radiation assumed in the reference problem.

4.2.2 Numerical errors

The norm

In order to measure the convergence properties of the method, one has to define a *norm* of the approximate solutions. The norm can be used for a quantitative measurement of the differences between the complex formal $(\mathbb{N} \times \mathsf{N})$-vectors in the solution space. In this work, I adopt the *Euclidean norm*,

$$\|\boldsymbol{x}\| = \frac{1}{\mathbb{N}} \sqrt{\sum_{i=1}^{\mathbb{N}} |x_i|^2}\,, \tag{4.4}$$

normalized with respect to the number of grid nodes, $\mathbb{N}$.

This norm has its advantages and disadvantages for the NLTE polarized problems. The advantage is that it can be easily evaluated and it is unique for the density matrix as a whole. On the other hand, the last property is also a disadvantage since it is clear that the norm $\|\boldsymbol{\rho}\|$ will be dominated by *populations* mostly from the regions close to the local thermodynamical equilibrium which are not particularly interesting (at least in the reference problem under consideration). These populations have usually much larger values than the coherences and populations close to the surface. However, this is not a big constraint for the purposes of measuring *convergence errors*, i.e., the differences between two approximate solutions $\|\boldsymbol{\rho} - \boldsymbol{\rho}'\|$: The equilibrium populations in the deep layers do not change between iterations hence do not contribute to the error. A similar conclusion can be made concerning the so-called truncation residual vector introduced below.

Measuring the convergence

From now on, grids with different finesse will be used. The individual grids will be identified by a lower index (G_ℓ). Similarly for other quantities related to a given grid: $\mathbb{N}_\ell$, $\boldsymbol{\rho}_\ell^{(k)}$, $\boldsymbol{\rho}_\ell$ etc.

There are three quantities usually used for an analysis of the convergence properties of the iterative solver (cf. Auer et al. 1994; Trujillo Bueno & Fabiani Bendicho 1995). These are *relative change* $\left\|\boldsymbol{\rho}_\ell^{(k)} - \boldsymbol{\rho}_\ell^{(k-1)}\right\|$, *convergence error* $\left\|\boldsymbol{\rho}_\ell^{(k)} - \boldsymbol{\rho}_\ell^{(\infty)}\right\|$, and *true error* $\left\|\boldsymbol{\rho}_\ell^{(k)} - \boldsymbol{\rho}_\infty^{(\infty)}\right\|$. These quantities are related to a given iteration k and the grid G_ℓ. They express, respectively, the difference between two successive iterations, the difference between the iteration k and the fully converged solution, and the difference between the iteration k and the exact solution on the grid with infinitely small spacing of grid nodes. In practice, one usually deals with following *relative* quantities:*relative change*

$$R_{\mathrm{c}}(k,\ell) = \frac{\left\|\boldsymbol{\rho}_\ell^{(k)} - \boldsymbol{\rho}_\ell^{(k-1)}\right\|}{\left\|\boldsymbol{\rho}_\ell^{(k)}\right\|}\,, \tag{4.5}$$

relative convergence error

$$C_{\mathrm{e}}(k,\ell) = \frac{\left\| \boldsymbol{\rho}_\ell^{(k)} - \boldsymbol{\rho}_\ell^{(\infty)} \right\|}{\left\| \boldsymbol{\rho}_\ell^{(\infty)} \right\|} , \tag{4.6}$$

and *relative true error*

$$T_{\mathrm{e}}(k,\ell) = \frac{\left\| \boldsymbol{\rho}_\ell^{(k)} - \boldsymbol{\rho}_\infty^{(\infty)} \right\|}{\left\| \boldsymbol{\rho}_\infty^{(\infty)} \right\|} . \tag{4.7}$$

Since the exact solution $\boldsymbol{\rho}_\infty^{(\infty)}$ is not known, it will be approximated by the solution calculated using the grid with very fine refinement of 23.4 points per decade (PPD). In the following, I will also use the notation $\boldsymbol{\rho}_\ell \equiv \boldsymbol{\rho}_\ell^{(\infty)}$ for the fully converged solutions.

Worth to say that different definitions can be used for norm (4.4) and the quantities (4.5)–(4.7). One often uses the α-norm to define the quantities above as

$$\tilde{R}_{\mathrm{c}} = \frac{1}{\mathbb{N}_\ell} \sqrt[\alpha]{\sum_{i=1}^{\mathbb{N}_\ell} \left| \frac{(\boldsymbol{\rho}_\ell^{(k)})_i - (\boldsymbol{\rho}_\ell^{(k-1)})_i}{(\boldsymbol{\rho}_\ell^{(k)})_i} \right|^\alpha} , \tag{4.8}$$

and analogously for the other quantities (see for instance Auer et al. 1994; Fabiani Bendicho et al. 1997). Such quantities, especially if $\alpha = \infty$, provide a good information on actual error of the individual *components* of the solution. In the models of the 1st kind, all the level populations are larger than zero. In contrast, it is common in the models of the 2nd kind that several elements of the density matrix are zero; either identically across the medium (due to a particular symmetry of the problem) or accidentally. It is always possible to determine the identically vanishing atomic multipoles and remove them from the model. For example, all ρ^1_q components would identically vanish in a cylindrically symmetric atmosphere in the Hanle effect regime if it is not illuminated by a circularly polarized radiation (cf. Manso Sainz & Trujillo Bueno 2003a). On the other hand, such removal can be more complicated if the element vanishes (or nearly vanishes) only in several nodes or in several iterations. This problem may arise in the large optical depths where the radiation becomes more or less isotropic and consequently the coherences become extremely small. Also in the regions where a density matrix multipole changes its sign the value of $|\rho_i|$ may become extremely small and the quantities $|\Delta\rho_i|/|\rho_i|$ behave unpredictably due to numerical perturbations. The definitions (4.4)–(4.7) guarantee a smooth variation of the relative change and the relative errors. A demonstration of typical convergence behavior of the ALI technique is shown in Figure 4.2.

Taking into account the asymptotic behavior of the iterative process discussed in Subsection 3.2.2 and the definitions (4.5) and (4.6), one can show (cf. Auer et al. 1994) that, in the asymptotic limit, the convergence error and the relative change are closely related by the expression

$$C_{\mathrm{e}} \approx R_{\mathrm{c}} \frac{\varrho}{1-\varrho} . \tag{4.9}$$

Moreover, if the estimation is close to the correct solution, one gets (cf. Trujillo Bueno & Fabiani Bendicho 1995)

$$\varrho = \lim_{k\to\infty} \frac{R_{\mathrm{c}}^{(k+1)}}{R_{\mathrm{c}}^{(k)}} = \lim_{k\to\infty} \frac{C_{\mathrm{e}}^{(k+1)}}{C_{\mathrm{e}}^{(k)}} , \tag{4.10}$$

hence the spectral radius of the method can be estimated even from the slope of R_{c} during the iterative process. It is important to note that these expressions are applicable regardless the particular definition of the norm and the errors (4.5)–(4.7).

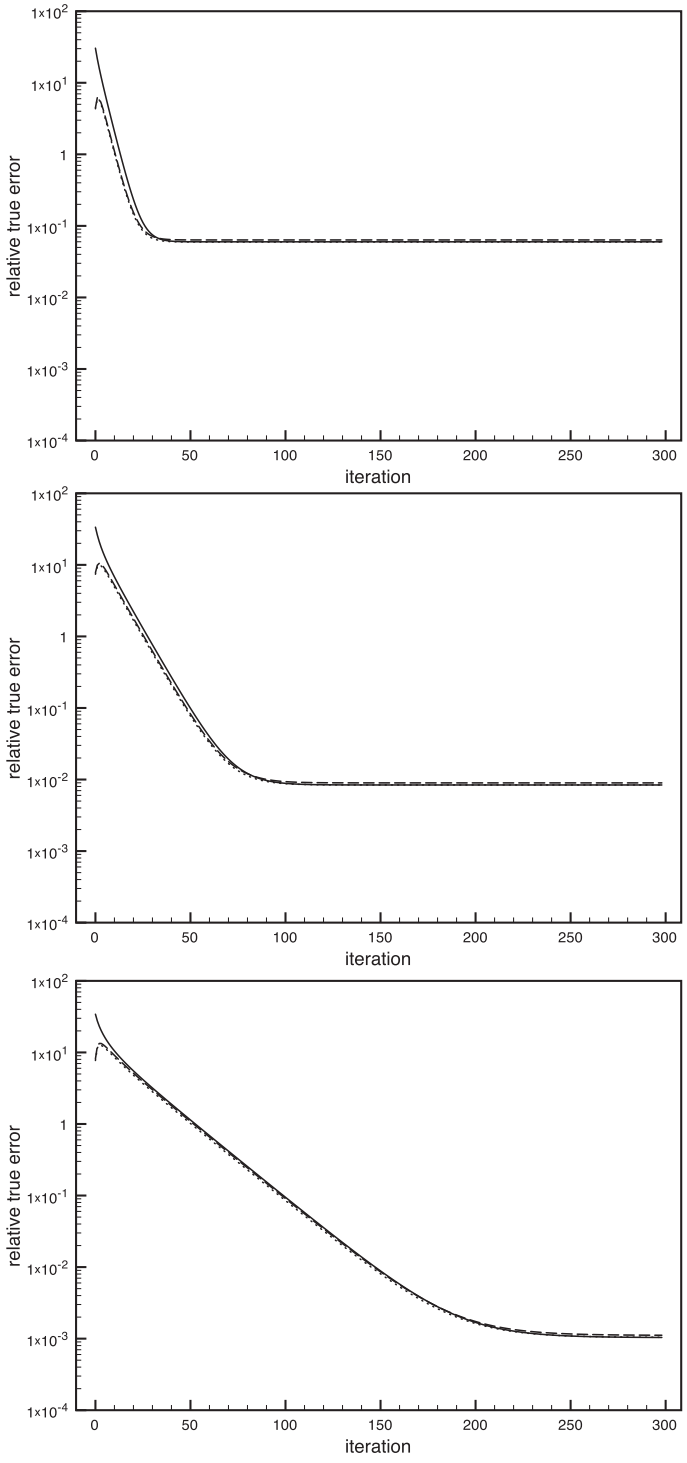

Figure 4.1: Variation of the relative true error with the iteration number of the *surface value* of the upper term invariants $\rho^0(J = 1, J' = 1)$ (solid line), $\rho^2(J = 1, J' = 1)$ (dashed line), and $\rho^3(J = 1, J' = 2)$ (dotted line). From up to bottom, the panels show the error variation on the grids with 3, 5.9, and 11.7 PPD (see Subection 4.3.1). The plateaus in the later iterations indicate that the truncation error is reached. The convergence is slower for the grids with smaller meshes. The error of solution in the finest grid is about 0.1% and it is almost the same for both population and coherence multipoles. As an initialization of the model, I always use the LTE populations of the levels.

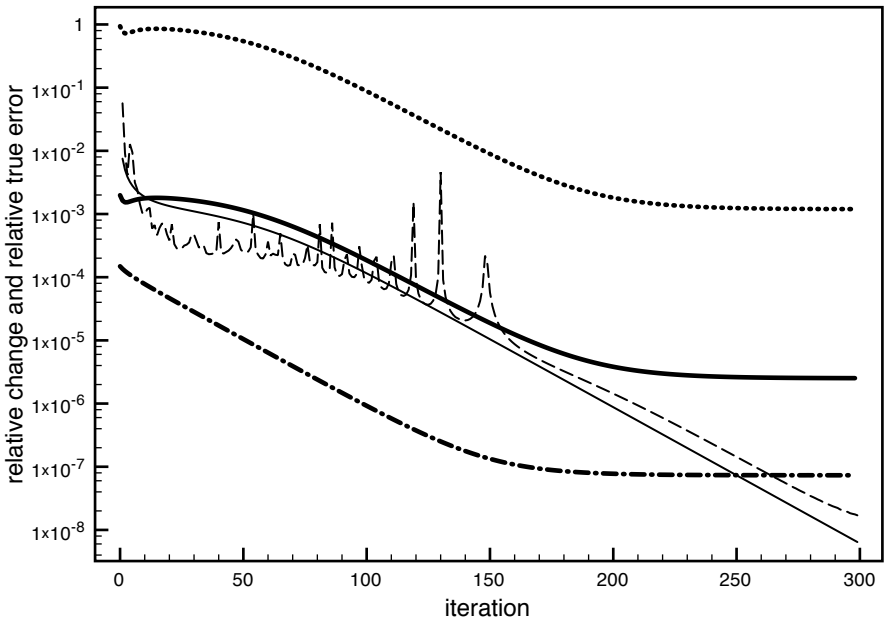

Figure 4.2: A comparison of different quantities describing the convergence process in the grid with 11.7 points per decade. The *thin* lines show the relative change of populations (solid line) and coherences (dashed line) of the atmosphere calculated using the Euclidean norm applied to the $|\Delta\rho_i|/|\rho_i|$ quantities (see text for details). The lower cut-off for coherences has been set to 10^{-4} multiple of the smallest population multipole to avoid divergencies. The *thick* lines show *true relative error* calculated using Eq. (4.7): The dash-dotted line corresponds to population multipoles, the dotted line corresponds to the multipoles of higher rank, and the solid line corresponds to the error of all multipoles.

4.3 Introduction to multigrid methods

4.3.1 Multiple grids

As it is clear from FS of RTE (3.85), radiative coupling of different points in the atmosphere decreases exponentially with their optical distance. In large optical depths of the atmosphere, the optical distance between two successive grid nodes is typically much higher than 1. The $\mathbf{\Lambda}$-matrix becomes strongly diagonally dominated in these regions and the convergence of the simple lambda-iteration process is quite bad. The use of approximate local operator Λ^* in the Jacobi method does analytically eliminate the dominating local photon scatterings and lets the wing photons to transfer the information effectively. Convergence of the Jacobi method in such nodes is very good. On the other hand, in the optically thin regions close to the surface, the off-diagonal elements of $\mathbf{\Lambda}$ become more important. The local scatterings become less crucial and the convergence deteriorates. The smaller is the grid spacing the stronger is the effect of the neighboring nodes and the slower is the convergence. This is the reason why Jacobi iteration convergence decreases significantly with increasing $\mathbb{N}$. In fact, Jacobi iteration acts as a *smoothing* procedure: It mostly averages the error among the neighboring points (see Figure 4.4), i.e., the *high-frequency errors*. On the other hand, reduction of the *low-frequency errors* is poor (Briggs et al. 2000). The observation that Jacobi iteration is efficient in smoothing the errors is advantageously applied in the MG technique below.

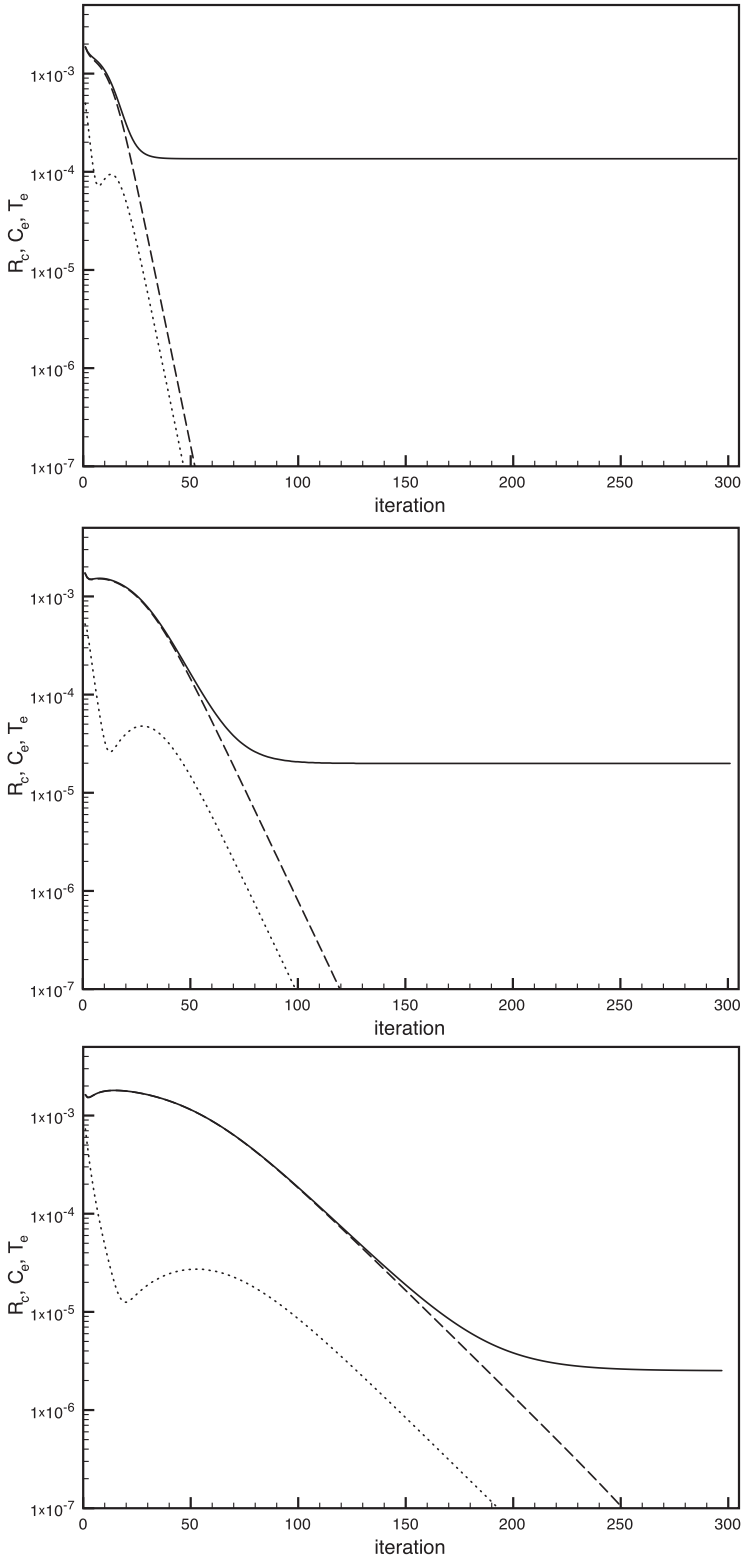

Figure 4.3: Evolution of $R_{\rm c}$ (dotted line), $C_{\rm e}$ (dashed line), and $T_{\rm e}$ (solid line) in the Jacobi iteration on the same grids as in Figure 4.1. The convergence radius of these models is, respectively, $\varrho_{3\,\rm PPD} = 0.78$, and $\varrho_{5.9\,\rm PPD} = 0.90$, $\varrho_{11.7\,\rm PPD} = 0.95$.

Progress in the multigrid techniques

The MG approach is based on *using the coarse grids to reduce the low frequencies* and the *fine grids to smooth the high-frequency components* (see Figure 4.5). Such a process can

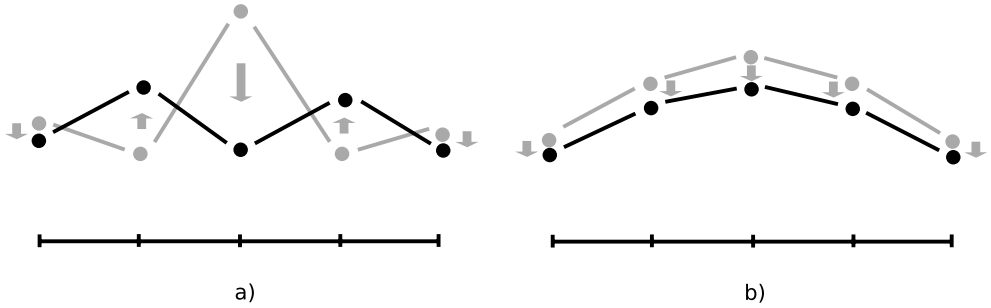

Figure 4.4: Jacobi error smoothing process. High-frequency error components are usually reduced quite effectively (a). On the other hand, the low frequencies survive quite well (b). It is shown in the numerical linear algebra that Jacobi acts more or less like an *error averaging process* in which the error e_i of solution in grid node i is smoothed to $\frac{1}{2}(e_{i-1} + e_{i+1})$ in the successive iteration (Briggs et al. 2000). The terms "low frequency" and "high frequency" is always relative to the mesh of a given grid.

lead to the asymptotically *optimal CPU time demands* of $O(\mathbb{N})$ in the number of grid nodes. The MG methods have been originally developed in order to get an efficient solver for the elliptic boundary value problems (Brandt 1977). Later the MG strategy has been used for a solution of the Fredholm integral equations of the second kind. The strong points of the MG methods are their generality and the possibility of solving *nonlinear* problems in the so-called full approximation storage (see the extensive monograph of Hackbush 1985). The first application of MG to the RT problems has been presented by the pioneering work of Steiner (1991) who used the MG strategy to solve the two-level unpolarized problem and showed the potential of this approach. This potential was used by implementation of these methods into the massively parallel *three-dimensional two-level atom* code of Väth (1994). The use of multiple grids (but not a MG method) in the so-called grid-doubling strategy has been applied to the nonlinear *multilevel* problems by Auer et al. (1994). This method has been further extended to the full MG technique by Fabiani Bendicho et al. (1997), who used the GS iteration as the smoothing method because it is more efficient than Jacobi (see Trujillo Bueno & Fabiani Bendicho 1995). These methods have been recently implemented in the models for studies of solar prominences by Léger et al. (2007). An extension to the case of one-dimensional *polarized* multilevel transfer in hydrogen lines of the non-magnetic atmosphere has been presented in Paper III.

Although the MG algorithms are of particular interest for multidimensional problems in which, typically, $\mathbb{N} \gtrsim 10^4$, an improvement of the convergence rate thanks to multigrid's $O(\mathbb{N})$ behavior is not only important in the asymptotic limit $\mathbb{N} \to \infty$. It also leads to a significant improvement of the solution time in one-dimensional problems with only $\mathbb{N} \sim 100$.

Multigrid for the one-dimensional RT

As indicated above, the MG methods are built on the advantageous use of the differently coarsened grids. In this work, I use the grids G_1, G_2, ..., $G_{\mathbb{M}}$, where $\mathbb{M}$ denotes the index of the *finest* grid whereas G_1 denotes the *coarsest* grid. The associated mesh sizes are h_1, h_2, ..., $h_{\mathbb{M}}$. The node spacing is constant for each grid and it is always $h_{\ell+1} = h_\ell/2$.[1] Since the density of the atmosphere increases exponentially with z, the spacing of the nodes in *optical depth scale* also increases exponentially with depth. In the problem under consideration, the line-center optical depth τ varies between 10^{-4} and 10^7, i.e., in the range of 11 decades of $\log_{10}\tau$.

[1]These conditions are not necessary. However, they are useful in most cases and straightforwardly generalized if necessary.

Figure 4.5: Philosophy of the MG technique. The picture of Josef Lada can be used for illustration of the effect of a different mesh size. A big brush can be used for efficient painting of large areas of a same color (panel 1). Corrections to this coarse painting can be done using smaller brushes until the desired accuracy is achieved (panels 2 to 4). The use of big brushes (coarse grids) is most efficient for finding the low-freqencies of the solution whereas the tinny brushes (fine grids) are used to find the small-scale corrections. (Note that the analogy is not perfect: In the MG methods one always uses the coarse grids to correct the solution in the fine-grid. That would correspond to repainting the detailed picture by a big brush...)

This number of grid nodes, $\mathbb{N}_\ell$, should vary from the lowest physically relevant approximation (typically 3 PPD) to a number leading to sufficiently precise predictions (typically 10 PPD). In the reference problem of this chapter, I usually use 3 grids with $\mathbb{N}_1 = 33$ (3 PPD) and $\mathbb{N}_3 = 129$ (11.7 PPD). The coarsest grid that has been considered in tests has 17 grid nodes (i.e., 1.5 PPD what is on the physical limits of the radiative transfer models). On the other hand, an extremely fine grid with $\mathbb{N} = 257$ (i.e., 23 PPD) has been used for estimation of the truncation error of the coarser grids and calculation of the Stokes profiles/Hanle diagrams in Section 4.6.

For discretization of the spatial directions $\mathbf{\Omega}$ I used 22 directions for the polar angle $\theta \in [0, \pi]$ and 28 directions in the azimuthal angle $\chi \in [0, 2\pi)$. The total number of ray directions considered in the model is thus 616 (see Subsection 3.2.1).

The wavelength quadrature of in the line profile Φ is always such that the constant spacing of the discrete wavelengths is $0.2\Delta\lambda_\mathrm{D}$.

4.3.2 Coarse grid correction

The more or less intuitive principles discussed in the previous subsection can be formulated in a more rigorous way (see also Hackbush 1985; Fabiani Bendicho et al. 1997). The discrete NLTE problem (3.4) can be formulated on each grid G_ℓ. Let us call G_ℓ the *fine grid* for the moment. Since only *estimates* $\boldsymbol{\mathcal{L}}_\ell^{(k)}$ are known in every successive iteration k, the problem to be solved reads

$$\boldsymbol{\mathcal{L}}_\ell^{(k)} \boldsymbol{\rho}_\ell^{(k+1)} = \boldsymbol{f}_\ell \,, \tag{4.11}$$

where $\boldsymbol{\mathcal{L}}_\ell^{(k)}$ is the matrix calculated from the density matrix $\boldsymbol{\rho}_\ell^{(k)}$ obtained in the *previous iteration* k (cf. Eq. 3.28). Using the approximate lambda operator technique from the previous chapter, one can preconditionate the system Eq. (4.11),

$$\boldsymbol{\mathcal{L}}_\ell'^{(k)} \boldsymbol{\rho}_\ell^{(k+1)} = \boldsymbol{f}_\ell \,, \tag{4.12}$$

from which one gets a new guess for the density matrix, $\boldsymbol{\rho}_\ell^{(k+1)}$.

A suitable measure of quality of a given approximation can be expressed in the form of residuum (cf. Eq. 3.8)

$$\boldsymbol{\mathcal{L}}_\ell \boldsymbol{\rho}_\ell - \boldsymbol{\mathcal{L}}_\ell^{(k)} \boldsymbol{\rho}_\ell^{(k)} = \boldsymbol{\mathcal{L}}_\ell (\boldsymbol{\rho}_\ell^{(k)} + \boldsymbol{e}_\ell^{(k)}) - \boldsymbol{\mathcal{L}}_\ell^{(k)} \boldsymbol{\rho}_\ell^{(k)} = \boldsymbol{f}_\ell - \boldsymbol{\mathcal{L}}_\ell^{(k)} \boldsymbol{\rho}_\ell^{(k)} = \boldsymbol{r}_\ell^{(k)} \,, \tag{4.13}$$

where

$$\boldsymbol{\rho}_\ell = \boldsymbol{\rho}_\ell^{(k)} + \boldsymbol{e}_\ell^{(k)} \,. \tag{4.14}$$

is the desired correct solution on G_ℓ. Residuum is the quantity of crucial importance since it contains an information about the error of solution. Note that since the problem is nonlinear, we cannot determine the *exact* value of residuum, $\boldsymbol{f}_\ell - \boldsymbol{\mathcal{L}}_\ell \boldsymbol{\rho}_\ell^{(k)}$, only the estimate given by Eq. (4.13) is available in every iteration. However, it is a good approximation if $\boldsymbol{\rho}_\ell^{(k)}$ is close to $\boldsymbol{\rho}_\ell$.

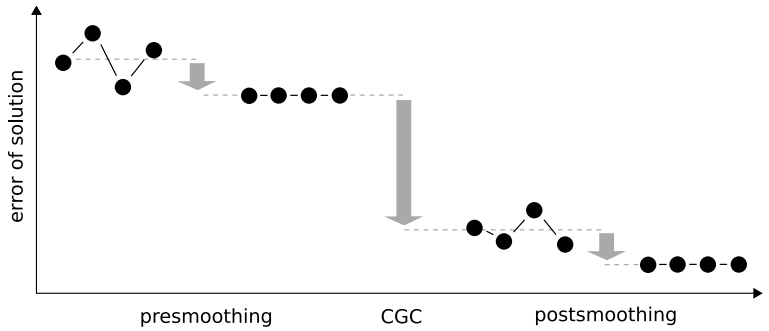

Figure 4.6: The effect of coarse grid correction. High-frequency components of the error are reduced by a few presmoothing Jacobi iterations. CGC reduces significantly the low-frequency error components but introduces a further noise into the fine-grid solution due to the interpolation process. This noise is swept out by the additional postsmoothing ALI iterations.

As stated above, Jacobi iteration smoothes effectively the high-frequency errors. In the following, the procedure of successive application of several Jacobi iterations will be symbolically represented by the *smoothing* (or *sweeping*) *operator* $\mathscr{S}$ acting on the formal density matrix vector $\boldsymbol{\rho}_\ell^{(k)}$. At this stage of solution, one uses ν_1 ($\nu_1 = 1, 2, 3, \dots$) of the so-called *presmoothing* iterations. This process can be represented by action of the $\mathscr{S}_{\nu_1}$ operator. Due to action of this operator the residuum becomes smooth, i.e., there are no high-frequecy Fourier components of the residuum in G_ℓ. The remaining low-frequency components can also be reduced via the coarser grids: The problem (4.13) can be transfered to the coarse grid $G_{\ell-1}$ without loss of accuracy,

$$\boldsymbol{\mathcal{L}}_{\ell-1} \boldsymbol{\rho}_{\ell-1} - \boldsymbol{\mathcal{L}}_{\ell-1}^{(k)} \mathscr{R}[\boldsymbol{\rho}_\ell^{(k)}] = \mathscr{R}[\boldsymbol{r}_\ell^{(k)}] \,, \tag{4.15}$$

where $\mathscr{R}$ is the so-called *restriction operator* mapping the vectors from the fine grid to the coarse grid,

$$\mathscr{R} : \; \boldsymbol{x}_\ell \mapsto \boldsymbol{x}_{\ell-1} \,. \tag{4.16}$$

The matrix $\boldsymbol{\mathcal{L}}_{\ell-1}^{(k)}$ has to be determined from $\mathscr{R}[\boldsymbol{\rho}_\ell^{(k)}]$ using an additional FS of in $G_{\ell-1}$ (see Algorithm 4.1). Eq. (4.15) is the so-called *coarse grid equation* (CGE, cf. Hackbush 1985) that can be used for estimation of the fine-grid error $\boldsymbol{e}_\ell^{(k)}$. Eq. (4.15) can be rewritten in the standard form of the (quasi)linear equation

$$\boldsymbol{\mathcal{L}}_{\ell-1} \boldsymbol{\rho}_{\ell-1} = \boldsymbol{f}_{\ell-1} \,. \tag{4.17}$$

Solution of this equation is equivalent to the solution of the NLTE problem on $G_{\ell-1}$ with a *modified right-hand side* $\boldsymbol{f}_{\ell-1}$. For this reason it is important to keep in mind that $\boldsymbol{\rho}_{\ell-1}$ is *not*

equivalent to the normal NLTE solution formulated on $G_{\ell-1}$. From Eq. (4.17) the vector $\boldsymbol{\rho}_{\ell-1}$ can be found and the correction

$$\Delta\boldsymbol{\rho}_{\ell-1} = \boldsymbol{\rho}_{\ell-1} - \mathscr{R}[\boldsymbol{\rho}_{\ell-1}^{(k)}] \tag{4.18}$$

can be *projected onto the fine grid* by the so-called *prolongation operator*,

$$\mathscr{P} : \ \boldsymbol{x}_\ell \mapsto \boldsymbol{x}_{\ell+1} \,. \tag{4.19}$$

It is obvious that $\mathscr{P}[\Delta\boldsymbol{\rho}_{\ell-1}]$ gives the low-frequency correction to the error $\boldsymbol{e}_\ell^{(k)}$,

$$\boldsymbol{e}_\ell^{(k)} \approx \mathscr{P}[\Delta\boldsymbol{\rho}_{\ell-1}] \,, \tag{4.20}$$

hence we arrive at the new guess for $\boldsymbol{\rho}_\ell$:

$$\boldsymbol{\rho}_\ell^{(k+1)} = \boldsymbol{\rho}_\ell^{(k)} + \mathscr{P}[\Delta\boldsymbol{\rho}_{\ell-1}] \,. \tag{4.21}$$

Finally, the high frequency corrections must be found by use of the so-called *postsmoothing* $\mathscr{S}_{\nu_2}$ in the fine grid. This is because the interpolation process introduced an additional noise into the fine-grid solution. The number of postsmoothing iterations will be denoted by ν_2. The process of solution of the NLTE problem by correcting the long-wavelength errors by the coarse grid is usually called the *coarse grid correction* (CGC, see Figure 4.6) or *full approximation storage (FAS)* (Brandt 1977).

repeat
- presmooth $\boldsymbol{\rho}_\ell^{(k-\nu_1)}$ by ν_1 Jacobi iterations, $\mathscr{S}_{\nu_1} \rightarrow \boldsymbol{\rho}_\ell^{(k)}$
- calculate one more FS to get $\boldsymbol{\mathcal{L}}_\ell^{(k)}$ consistent with $\boldsymbol{\rho}_\ell^{(k)}$
- calculate residuum $\boldsymbol{r}_\ell^{(k)} := \boldsymbol{f}_\ell - \boldsymbol{\mathcal{L}}_\ell^{(k)}\boldsymbol{\rho}_\ell^{(k)}$
- restrict $\boldsymbol{r}_\ell^{(k)}$ to $G_{\ell-1} \rightarrow \mathscr{R}[\boldsymbol{r}_\ell^{(k)}]$
- restrict $\boldsymbol{\rho}_\ell^{(k)}$ to $G_{\ell-1} \rightarrow \mathscr{R}[\boldsymbol{\rho}_\ell^{(k)}]$
- restrict $\boldsymbol{f}_\ell$ to $G_{\ell-1} \rightarrow \mathscr{R}[\boldsymbol{f}_\ell]$
- calculate FS in $G_{\ell-1}$ consistent with $\mathscr{R}[\boldsymbol{\rho}_\ell^{(k)}] \rightarrow \boldsymbol{\mathcal{L}}_{\ell-1}^{(k)}$
- get $\boldsymbol{f}_{\ell-1}$ and $\boldsymbol{\tau}_{\ell-1}$ form Eq. (4.22)
- solve CGE $\rightarrow \boldsymbol{\rho}_{\ell-1}$
- calculate $\Delta\boldsymbol{\rho}_{\ell-1}$ from Eq. (4.18)
- project these corrections onto $G_\ell \rightarrow \boldsymbol{\rho}_\ell^{(k+1)}$
- perform ν_2 postsmoothing iterations, $\mathscr{S}_{\nu_2} \rightarrow \boldsymbol{\rho}_\ell^{(k+1+\nu_2)}$
- $\|\boldsymbol{\tau}_\ell\| := \frac{1}{3}\,\|\boldsymbol{\tau}_{\ell-1}\|$
- calculate the residuum $\boldsymbol{r}_\ell := \boldsymbol{f}_\ell - \boldsymbol{\mathcal{L}}_\ell^{(k+\nu_2-1)}\boldsymbol{\rho}_\ell^{(k+\nu_2-1)}$

until $\|\boldsymbol{r}_\ell\| < \|\boldsymbol{\tau}_\ell\|$

Algorithm 4.1: Coarse grid correction.

From Eqs. (4.13), (4.15), and (4.17) one obtains for the right-hand side of CGE,

$$\boldsymbol{f}_{\ell-1} = \mathscr{R}[\boldsymbol{f}_\ell] + \boldsymbol{\mathcal{L}}_{\ell-1}^{(k)}\mathscr{R}[\boldsymbol{\rho}_\ell^{(k)}] - \mathscr{R}[\boldsymbol{\mathcal{L}}_\ell^{(k)}\boldsymbol{\rho}_\ell^{(k)}] = \mathscr{R}[\boldsymbol{f}_\ell] + \boldsymbol{\tau}_{\ell-1} \,. \tag{4.22}$$

$\boldsymbol{\tau}_{\ell-1}$ has a direct numerical interpretation. It is the so-called *relative truncation error* (or relative truncation residual) of $G_{\ell-1}$ with respect to G_ℓ (Press et al. 1994). As already mentioned in Section 3.2, solution of the problem on a given grid is always affected by a truncation error. The

presence of $\boldsymbol{\tau}_{\ell-1}$ guarantees that the solution on the coarse grid will have the same precision as the fine-grid solution.[2] In terms of the analogy in Figure 4.5 one would say that $\boldsymbol{\tau}_{\ell-1}$ guarantees that colors in the coarser paintings correspond to the averaged colors of the fine-brush painting. If the truncation error is ignored then it would lead to systematically darker/brighter colors of the coarse spots. Such a ground-color would be useless since it would need to be completely repainted by the fine brush in the same way the low-frequency errors would need to be corrected in the fine grids.[3] Algorithm 4.1 summarizes the CGC process.

A crucial observation is now the following: Time required to solve the RT problem on the *fine* grid is *constant*, i.e., there are only few $\nu_1+\nu_2$ sweeps necessary to reduce the high-frequency errors. The CPU time required is thus proportional to the size $\mathbb{N}_\ell$ of the problem. Evidently, the time required for solution of CGE can be significant but it will turn out in Section 4.4 that the conclusion on $O(\mathbb{N}_\ell)$ behavior of MG does not have to be modified if clever approach is used.

Restriction and prolongation operators

Mapping of the solution formal vectors between the fine and coarse grids is done by use of the restriction and prolongation operators. For the applications in the numerical radiative transfer a suitable choice of these operators is as follows.

The most straightforward type of the restriction operator is a direct injection of the density matrix from the fine-grid nodes to the corresponding coarse-grid nodes. A better and more accurate choice for $\mathscr{R}$ is the *adjoint to the linear interpolation operator*. This operator is used in our implementation. For a discussion of this restriction operator see (Press et al. 1994).

The lowest-order prolongation operator would use a linear interpolation of the coarse grid to the fine grid. Again, it is more accurate to use a higher order projection in the RT applications. A common choice is the *cubic centered interpolation* operator (see Press et al. 1994; Hackbush 1985, for detals).

Application of the $\mathscr{R}$ and $\mathscr{P}$ operators is rather efficient. It requires $O(\mathbb{N}_\ell \mathsf{N})$ operations and it is much faster than solution of ESE which is a $O(\mathbb{N}_\ell \mathsf{N}^3)$ process.

Consistency of density matrix

Processing $\mathscr{R}$ and $\mathscr{P}$ involves construction of the linear combinations of density matrices. Let, in the notation of Eq. (2.4), $\rho_{mn}(i)$ be the density matrix coherence in the grid node i. Both $\mathscr{R}$ and $\mathscr{P}$ are supposed to be linear operators mixing the density matrices of different grid nodes into a new density matrix of another grid,

$$\tilde{\rho}_{mn} = \sum_i c_i \rho_{mn}(i)\,. \tag{4.23}$$

It is easy to show that both normalization, $\mathrm{Tr}\,\tilde{\rho} = 1$, and the Hermiticity, $\tilde{\rho}^*_{mn} = \tilde{\rho}_{nm}$, are satisfied if $\sum_i c_i = 1$ and c_i's are real. Both conditions are satisfied by the operators described above. The MG process thus does not violate the consistency of the solution.

[2] In the sense that a value of the density matrix elements in both grids will be approximately the same. The coarse grid can describe the same solution as the fine grid with exception of the highest frequencies due to the Nyquist theorem.

[3] However, the analogy is not perfect. The coarse grids can be advantageously used for finding an *initial guess* of the fine-grid the solution. See Section 4.5 for details.

Stopping criterion

It is pointless to iterate the model anymore if the error of solution is dominated by the truncation error. A suitable measure of the error is the residuum vector: It is only worth to iterate until

$$\|\boldsymbol{r}_\ell\| < \|\boldsymbol{\tau}_\ell\| \ . \tag{4.24}$$

It is difficult to estimate the truncation error in the common ALI models with one grid only. However, if multiple grids are used, the relative truncation error of the coarse grid, $\boldsymbol{\tau}_{\ell-1}$, can be used for estimation of the fine-grid truncation error. It can be shown (Press et al. 1994) that for the method of second order and for the mesh-size relation $h_\ell = 2h_{\ell+1}$ the fine-grid truncation error can be approximated by

$$\|\boldsymbol{\tau}_\ell\| \approx \frac{1}{3} \|\boldsymbol{\tau}_{\ell-1}\| \ , \tag{4.25}$$

(cf. also Fabiani Bendicho et al. 1997). This general criterion should be used for verification of the CGC after performing the postsmoothing iterations. If the criterion is not satisfied one should run another CGC for the finest grid. For a different criterion based on an estimation of the relative truncation error T_e see Auer et al. (1994).

4.4 Standard multigrid method

There is a number of approaches to the MG philosophy. The so-called *Standard MG* is a natural generalization of the CGC described in the preceding section.

One easily realizes that the coarse-grid equation can be solved *recursively*: A solution of Eq. (4.17) can also be found using CGC with $G_{\ell-2}$ and so forth. Since the presmoothing and postsmoothing Jacobi iterations always cost a constant CPU time, the whole process remains $O(\mathbb{N}_\ell)$. The Jacobi sweeps are only used to find a solution in the coarsest grid G_1. Since there is only small number of grid nodes in this grid, the time to find this solution is quite small.

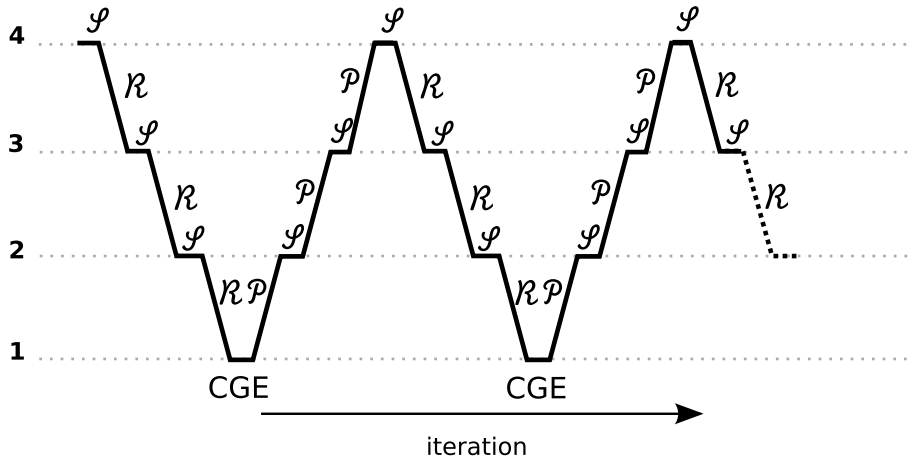

Figure 4.7: Standard MG iterations. The V-cycles are drawn for the case of 4 grids. As mentioned in the text, $\mathscr{S}$, $\mathscr{R}$, and $\mathscr{P}$ denote, respectively, the Jacobi smoothing procedure, restriction, and prolongation operators. In the lowest grid, the coarse grid equation must always be solved with a sufficient accuracy.

It is not necessary to find an exact solution on each grid within just one Standard MG iteration from $G_\mathbb{M}$ to G_1 and back. Instead, few of these so-called *V-cycles* (see Figure 4.7)

can be employed to find the successive approximations to the solution on $G_{\mathbb{M}}$. The solution on a given grid G_ℓ can also be obtained by a few CGC iterations before the corrections are projected onto $G_{\ell+1}$. In this way, one can develop the more complicated iterative shemes (V-cycles, W-cycles, etc.; see Hackbush 1985; Fabiani Bendicho et al. 1997). In this work I only consider the V-cycle scheme. The extension of CGC to the Standard MG scheme is described in Algorithm 4.2.

initialize LTE populations on $G_{\mathbb{M}}$
repeat
  if $\ell = 1$ **then**
    solve CGE by $\mathscr{S}$
    exit the function
  else
    presmooth $\boldsymbol{\rho}_\ell^{(k-\nu_1)}$ by ν_1 Jacobi iterations, $\mathscr{S}_{\nu_1} \rightarrow \boldsymbol{\rho}_\ell^{(k)}$
    calculate one more FS to get $\boldsymbol{\mathcal{L}}_\ell^{(k)}$ consistent with $\boldsymbol{\rho}_\ell^{(k)}$
    calculate residuum $\boldsymbol{r}_\ell^{(k)} := \boldsymbol{f}_\ell - \boldsymbol{\mathcal{L}}_\ell^{(k)} \boldsymbol{\rho}_\ell^{(k)}$
    restrict $\boldsymbol{r}_\ell^{(k)}$ to $G_{\ell-1} \rightarrow \mathscr{R}[\boldsymbol{r}_\ell^{(k)}]$
    restrict $\boldsymbol{\rho}_\ell^{(k)}$ to $G_{\ell-1} \rightarrow \mathscr{R}[\boldsymbol{\rho}_\ell^{(k)}]$
    restrict $\boldsymbol{f}_\ell$ to $G_{\ell-1} \rightarrow \mathscr{R}[\boldsymbol{f}_\ell]$
    calculate FS in $G_{\ell-1}$ consistent with $\mathscr{R}[\boldsymbol{\rho}_\ell^{(k)}] \rightarrow \boldsymbol{\mathcal{L}}_{\ell-1}^{(k)}$
    get $\boldsymbol{f}_{\ell-1}$ and $\boldsymbol{\tau}_{\ell-1}$ form Eq. (4.22)
    call recursively this algorithm for $G_{\ell-1}$
    calculate $\Delta\boldsymbol{\rho}_{\ell-1}$ from Eq. (4.18)
    project these corrections onto $G_\ell \rightarrow \boldsymbol{\rho}_\ell^{(k+1)}$
    perform ν_2 postsmoothing iterations, $\mathscr{S}_{\nu_2} \rightarrow \boldsymbol{\rho}_\ell^{(k+1+\nu_2)}$
    if $\ell = \mathbb{M}$ **then**
      $\|\boldsymbol{\tau}_\ell\| := \frac{1}{3}\|\boldsymbol{\tau}_{\ell-1}\|$
      calculate the residuum $\boldsymbol{r}_\ell := \boldsymbol{f}_\ell - \boldsymbol{\mathcal{L}}_\ell^{(k+\nu_2)} \boldsymbol{\rho}_\ell^{(k+\nu_2)}$
    else
      exit the function
    end
  end
until $\|\boldsymbol{r}_\ell\| < \|\boldsymbol{\tau}_\ell\|$

Algorithm 4.2: Standard MG scheme.

The convergence properties of the Standard MG method are shown in Figure 4.8. A comparison with the convergence behavior of the ALI technique (the bottom panel of Figure 4.3) shows that the iteration to the level of the truncation error is not only faster in the Standard MG case but also that the relative convergence error C_e is always smaller than the relative change of density matrix corresponding to the same iteration (cf. Fabiani Bendicho et al. 1997). R_c is thus a sufficient estimate of the upper limit of C_e. From Eq. (4.10) one obtains the spectral radius of the problem of about $\varrho \approx 0.015$ which is rather small. If follows from Eq. (3.23) that number of iterations required to minimize the error is quite small. Typically only two or three MG iterations are sufficient to reach the convergence.

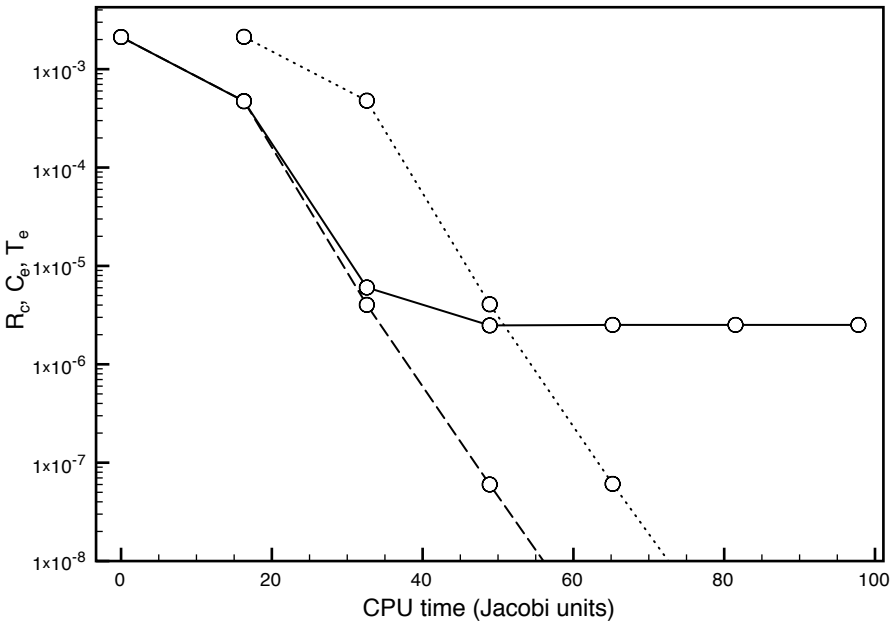

Figure 4.8: Evolution of R_c (dotted line), C_e (dashed line), and T_e (solid line) in the Standard MG scheme with 4 grids. The finest grid was the one with 11.7 PPD. The numbers $\nu_1 = 4$ and $\nu_2 = 5$ of the pre/postsmoothing iterations have been used. CGE was solved by Jacobi iteration which was stopped once the *maximum relative change of populations* was below 10^{-4}. The finest grid with 11.7 PPD has been considered. It follows from Eq. (4.9) that the spectral radius is $\varrho = 0.015$. Since $\varrho \ll 1$ it is also $C_\mathrm{e} \ll R_\mathrm{c}$ in contrast to the ALI method. The full convergence is reached after very few MG iterations and within a significantly shorter CPU time.

CPU time demands

It follows from Algorithm 4.2 that number of Jacobi iterations performed in each grid is $(\nu_1 + \nu_1 + 1)$. Let $t_\mathbb{M}$ the CPU time required for one Jacobi iteration on the *finest* grid $G_\mathbb{M}$ and let t_CGE be the time of solution of CGE. Since the time spent on one Jacobi iteration is proportional to $\mathbb{N}_\ell$, one gets for the Standard MG V-cycle with $\mathbb{M}$ grids a total computation time[4] of

$$t_\mathrm{CGE} + (\nu_1 + \nu_1 + 1)t_\mathbb{M} \sum_{\ell=1}^{\mathbb{M}} \left(\frac{1}{2}\right)^{\ell-1} = t_\mathrm{CGE} + (\nu_1 + \nu_1 + 1)t_\mathbb{M} \left(2 - \frac{1}{2^{\mathbb{M}-1}}\right) . \qquad (4.26)$$

We see that the computation time only slowly increases with the number of grids. In fact, it saturates at the limit $t_\mathrm{CGE} + 2(\nu_1 + \nu_1 + 1)t_\mathbb{M}$. Since $t_\mathbb{M} \propto \mathbb{N}_\mathbb{M}$, we see that the the computational time scales linearly with $\mathbb{N}_\ell$ if $t_\mathrm{CGE} \ll t_\ell$.

The effectivity of the MG methods is even better in the multidimensional geometry. Not only that the solution time scales linearly with $\mathbb{N}_\mathbb{M}$ but also the number $\frac{1}{2}$ in the sum of Eq. (4.26) becomes $\frac{1}{4}$ and $\frac{1}{8}$ in the two and three dimensions respectively.

Worth to say that the smoothing ability of the Jacobi iteration is not quite optimal (see also Trujillo Bueno & Fabiani Bendicho 1995). The use of Gauss-Seidel iteration in $\mathscr{S}$ can lead to a decrease of $(\nu_1 + \nu_2 + 1)$ by factor of 2 or 3 with virtually same $t_\mathbb{M}$. For a very detailed convergence analysis of the MG technique with a Gauss-Seidel smoother see Fabiani Bendicho et al. (1997).

[4]Note that the time demands of restrictions and prolongations have been neglected.

4.5 Nested multigrid method

Another approach to the MG technique is possible. In the so-called *Nested MG* method one starts in the *coarsest* grid G_1 and successively interpolates the approximate solutions onto the finer grids by $\mathscr{P}$. The Standard MG iteration is then applied in each grid to find the correct solution. The process can be visualized as in Figure 4.9.

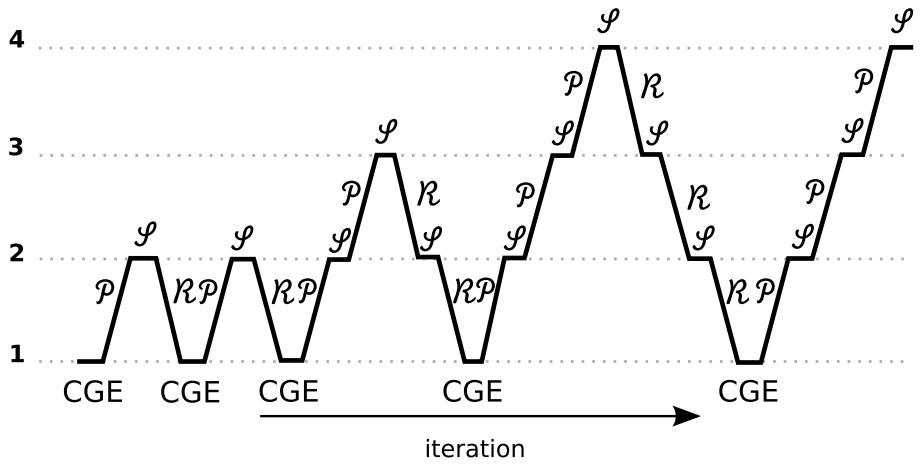

Figure 4.9: Nested MG iteration for an example of 4 grids.

initialize LTE populations on G_1
solve CGE by $\mathscr{S}$
project the solution onto G_2: $\boldsymbol{\rho}_2 := \mathscr{P}[\boldsymbol{\rho}_1]$
for ℓ *from* 2 *to* $\mathbb{M}$ **do**
  solve for $\boldsymbol{\rho}_\ell$ by Algorithm 4.2 in which $\mathbb{M} \to \ell$
  if $\ell < \mathbb{M}$ **then** project the solution onto $G_{\ell+1}$: $\boldsymbol{\rho}_{\ell+1} := \mathscr{P}[\boldsymbol{\rho}_\ell]$
end

Algorithm 4.3: Nested MG scheme.

This approach is generally more efficient than Standard MG since one starts the iteration in the fine grid using a more accurate guess for solution provided by the coarse grid (and contaminated by the relative truncation error, of course). From Figure 4.10 it becomes clear that the Nested MG method has rather fast convergence towards the correct solution. It is about a factor 2 faster than the Standard MG method. In the typical applications, one only needs one nested iteration cycle to reach the convergence.

4.6 Examples of solution

In addition to the convergence analysis, it is worth to illustrate the model by a particular solution. In this section, two figures are presented to demonstrate the properties of the emergent radiation of the ^{3}S–^{3}P triplet.

There are the so-called *Hanle* (or *polarization*) *diagrams* in Figure 4.11. They show a fractional linear polarization of Q/I and U/I of in the line core. These diagrams are plotted for three different polar angles of observation and reflect the effect of magnetic field on the linear polarization state. Typical signatures of level-crossings in the incomplete Paschen-Back effect

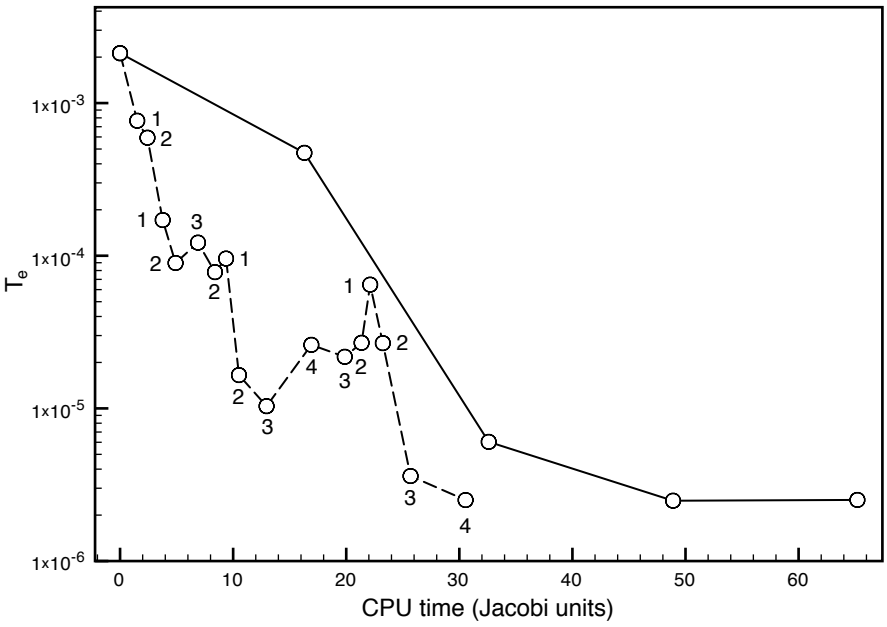

Figure 4.10: Comparison of the convergence behavior of Standard MG (solid line) and Nested MG (dashed line). There is the true relative error T_e of the solution in the vertical axis plotted against the CPU time in the horizontal axis. The circles on the Nested MG line indicate the value of T_e after a postsmoothing iteration on a given grid, which itself is indicated by the number 1 to 4 for grids G_1 to G_4.

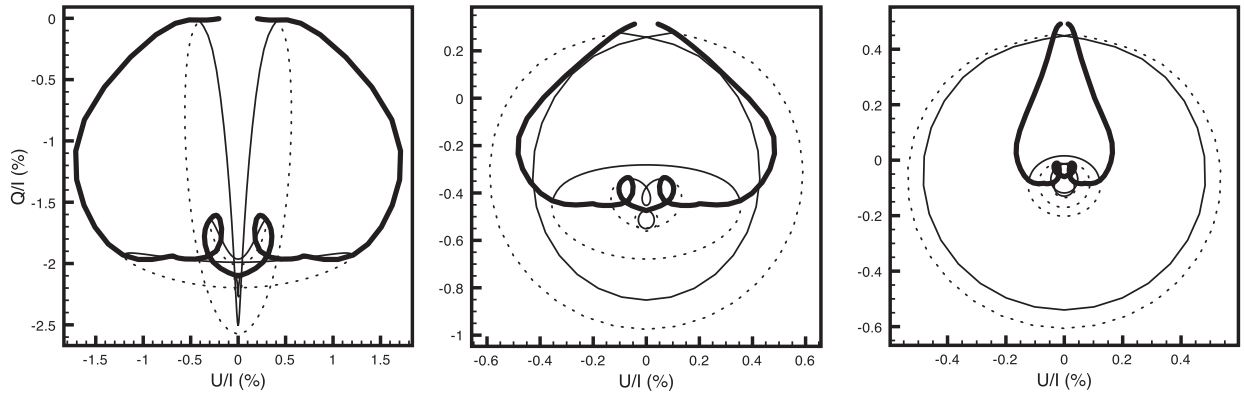

Figure 4.11: Hanle diagrams for the line centre of the ^{3}S – ^{3}P triplet observed at $\mu = 0.085$ (left panel), 0.56 (central panel), and 0.89 (right panel) and horizontal magnetic field. Thick line in each diagram corresponds to a fixed line-of-sight azimuth with respect to magnetic field vector: $\chi - \chi_B = 0°$ (left branch), and $\chi - \chi_B = 180°$ (right branch). Thin lines correspond to a fixed magnetic field strength of $\gamma = 0.01$, 0.3, 1.2, and 6.0. Solid parts of the curves correspond to $0° \leq \chi - \chi_B \leq 180°$, dotted lines correspond to the case $180° \leq \chi - \chi_B \leq 360°$. As expected, polarization degree decreases towards the disk centre. However, a non-negligible amount of linear polarization is present even in the disk centre. Note the various scaling of the axes.

regime of the upper term are found: The closed loops are due to evolution of the coherence between the crossing Zeeman sublevels with $\Delta M = \pm 2$ (Bommier 1980).

Figure 4.12 contains the synthetic emergent line *Stokes profiles* for several strengths of the magnetic field and for different inclinations of the line of sight (LOS). The LOS is always

such that $\chi - \chi_B = 0°$. Both Hanle and Zeeman effects are taken consistently into account. By comparison of the linear polarization profiles at $B = 0\,\mathrm{G}$ with the results of the $^1\mathrm{S}$–$^1\mathrm{P}$ singlet line transfer (Rees & Saliba 1982; Trujillo Bueno 1999) the depolarizing effect of the fine structure is well exhibited (cf. Section 10.16 of Landi Degl'Innocenti & Landolfi 2004).

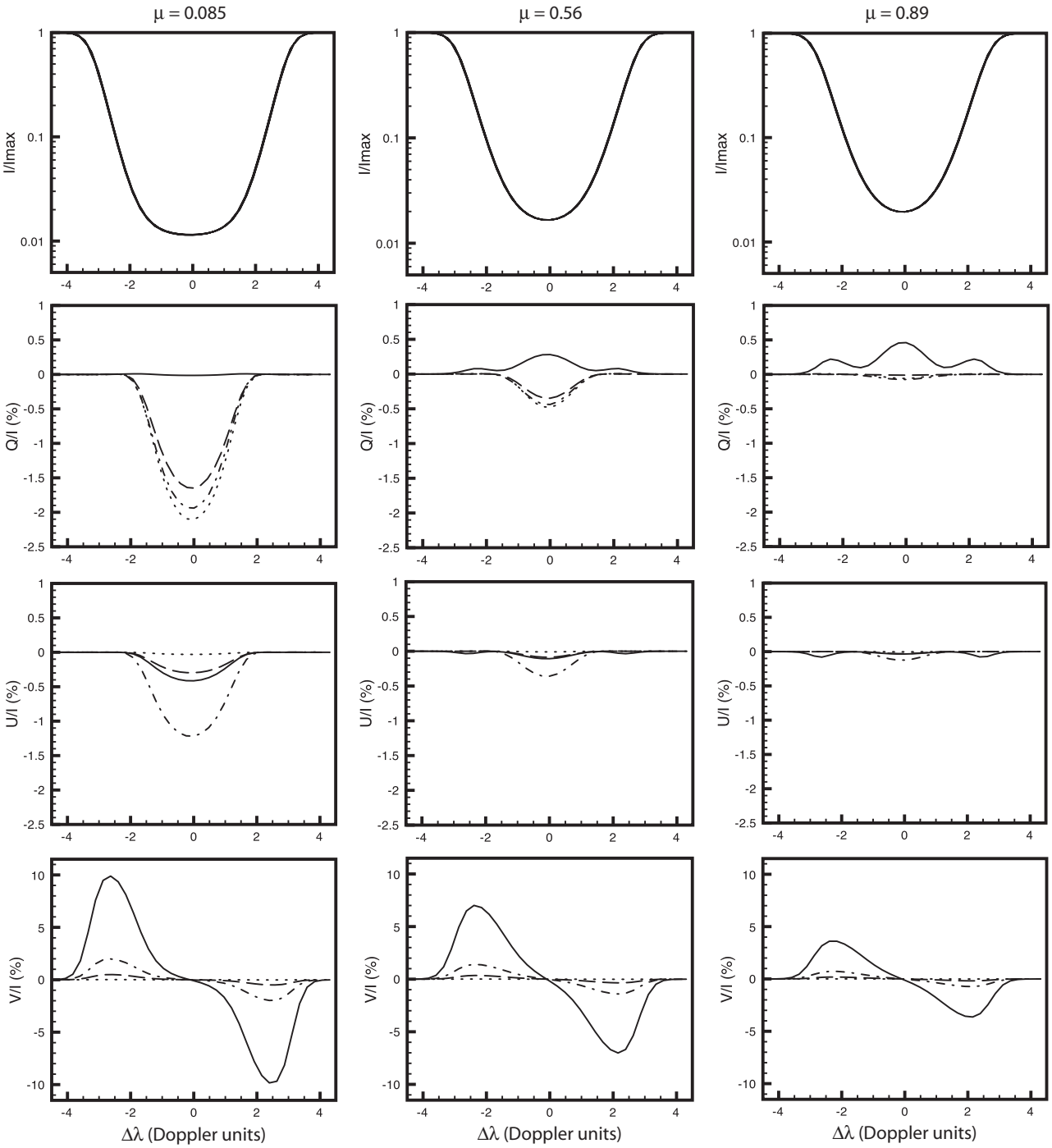

Figure 4.12: Stokes profiles of the ^{3}S – ^{3}P triplet observed at azimuth $\chi - \chi_B = 0°$. The observation is made close to the limb ($\mu = 0.085$, left column), at $\mu = 0.56$ (central column), and close to the disk centre ($\mu = 0.89$, right column). The profiles have been synthesized for four different magnetic field strengths: $\gamma = 0.01$ (dotted line), 0.3 (dashed line), 1.2 (dash-dotted line), and 6.0 (solid line). The intensity profiles are not significantly modified by the Zeeman splitting of the strength considered. The Stokes-V profiles are not perfectly antisymmetric since there is a small contribution of symmetric component due to the alignment-to-orientation mechanism (Landi Degl'Innocenti & Landolfi 2004). However it is only small contribution in the present configuration. Note that negative Q corresponds to the linear polarization parallel with the limb.

Chapter 5

Hydrogen Hα impact polarization in solar flares

This chapter deals with the problem of impact atomic polarization of the hydrogen Hα line in the flaring solar chromosphere due to bombardment by the directive proton beams. The detailed results of the theoretical modeling of this process can be found in Štěpán et al. (2007a) (from now on referred to as Paper IV, see also Appendix F). This chapter is just a very brief summary of this work. For more reviews see also Štěpán et al. (2006) and Štěpán (2007).

The observations of the solar flares in the hard X-ray band indicate a bremsstrahlung radiation of the electron beams with energies of the order of 10-100 keV or even more. These beams are injected into the matter of the chromosphere from a coronal magnetic reconnection site. However, the superthermal electron beams are not a satisfactory explanation of all flare observations (e.g. Doschek et al. 1996). Furthermore, different accelerating mechanisms can also lead to acceleration of protons (Orrall & Zirker 1976). In contrast to electrons, it is difficult to detect the bremsstrahlung radiation of the proton beams at the energies below 1 MeV because they do not radiate with enough efficiency (Brown et al. 1990).

Different techniques have to be used in order to detect the low-energy proton beams: One of the candidates for such a measurement is the Stokes polarimetry of the hydrogen lines. As explained in Subsection 2.5.7, anisotropic bombardment by charged particles can lead to impact atomic polarization and consequently to emission of linearly polarized radiation (Hénoux et al. 1990). In the case of vertical beams, the maximum degree of linear polarization is expected close to the solar limb.

In fact, there are observations indicating the existence of linear polarization of the Hα line in solar flares. The degree of such polarization is often of the *order of 5% or higher* and is usually interpreted as due to the impact polarization by proton beams (Hénoux & Chambe 1990; Vogt & Hénoux 1996; Xu et al. 2005). The preferential orientation of the polarization is towards the disk center (radial) or parallel to the limb (tangential) in some cases.

There are also observations of other authors which indicate *no linear polarization* in an extensive group of flares (Bianda et al. 2003, 2005). These authors argue for isotropization of the proton beam in the relevant atmospheric depths where the hydrogen Balmer line core is formed. Another crucial effect that has to be taken into account is an increase of density of the background electrons and protons due to higher degree of plasma ionization. Consequently, the collisions can lead to a significant depolarization effect (Bommier et al. 1986; Sahal-Bréchot et al. 1996).

The first quantitative models taking into account the effect of collisional depolarization have been considered by Vogt et al. (1997) and Vogt et al. (2001). Basically, these models consisted of the two parts: (1) A self-consistent *unpolarized* NLTE radiative transfer model of

the chromosphere affected by the proton beam. This model provided the hydrogen ionization degree and the average radiation intensity at the Hα line optical depth equal to 1. To this end, several semiempirical models of the chromosphere have been considered by the authors: the quiet atmosphere model VAL C, the hotter plage model VAL F (Vernazza et al. 1981), and the flaring atmosphere model F1 (Machado et al. 1980). The effect of proton beam was taken into account in the calculation following the approach of Hénoux et al. (1990). (2) The equations of statistical equilibrium and the radiation transfer equations have been decoupled and the Hα line has been assumed to be optically thin. The proton beam energy distribution at the injection site has been taken to be similar to the one deduced for the electron beams, i.e., the power law

$$F(E) = \begin{cases} \kappa E^{-\delta} & \text{for } E \geq E_{\rm c} \\ 0 & \text{for } E < E_{\rm c} \end{cases} \tag{5.1}$$

where $E_{\rm c}$ is the lower energy cut-off, κ is the normalization constant, and δ is the spectral index. The lower energy cut-off is usually considered between 100 to 200 keV. This energy approximately corresponds to the energy necessary for the proton to reach the Hα line-forming layers. The authors used the assumptions that the power-law distribution retains its shape as the beam propagates in the upper chromospheric plasmas. Taking into account the effect of depolarizing collisions, the rates of anisotropic excitation by the proton beam, and the anisotropy of radiation (in Vogt et al. 2001), the authors calculated the polarization degree ϵ_Q/ϵ_I of the radiation emitted at the unit optical depth. Depending on the atmosphere model and the particular beam properties (the spectral index $\delta = 3, 4, 5$, the energy cut-off, the total energy flux $\mathcal{E}$) they found the polarization degree of Hα up to 4.5 %, i.e., consistent with the reported measurements.

It is worthwhile to calculate the line profiles self-consistently to verify whether the emergent linear polarization is significantly affected by radiation transfer. The aim of this chapter is thus to show a *self-consistent* solution of the problem taking into account the NLTE radiative transfer of the 2nd kind. The goal is to clarify whether the proton beams are likely to be a source of the observed linear polarization.

Description of the atomic model

We use a one-dimensional static atmosphere model with a fixed temperature structure and we solve the NLTE radiative transfer model to find the *differential effects* of the proton beam on the line Stokes profiles. The initial properties of the atmosphere are given by the semiempirical models F1 and VAL F. The atomic model is restricted to the three Bohr levels $n = 1, 2, 3$ plus the continuum. In the range of electron and proton densities in our model, the adequate description of the hydrogen state is in terms of the fine structure levels (see Sahal-Bréchot et al. 1996, for the discussion of this approximation). Hyperfine splitting is neglected. The magnetic field in the chromosphere is supposed to be vertical. We neglect the Zeeman splitting of the levels. This approximation seems to be adequate for typical fields in the chromospheric flares which are well below ≈ 1 kG for which the Zeeman sublevels of a given term overlap (Vogt et al. 1997). For symmetry reasons, there are no Zeeman coherences ($Q \neq 0$) in the atomic density matrix once the quantization axis is set to be vertical. The only non-vanishing density matrix multipoles of the levels are populations, ρ^0_0, and alignments, ρ^2_0. Due to cylindrical symmetry of the problem, the only non-vanishing Stokes parameters are I and Q, i.e., the linear polarization is either radial or tangential.

Beam propagation

We suppose that the proton beam penetrates the chromosphere vertically. A horizontal motion of the protons is neglected in order to keep the calculation simple and also to maximize the effect of impact polarization (Hénoux et al. 1993). We adopt the power-law energy distribution of the beam number flux given by Eq. (5.1). In a partially ionized medium, the superthermal proton beam is decelerated by the collisions with the background electrons, ions and by the (in)elastic collisions with neutral atoms (Emslie 1978). The injection energy of the protons necessary to reach the Hα line-core formation region is of the order of 100 keV. A typical example of the shape of the differential energy distributions of the beam at different atmosphere depths is plotted in Figure 5.1.

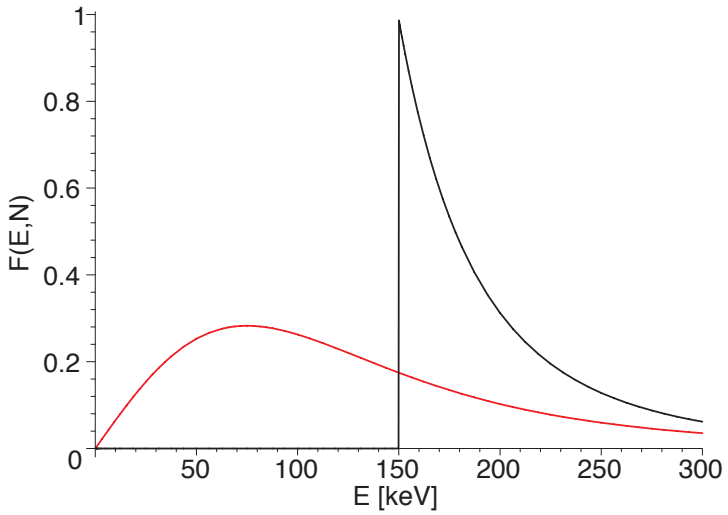

Figure 5.1: Energy distribution $F(E, N)$ of the proton beam with $\delta = 4$ and $E_c = 150$ keV in two different column depths N of the chromosphere: The upper curve represents the initial distribution at the injection site whereas the lower curve is the typical distribution of protons in the Hα formation layer. The vertical axis of the plot is in arbitrary units. See Canfield & Chang (1985) for details.

Collisional rates

For the purpose of calculation of the superthermal proton-hydrogen excitation rates of the key transitions $1s^{1/2} \rightarrow nlj$,

$$C^{K\leftarrow 0}_{nlj\leftarrow 1s^{1/2}} = \mathcal{N} \int \mathrm{d}^3\boldsymbol{v} f(\boldsymbol{v}) v \sigma^{K\leftarrow 0}_{nlj\leftarrow 1s^{1/2}}(\boldsymbol{v}) \tag{5.2}$$

we use the close-coupling cross-sections of Balança & Feautrier (1998). It can be shown (Vogt et al. 2001) that the other nonthermal rates are negligible. The impact polarization of the $n = 3$ level is most efficient for collision energies below 10 keV and the emitted light has the *radial* direction of polarization for the collision energies below approximately 200 keV (Hénoux et al. 1990). The cross-sections of depolarizing dipolar transitions $nlj \rightarrow n\,l \pm 1\,j'$ induced by the background electrons and protons are calculated via the semiclassical perturbation method of Sahal-Bréchot et al. (1996). The other collisional rates are calculated from the data of Atomic and Molecular Data Information System (http://www-amdis.iaea.org). For more details see Paper IV.

Results and conclusions

We found that the approximation of the energy distribution of the proton beam used in the previous works is inadequate. The initial power-law distribution is dramatically modified in the Hα formation layers (cf. Figure 5.1). The use of the power-law distribution at this layer (Vogt et al. 1997, 2001) leads to an overestimation of the number of low-energy ($\lesssim 10$ keV) protons which are most efficient in creation of the atomic alignment. Consequently, a polarization degree of the emitted radiation is overestimated.

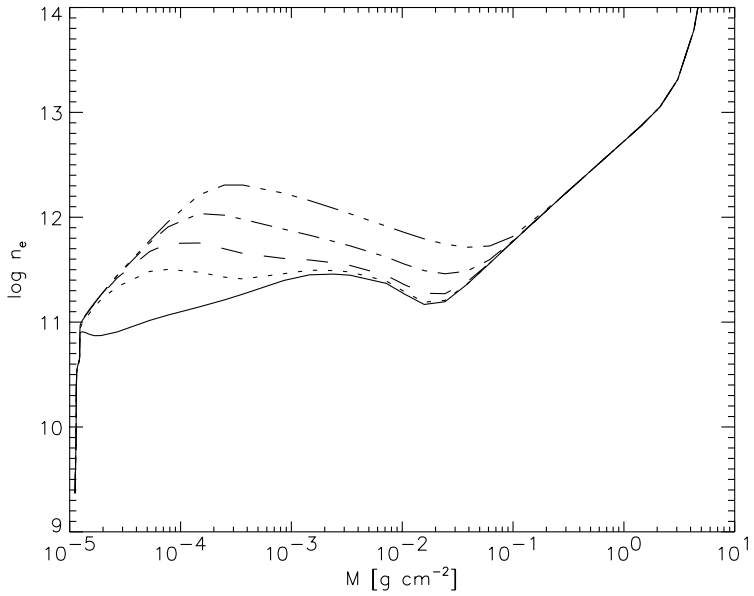

Figure 5.2: Electron density of the VAL F chromosphere affected by the nonthermal proton beams with $\delta = 4$ and $E_c = 150$ keV. The thermal case is plotted by the solid line. The models including the beam are calculated for the total energy fluxes of 10^8 (dotted line), 10^9 (dashed line), 10^{10} (dash-dotted line), and 10^{11} erg cm^{-2} s^{-1} (the line with three dots per dash).

The unpolarized NLTE model of Vogt et al. (1997, 2001) was based on the lambda iteration method. We have verified that these models did not provide a fully converged solution. The ionization degree of the chromosphere predicted by these models was underestimated. Consequently, the rates of collisional depolarization by the thermal electrons and protons were also underestimated. Even in the cooler model VAL F, the fully converged solution leads to a significant increase of the electron density (see Figure 5.2).

Even though the excitation collisions at energies below approximately 200 keV lead to emission of polarization with *radial direction*, the typical line polarization obtained from our models is not only very small but also *tangential*. This orientation is due to the resonance scattering polarization. A typical synthetic Q/I profile of Hα is plotted in Figure 5.3. In the VAL F model,[1] the degree of fractional polarization is about 0.3% and only a small contribution of impact polarization is seen. In the F1 flare model the degree of linear polarization is of the order of 0.01% since the depolarizing collisions are strong (see Appendix F). In all our models the effect of the proton beam on the Q/I profile is practically negligible and the polarization degree is well below the value of 5% suggested by the observations of Hénoux and collaborators.

Our conclusion is that the proton beams are very unlikely to be a source of the observed linear polarization of the Hα line as long as the approximations introduced above are applicable.

[1]This cooler model seems to be more reliable than F1 since the linear polarization of Hα is mostly found out of the brightest footpoints of the flares (Xu et al. 2005).

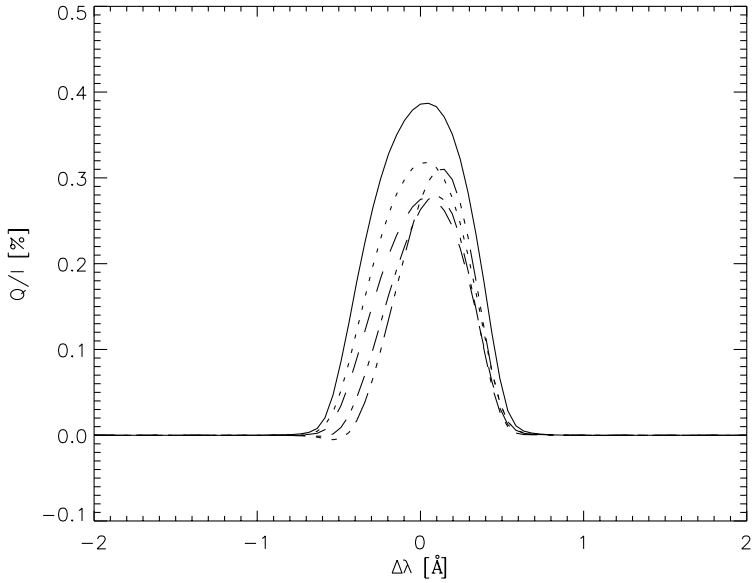

Figure 5.3: A fractional linear polarization profile of the emergent Hα line close to the limb ($\mu = 0.11$). The semiempirical model VAL F has been used and the effect of nonthermal proton beam has been included. The individual profiles represent the same beam fluxes as in Figure 5.2. Note that in the current definition, the positive-Q sign means tangential polarization. The polarization signal is mainly due to resonance scattering of the photons. The effect of the proton beams is small and it cannot be distinguished from the effect of collisional depolarization in these profiles. Note that there is always a change of the optical depth scale of the atmosphere due to nonthermal bombardment resulting in modification of the polarization profile.

However, the joint effect of the beam, of the magnetic fields, and of the dynamics of the flare event is quite complicated. The same applies to the complicated measurements of the emergent linear polarization in flares. It is thus possible that a stationary one-dimensional model like ours is not sufficient for drawing definitive conclusions about this issue.

Chapter 6

Hydrogen Balmer line formation affected by electric return currens

There is another promising mechanism that could be possibly responsible for creation of the Hα linear polarization in solar flares. The *electron beams* propagating in the solar chromosphere can be accompanied by the so-called *electric return currents* (RC). The importance of RC in formation of the spectral lines in solar flares has been recently pointed out by Karlický & Hénoux (2002) and Karlický et al. (2004). These authors suggested that the role of the neutralizing RC can be at least as important as the role of the primary beam itself. This results from the fact that RC's are expected to have typical energies of few deca-eV, i.e., the range of energies for which the excitation cross-sections of hydrogen are high. Moreover, a number density flux of the return-current electrons is enough to *neutralize* the electric flux of the primary beam. These two facts make the RC problem of interest for the line formation studies.

In this chapter, I briefly recall some of the results of the recent modeling of the Balmer line formation under the conditions of flaring atmosphere affected by the primary electron beam and the associated RC formed by the so-called *runaway electrons* (Rowland & Vlahos 1985; van den Oord 1990; Norman & Smith 1978). These preliminary calculations do *not* take into account the polarization state of radiation. Only the intensity component of the Stokes vector is considered. However, qualitative conclusions concerning polarization of the emergent radiation can be made and this work can be considered as a first step towards modeling of the linear polarization signal. Since the matter contained in this chapter is discussed in detail in Štěpán et al. (2007b) (from now on referred to as Paper V, see also Appendix G), only a brief review of motivations and results is presented here.

The models of the RC formation

The electron beam injected into the cold chromosphere evolves under the influence of several processes (e.g., Karlický (1997), Paper V): (a) the beam generates RC that decelerates the beam in the RC electric field, (b) the beam generates the plasma waves causing the quasi-linear relaxation of the beam, and (c) the beam electrons are decelerated and scattered due to collisions with the background plasma particles. In our model, the plasma waves are neglected and RC is supposed to be formed by the runaway electrons. The RC losses are thus strongly reduced (Rowland & Vlahos 1985; Karlický et al. 2004) and only the collisional losses are responsible for deceleration of the electron beam (Emslie 1978).

The physics of RC formation in the chromospheric conditions is quite complicated and it is not yet fully understood. However, one can use several approximations. Our model of the RC formation is the following. For the reasons of simplicity, we approximate the power-law energy

distribution of the electron beam by a *monoenergetic beam*. Taking high-energy electrons into account (i.e. releasing the monoenergetic approximation) would lead to modification of the line wings (cf. Kašparová & Heinzel 2002). However, the importance of RC in the lower layers of the chromosphere is supposed to be of secondary importance.

Let $\Phi = n_{\rm B} v_{\rm B}$ be the number density flux of the beam, where $n_{\rm B}$ is the number density of the beam electrons, and $v_{\rm B}$ is its velocity. We suppose that the beam is propagating vertically along the magnetic field lines. According to Norman & Smith (1978) and Karlický et al. (2004), a fraction of background thermal electrons, $\alpha = n_{\rm R}/n_{\rm e}$, forms the current that moves in the *opposite direction* in order to neutralize the electric current $e\Phi$ associated with the primary beam. Thus we have the condition

$$e n_{\rm R} v_{\rm R} = e\Phi \,. \tag{6.1}$$

In this equation $n_{\rm R}$ is the number density of the the RC electrons and $v_{\rm R}$ is their velocity. Like in the case of the primary beam, we assume that all the RC electrons move with the same superthermal velocity.

Two models estimating $n_{\rm R}$ have been used in Paper V: Following Norman & Smith (1978) we have set

$$\alpha = \frac{n_{\rm R}}{n_{\rm e}} = \frac{1}{2} \exp \left[-\frac{1}{2} \left(\sqrt{\frac{\mathcal{E}_{\rm D}}{\mathcal{E}}} - \frac{\mathcal{E}}{\mathcal{E}_{\rm D}} \right)^2 \right] , \tag{6.2}$$

where $\mathcal{E}/\mathcal{E}_{\rm D} = n_{\rm B} v_{\rm B} / n_{\rm e} v_{T_{\rm e}}$ is the ratio of the electric field generated by the electron beam and the so-called the Dreicer electric field (see Karlický et al. 2004; Xu et al. 2005), and $v_{T_{\rm e}}$ denotes the thermal velocity of the background electrons. In the second model, we have assumed that RC is formed by a *fixed* fraction of the background electrons everywhere in the relevant layers of the upper chromosphere,

$$\alpha = \frac{n_{\rm R}}{n_{\rm e}} = \text{const.} \tag{6.3}$$

In our approach, α has been obtained by averaging the values from the previous model in the Balmer line formation layers. The value of α depends on the total flux of the beam. In the range of fluxes we have considered in our solution (i.e., 4×10^{11} to $1.0 \times 10^{12}\,\mathrm{erg\,cm^{-2}\,s^{-1}}$), the typical value of α is of the order of 0.1 (see Paper V, for details).

The model inputs and outputs

For the purposes of this work, we have used the 5-Bohr-level plus continuum model of hydrogen atom. The atmosphere has been approximated by the plane-parallel F1 model with a fixed temperature structure (see the preceding chapter). The initial energy of the beam electrons at the injection site has been set to 10 keV. This energy is typical for the electron distribution cut-offs considered in the previous models (e.g. Kašparová & Heinzel 2002). We have calculated the differential effect of the beam and RC on the profiles of the hydrogen Hα, Hβ, and Hγ line.

Results and conclusions

The excitation and ionization cross-sections of the low-energy return-current electrons are larger than those for the fast beam electrons. Along with the fact that the collisional rates of the beam and RC are both proportional to Φ, the return-current effects on line formation become important.

The synthesized Balmer line profiles can be found in Figure 6.1. The approach to the calculations *with RC neglected* is analogous to that of Fang et al. (1993) and Kašparová & Heinzel

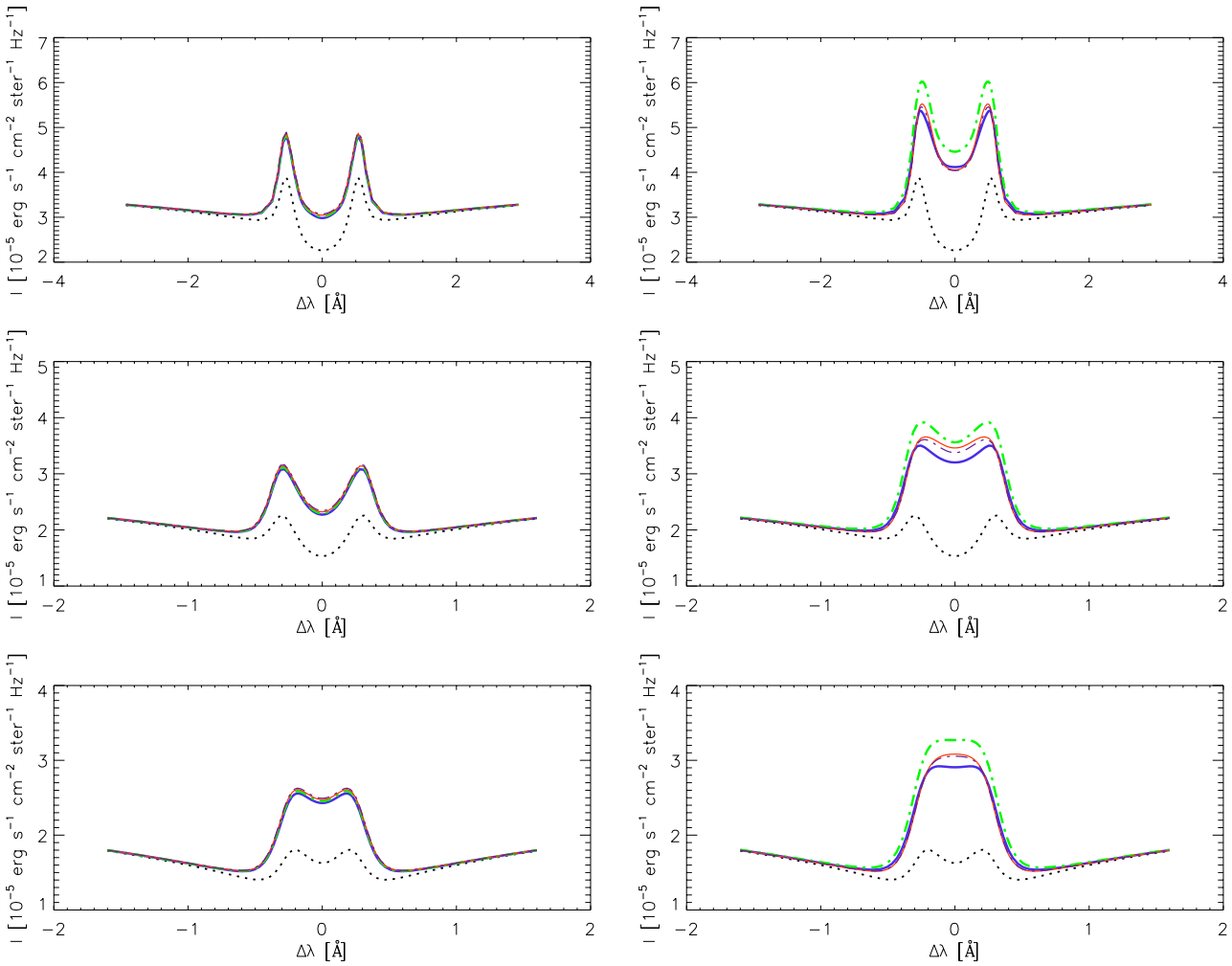

Figure 6.1: Hydrogen Balmer line profiles affected by 10 keV electron beams (left panels) and by the beam associated with RC (right panels). From upper to lower panel: Hα, Hβ, and Hγ disk-center line profiles for $\mathcal{E} = 0$ (dotted line / black), 4×10^{11} (thick solid line / blue), 6×10^{11} (thick dash-dotted line / green), 8×10^{11} (thin solid line / red), and 1.0×10^{12} erg cm^{-2} s^{-1} (thin dash-dotted line / violet). Note that the nonthermal profiles in the "beam-only solution" almost overlap because the range of the beam fluxes is small. In contrast, the spectral line response to the RC effects is more sensitive.

(2002). Taking RC into account by means of the theory of Norman & Smith (1978) (Eq. 6.2) leads to the new line profiles shown in the right-hand side of the figure. One can see that RC leads to a significant increase of emission in the line center of all the Balmer lines. Our calculations indicate that, in the layers of Balmer line formation, α remains approximately independent of depth. Similar profiles are thus obtained for the approximation of α given by Eq. (6.3) (see Figure 3 of Paper V).

In the region of Balmer line formation the energy of RC is comparable to the excitation threshold of the $n \geq 3$ levels. Since the RC energy and density are sensitive to the beam flux, the resulting variation of the nonthermal collisional rates leads to a significant variation of the line profiles. For both models under consideration, a maximum emission is found for the beam flux of 6×10^{11} erg cm^{-2} s^{-1}. The reason that the higher beam fluxes lead to a lower emission in the lines is that the energy of the return current is not sufficient to excite the hydrogen atoms. The excitation threshold effects seem to play an important role for higher fluxes, but they are

very likely only a consequence of the monoenergetic approximation we have used.

Outlook

Recent numerical simulations of Karlický (2008) indicate that the electron velocity distribution in the chromospheric plasmas can be dramatically modified by the presence of the beam and RC: It is no longer possible to distinguish the beam, RC, and the thermal component of the velocity distribution. Instead, one has to take into account a complicated distribution function with a significant anisotropy in the vertical direction. Such a distribution is to be considered in the Balmer line impact polarization studies. The resulting impact linear polarization can be high since a huge number of anisotropic electrons has the energies in the interval of 10 – 100 eV. The linear polarization observed in flares by Hńoux and collaborators is predominantly radial. That is consistent with this range of energies since the electron impacts imply the polarization direction *parallel* to the direction of the velocity anisotropy for energies $\lesssim 200$ eV. A detailed study of the effect of RC on the Balmer line polarization is now in progress.

Chapter 7

Conclusions and future prospects

The methods developed in chapters 2 to 4 and implemented in the computer code described in Appendix A allow to solve the NLTE problems of the 2nd kind for a wide variety of spectral lines and the one-dimensional plane-parallel geometry of the medium. The basic properties of the solver can be summarized as follows:

- The density matrix formalism for description of the atomic state.
- Representation of the irreducible tensorial operators.
- A unified notation for the NLTE equations useful for a general iterative scheme based on the Jacobi method.
- Short-characteristics formal solver for RTE.
- The solution can be performed for the problems formulated in terms of atomic manifolds satisfying the flat-spectrum approximation (the explicit expressions for multilevel, multiterm, and multilevel picture with hyperfine splitting were given).
- Multigrid method: Implementation of the nonlinear multigrid methods (Standard MG, Nested MG) leads to a significant decrease of the time required for solution of the problem.
- As a result, the problems involving a joint action of both Hanle and Zeeman effect can be solved. All the basic radiative and collisional processes are taken into account.

In Chapter 5 it was shown by solution of the NLTE radiative transfer in hydrogen lines of solar chromosphere that proton beams are the unlikely explanation of the linear polarization of the Hα line. The study of the effect of electric return currents in Chapter 6 shows that return currents can affect significantly the line profiles of the hydrogen Hα, Hβ, and Hγ lines. A future work should reveal whether the electron beams accompanied by return currents can also lead to a significant modification of the emergent linear polarization.

Extension of the NLTE code to the multi-dimensional geometries would allow to model the realistic optically thick structures of outer solar atmosphere. These regions are known to be highly structured and the approximation of one-dimensional geometry is not adequate in most cases. Diagnostics of the magnetic fields in such a regions is a non-trivial task. The use of the forward NLTE modeling of the emergent spectra in optically thick lines (such as those of H I or He I) can provide a useful quantitative information on the actual atmospheric plasma conditions.

Appendix A

Design of Monopost

Monopost (for *mo*deler of the *no*n-LTE *po*larized *st*ructures) is the computer code implementing the numerical techniques described in the preceding chapters. The code has been developed in the C++ language and it is based upon the object-oriented design. This appendix contains few remarks to the algorithms and design of the code.

Monopost structure

The code consists of several components (see Figure A.1). The *parser* interprets a list of commands stored in a text file (the *model script*). The scripts are written using a simple high-level language and providing a functionality of the *core*. The core encapsulates all the classes used in the numerical calculations. The data describing the model (description of the levels, collisional rates, magnetic fields, structure of the atmosphere, ...) are stored in the *data files*. These data are accessed by the core via the *data input layer*. The results of a particular model (as specified in the model script) are provided by the core through the *output layer*.

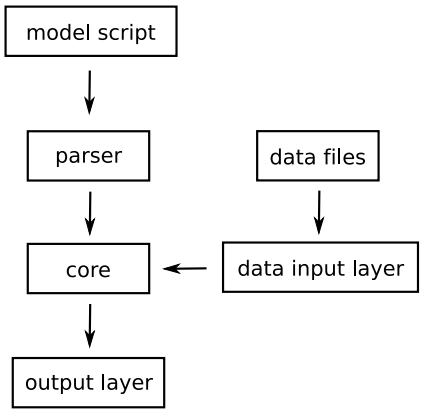

Figure A.1: Monopost code design.

The Monopost system can be used for the studies of a wide variety of the radiation-matter interactions from modeling of a single resonance scattering event to the complex NLTE multigrid models of realistic atmospheres. The system provides a set of advanced data types for the density matrices, radiation tensors, and model grids. These high-level structures make the use of the scripting language quite straightforward a efficient.

An example: Internal representation of the atomic density matrix

The atomic structure is read from a data file. An appropriate classes are used by the core to represent the atomic model taking into account any eventual symmetries of the problem and the magnetic field regime (see Figure A.2).

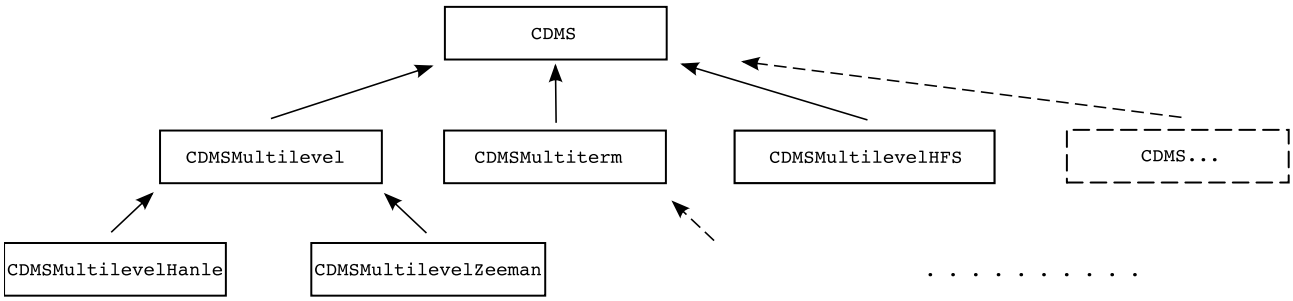

Figure A.2: Inheritance of the density matrix structure classes. The generic class `CDMS` provides the basic data structures for a data storage and manipulation with the atomic multipoles (preconditioning, solution of ESE, calculation of residuals, etc.). The inherited layer of classes provide an additional functionality specific for a particular picture of levels (such as reading of the atomic data, generation of the lists of $s_{ij}(\alpha KQ)$ and s^{E}_{ij} coefficients, treatment of the magnetic kernels, etc.). The third layer can be used if more specific constrains can be applied. For example, `CDMSMultilevelHanle` is a class providing only the atomic population a alignment components that can be used for an efficient solution of the problems in which the Zeeman splitting is negligible, circular polarization is neglected, and only Hanle effect takes place (in fact, this model corresponds to the multilevel picture considered in Table 3.2). An extreme case is the model taking into account only the populations of levels.

The classes for the density matrix data ρ_i are derived from the generic class `CDM`. One instance of such an object is allocated in every grid node. The reference frame for ρ_i is selected in every point of the atmosphere so that the quantization axis is parallel to the magnetic field.

Construction of $s_{ij}(\alpha KQ)$ and s^{E}_{ij} coefficients

The coefficients $s_{ij}(\alpha KQ)$ and s^{E}_{ij} are generated once the atomic model is loaded. A list of the non-vanishing coefficients is generated for each of these quantities. The radiation part of ESE is then always generated from these lists and from the local radiation field tensors $J^K_Q(\alpha\beta)$. In the NLTE model, the equations are then modified according to the precondition strategy by the use of the coefficients $L_{\alpha\beta\bar{i}}$ defined in Eq. (3.122). The use of the lists makes the construction of ESE optimal since it reduces the numerical work to a minimum possible number of operations (note that radiation field changes between iterations).

Collisional rates are added into ESE as well as the magnetic kernels which need to be precalculated and stored in every grid node.

Solution of ESE

Atomic density matrix obeys the conjugation relation (B.6). It follows that each multipole ρ_i has its unique counterpart $\rho_{\bar{i}}$ such that

$$\rho^*_i = Z_i \rho_{\bar{i}}\,, \tag{A.1}$$

where $Z_i = Z_{\tilde{i}}$ is either $+1$ or -1. Each pair of multipoles $\{\rho_i, \rho_{\tilde{i}}\}$ is fully described by the two real numbers. If ρ_i is identically real then $i \equiv \tilde{i}$. In conclusion, the number of real numbers needed for a full description of the state of the ensemble is the same as the total number of complex multipoles ρ_i. This number is denoted by N in this thesis. In the following, I will adopt the notation $\bar{\rho}_i = \mathrm{Re}\,\rho_i$ and $\hat{\rho}_i = \mathrm{Im}\,\rho_i$.

The use of the real arithmetics leads to an improvement of the ESE solution time approximately by a factor of 4.

The ESE matrix has obviously to satisfy certain conjugation relations in order to lead to the solution of the form given by Eq. (B.6). The algorithm transforming the complex ESE matrix to the real matrix of the same dimension follows. From

$$\frac{\mathrm{d}\rho_a}{\mathrm{d}t} = \sum_b \Pi_{ab}\rho_b\,, \tag{A.2}$$

and Eq. (A.1) it follows that

$$\frac{\mathrm{d}\rho_{\tilde{a}}}{\mathrm{d}t} = Z_a\frac{\mathrm{d}\rho^*_{\tilde{a}}}{\mathrm{d}t} = \sum_b \Pi_{\tilde{a}b}\rho_b\,, \tag{A.3}$$

from which

$$\frac{\mathrm{d}\rho^*_a}{\mathrm{d}t} = \sum_b \Pi_{\tilde{a}b}Z_a\rho_b\,. \tag{A.4}$$

Using the definitions

$$K_{ab} = \Pi_{ab} + Z_a\Pi_{\tilde{a}b}\,, \tag{A.5}$$
$$L_{ab} = \Pi_{ab} - Z_a\Pi_{\tilde{a}b}\,, \tag{A.6}$$

we can write the summation and subtraction of the equations (A.2) and (A.4) as

$$2\frac{\mathrm{d}\bar{\rho}_a}{\mathrm{d}t} = \sum_b \rho_b K_{ab}\,, \tag{A.7}$$
$$2\frac{\mathrm{d}\hat{\rho}_a}{\mathrm{d}t} = \sum_b \rho_b L_{ab}\,. \tag{A.8}$$

We can formally split the summation over the *independent* multipoles ρ_b and the associated dependent multipoles $\rho_{\tilde{b}}$ by rewriting the sums in the form

$$2\frac{\mathrm{d}\bar{\rho}_a}{\mathrm{d}t} = \sum_b \rho_b K_{ab} + \sum_{\tilde{b}} \rho_{\tilde{b}} K_{a\tilde{b}}\,, \tag{A.9}$$
$$2\frac{\mathrm{d}\hat{\rho}_a}{\mathrm{d}t} = \sum_b \rho_b L_{ab} + \sum_{\tilde{b}} \rho_{\tilde{b}} L_{a\tilde{b}}\,. \tag{A.10}$$

Using the fact that $\Pi^*_{ab} = Z_a Z_b \Pi_{\tilde{a}\tilde{b}}$ it is easy to verify that

$$K_{a\tilde{b}} = Z_b K^*_{ab}\,, \tag{A.11}$$
$$L_{a\tilde{b}} = -Z_b L^*_{ab}\,, \tag{A.12}$$

from which we arrive at

$$2\frac{\mathrm{d}\bar{\rho}_a}{\mathrm{d}t} = \sum_b (K_{ab}\rho_b + K^*_{ab}\rho^*_b) = 2\sum_b \mathrm{Re}\,K_{ab}\rho_b\,, \tag{A.13}$$
$$2\frac{\mathrm{d}\hat{\rho}_a}{\mathrm{d}t} = \sum_b (L_{ab}\rho_b - L^*_{ab}\rho^*_b) = 2\sum_b \mathrm{Im}\,L_{ab}\rho_b\,. \tag{A.14}$$

where the summations run only over the *independent* multipoles ρ_b. Finally, we can write

$$\frac{\mathrm{d}\bar{\rho}_a}{\mathrm{d}t} = \sum_b (\bar{\rho}_b \bar{K}_{ab} - \hat{\rho}_b \hat{K}_{ab}) \,, \tag{A.15}$$

$$\frac{\mathrm{d}\hat{\rho}_a}{\mathrm{d}t} = \sum_b (\bar{\rho}_b \hat{L}_{ab} + \hat{\rho}_b \bar{L}_{ab}) \,, \tag{A.16}$$

what is the desired recipe for the construction of the real ESE. Note that summations over the $\bar{\rho}_b$ and $\hat{\rho}_b$ are still restricted to the *independent* components and the equations are restricted to the independent components of ρ_a.

Generation of $\boldsymbol{a}$ and $\boldsymbol{b}$ matrices

Efficient calculation of the $\boldsymbol{a}$ and $\boldsymbol{b}$ matrices (see Subsection 3.3.3) is a crucial point of the solution since the formal solution of RTE is usually a "bottleneck" of the code.

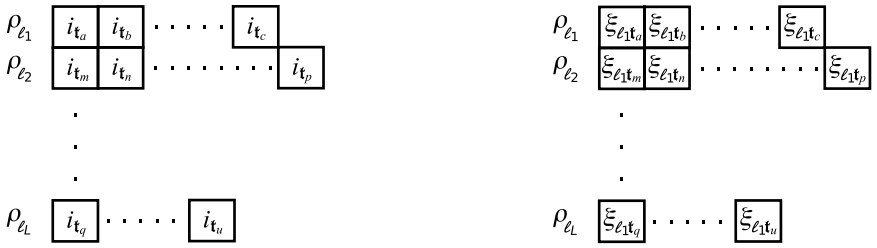

Figure A.3: Indexing of the ξ-coefficients. A list of the transition indices $i_{\mathfrak{t}_j}$ is constructed for each *lower-level* multipole ρ_{ℓ_k}. Only exciting transitions from the manifold containing ρ_{ℓ_k} are taken into account for each multipole. At first, the list of the relevant transition indices is constructed (left). Then the coefficients $\xi_{\mathfrak{t}_j}$ are calculated by the summation over the quantum numbers as described in Subsection 3.3.3 (right).

In every iteration, these matrices (or the blocks from which they are composed of) have to be calculated in every point of the grid and for every characteristic direction. To this end it is useful to precalculate and store the coefficients ξ and χ defined in Eqs. (3.78) and (3.79) in every grid node. These coefficients depend, in general, on the local magnetic field and they are calculated by the diagonalization coefficients C_J^j (cf. Subsection 2.3.3). Precalculation of the ξ and χ coefficients before the iteration process starts can be performed quite efficiently. Note that the calculation of the decoupling matrices $\boldsymbol{a}$ and $\boldsymbol{b}$ (in other words, the calculation of the transfer coefficients of RTE) directly from the definition would lead to unbearable time demands. To save the memory and to maximize the efficiency, Monopost uses the data structures described in Figure A.3 for the storage of the ξ coefficients (and analogously for χ).

Note that there are 19 non-trivial tensors $\mathcal{T}_Q^K(p, \boldsymbol{\Omega})$ (including the negative-Q tensors; see Table B.1). The $\xi_{i\mathfrak{t}}(p, K, Q)$ and $\chi_{i\mathfrak{t}}(p, K, Q)$ coefficients have to be stored for each of these tensors.

Calculation of the $\boldsymbol{a}(\boldsymbol{\Omega})$ matrix proceeds following the Algorithm A.1. An analogous algo-

rithm can be used for calculation of the $\boldsymbol{b}(\boldsymbol{\Omega})$ matrix.

input : direction of propagation $\boldsymbol{\Omega}$, Stokes parameter index p, profiles $\Phi_{\mathfrak{t}}$
output: complex $(\mathsf{N} \times \mathsf{F})$-matrix $\boldsymbol{a}(\boldsymbol{\Omega})$

initialize the $\boldsymbol{a}(\boldsymbol{\Omega})$ matrix
forall *Stokes parameters p and KQ multipoles for which* $(\mathcal{T}^K_Q(p, \boldsymbol{\Omega}) \neq 0)$ **do**
  get geometrical tensor $\mathcal{T}^K_Q(\boldsymbol{\Omega})$
  forall *lower-level multipoles* ρ_i **do**
    forall *absorption transitions* $\mathfrak{t}$ *from* ρ_i **do**
      get $\xi_{i\mathfrak{t}}(p, K, Q)$-matrix value
      forall *frequencies* ω *involved in* $\mathfrak{t}$ **do**
        add $\mathcal{T}^K_Q(p, \boldsymbol{\Omega})\Phi_{\mathfrak{t}}(\omega)\xi_{i\mathfrak{t}}(p, K, Q)$ to $a_{i\omega}$
      end
    end
  end
end

Algorithm A.1: Calculation of the $a_{i\omega}$ matrix. Note that several optimizations can be made in the algorithm to avoid the repetitive calculations. The present version of the algorithm is just to demonstrate the approach to the generation of the matrix.

Note that ξ and χ coefficients depend on the reference frame. In Monopost, they are calculated in the atomic frame (see Subsection 3.2.4). For calculations of FS in the observer's frame it is necessary to transform the absorption (η_Q, η_U, ρ_Q, ρ_U) and emission (ϵ_Q, ϵ_U) coefficients of the linear polarization components. The remaining coefficients are invariant under rotation (see Section 5.5 of Landi Degl'Innocenti & Landolfi 2004). The time penalty of this approach is small when compared to the total time needed for FS of RTE.

Appendix B

Representation of the irreducible spherical tensors

Irreducible components of the atomic density matrix

The vectors of the standard basis, $|\alpha JM\rangle$, transform under rotation of the reference frame as

$$[|\alpha JM\rangle]_{\rm new} = \sum_{M'} [|\alpha JM'\rangle]_{\rm old} \mathscr{D}^J_{M'M}(R)\,, \tag{B.1}$$

where R is the rotation that brings the old reference frame into the new one, and $\mathscr{D}^J_{MM'}(R)$ is the associated *rotation matrix* (Fano & Racah 1959). The density matrix elements expressed in the standard basis thus transform according to the rule (Brink & Satchler 1962)

$$[\rho_{\alpha JM,\alpha' J'M'}]_{\rm new} = \sum_{\mu\mu'} \mathscr{D}^J_{\mu M}(R)^* [\rho_{\alpha J\mu,\alpha' J'\mu'}]_{\rm old} \mathscr{D}^{J'}_{\mu' M'}(R)\,. \tag{B.2}$$

It is more convenient to use the *irreducible representation* of the density matrix (Sahal-Bréchot 1977),

$$\rho^K_Q(\alpha J,\alpha' J') = \sum_{MM'} (-1)^{J-M} \sqrt{[K]} \begin{pmatrix} J & J' & K \\ M & -M' & -Q \end{pmatrix} \rho_{\alpha JM,\alpha' J'M'}\,, \tag{B.3}$$

where

$$|J-J'| \le K \le J+J' \qquad \text{and} \qquad -K \le Q \le K\,. \tag{B.4}$$

In this representation, the transformation law for the rotation becomes

$$[\rho^K_Q(\alpha J,\alpha' J')]_{\rm new} = \sum_{Q'} [\rho^K_{Q'}(\alpha J,\alpha' J')]_{\rm old} \mathscr{D}^K_{Q'Q}(R)\,, \tag{B.5}$$

which is obviously simpler than Eq. (B.2). It is more convenient for use in the numerical codes because only one matrix multiplication is necessary for calculation of the rotation. Moreover, only the multipoles of the same rank K are coupled by the rotation.

Since the density matrix $\rho_{\alpha JM,\alpha' J'M'}$ is self-adjoint, we deduce from Eq. (B.3) that

$$\rho^K_Q(\alpha J,\alpha' J')^* = (-1)^{J-J'-Q} \rho^K_{-Q}(\alpha' J',\alpha J)\,. \tag{B.6}$$

The number of complex elements representing a state of the isolated J-level is $[J]^2$. Thanks to the relation (B.6) the number of *independent real numbers* required for representation of this level is the same. If the level-crossing coherences are taken into account ($\alpha J \neq \alpha' J'$) then the

number of required elements increases but the conjugation relation still guarantees that the total number of complex and independent real elements is the same.

A physical interpretation of the multipoles (B.3) is more intuitive than is the interpretation in the standard basis. The rank $K = 0$ components stand for *populations* of the levels,

$$\rho^0_0(\alpha J) = \frac{N(\alpha J)}{\sqrt{[J]}}\,, \tag{B.7}$$

and they are invariant under rotation of the reference frame. The ρ^K_0 $(K > 0)$ multipoles express an *imbalance of populations of the Zeeman sublevels*. The $Q \neq 0$ multipoles stand for the quantum *coherences* in a given basis. The elements of an even rank $(K = 2, 4, \dots)$ are called the *alignment* components. They represent an imbalance of populations of the Zeeman sublevels of different $|M|$, i.e., an alignment of the atomic angular momentum. The elements with odd rank $(K = 1, 3, \dots)$ are called the *orientation* components are they represent an imbalance of populations of the Zeeman sublevels $|\alpha JM\rangle$ and $|\alpha J\ -M\rangle$.

Irreducible representation of the radiation field tensors

The radiation enters ESE through the angle-averadged Stokes parameters. One can introduce the *irreducible radiation field tensor* (Landi Degl'Innocenti 1984)

$$J^K_Q(\omega) = \sum_{p=0}^{3} \oint \frac{\mathrm{d}\boldsymbol{\Omega}}{4\pi} \mathcal{T}^K_Q(p, \boldsymbol{\Omega}) I_p(\boldsymbol{k})\,, \tag{B.8}$$

where $I_p(\boldsymbol{k})$ are the Stokes parameters and $\mathcal{T}^K_Q(p, \boldsymbol{\Omega})$ is the geometrical tensor whose components in a given reference frame are obtained from the components of the rotation matrix $\mathscr{D}$. The explicit expressions for $\mathcal{T}^K_Q(p, \boldsymbol{\Omega})$ are given in Table B.1.

The important property of the irreducible radiation tensor of the zeroth rank follows directly form its definition, namely

$$J^0_0(\omega) = \oint \frac{\mathrm{d}\boldsymbol{\Omega}}{4\pi} I_0(\boldsymbol{k}) = J(\omega)\,, \tag{B.9}$$

where $J(\omega)$ is the mean radiation intensity.

$p=0$	$p=1$
$\mathcal{T}_0^0(0,\mathbf{\Omega}) = 1$	$\mathcal{T}_0^0(1,\mathbf{\Omega}) = 0$
$\mathcal{T}_0^1(0,\mathbf{\Omega}) = 0$	$\mathcal{T}_0^1(1,\mathbf{\Omega}) = 0$
$\mathcal{T}_1^1(0,\mathbf{\Omega}) = 0$	$\mathcal{T}_1^1(1,\mathbf{\Omega}) = 0$
$\mathcal{T}_0^2(0,\mathbf{\Omega}) = \frac{1}{2\sqrt{2}}(3\cos^2\theta - 1)$	$\mathcal{T}_0^2(1,\mathbf{\Omega}) = -\frac{3}{2\sqrt{2}}\cos 2\gamma \sin^2\theta$
$\mathcal{T}_1^2(0,\mathbf{\Omega}) = -\frac{\sqrt{3}}{2}\sin\theta\cos\theta \mathrm{e}^{\mathrm{i}\chi}$	$\mathcal{T}_1^2(1,\mathbf{\Omega}) = -\frac{\sqrt{3}}{2}(\cos 2\gamma\cos\theta + \mathrm{i}\sin 2\gamma)\sin\theta \mathrm{e}^{\mathrm{i}\chi}$
$\mathcal{T}_2^2(0,\mathbf{\Omega}) = \frac{\sqrt{3}}{4}\sin^2\theta \mathrm{e}^{2\mathrm{i}\chi}$	$\mathcal{T}_2^2(1,\mathbf{\Omega}) = -\frac{\sqrt{3}}{4}\left[\cos 2\gamma(1+\cos^2\gamma) + 2\mathrm{i}\sin 2\gamma\cos\theta\right]\mathrm{e}^{2\mathrm{i}\chi}$
$p=3$	$p=2$
$\mathcal{T}_0^0(3,\mathbf{\Omega}) = 0$	$\mathcal{T}_0^0(2,\mathbf{\Omega}) = 0$
$\mathcal{T}_0^1(3,\mathbf{\Omega}) = \sqrt{\frac{3}{2}}\cos\theta$	$\mathcal{T}_0^1(2,\mathbf{\Omega}) = 0$
$\mathcal{T}_1^1(3,\mathbf{\Omega}) = -\frac{\sqrt{3}}{2}\sin\theta \mathrm{e}^{\mathrm{i}\chi}$	$\mathcal{T}_1^1(2,\mathbf{\Omega}) = 0$
$\mathcal{T}_0^2(3,\mathbf{\Omega}) = 0$	$\mathcal{T}_0^2(2,\mathbf{\Omega}) = \frac{3}{2\sqrt{2}}\sin 2\gamma \sin^2\theta$
$\mathcal{T}_1^2(3,\mathbf{\Omega}) = 0$	$\mathcal{T}_1^2(2,\mathbf{\Omega}) = \frac{\sqrt{3}}{2}(\sin 2\gamma\cos\theta - \mathrm{i}\cos 2\gamma)\sin\theta \mathrm{e}^{\mathrm{i}\chi}$
$\mathcal{T}_2^2(3,\mathbf{\Omega}) = 0$	$\mathcal{T}_2^2(2,\mathbf{\Omega}) = \frac{\sqrt{3}}{4}\left[\sin 2\gamma(1+\cos^2\theta) - 2\mathrm{i}\cos 2\gamma\cos\theta\right]\mathrm{e}^{2\mathrm{i}\chi}$

Table B.1: Components of the irreducible spherical tensors $\mathcal{T}_Q^K(p,\mathbf{\Omega})$ (Landi Degl'Innocenti & Landolfi 2004). For the definition of the angles θ and χ see Figure 3.1. The angle γ defines the orientation of the reference polarization vector $\boldsymbol{e}_a$ with respect to the meridian (see Figure 5.14 of Landi Degl'Innocenti & Landolfi 2004). In our definition it is always $\gamma = 0$ with the exception of Chapter 5 where $\gamma = \pi/2$. The negative-Q components of the tensors are given by the relation $\mathcal{T}_{-Q}^K(p,\mathbf{\Omega}) = (-1)^Q \mathcal{T}_Q^K(p,\mathbf{\Omega})^*$.

Appendix C

Paper I: A generalized $\sqrt{\epsilon}$-law

A&A 468, 797–801 (2007)
DOI: 10.1051/0004-6361:20066507

Astronomy & Astrophysics

A generalized $\sqrt{\epsilon}$-law *(Research Note)*

The role of unphysical source terms in resonance line polarization transfer and its importance as an additional test of NLTE radiative transfer codes

J. Štěpán[1,2] and V. Bommier[2]

[1] Astronomical Institute, Academy of Sciences of the Czech Republic, 251 65 Ondřejov, Czech Republic
e-mail: stepan@asu.cas.cz
[2] LERMA, Observatoire de Paris–Meudon, CNRS UMR 8112, 5 place Jules Janssen, 92195 Meudon Cedex, France
e-mail: [jiri.stepan;V.Bommier]@obspm.fr

Received 4 October 2006 / Accepted 26 March 2007

ABSTRACT

Context. A derivation of a generalized $\sqrt{\epsilon}$-law for nonthermal collisional rates of excitation by charged perturbers is presented.
Aims. Aim of this paper is to find a more general analytical expression for a surface value of the source function which can be used as an additional tool for verification of the non-LTE radiative transfer codes.
Methods. Under the impact approximation hypothesis, static, one-dimensional, plane-parallel atmosphere, constant magnetic field of arbitrary strength and direction, two-level atom model with unpolarized lower level and stimulated emission neglected, we introduce the unphysical terms into the equations of statistical equilibrium and solve the appropriate non-LTE integral equations.
Results. We derive a new analytical condition for the surface values of the source function components expressed on the basis of irreducible spherical tensors.

Key words. line: formation – polarization – radiative transfer

1. Introduction

In the series of papers of Landi Degl'Innocenti et al. (1991a,b), Landi Degl'Innocenti & Bommier (1994) (from now on referenced as Paper I), the general formalism of resonance line polarization scattering for a two-level atom has been developed. The non-LTE problem of the 2nd kind for an arbitrary magnetic field, three-dimensional geometry of the medium and arbitrary irradiation by external sources has been discussed. The effect of inelastic collisions with charged perturbers has been considered for the particular case of a relative Maxwellian velocity distribution.

Paper I analysed the analytical properties of the solutions in the particular case of a one-dimensional, semi-infinite, static atmosphere with a constant magnetic field of arbitrary strength and direction and assuming zero external irradiation of the atmosphere. They derived a generalization of the well known $\sqrt{\epsilon}$-law (e.g. Avrett & Hummer 1965; Mihalas 1970; Hubený 1987) for the case of polarized radiation and extended the previous results of Ivanov (1990) who studied scattering in a non-magnetic regime.

In most cases of practical interest the polarization degree is rather small. The purpose of this paper is to find a new analytical solution of the non-LTE problem in unphysical conditions in order to better verify the accuracy of the polarized radiation transfer codes. This is done by introduction of an unphysical source term in the polarization into the equations of statistical equilibrium. Such a generalization can be useful in testing the accuracy of the radiative transfer codes whose purpose is to deal with the non-thermal collisional processes (for instance in the impact polarization studies of solar flares).

Following the approach of the papers quoted above, we adopt the formalism of density matrix in the representation of irreducible tensorial operators (e.g. Fano 1957). We consider the lower level with total angular momentum j to be unpolarized. This level is completely described by the overall population which is set to 1 for normalization reasons. The upper level with angular momentum j' is described by the multipole components of the statistical tensor ρ^K_Q. Coherences between different levels j and j' are neglected but coherences between Zeeman sublevels of level j' are in general taken into account. The calculation is performed in the Wien limit of line frequency whose assumption makes it possible to neglect stimulated emission effect, and to preserve the linearity of the non-LTE problem.

2. Equations of statistical equilibrium

The suitable coordinate system Σ_0 for atomic state description is the one with the z-axis directed along the magnetic field (see Fig. 1).

Radiative rate contributions to the evolution of statistical operator ρ^K_Q are given by (Landi Degl'Innocenti 1985)

$$\left[\frac{\mathrm{d}\rho^K_Q}{\mathrm{d}t}\right]_{\mathrm{RAD}} = -\mathrm{i}A_{j'j}\Gamma Q\rho^K_Q - A_{j'j}\rho^K_Q + \frac{w^{(K)}_{j'j}(-1)^Q}{\sqrt{2j'+1}}B_{jj'}\bar{J}^K_{-Q}. \quad (1)$$

In this equation $A_{j'j}$ ($B_{jj'}$) is the Einstein coefficient of spontaneous emission (absorption) from level j' (j) to level j (j').

$\Gamma = 2\pi g_{j'} \nu_L / A_{j'j}$ with $g_{j'}$ being the Landé factor of the level j' and ν_L is the Larmor frequency. The transition-dependent numerical factor $w^{(K)}_{j'j}$ has been defined by Landi Degl'Innocenti (1984) as have the irreducible components of the mean radiation tensor $\overline{J}^K_Q$. Besides the radiative rates, collisional rates have to be considered in the statistical equilibrium, because the source of radiation in a semi-infinite atmosphere is the collisional excitation followed by radiative de-excitation. Thus, the source term of the radiative transfer equation originates in the inelastic collision effect. As the purpose of the present paper is to consider unphysical source terms in the non-zero ranks (K, Q) of the irreducible tensorial operator basis T^K_Q, we will introduce an unphysical (K, Q)-dependence to the inelastic collisional rates of the statistical equilibrium equation below. The purpose here is not to thus describe anisotropic collisions, which would require a proper formalism that is out of the scope of the present paper (see, for instance, Landi Degl'Innocenti & Landolfi 2004, for a two-level atom, and Derouich 2006, for polarization transfer rates in a multi-level atom due to isotropic collisions). We introduce as usual the depolarizing rate due to isotropic elastic collisions. Thus, the contribution of collisional rates reads

$$\left[\frac{\mathrm{d}\rho^K_Q}{\mathrm{d}t}\right]_{\mathrm{COLL}} = (C_{jj'})^K_Q - (C^{\mathrm{R}}_{j'j})^K_Q \rho^K_Q - D^{(K)} \rho^K_Q. \tag{2}$$

The terms $(C_{jj'})^K_Q$ and $(C^{\mathrm{R}}_{j'j})^K_Q$ on the right-hand side of Eq. (2) are the multipole components of collisional rates of excitation and relaxation respectively. $D^{(K)}$ is the depolarization rate due to elastic collisions[1].

The radiative and collisional rates can be added under the impact approximation hypothesis (Bommier & Sahal-Bréchot 1991) $\mathrm{d}\rho^K_Q/\mathrm{d}t = [\mathrm{d}\rho^K_Q/\mathrm{d}t]_{\mathrm{RAD}} + [\mathrm{d}\rho^K_Q/\mathrm{d}t]_{\mathrm{COLL}}$. Using Eqs. (1), (2), and the condition for static atmosphere, $\mathrm{d}\rho^K_Q/\mathrm{d}t = 0$, we obtain the equations of statistical equilibrium

$$\left[\mathrm{i}A_{j'j}\Gamma Q + A_{j'j} + (C^{\mathrm{R}}_{j'j})^K_Q + D^{(K)}\right]\rho^K_Q = \frac{w^{(K)}_{j'j}(-1)^Q}{\sqrt{2j'+1}} B_{jj'} \overline{J}^K_{-Q} + (C_{jj'})^K_Q. \tag{3}$$

By applying the relation between Einstein coefficients for spontaneous emission and absorption,

$$B_{jj'} = \frac{2j'+1}{2j+1}\frac{c^2}{2h\nu_0^3} A_{j'j}, \tag{4}$$

and dividing formula (4) by $A_{j'j}$, we obtain the equation

$$\left(1 + \epsilon^K_Q + \delta^{(K)} + \mathrm{i}\Gamma Q\right)\rho^K_Q = (-1)^Q w^{(K)}_{j'j} \overline{J}^K_{-Q} \frac{\sqrt{2j'+1}}{2j+1} \times \frac{c^2}{2h\nu_0^3} + \frac{(C_{jj'})^K_Q}{A_{j'j'}}. \tag{5}$$

One can introduce the dimensionless parameter of the depolarization rate

$$\delta^{(K)} = \frac{D^{(K)}}{A_{j'j}}, \tag{6}$$

[1] This process cannot change a total population of the level. Therefore it is always $D^{(0)} = 0$. We take formally into account only the depolarization rate $D^{(K)}$ to use a formalism coherent with the previous papers. A general treatment of physically more relevant transfer of multipole components of the upper level is out of scope of this paper.

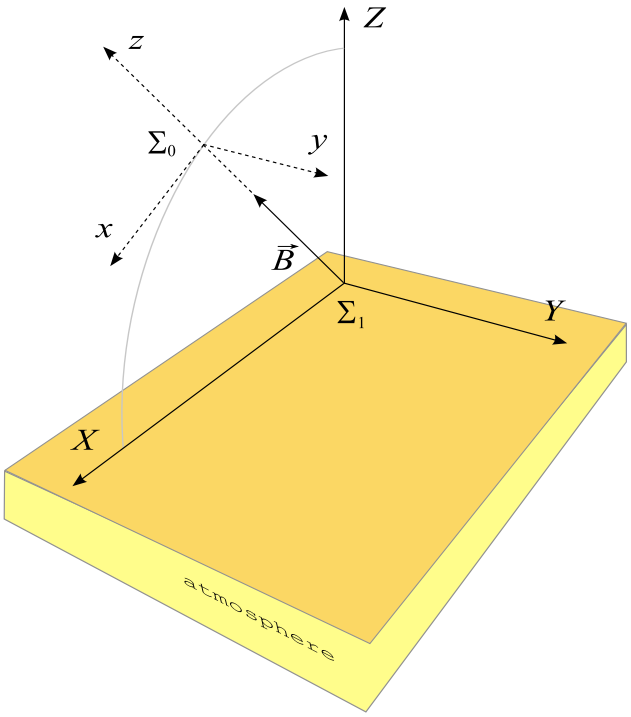

Fig. 1. The reference frame Σ_1 has its Z-axis oriented vertically with respect to the atmosphere, while the z-axis of the reference frame Σ_0 is parallel to the direction of magnetic field $\boldsymbol{B}$. The axes X and x lie in the same plane defined by Z-axis and $\boldsymbol{B}$; the axes Y and y are defined to complement the right-handed orthogonal coordinate systems.

and the irreducible tensor which plays the role of generalized photon destruction probability

$$\epsilon^K_Q = \frac{(C^{\mathrm{R}}_{j'j})^K_Q}{A_{j'j'}}. \tag{7}$$

If the relation $(C^{\mathrm{R}}_{j'j})^K_Q \neq 0$ is satisfied we may define the quantity

$$B^{(KQ)} = \frac{2h\nu_0^3}{c^2}\frac{2j+1}{\sqrt{2j'+1}}\frac{(C_{jj'})^K_Q}{(C^{\mathrm{R}}_{j'j})^K_Q}. \tag{8}$$

It is easy to show (see below) that in the particular case of a Maxwellian velocity distribution of colliders the relation $B^{(00)} = B_{\mathrm{P}}$ is satisfied, where B_{P} is the Planck function in the Wien limit at given temperature. Using the definition of irreducible components of the two-level source function (cf. Paper I)

$$S^K_Q = \frac{2h\nu_0^3}{c^2}\frac{2j+1}{\sqrt{2j'+1}}\rho^K_Q, \tag{9}$$

we obtain the statistical equilibrium equations in the compact form

$$\left(1 + \epsilon^K_Q + \delta^{(K)} + \mathrm{i}\Gamma Q\right) S^K_Q = w^{(K)}_{j'j}(-1)^Q \overline{J}^K_{-Q} + \epsilon^K_Q B^{(KQ)}. \tag{10}$$

3. Solution of the Wiener-Hopf equations

From now on we reduce our analysis to the case of semi-infinite, plane-parallel geometry with constant magnetic field along the

atmosphere. The velocity distribution and volume density of colliders is also constant along the atmosphere but it is in general non-thermal. The only position coordinate is the common line optical depth τ.

Following the procedure of Paper I a formal solution of radiative transfer equation is substituted into the definition of tensor $\overline{J}^K_Q$; after that we obtain a set of integral Wiener-Hopf equations of the 2nd kind,

$$(1 + \epsilon^K_Q + \delta^{(K)} + \mathrm{i}\Gamma Q) S^K_Q(\tau) = \sum_{K'Q'} \int_0^\infty \widetilde{K}_{KQ,K'Q'}(\tau,\tau') S^{K'}_{Q'}(\tau')\mathrm{d}\tau' + \epsilon^K_Q B^{(KQ)}, \quad (11)$$

which describe coupling of the tensors $\rho^K_Q(\tau)$ at different optical depths via radiation. Several important properties of kernels $\widetilde{K}_{KQ,K'Q'}(\tau,\tau')$ have been discussed by Landi Degl'Innocenti et al. (1990) and in Paper I. Using their indexing notation one can rewrite the Eq. (11) in the shorthanded form

$$a_i S_i(\tau) = \sum_j \int_0^\infty K_{ij}(|\tau - \tau'|) S_j(\tau')\mathrm{d}\tau' + b_i, \quad (12)$$

with

$$a_i = 1 + \epsilon^K_Q + \delta^{(K)} + \mathrm{i}\Gamma Q, \quad (13)$$

$$b_i = \epsilon^K_Q B^{(KQ)}. \quad (14)$$

The index i in these expressions runs between the limits 1 and N, where N is the number of ^K_Q-multipoles. In the following we briefly repeat the derivation performed by Frisch & Frisch (1975) emphasizing the differences due to presence of b_i terms.

Calculation of the derivative of (12) with respect to τ, splitting the integral on the right-hand side into two parts, multiplication of the equation by $S_i(\tau)$, summation over index i, and finally integration with respect to τ leads to the set of equations

$$\sum_i a_i \int_0^\infty S_i(\tau)\frac{\mathrm{d}S_i(\tau)}{\mathrm{d}\tau}\mathrm{d}\tau = \sum_{i,j} S_j(0) \int_0^\infty K_{ij}(\tau) S_i(\tau)\mathrm{d}\tau + \sum_{i,j} \int_0^\infty \mathrm{d}\tau S_i(\tau) \int_0^\infty \mathrm{d}\tau' K_{ij}(|\tau' - \tau|)\frac{\mathrm{d}S_j(\tau')}{\mathrm{d}\tau'}. \quad (15)$$

The left-hand side of (15) is easily evaluated as

$$\frac{1}{2}\sum_i a_i \left[S_i(\infty)^2 - S_i(0)^2\right]. \quad (16)$$

The first term on the right-hand side of (15) is evaluated using the kernels symmetry $K_{ij}(t) = K_{ji}(t)$ and Eq. (12), so that we obtain

$$\sum_i S_i(0)\left[a_i S_i(0) - b_i\right], \quad (17)$$

while the second term equals

$$\frac{1}{2}\sum_i a_i \left[S_i(\infty)^2 - S_i(0)^2\right] - \sum_i b_i \left[S_i(\infty) - S_i(0)\right]. \quad (18)$$

We put these results into (15) to get

$$\sum_i a_i S_i(0)^2 = \sum_i b_i S_i(\infty). \quad (19)$$

Calculation of the limit $\tau \to \infty$ of both sides of Eq. (12) leads to the set of linear algebraic equations for the components of source function tensor in the infinite depth:

$$\sum_j \left[a_j\delta_{ij} - \int_{-\infty}^\infty K_{ij}(t)\mathrm{d}t\right] S_j(\infty) = b_i. \quad (20)$$

We can solve these equations and write

$$\boldsymbol{S}(\infty) = \boldsymbol{L}^{-1}\boldsymbol{b}, \quad (21)$$

where $\boldsymbol{S}$ is the formal vector of S_i components, $\boldsymbol{b}$ is the formal vector of b_i components, and the elements of matrix $\boldsymbol{L}$ are defined by relation

$$\{\boldsymbol{L}\}_{ij} = a_j\delta_{ij} - \int_{-\infty}^\infty K_{ij}(t)\mathrm{d}t. \quad (22)$$

Establishing a new matrix $\boldsymbol{\ell} = \boldsymbol{L}^{-1}$ and substituting (21) into (19) leads to the generalized form of the $\sqrt{\epsilon}$-law

$$\sum_i a_i S_i(0)^2 = \sum_{i,j} b_i b_j \ell_{ij}. \quad (23)$$

4. Particular solutions

Setting the special conditions for magnetic field and collisional rates, one recovers the less general but more common and explicit formulations of the $\sqrt{\epsilon}$-law than the one given by (23). In the following sections we will verify this result in the limiting conditions assumed in recent papers and we will analyse the simple examples of non-thermal collisional excitation.

4.1. Maxwellian velocity distribution of colliders

In the case of Maxwellian velocity distribution of colliders, relaxation rates of all multipole components ρ^K_Q are the same:

$$(C^{\mathrm{R}}_{j'j})^K_Q = C^{\mathrm{R}}_{j'j}, \quad (24)$$

where $C^{\mathrm{R}}_{j'j}$ is the usual relaxation rate for collisional deexcitation from j' to j. For excitation rates one has

$$(C_{jj'})^K_Q = \frac{C_{jj'}}{\sqrt{2j'+1}}\delta_{K0}\delta_{Q0}, \quad (25)$$

where the factor $(2j'+1)^{-1/2}$ has been introduced to make a connection with the usual collisional rate $C_{jj'}$ of standard unpolarized theory. In this isotropic case, there is no collisional excitation of higher ranks of density matrix. From the assumption of thermodynamic equilibrium one has

$$\frac{C_{jj'}}{C^{\mathrm{R}}_{j'j}} = \frac{2j'+1}{2j+1}\mathrm{e}^{-h\nu_0/k_{\mathrm{B}}T}, \quad (26)$$

where k_{B} stands for the Boltzmann constant and T for a temperature of the atmosphere. From (24) and (7) it is evident that $\epsilon^K_Q = \epsilon$ for all possible K and Q, where ϵ is the common photon destruction probability. Further

$$B^{(KQ)} = B_{\mathrm{P}}\delta_{K0}\delta_{Q0}. \quad (27)$$

Substituting the rates (24) and (25) into formula (22) and employing the general identity $\int_{-\infty}^\infty K_{i1}(t)\mathrm{d}t = \delta_{i1}$ (see Paper I)

together with $b_i = \delta_{i1}$, we recover form (23) the formula (16) of the previously cited paper:

$$\sum_{KQ}(1+\epsilon+\delta^{(K)}+\mathrm{i}\Gamma Q)[S^K_Q(0)]^2 = \epsilon B_\mathrm{P}^2. \tag{28}$$

Assuming that there is zero magnetic field, i.e. $\Gamma = 0$, the source function tensor reduces due to symmetry reasons to the two non-vanishing components S^0_0 and S^2_0 in the reference frame Σ_1. This reference frame is suitable for descriptions of the atomic system under these conditions, so that we may identify $\Sigma_0 \equiv \Sigma_1$, with X and Y axes oriented arbitrary in the plane parallel to atmospheric surface. Further, assuming that there is no depolarization of the upper level ($\delta^{(K)} = 0$), we realize from (28):

$$\sqrt{\left[S^0_0(0)\right]^2+\left[S^2_0(0)\right]^2} = \sqrt{\frac{\epsilon}{1+\epsilon}}B_\mathrm{P} = \sqrt{\epsilon'}B_\mathrm{P}, \tag{29}$$

which is the same result derived in different notation by Ivanov (1990). For simplicity the common alternative to the photon destruction probability has been introduced: $\epsilon' = \epsilon/(1+\epsilon)$.

If depolarization of the upper level is high enough to destroy atomic level polarization ($\delta^{(K)} \to \infty$ for $K > 0$), or the upper level is unpolarizable, the common $\sqrt{\epsilon}$-law for scalar radiation is recovered,

$$S^0_0(0) = \sqrt{\frac{\epsilon}{1+\epsilon}}B_\mathrm{P} = \sqrt{\epsilon'}B_\mathrm{P}. \tag{30}$$

4.2. Anisotropic alignment (de)excitation

The relation $\epsilon^K_Q = \epsilon$ is not in general satisfied for all the multipoles because the relaxation of the ρ^K_Q state depends on the velocity distribution of colliders. In the following text we will neglect the effects of magnetic field.

Let us assume an example of a relative velocity distribution of particles that is axially symmetric with the axis of symmetry parallel to the vertical of the atmosphere (so that it is as in the former case $\Sigma_0 \equiv \Sigma_1$) and that the collisional interaction can be fully described by only the first two even multipole components of this distribution. Thanks to these assumptions the only non-vanishing excitation collisional rates are $(C_{jj'})^0_0$ and $(C_{jj'})^2_0$, the relaxation rates $(C^\mathrm{R}_{j'j})^0_0$ and $(C^\mathrm{R}_{j'j})^2_0$ and for the same reasons the only non-zero source function components are S^0_0 and S^2_0.

An explicit evaluation of the integrals of kernels $\int_{-\infty}^{\infty}\widetilde{K}_{KQ,K'Q'}(\tau,\tau')\mathrm{d}\tau'$ under these conditions shows that the only non-zero ones are given by (A5) and (A12) of Landi Degl'Innocenti et al. (1991b). In our notation they read

$$\int_{-\infty}^{\infty}\widetilde{K}_{00,00}(\tau,\tau')\mathrm{d}\tau' = 1, \tag{31}$$

$$\int_{-\infty}^{\infty}\widetilde{K}_{20,20}(\tau,\tau')\mathrm{d}\tau' = \frac{7}{10}W_2, \tag{32}$$

with $W_2 = (w^{(2)}_{j'j})^2$. Substituting these results into (23) we see that

$$\left(1+\epsilon^0_0\right)\left(S^0_0\right)^2+\left(1+\epsilon^2_0\right)\left(S^2_0\right)^2 = \epsilon^0_0\left(B^{(00)}\right)^2 + \frac{\left(\epsilon^2_0 B^{(20)}\right)^2}{1+\epsilon^2_0-\frac{7}{10}W_2}. \tag{33}$$

To check the validity of polarized radiative transfer codes, it is advantageous if one can verify that the transfer of higher ranks of the radiation tensor is accurate enough. In the realistic scattering polarization models the polarization degree does not exceed a few percent so that $|S^0_0(0)| \gg |S^K_Q(0)|$. By setting arbitrary (even unphysical) collisional rates it is possible to verify transfer codes in conditions with $|S^0_0| \ll |S^K_Q|$.

To privilege transfer in higher ranks of the radiation tensor one can artificially suppress the excitation rate $(C_{jj'})^0_0$. In the extremal case one can set $(C_{jj'})^0_0 \to 0$. The easiest way to do this is the formal interchange of the role of excitation rates of population and alignment, i.e. $(C_{jj'})^0_0 \leftrightarrow (C_{jj'})^2_0$ of the original Maxwellian velocity distribution:

$$(C_{jj'})^0_0 = 0, \quad (C_{jj'})^2_0 = \frac{C_{jj'}}{\sqrt{2j'+1}} \tag{34}$$

(no collisional excitation to upper level population) and the relaxation rates set to the Maxwellian ones

$$(C^\mathrm{R}_{j'j})^0_0 = (C^\mathrm{R}_{j'j})^2_0 = C^\mathrm{R}_{j'j}. \tag{35}$$

In this case we have

$$B^{(00)} = 0, \quad B^{(20)} = B_\mathrm{P}, \tag{36}$$

and again

$$\epsilon^0_0 = \epsilon^2_0 = \epsilon. \tag{37}$$

Substituting this into (33) we find out the $\sqrt{\epsilon}$-law in the form

$$\sqrt{[S^0_0(0)]^2+[S^2_0(0)]^2} = \frac{\epsilon'}{\sqrt{1-\frac{7}{10}W_2(1-\epsilon')}}B_\mathrm{P}. \tag{38}$$

The particular collisional rates (34) are in fact arbitrary and have been chosen to obtain a formula similar to the one of the Maxwellian distribution case.

This relation is useful to test polarized radiative transfer codes, because in this unphysical case $S^2_0(0)$ is the largest term, unlike the physical case where the largest term is $S^0_0(0)$ and $S^2_0(0)$ is only a few percent of it. By applying Eq. (38) the test is much more sensitive to the polarization, and the polarization is better tested. We have thus successfully tested a multilevel non-LTE radiative transfer code that we are developing, but this code and its results are the subjects of a forthcoming paper.

5. Conclusions

We have derived a more general formulation of the so-called $\sqrt{\epsilon}$-law of radiation transfer. This analytical condition couples the value of source function tensor of a two-level atom with other physical properties of the atmosphere. The simplest result obtained in conditions of a non-magnetic, isothermal, plane-parallel, semi-infinite atmosphere with thermal velocity distribution of particles and unpolarized atomic levels (e.g. Mihalas 1970) has been generalized by Ivanov (1990) to account for scattering of polarized radiation and polarized upper atomic level. Further generalizations done in Paper I, which account for a magnetic field of arbitrary strength and direction, has been extended in the present paper to account for non-thermal collisional interactions. It was done by introducing the tensor of the photon destruction probability ϵ^K_Q and by defining the function $B^{(KQ)}$.

The resulting formula (23) reduces to the cases mentioned above if the physical conditions become more symmetric. On

the other hand, situations with a high degree of perturbers velocity distribution anisotropy and especially ones with unphysical collisional rates result in a wide range of models which can be calculated both numerically and analytically. Thus they offer new possibilities for verification of the non-LTE radiation transfer codes.

References

Avrett, E. H., & Hummer, D. G. 1965, MNRAS, 130, 295
Bommier, V., & Sahal-Bréchot, S. 1991, Ann. Phys. Fr., 16, 555
Derouich, M. 2006, A&A, 449, 1
Fano, U. 1957, Rev. Mod. Phys., 29, 74
Frisch, U., & Frisch, H. 1975, MNRAS, 173, 167
Hubený, I. 1987, A&A, 185, 332
Ivanov, V. V. 1990, Soviet Astron., 34, 621
Landi Degl'Innocenti, E. 1984, Sol. Phys., 91, 1
Landi Degl'Innocenti, E. 1985, Sol. Phys., 102, 1
Landi Degl'Innocenti, E., & Bommier, V. 1994, A&A, 284, 865
Landi Degl'Innocenti, E., & Landolfi, M. 2004, Polarization in Spectral Lines (Kluwer Acad. Publ.)
Landi Degl'Innocenti, E., Bommier, V., & Sahal-Bréchot, S. 1990, A&A, 235, 459
Landi Degl'Innocenti, E., Bommier, V., & Sahal-Bréchot, S. 1991a, A&A, 244, 391
Landi Degl'Innocenti, E., Bommier, V., & Sahal-Bréchot, S. 1991b, A&A, 244, 401
Mihalas, D. 1970, Stellar Atmospheres (W. H. Freeman and Company)

Appendix D

Paper II: NLTE effects in the formation of polarized lines of multiterm atoms

NLTE effects in the transfer of polarized lines of multiterm atoms

J. Štěpán

Astronomical Institute, Academy of Sciences of the Czech Republic, v.v.i., Fričova 298, 25165 Ondřejov, Czech Republic,
LERMA, Observatoire de Paris – Meudon, CNRS UMR 8112, 5 place Jules Janssen, 92195 Meudon Cedex, France

Abstract. The formation of spectral lines in a magnetized atmosphere is a complex issue both from the conceptual and computational point of view. The NLTE effects have been shown to play a significant role in many astrophysical situations both for unpolarized and polarized cases. We present a code for the NLTE radiative transfer calculations in a plane-parallel magnetized atmosphere for the so-called multiterm picture of atomic levels. We discuss the effects of NLTE radiative transfer on the polarization state of emergent radiation.

1. Introduction

We have developed a numerical code for the self-consistent NLTE modeling of polarized radiative transfer in spectral lines. Here we present a brief overview of the capabilities of the code. We also show a solution of a simple 1D model. We adopted the so-called multiterm picture of atomic levels in the Paschen-Back effect regime. Coherences between different J-levels of the same term are taken into account (Landi Degl'Innocenti & Landolfi 2004). The main attributes of the code are summarized below.

1. Density matrix description of the atomic state. Density matrix is expressed within the spherical tensors representation.
2. LS coupling. Quantum interferences between fine structure levels pertaining to the same term are allowed. Density matrix elements have the form ${}^{\delta LS}\rho^K_Q(J,J')$.
3. Incomplete Paschen-Back effect regime. Atomic Hamiltonian is diagonalized at each point of the atmosphere.
4. Collisional effects can be added within the impact approximation.
5. Flat-spectrum approximation. Spectrum of the radiation must be flat over the frequency interval larger than separation of the J-levels pertaining to the same term and than their width (cf. Landi Degl'Innocenti & Landolfi 2004)
6. Formal solution of the radiative transfer equation is calculated using the parabolic version of the short characteristics method (DELOPAR, Trujillo Bueno 2003). The full Stokes vector $\boldsymbol{I} = (I, Q, U, V)$ is treated.

7. Efficient self-consistent NLTE. Multigrid technique (MG) with modified accelerated lambda iteration method as a smoother is implemented. Linear convergence rate in the number of grid nodes is guaranteed.

2. Iterative scheme

We follow the operator-splitting ideas of Rybicki & Hummer (1992) (unpolarized multilevel radiative transfer of *overlapping lines*) and Trujillo Bueno (1999) (first formulation of the *multilevel* preconditioning strategy for the *polarized* case). We use a rather general lambda-operator splitting that leads to the preconditioning of the equations of statistical equilibrium (ESE) of the multiterm atom. A kind of accelerated lambda iteration (ALI) or Jacobi technique is obtained after linearization of the equations. We use these ALI iterations as a smoothing procedure in our implementation of the multigrid method (Štěpán 2006). Below, we give a brief overview of several aspects of the ALI method.

The formal solution of the radiative transfer equation

$$\frac{\mathrm{d}\boldsymbol{I}}{\mathrm{d}s} = \boldsymbol{J} - \boldsymbol{K}\boldsymbol{I} \tag{1}$$

can be expressed in the form

$$\boldsymbol{I} = \Lambda\boldsymbol{S} - \Lambda\boldsymbol{K}'\boldsymbol{I} + \boldsymbol{T}\,, \tag{2}$$

where $\boldsymbol{T}$ is the transmitted part of radiation from the surface, Λ is the common Λ-operator of the radiative transfer theory, $\boldsymbol{S} = \boldsymbol{J}/\eta_I$ is the formal source function vector, and $\boldsymbol{K}' = \boldsymbol{K}/\eta_I - \boldsymbol{1}$ is the modified propagation matrix (Rees et al. 1989). Expressing $\boldsymbol{S}$ as a linear combination of unknown density matrix elements of the *upper* term, splitting the *first* Λ-operator in the r.h.s. of Eq. (2) into its diagonal and off-diagonal parts ($\Lambda \to \Lambda^* + (\Lambda - \Lambda^*)$), one arrives, after several steps, at the preconditioning scheme

$$J^0_0(\alpha\beta)\rho_j \;\;\to\;\; J^0_0(\alpha\beta)^+\rho_j + \sum_{\overline{k}} L_{\alpha\beta\overline{k}}(\rho_{\overline{k}}\rho^+_j - \rho^+_{\overline{k}}\rho_j)\,, \tag{3}$$

$$J^K_Q(\alpha\beta)\rho_j \;\;\to\;\; J^K_Q(\alpha\beta)^+\rho_j\,, \qquad (K>0)\,. \tag{4}$$

Here index j is the abbreviation of density matrix multipole (i.e., $j \equiv \delta LSJJ'KQ$). $\overline{k}$ is the index of the *population* multipoles of the density matrix, i.e. the ρ^0_0 elements of the upper term. The α and β indices identify the lower and upper term of the transition respectively. $J^K_Q(\alpha\beta)$ is the mean radiation field tensor of the α–β line. The exlicit form of the coefficient $L_{\alpha\beta\overline{k}}$ will be given elsewhere. It can be calculated at each point of the atmosphere quite efficiently along with the formal solution. The superscript "+" means a guess of the quantities calculated in the previous iteration step.

It is worth to say that the method of Manso Sainz & Trujillo Bueno (2003) for the multilevel atoms in the Zeeman effect regime is obtained as a limiting case of the present scheme for low magnetic fields and multilevel picture of the levels.

The ALI scheme plotted above is used as an error-smoother in the efficient MG technique. A detailed description of the implementation of the method is out of scope of this work and it will be given in a forthcoming paper. For a brief review of the subject see also Štěpán (2006).

3. Toy model

In this section, we show a simple demonstration of the NLTE solution. We consider the transfer in the multiplet ^{3}S–^{3}P. Both lower and upper terms can be polarized, stimulated emission is taken into account. The ratio of the fine-structure levels splitting of the upper term and their natural width is set to $x = 0.5$ (see Eq. (10.142) of Landi Degl'Innocenti & Landolfi (2004) for the exact definition of x). We assume pure radiation scattering. All collisional effects, both inelastic and elastic, have been neglected.

Worth to emphasize that the method can only be used if the flat-spectrum approximation holds (cf. point 5 in the Section 1). That is not true in general for the fine-structure splitting. However, we suppose that both natural width and frequency separation of the J-levels are much smaller than the Doppler width of the line, hence the spectrum is well smoothed out by the Doppler motions.

A geometry scenario of the model is showed in Fig. 1. The optical thickness of the homogeneous slab has been varied to discover the radiation transfer effects on the linear polarization state of the emergent radiation (we ignore the Stokes V parameter in this work).

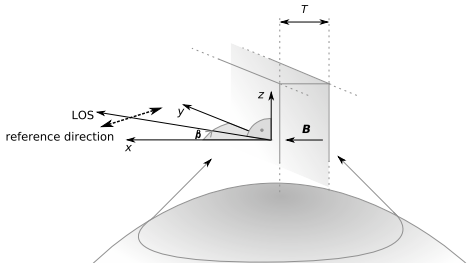

Figure 1. Infinite slab with the line-center optical thickness T is irradiated by the unpolarized anisotropic radiation from solar surface. Anisotropy factor of the incident radiation is $w = 0.1$. The magnetic field is perpendicular to the slab and the line-of-sight is perpendicular to the solar radius (the prominence case). Number of incoming photons per mode at the line frequency is $\overline{n} = 0.03$.

Polarization diagrams for three optical thicknesses of the slab are plotted in Fig. 2. As expected (cf. Landi Degl'Innocenti et al. 1987) the polarization direction is rotated with respect to the limb even in the zero magnetic field case. It is a pure radiation transfer effect. Linear polarization degree is obviously decreased due to transfer. The Hanle effect demonstrates itself in the diagrams as a rotation of the linear polarization direction and by modification of the polarization degree. Increased magnetic field leads to transition from the Zeeman to Paschen-Back effect regime. One can see the signatures of the level-crossing coherences in the ^3P term as the closed loops in the plots (see Bommier (1980)

for details). The symmetry of the Hanle diagram (the fundamental ambiguity) is obviously broken in the optically thick case.

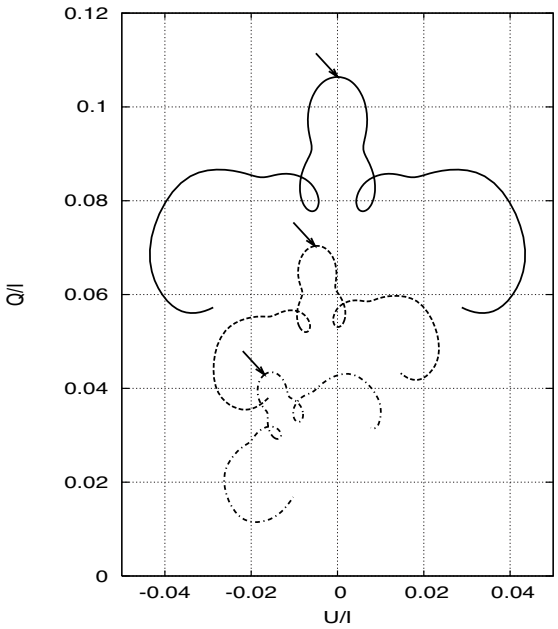

Figure 2. Hanle diagram of the emergent radiation observed at $\beta = 37°$ (right branch) and $\beta = 143°$ (left branch; see Figure 1). Solution for three different line-center optical thicknesses of the slab are plotted: $T = 0$ (solid line), $T = 1$ (dashed line), and $T = 3$ (dash-dotted line). The integral fractional linear polarization in Q/I and U/I are calculated for the magnetic field intensity varying between $\gamma = 0$ (pointed by the arrows) to $\gamma = 2.8$ in all plots (see Eq. (3.63) of Landi Degl'Innocenti & Landolfi (2004) for the definition of γ).

Acknowledgments. This work was supported by the project LC06014 of Center for Theoretical Astrophysics.

References

Bommier, V. 1980, A&A, 87, 109

Landi Degl'Innocenti, E. & Bommier, V. & Sahal-Bréchot, S. 1987, A&A, 186, 335

Landi Degl'Innocenti, E., & Landolfi, M. 2004, Polarization in Spectral Lines (Dordrecht: Kluwer)

Manso Sainz, M., & Trujillo Bueno, J. 2003, in ASP Conf. Ser. Vol. 307, Solar Polarization, eds. J. Trujillo Bueno and J. Sánchez Almeida, (San Francisco: ASP) 251

Rees, D. E., Durrant, C. J., & Murphy, G. A. 1989, ApJ, 339, 1093

Rybicki, G. B. & Hummer, D. G. 1992, A&A, 262, 209

Štěpán, J. 2006, in ASP Conf. Ser. Vol. 358, Solar Polarization 4, eds. R. Casini and B. W. Lites J., (San Francisco: ASP), 148

Trujillo Bueno, J. 1999, in ASSL Ser. 243, Solar Polarization, eds. K. N. Nagendra & J. O. Stenflo, (Dordrecht: Kluwer), 73

Trujillo Bueno, J. 2003, in ASP Conf. Ser. Vol. 288, Stellar Atmosphere Modeling, ed. Ivan Hubeny, Dimitri Mihalas & Klaus Werner (San Francisco: ASP), 551

Appendix E

Paper III: Multigrid methods for polarized radiative transfer

Solar Polarization 4
ASP Conference Series, Vol. 358, 2006
R. Casini and B. W. Lites

Multigrid Methods for Polarized Radiative Transfer

J. Štěpán

Astronomical Institute, Academy of Sciences of the Czech Republic, CS-25165 Ondřejov, Czech Republic

LERMA, Observatoire de Paris-Meudon, 5 Place Jules Janssen, F-92195 Meudon, France

Abstract. A new iterative method for non-LTE multilevel polarized radiative transfer in hydrogen lines is presented. Iterative methods (such as the Jacobi method) tend to damp out high-frequency components of the error fast, but converges poorly due to slow reduction of low-frequency components. The idea is to use a set of differently coarsed grids to reduce both the short- and long-period errors. This leads to the so-called multigrid (MG) methods. For the grid of N spatial points, the number of iterations required to solve a non-LTE transfer problem is of the order of $O(N)$. This fact could be of great importance for problems with fine structure and for multi-dimensional models. The efficiency of the so-called standard MG iteration in comparison to Jacobi iteration is shown. The formalism of density matrix is applied to the demonstrative example of 1D, semi-infinite, non-magnetic, 3-principal level hydrogen atmospheric model. The effect of depolarizing collisions with thermal electrons is taken into account as well as general treatment of overlapping profiles.

1. Formulation of the Problem

In this paper we briefly discuss the usage of multigrid (MG) iteration schemes to solve the non-LTE problem of the 2nd kind as defined by Landi Degl'Innocenti (1987). The era of extensive development of MG methods started in 1970's by the work of Brandt (1977). Several steps in using MG methods applied to radiative transfer were made by Steiner (1991), Väth (1994), and Fabiani Bendicho, Trujillo Bueno, & Auer (1997). These authors showed that this technique leads to a great improvement of the convergence rate. This paper demonstrates how to apply these methods to a more general solution of polarized radiative transfer with realistic multilevel atomic models and complicated structure of overlapping lines. The effects of depolarizing collisions is taken into account.

For the description of the atomic state, we adopt the density-matrix formalism and the representation in the basis of irreducible tensorial operators (e.g., Fano 1957). The elements of atomic density matrix have the usual form[1] $\rho^k_q(\alpha j)$, where αj is the energy level of total angular momentum j, and (k, q) are the multipolar components of the level ($k = 0, \ldots, 2j$, $q = -k, \ldots, k$). In stationary

[1] We suppose that all coherences between different energy levels vanish due to further assumptions.

regime, the density-matrix elements are solutions of the local statistical equilibrium equations,

$$\sum_{\alpha jkq} \Pi_{\alpha' j' k' q',\, \alpha jkq}\, \rho^k_q(\alpha j) = 0 \,. \tag{1}$$

The structure of the Π-matrix has been extensively discussed by Sahal-Bréchot (1977), Bommier (1978), and Bommier (1980). We assume that this matrix has the form $\mathbf{\Pi} = \mathbf{R} + \mathbf{C}$, where $\mathbf{R}$ is the matrix of radiative rates, and $\mathbf{C}$ is the matrix of collisional rates (impact approximation).

The radiative transfer equation for the set of four Stokes parameters $\boldsymbol{S} \equiv (I, Q, U, V)^{\mathrm{T}}$ has the usual form

$$\frac{\mathrm{d}\boldsymbol{S}}{\mathrm{d}s} = \boldsymbol{J} - (\mathbf{K} - \mathbf{K}^{\mathrm{s}})\, \boldsymbol{S} \,,$$

where $\boldsymbol{J}$ is the emission vector of the local sources, $\mathbf{K}$ is the absorption matrix, and $\mathbf{K}^{\mathrm{s}}$ is the matrix of stimulated emission. All these quantities are dependent on radiation frequency, ν, position vector, $\boldsymbol{x}$, and direction of propagation determined by the unit vector $\mathbf{\Omega}$. Finally, s is the parametrization of the radiation path along the $\mathbf{\Omega}$ direction.

2. Standard Multigrid Method

Most of the existing non-LTE solvers use the methods based on Λ-operator splitting similar to the one of Rybicki & Hummer (1991, 1992). Depending on organization, these schemes are numerically equivalent to the Jacobi or Gauss-Seidel smoothing procedures (for details, see Paletou & Léger 2005). These smoothing procedures do reduce high frequencies of the solution fast, but poor convergence is achieved for low frequencies. (With "high frequencies" we mean those which are comparable to the spatial frequency of grid points approximating the continuous scale.) The principles of MG schemes are based on the idea of using coarse grids to reduce the low frequencies, and fine grids to smooth their high-frequency components. It can be showed that such a process may lead to the optimal CPU time demands of $O(N)$, N being the number of points per decade of optical scale. For comparison, the Jacobi and Gauss-Seidel methods scales approximately as $O(N^2)$. We have applied the non-linear version of the *standard multigrid* scheme based on the coarse grid correction (CGC) technique (for details, see Hackbush 1985).

CGC is the process of correction of the fine-grid approximation of the solution using the solutions on the coarse grids. Schematically, it can be described in the following way: the defect (or residuum) of the fine-grid approximation is computed by several calls of the sweeping procedure (Jacobi, etc.); then both defect and the initial guess of the solution are restricted to the coarse grid, and a new solution on the coarse grid is obtained using these data. This coarse-grid solution is interpolated to the fine grid, and the density-matrix components are corrected. This process can be repeated recursively for every grid in order of increasing grid steps. This recursive process leads to the so-called V, W, or more complicated diagrams, depending on the way in which the recursion is implemented (Hackbush 1985).

In our code we use the parabolic short-characteristics technique of Kunasz & Auer (1988), and as a smoothing algorithm we use the Jacobi iteration, similar to the one of Manso Sainz & Trujillo Bueno (2003), with modifications to include the effects of line overlapping.

3. Detailed Model Parameters

For demonstrating the possibilities of this technique, we chose the model of a semi-infinite, plane-parallel, H I atmosphere. The atmosphere is isothermal ($T = 5300\,\mathrm{K}$), with constant volume density of neutral hydrogen, $N_\mathrm{H} = 10^{12}\,\mathrm{cm}^{-3}$, thermal electrons, $N_\mathrm{e} = 10^{10}\,\mathrm{cm}^{-3}$, and protons, $N_\mathrm{p} = N_\mathrm{e}$. No magnetic field is taken into account. The scattering of radiation is supposed to fulfill the conditions of complete frequency redistribution, and the U and V Stokes parameters vanish due to the symmetries of the problem.

We adopted a hydrogen atomic model with 9 fine-structure energy levels ($1\,\mathrm{s}^{1/2}$ to $3\,\mathrm{d}^{5/2}$) and all the non-vanishing multipole components $\rho^k_0(nlj)$ of density matrix. All the coherence elements ($q \neq 0$) are identically zero due to the model's symmetries. The coherences between different energy levels have been neglected due to the small natural widths of the levels in comparison to their separations, and due to the selection rules for dipole radiative transitions.

Collisional rates with thermal electrons and protons for fine structure transitions, $C^{k\to k'}_{nlj\to n'l'j'}$, were computed in part using the semiclassical theory of Sahal-Bréchot et al. (1996), for transitions within the same shell, and in part using the data of collisional cross-sections from the Atomic and Molecular Data Information System (AMDIS; `http://www-amdis.iaea.org/`), for transitions between different shells.

The number of logarithmically spaced nodes in the fine grid is $N_5 = 257$ and 5 grids were used in total. The number of nodes in the "$G-1$" grid is equal to $N_{G-1} = (N_G - 1)/2 + 1$. The initial guess for the atomic density-matrix elements is given by the LTE populations determined in the unpolarized case.

4. Convergence Properties and Conclusions

Figure 1 shows a comparison between the convergence rates of the Jacobi and the MG methods. The effect of coarse-grid solutions is reflected by the dramatic evolution of the maximum relative change of the populations. The coarser the grid the shorter the evaluation time, and the higher the rate of approaching to the truncation error of the grid. The maximum relative error dominated by the long-period components is strongly reduced by the recursive CGC during the V-cycles.

The time saving of the MG method in this particular model is about a factor 4 compared to the Jacobi method. It must be noticed that the efficiency of MG increases as fast as the efficiency of the smoothing procedure. The most important benefit from MG's is the asymptotical $O(N)$ behavior, which designates the method for use in solutions of problems that necessitate strong refinements. Moreover the presented 1D geometry is the slowest case as pointed out by Steiner (1991) and Fabiani Bendicho et al. (1997).

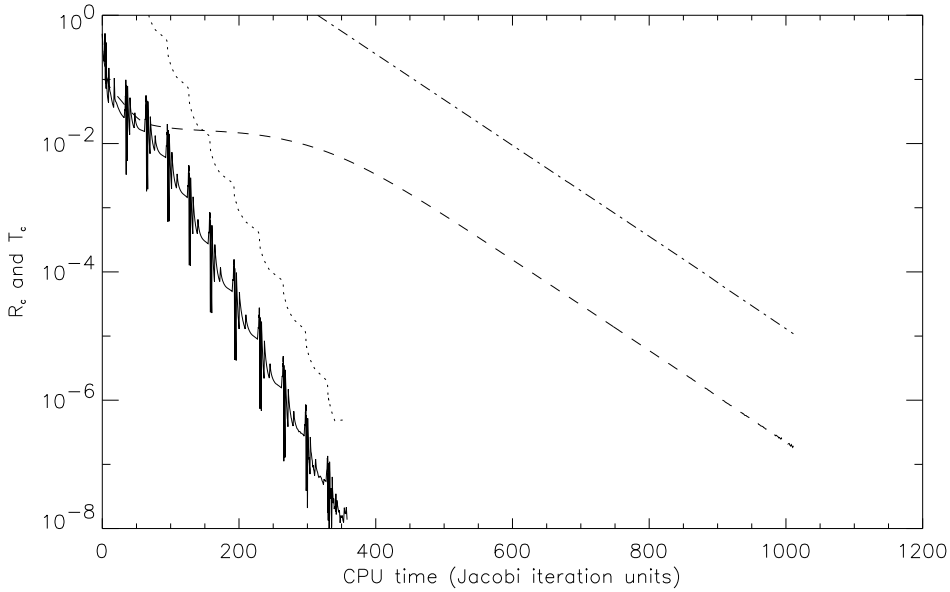

Figure 1. Convergence of the MG method with Jacobi smoothing procedure compared to the Jacobi method. The maximum relative change R_c of atomic populations, ρ^0_0, in the MG case (solid line) is compared to the Jacobi solution (dashed line). The maximum relative error T_e (with respect to the fully converged solution) for MG case (dotted line) and Jacobi case (dot-dashed line) is showed as well. The norm used is $\|\cdots\|_\infty$ (see Fabiani Bendicho et al. 1997). The graph shows the effect of 11 V-cycles with 2 pre- and 15 post-smoothing Jacobi iterations.

Acknowledgments. I'm grateful to my Ph.D. supervisors, Petr Heinzel and Sylvie Sahal-Bréchot, for their useful comments.

References

Bommier, V., & Sahal-Bréchot, S. 1978, A&A, 69, 57
Bommier, V. 1980, A&A, 87, 109
Brandt, A. 1977, Math.Comp., 31, 333
Fabiani Bendicho, P., Trujillo Bueno, J., & Auer, L. 1997, A&A, 324, 161
Fano, U. 1957, Rev.Mod.Phys., 29, 74
Hackbush, W. 1985, Multi-Grid Methods and Applications (Berlin: Springer)
Kunasz, P., & Auer, L. H. 1988, JQSRT, 39, 67.
Landi Degl'Innocenti, E. 1987, in Numerical Radiative Transfer, ed. W. Kalkofen (Cambridge: Cambridge Univ.), 265
Manso Sainz, R., & Trujillo Bueno, J. 2003, in ASP Conf. Ser. Vol. 307, Solar Polarization 3, ed. J. Trujillo Bueno & Sánchez Almeida (San Francisco: ASP), 251
Paletou, F., & Léger, L. 2005 (`astro-ph/0507021`)
Rybicki, G. B., & Hummer, D. G. 1991, A&A, 245, 171
Rybicki, G. B., & Hummer, D. G. 1992, A&A, 262, 209
Sahal-Bréchot, S. 1977, ApJ, 213, 887
Sahal-Bréchot, S., Vogt, E., Thoraval, S., & Diedhiou, I. 1996, A&A, 309, 317
Steiner, O. 1991, A&A, 242, 290
Väth, H. M. 1994, A&A, 284, 319

Appendix F

Paper IV: Hydrogen Hα line polarization in solar flares

A&A 465, 621–631 (2007)
DOI: 10.1051/0004-6361:20066329

Astronomy & Astrophysics

Hydrogen Hα line polarization in solar flares

Theoretical investigation of atomic polarization by proton beams considering self-consistent NLTE polarized radiative transfer

J. Štěpán[1,2], P. Heinzel[1], and S. Sahal-Bréchot[2]

[1] Astronomical Institute, Academy of Sciences of the Czech Republic, Fričova 298, 251 65 Ondřejov, Czech Republic
e-mail: [stepan;pheinzel]@asu.cas.cz
[2] LERMA, Observatoire de Paris – Meudon, CNRS UMR 8112, 5 place Jules Janssen, 92195 Meudon Cedex, France
e-mail: [jiri.stepan;sylvie.sahal-brechot]@obspm.fr

Received 31 August 2006 / Accepted 20 December 2006

ABSTRACT

Context. We present a theoretical review of the effect of impact polarization of a hydrogen Hα line due to an expected proton beam bombardment in solar flares.
Aims. Several observations indicate the presence of the linear polarization of the hydrogen Hα line observed near the solar limb above 5% and preferentially in the radial direction. We theoretically review the problem of deceleration of the beam originating in the coronal reconnection site due to its interaction with the chromospheric plasma, and describe the formalism of the density matrix used in our description of the atomic processes and the treatment of collisional rates.
Methods. We solve the self-consistent NLTE radiation transfer problem for the particular semiempirical chromosphere models for both intensity and linear polarization components of the radiation field.
Results. In contrast to recent calculations, our results show that the energy distribution of the proton beam at Hα formation levels and depolarizing collisions by background electrons and protons cause a significant reduction of the effect below 0.1%. The radiation transfer solution shows that tangential resonance-scattering polarization dominates over the impact polarization effect in all considered models.
Conclusions. In the models studied, proton beams are unlikely to be a satisfying explanation for the observed linear polarization of the Hα line.

Key words. Sun: flares – polarization – atomic processes – radiative transfer – line: formation

1. Introduction

Observations of solar flares in the hard X-ray spectral region indicate a non-thermal origin of this radiation (Frost 1969). There are several mechanisms that can be identified as a possible source of this emission (Korchak 1967). Presently, there is wide consensus among solar physicists that the most likely explanation is the bremsstrahlung radiation of electron beams with energies of the order 10−100 keV, which are injected into denser layers of the solar atmosphere from a coronal reconnection site. The differential energy spectrum of these beams at the injection site is usually assumed to have a power-law distribution $\sim E^{-\delta}$ with δ between 3 and 5 (Brown 1971).

Although there is also observational evidence of high energetic protons (above 10 MeV) in the γ-ray spectrum, radiation induced by protons at energies below 1 MeV is difficult to detect because they do not radiate efficiently at such energies. Several processes that lead to electron acceleration at the reconnection site can also lead to acceleration of protons (see Orrall & Zirker 1976, and references therein) The existence of low energy proton beams in solar flares is still uncertain, but it is believed that they may also play a significant role in flare physics. Furthermore, energetic electron beams cannot be used as a satisfactory explanation for all flare observations (e.g., Doschek et al. 1996). For a comparison of the effects of electron and proton beams see Brown et al. (1990).

There are several techniques that can be used to detect low energy proton beams. The emission peak in the Hα core due to proton beam bombardment was proposed by Hénoux et al. (1993). It has been recently shown by Xu et al. (2005a) that this effect does not exist. Another technique is based on measurements of the red-shifted emission in line wings, especially in the hydrogen Lyα line, which is a consequence of the charge exchange effect (Orrall & Zirker 1976; Canfield & Chang 1985; Brosius et al. 1995; Fang et al. 1995; Zhao et al. 1998; Brosius & Woodgate 1999). A different approach is based on the fact that anisotropic excitation of the chromosphere atoms by a directed proton (or electron) beam induces a preferential population of particular Zeeman sublevels, i.e., the impact atomic polarization and, consequently, an emission of linearly polarized radiation (Hénoux et al. 1990).

Some observations indicate the existence of linear polarization of the Hα line in solar flares above 5% or even as high as 10% (Hénoux & Chambe 1990; Vogt & Hénoux 1996; Xu et al. 2005b) and preferentially oriented towards the disk center (it will be denoted as *radial* in this paper) and also parallel to the limb (i.e., *tangential*). This effect is usually interpreted as a consequence of the impact polarization by a vertical proton beam with energy below 200 keV in the Hα core forming layers. Contrary to these measurements, there are observations that indicate no linear polarization in a wide range of flares (Bianda et al. 2005) and argue for isotropization of

the beam at crucial atmospheric depths. Studies of Hα polarization in solar prominences show that transitions between fine structure levels within the shell $n = 3$ of hydrogen caused by collisions with background electrons and protons lead to a significant depolarizing effect (Bommier et al. 1986b) even at densities of the order of 10^{10} cm^{-3}. The electron (proton) density in a flaring solar chromosphere at the Hα formation levels is above 10^{12} cm^{-3}, therefore this effect could significantly reduce measurable polarization.

In recent years, a first quantitative estimation of the hydrogen impact polarization under the flare conditions has been done by Vogt et al. (1997) and Vogt et al. (2001). In these calculations, a self-consistent radiative transfer code for unpolarized radiation has been used to find the hydrogen ionization degree and the radiation intensity at unit optical depth of Hα for several semiempirical atmospheric models and under the effect of proton beams having several parameters. In these calculations, the following approximation has been used: The equations of statistical equilibrium and the radiation transfer equations have been decoupled and the Hα line has been assumed to be optically thin. The proton beam energy distribution at an injection site has been assumed to be similar to the one deduced for electron beams, i.e., a power law. The lower energy cut-off E_c is usually set between 100 to 200 keV. This energy approximately corresponds to the energy necessary for a proton to reach the Hα line-forming layers. Using an assumption that the power-law distribution preserves its character while the beam propagates to the upper chromosphere, these authors calculated the polarization degree of emitted radiation. Depolarization by collisions with electrons and protons of the ambient medium have also been taken into account. Depending on the atmosphere model and beam parameters, the predicted polarization degree has been up to 4.5%. However, a complete solution of the coupling of the polarized radiative transfer to the atomic equilibrium has not been tackled.

The aim of this paper is to present a theoretical analysis of the proton impact polarization phenomenon in the hydrogen Hα line based on NLTE polarized radiative transfer. Our goal is to verify the assumption that the measured linear polarization can be interpreted as due to this mechanism. In particular, we have focused our attention to a limiting case of unidirectional non-deflecting beams, which are supposed to generate highest polarization due to their extremal anisotropy. For simplicity we use a static 1D model of the flaring chromosphere.

In the second section, the deceleration effect of the chromosphere on proton beams is reviewed and some conclusions are made about the low-energy beam fluxes in Hα-forming layers. These are compared with the assumptions made in the previous works. The third section describes our NLTE solution of the unpolarized transfer in an atmosphere affected by non-thermal excitation and ionization by proton beam. This solution is similar to that of Kašparová & Heinzel (2002), which has been performed for electron beams. We use the same approach to calculate the volume densities of thermal electrons and protons in the chromosphere. These densities are then used in our polarized transfer code. After that we describe the framework of the quantum density matrix and equations of atomic statistical equilibrium on the basis of irreducible tensorial operators. The fifth section is dedicated to the problem of collisional rates for all transitions used in our modeling. Section 6 contains a comparison of results obtained by Vogt et al. (2001) with our calculations in the last scattering approximation. A brief description of polarized transfer solution and the method used in our calculations can be found in Sect. 7. The results and their discussion are summarized in Sect. 8. In the last section our conclusions are made and the main consequences for the interpretation of observations are pointed out. All expressions in this paper are written using the CGS system of units.

2. Solar atmosphere models and beam propagation

2.1. Proton beam propagation

Let us briefly review the interaction of a proton beam with the solar chromosphere. We assume a beam in the coronal reconnection site, which vertically penetrates the chromosphere. A horizontal motion of the protons is neglected to obtain as anisotropic a velocity distribution as possible. The energy of protons necessary to reach the Hα formation levels is of the order of 100 keV at the top of the chromosphere (see below). Protons of such high energy do not lose a lot of energy in the interaction with extremely hot coronal plasma (Hénoux et al. 1993), hence we may neglect any interaction with the coronal mass in this paper. In all our calculations, the energy of the superthermal protons (>1 keV) of the beam is high above the average energy of thermal motions in the chromosphere where Hα is formed, thus we can use the so-called cold target approximation (Emslie 1978).

In a partially ionized medium, a superthermal proton beam is decelerated by collisions with the background electrons and ions and also by elastic and inelastic collisions with neutral atoms, especially the atmosphere's main constituent, hydrogen. We will use the approach of Emslie (1978) to describe this deceleration and the beam energy deposition into the atmosphere. The deceleration by charged electrons and protons can be quantified by means of the Coulomb logarithm Λ. The inelastic and elastic scattering on the neutral hydrogen is similarly described by Λ' and Λ'', respectively. These logarithms vary slightly according to atmospheric properties, but these changes are small within a wide range of physical characteristics and it will not affect our results significantly if we suppose these quantities to be constant. The values adopted in this paper have been set according to typical physical properties of the upper chromosphere: $\Lambda = 23$, $\Lambda' = 3$. Elastic scattering of the proton beam on neutral hydrogen is negligible in comparison to other processes and will be neglected.

Let $F(E, N)$ be the energy distribution of the number flux of beam particles at the column depth N. At the injection level we set $N = 0$. The general form of this distribution is (Canfield & Chang 1985)

$$F(E,N) = F(\sqrt{E^2 + E_N^2}, 0)\frac{E}{\sqrt{E^2 + E_N^2}}. \quad (1)$$

For the purposes of our calculations, we have used an initial power-law energy distribution at the injection site, which is usually considered in the non-thermal flare heating problems (Brown 1971)

$$F(E,0) = (\delta - 2)E_c^{\delta-2}\mathcal{E}_0 E^{-\delta}\theta(E - E_c), \quad (2)$$

where

$$\theta(x) = \begin{cases} 1 & (x > 0) \\ 0 & (x < 0) \end{cases} \quad (3)$$

is the Heaviside function, E_c is the lower energy cut-off of the distribution, and $\mathcal{E}_0$ is the total initial energy flux of the beam. E_c is usually assumed to lie between 100 keV and 200 keV, according to minimal energy necessary for protons to reach the

Hα formation layers. The formula (1) for the particular case of initial distribution (2) gives (Zhao et al. 1998)

$$F(E,N) = (\delta-2)E_{\rm c}^{\delta-2}\mathcal{E}_0\frac{E}{(E^2+E_N^2)^{\frac{\delta+1}{2}}},\ \text{for } E \geq E_{\rm m}\ , \tag{4}$$

where

$$E_{\rm m}(N) = \begin{cases} \sqrt{E_{\rm c}^2 - E_N^2}, & (E_N \leq E_{\rm c}) \\ 0, & (E_N > E_{\rm c}) \end{cases} \tag{5}$$

is the minimum energy of the distribution at a given depth.

The energy deposition rate into the neutral hydrogen is given by

$$I_{\rm H\,I}(N) = \frac{Kn_{\rm H}}{2}(\delta-2)(1-x)\Lambda'\frac{m_{\rm p}}{m_{\rm e}}\frac{\mathcal{E}_0}{E_{\rm c}^2}\left(\frac{N}{N_{\rm c}}\right)^{-\frac{\delta}{2}} B_{x_{\rm c}}\left(\frac{\delta}{2},\frac{1}{2}\right)\ , \tag{6}$$

where

$$x_{\rm c} = \begin{cases} N/N_{\rm c}, & (N < N_{\rm c}) \\ 1, & (N > N_{\rm c}), \end{cases} \tag{7}$$

and $B_x(a,b)$ is the incomplete beta function. $N_{\rm c}$ is the depth that can be reached by protons with the initial energy $E_{\rm c}$. Eq. (6) is a special case of the Eq. (1) of Kašparová & Heinzel (2002), here for a non-deflecting vertical proton beam. This energy deposition rate has been used in calculations of the ionization degree of the chromosphere described in Sect. 3.

2.2. Flux distribution at Hα formation level

The distribution (4) has been plotted in Fig. 1 for several values of E_N, typical energy cut-off $E_{\rm c} = 150$ keV and two initial spectral indices δ. The first fact that should be pointed out is that the energy cut-off does not significantly depend on E_N if $E_N < E_{\rm c}$ until $E_N \approx E_{\rm c}$. It is because high energy protons are decelerated inefficiently. Only if $E_N \to E_{\rm c}$, protons are slowed to energies close to 5 keV[1]. Using Eq. (4) we find that the flux of the beam at the local energy cut-off $E_{\rm m}$ is lower by factor $(E_{\rm c}/E_N)^{\delta}E_{\rm m}/E_N$ compared to the flux $F(E_{\rm c},0)$. Hence we have a strong decrease of flux close to the interesting energy range (i.e., $E_{\rm m} \ll E_{\rm c}$) by the factor of approximately $E_{\rm m}/E_{\rm c}$. The total flux is rapidly reduced in deeper layers ($E_N > E_{\rm c}$). It can be shown that the flux maximum is at the energy $E_N/\sqrt{\delta}$. After crossing some critical depth, the flux of the beam with lower δ dominates the one with higher δ at all energies – because initially there is a higher number of high energy protons in the small-δ case, which are now decelerated to low energies. As a result, energy is more effectively deposited by small-δ beams in lower depths, while high-δ beams are decelerated in upper layers. In any case, the decrease of flux $\partial F(E,E_N)/\partial E_N$ is steep for any δ and one could expect that impact polarization will be sensitive to the $E_{\rm c}$ value because there is only a small ΔE_N interval in which low-energy flux is not negligible, and this depth interval should overlap with the Hα line center formation region as much as possible. It is not possible to have a power-law-like distribution at this layer with a local cut-off of about 5 keV for beams starting at the top of chromosphere with energies above 100 keV or higher.

This leads us to the second conclusion. The energy distribution of the flux cannot be approximated by the power-law curve if E_N is close to $E_{\rm c}$. If these energies are comparable (and that is the case of our interest here because we have for maximum impact polarization $E_{\rm c} \approx 5$ keV $\ll E_{\rm c}$), the use of the power-law distribution leads to an unrealistic overestimation of the polarization degree. Such an approximation has been used by Vogt et al. (1997) and by Vogt et al. (2001) with lower energy cut-off varied from 1 keV to 20 keV and with a total beam number flux and δ conserved. The theoretical values of polarization obtained from these calculations should therefore be revised.

[1] As we will show later, the low-energy protons (4–5 keV) are most effective in producing impact polarization of $n = 3$ hydrogen level.

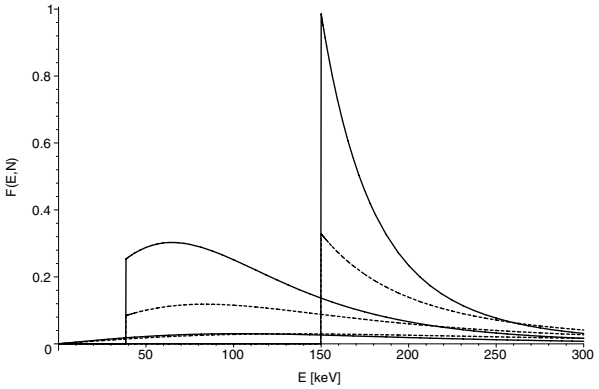

Fig. 1. Energy distribution of the beam with initial energy cut-off $E_{\rm c}$ = 150 keV at depths with different E_N. Solid curves correspond to spectral index $\delta = 5$, dashed curves to $\delta = 3$. From upper to lower, the curves are plotted for $E_N = 0$, 145 and 230 keV. The cut-off energy at depths close to $N_{\rm c}$ is still of the order of $E_{\rm c}$. At deeper depths the distribution $\delta = 3$ dominates over $\delta = 5$ at all energies.

3. Unpolarized radiation modeling and background electron and proton densities

Our solution of unpolarized radiation transfer follows the approach of Hénoux et al. (1993) and Kašparová & Heinzel (2002). We take a 1D static atmosphere with fixed temperature structure and other plasma properties given by the semiempirical chromosphere model of the flaring atmosphere F1 (Machado et al. 1980), and following Vogt et al. (1997) and Vogt et al. (2001) we also use the model VAL F (Vernazza et al. 1981) for comparison. These models have been created using a number of line and continuum observations.

The non-thermal proton beam dissipates its energy while propagating through the matter of the chromosphere causing its heating and the modification of atomic level populations and ionization. The non-thermal heating is already included in the semiempirical flare models to explain the observed emission. Our approach to the modeling follows the approach of Hénoux et al. (1993) and Kašparová & Heinzel (2002). We consider a fixed temperature structure of the atmosphere as given by the semiempirical atmosphere models. The pressure and statistical equilibrium equations are solved together with radiation transfer. Then we study an influence of the non-thermal collisional rates on the line profiles in comparison to the thermal model (differential approach). It is important to notice that the temperature of the flaring atmosphere described by semiempirical models is in general overestimated because it has been determined to explain the increased radiation emission regardless of the non-thermal excitation and ionization. The same approach has been used for the solution of the polarized radiative transfer (Sect. 7) to obtain the changes of the Hα Q/I-profiles after introduction of the non-thermal collisional rates into statistical equilibrium equations. The only difference is that the polarized solution uses the

electron and proton densities precalculated by the unpolarized transfer code. We have used the same MALI code as Kašparová & Heinzel (2002), now adapted to treat proton beam bombardment described in Sect. 2. The code has been run with a four-level plus continuum hydrogen atomic model and non-thermal collisional rates have been calculated from the energy deposition rate into hydrogen (6) using the expressions (10) and (11) of Hénoux et al. (1993).

The electron densities (which are close to proton densities at Hα core formation layers) are plotted in Figs. 2 and 3 for both models under consideration, several beam fluxes, and three different values of δ. These calculations show that ambient electron (and proton) densities used by Vogt et al. (1997) are underestimated (cf. Tables 2 and 3 therein) and the same is true for the mean radiation intensities. These values have been computed in the layers of total (coronal + chromospheric above Hα-forming layers) column mass depth 2.484×10^{-4} g cm^{-2} (VAL F, see Table 15 of Vernazza et al. 1981) and 3.186×10^{-4} g cm^{-2} (F1, see Table 3 of Machado et al. 1980), where the optical depth of Hα is approximately unity. Because our background particle densities did not correspond to the ones presented by Vogt et al. (1997), we have used their radiation transfer code which is based on the standard Λ-iteration process. We have found that this code setting (the accuracy of 10^{-3} in maximum relative change of atomic populations between subsequent iterations) leads to insufficient convergence and consequently to the underestimation of electron and proton densities. An increase of accuracy led to values close to ours, but at the cost of an extremely large number of Λ-iterations (for similar tests see also Kašparová & Heinzel 2002).

In Fig. 4 one can see the theoretical Hα line profile for the same beam fluxes as in Fig. 2. These profiles are consistent with the results of Xu et al. (2005a). In comparison to profiles presented by Hénoux et al. (1993), the central emission in the line core does not appear.

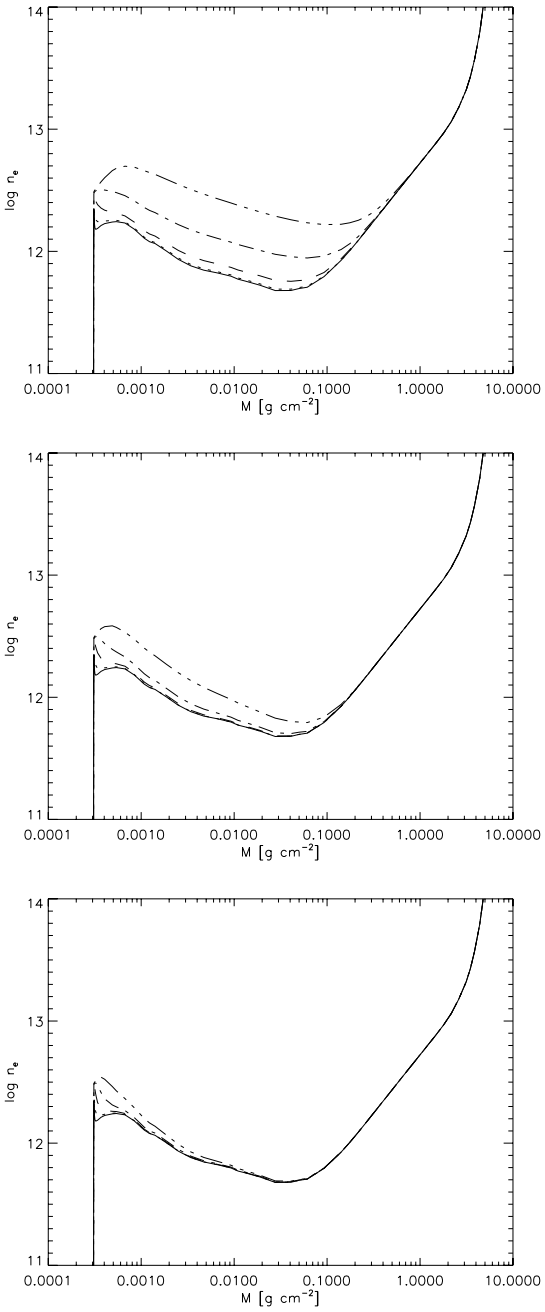

Fig. 2. Electron density for the model F1. The plots correspond to the case $\delta = 3$ (*upper panel*), $\delta = 4$ (*middle panel*), and $\delta = 5$ (*lower panel*). The thermal case is plotted by a solid line, the non-thermal beam fluxes are $\mathcal{E}_0 = 10^8$ (dot), 10^9 (dash), 10^{10} (dash-dot), and 10^{11} erg cm^{-2} s^{-1} (dash-dots). All beams have $E_c = 150$ keV.

4. Formalism of density matrix and local equilibrium

The electron densities in the layers of interest do not exceed 10^{13} cm^{-3}. Following Bommier & Sahal-Bréchot (1982) and Bommier et al. (1986a), the hyperfine splitting of the hydrogen levels is completely negligible. In fact the hyperfine splitting of the relatively long-living $3s^{1/2}$ level (about 50 MHz) is higher than its inverse radiative lifetime (of the order of 1 MHz) and thus the hyperfine levels do not overlap. However, it was verified by Bommier et al. (1986a) that taking the hyperfine structure into account does not affect the linear polarization of the Balmer lines in any significant way. Moreover, in the conditions under consideration, the lifetimes of the levels are strongly reduced by collisions with the charged perturbers. The lifetimes of the $n = 3$ levels are of the order of a few 100 MHz in the Hα core-forming layers due to the dipolar transitions $nlj \rightarrow nl \pm 1j'$ (cf. Sahal-Bréchot et al. 1996); hence, much greater than hyperfine splitting. Therefore, we take into account only the fine structure splitting of the levels. We suppose that there are no quantum coherences between different energy levels. This assumption is valid in our model of the hydrogen atom where the individual level widths are smaller than distances between them or where the selection rules for dipolar optical transitions prevent creation of coherences. As a result, the fine structure levels are supposed to be completely separated.

To describe the state of hydrogen atoms in an equilibrium with the radiation field and charged colliders, we adopt the framework of the atomic density matrix ρ (e.g., Fano 1957). In the dyadic basis $|nljm\rangle$ of hydrogen states, we adopt the common notation: n is the principal quantum number, l the orbital one, and j is the total angular momentum. Magnetic quantum number is represented by m. The natural basis for the density matrix operator in polarization studies is that of irreducible tensorial operators (ITO or the multipole expansion) T^k_q (Sahal-Bréchot 1977). In all our development we suppose that all the particle velocity

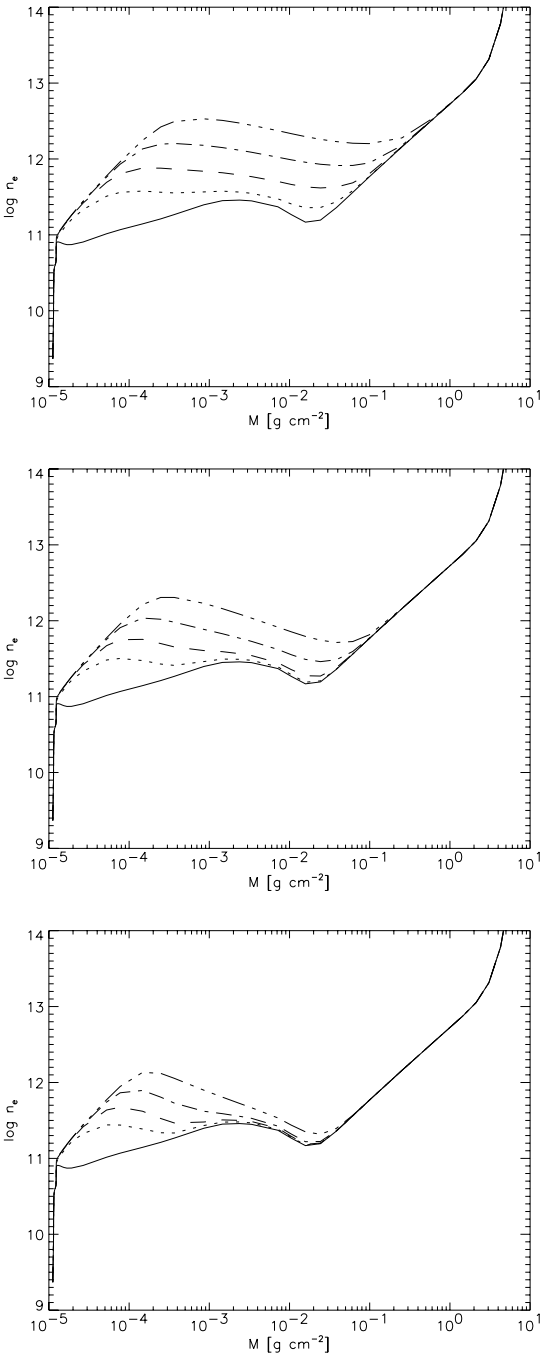

Fig. 3. Same as Fig. 2; here for the VAL F model.

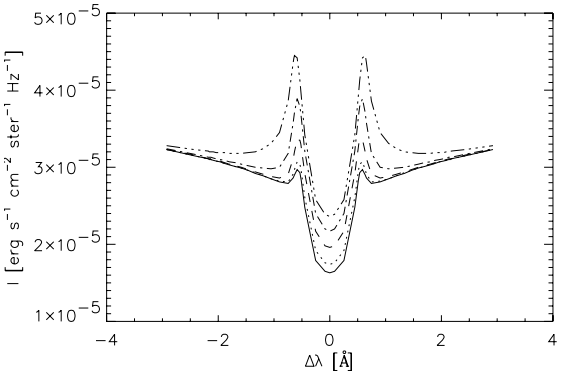

Fig. 4. Hα line profiles for the model F1 and $\delta = 4$. The particular profiles correspond to the same beam fluxes as in Fig. 2.

distributions and the radiation field are axially symmetric with the symmetry axis in a vertical direction. We also assume that the magnetic field lines are oriented along the vertical axis and that the strength of the magnetic field is at most a few hundred gauss (thus we can neglect the Zeeman splitting of the levels). All of these assumptions lead to a great simplification of calculations because most of the density matrix elements vanish: All the coherences between the wave functions of the states vanish. In the basis of ITO only the components ${}^{nlj}\rho^k_0$ remain. These diagonal elements represent population ($k = 0$) and alignment ($k = 2$) components of the different levels. Again, due to symmetry reasons ($\rho_{nljm} = \rho_{nlj-m}$), the elements with odd k vanish. One could take into account the anti-level-crossing effect (Bommier 1980) related to the so-called alignment-to-orientation mechanism (cf. Landi Degl'Innocenti 1982), which can lead to creation of some non-zero density matrix components of odd rank (so-called orientation), even if no circularly polarized radiation is present. In fact, this effect is of little importance in our current model because the magnitude of the created orientation remains well below the magnitude of the alignment. Therefore we can safely exclude this effect from our study. The higher multipoles ($k > 2$) do not affect the solution under given the physical conditions and they have been neglected[2]. We limit our analysis to the three principals levels of the hydrogen atom.

Our calculations concern a static model. The local hydrogen equilibrium is expressed by the equations of statistical equilibrium (ESE)

$$\Pi\rho = u \; . \tag{8}$$

The elements of matrix Π consist (in the impact approximation) of the collisional and radiative rates simply summed together: $\Pi^{k\to k'}_{nlj\to n'l'j'} = R^{k\to k'}_{nlj\to n'l'j'} + C^{k\to k'}_{nlj\to n'l'j'}$ (Bommier & Sahal-Bréchot 1991). The diagonal elements in $nlj \equiv n'l'j'$ stand for relaxation of the level nlj to another levels, while the nondiagonal elements stand for populating a given multipole component. The relaxation rates will be marked by the index "R" in this paper. The detailed analysis of the structure of Π can be found in Sahal-Bréchot (1977). ρ is the formal vector of density matrix components ${}^{nlj}\rho^k_0$. The normalization condition on the density matrix has to be introduced: The sum of all level populations is equal to 1. We know that the relative population of level nlj is equal to $\sqrt{2j+1}\,{}^{nlj}\rho^0$, and hence we may replace the first row of Π by the appropriate constant elements and the right-hand-side of Eq. (8) reads $u = (1, 0, \ldots, 0)^{\mathrm{T}}$.

The particular expressions for the R-matrix elements can be found in Landi Degl'Innocenti (1984). They are calculated in the lowest order of quantum electrodynamics from a known radiation field. Only the single events of emission and absorption are considered. We adopt the approximation that there is no coherence between the frequency of absorbed and emitted photons. This approximation is known as a complete frequency redistribution (CRD; cf. also Sect. 7). The elements of the matrix of

[2] The only non-zero multipole $k \geq 4$ in the third-principal level hydrogen is ${}^{3d\frac{5}{2}}\rho^4_0$ and one has ${}^{3d\frac{5}{2}}\rho^4_0 \ll {}^{3d\frac{5}{2}}\rho^2_0 \ll {}^{3d\frac{5}{2}}\rho^0_0$.

collisional rates C can be calculated taking into account several collisional processes as will be described in the following section.

5. Collisional rates in detail

First of all we stress that we limit our analysis of collisional transitions to density matrix multipoles of $k = 0$ and $k = 2$. Higher ranks do not significantly affect polarization in the studied problem and will be neglected. Collisional rates $C^{k\to k'}_{nlj\to n'l'j'}$ and ${}^{\mathrm{R}}C^{k\to k'}_{nlj\to n'l'j'}$ of hydrogen can be calculated from cross-sections $\sigma^{k\to k'}_{nlj\to n'l'j'}(\boldsymbol{v})$ of appropriate transitions by integration over the relative velocity distribution $f(\boldsymbol{v})$ of particles

$$C^{k\to k'}_{nlj\to n'l'j'} = N_{\mathrm{P}} \int \mathrm{d}^3 v\, f(\boldsymbol{v}) v \sigma^{k\to k'}_{nlj\to n'l'j'}(\boldsymbol{v}), \tag{9}$$

and similarly for relaxation rates. N_{P} stands for the perturbers volume density.

The processes taken into account in our analysis are the following:

1. Fine structure dipole transitions induced by ambient electrons $\mathrm{e}^- + (\mathrm{H\,I})^{nlj} \to \mathrm{e}^- + (\mathrm{H\,I})^{nl\pm1j'}$.
2. Fine structure dipole transitions induced by ambient protons $\mathrm{p}^+ + (\mathrm{H\,I})^{nlj} \to \mathrm{p}^+ + (\mathrm{H\,I})^{nl\pm1j'}$.
3. (De)excitation by ambient electrons $\mathrm{e}^- + (\mathrm{H\,I})^{nlj} \to \mathrm{e}^- + (\mathrm{H\,I})^{n'l'j'}$.
4. Excitation by proton beam $\mathrm{p}^+_{\mathrm{B}} + \mathrm{H\,I} \to \mathrm{p}^+_{\mathrm{B}} + (\mathrm{H\,I})^*$.
5. Charge exchange excitation $\mathrm{p}^+_{\mathrm{B}} + \mathrm{H\,I} \to (\mathrm{H\,I})^*_{\mathrm{B}} + \mathrm{p}^+$.

The index "B" is reserved for particles of the beam and an asterisk (*) is used for an excited state of the neutral hydrogen H I. p^+ and e^- denote protons and electrons, respectively. The other possible collisional transitions have been neglected due to their negligible effect. The cross-sections of these processes have been obtained in several ways.

The fine structure transitions within the same shell ($nlj \to nl \pm 1j'$) have been calculated using the semiclassical perturbation method (Sahal-Bréchot et al. 1996). This approach is accurate for calculation of transitions between close levels (in comparison to collision energy) in a dipolar approximation. Using the formalism of the previously referenced paper, rates can be expressed in the form

$$\begin{aligned} C^{k\to k'}_{nlj\to n'l'j'} &= N_{\mathrm{P}}\Big(\delta_{kk'} c^{(0)}_{k,j\to j'} \alpha^{(0)}_{nlj\to n'l'j'} \\ &\quad + c^{(2)}_{k\to k',j\to j'} \alpha^{(2)}_{nlj\to n'l'j'}\Big), \end{aligned} \tag{10}$$

$$\begin{aligned} {}^{\mathrm{R}}C^{k\to k'}_{nlj\to n'l'j'} &= N_{\mathrm{P}}\Big(\delta_{kk'} {}^{\mathrm{R}}c^{(0)}_{k,j\to j'} \alpha^{(0)}_{nlj\to n'l'j'} \\ &\quad + {}^{\mathrm{R}}c^{(2)}_{k\to k',j\to j'} \alpha^{(2)}_{nlj\to n'l'j'}\Big), \end{aligned} \tag{11}$$

with

$$\alpha^{(0)}_{nlj\to n'l'j'} = \sqrt{4\pi} \int_0^\infty \sigma^{(0)}_{nlj\to n'l'j'}(v) f_0(v) v^3 \mathrm{d}v, \tag{12}$$

$$\alpha^{(2)}_{nlj\to n'l'j'} = \sqrt{\frac{4\pi}{5}} \int_0^\infty \sigma^{(2)}_{nlj\to n'l'j'}(v) f_2(v) v^3 \mathrm{d}v. \tag{13}$$

The cross sections $\sigma^k_{nlj\to n'l'j'}$ have been defined by expressions (59) and (60) of the referenced paper. f_0 and f_2 are the monopole and quadrupole components of the relative velocity distribution with axial symmetry. The angular coefficients c have been defined by expressions (66)–(69) of Sahal-Bréchot et al. (1996). Although this method is limited only to treatment of dipolar transitions $l \to l \pm 1$, these transitions are dominant in the important range of collisional energies at chromospheric temperatures.

Excitation transition probabilities from the ground state $1\mathrm{s}\frac{1}{2}$ to upper levels induced by thermal electrons have been calculated using the cross-section data of database AMDIS[3]. These data are provided for $1\mathrm{s} \to nl$ transitions neglecting the fine structure of the levels, and therefore we use an approximation by the angular coefficient to obtain the fine structure cross-sections (Vogt et al. 2001).

$$\sigma^{0\to k}_{1\mathrm{s}\frac{1}{2}\to nlj} = (-1)^{j+l+k+\frac{1}{2}} \frac{2j+1}{\sqrt{2}} \begin{Bmatrix} l & l & k \\ j & j & \frac{1}{2} \end{Bmatrix} \sigma^{0\to k}_{1\mathrm{s}\to nl}. \tag{14}$$

At the present time, we do not have any adequate cross-section data for the fine structure transitions between levels $n = 2$ and $n = 3$. Therefore we have calculated these cross sections using the same semiclassical perturbation method, although these cross sections are overestimated and cannot be used for non-dipolar transitions $2\mathrm{s} \to 3\mathrm{d}$.

The cross sections of direct excitation to levels $n = 2$ and $n = 3$ by protons have been calculated using the data of Balança & Feautrier (1998). These authors give cross sections $\sigma^{0\to k}_{1\mathrm{s}\to nl}$ for population and alignment excitation in the energy range of 1 keV to 100 keV. As well as in the case of excitation by thermal electrons, we use the expression (14) to obtain data for the fine structure transitions. The transitions $n = 2 \to n = 3$ have been neglected. The self-consistent solution of radiation transfer requires us to know the cross sections at energies above 100 keV. This is due to the behavior of the energy distribution of proton beams at different depths. Although the total flux of the beam decreases quickly as the depth exceeds N_{c}, the role of high energy protons increases: the maximum of the distribution $F(E, N > N_{\mathrm{c}})$ is at the energy $E_N/\sqrt{\delta}$. This leads to the emission in the near Hα line wings and neglecting these energies leads to unrealistic line profiles. We have used the semiclassical perturbation method to calculate dipolar cross sections at energies above 100 keV. The transitions $1\mathrm{s} \to 3\mathrm{d}$ cannot be calculated by this method, and therefore we used a similar approximation as Vogt et al. (1997) and set these transitions to one tenth of the value of $1\mathrm{s} \to 3\mathrm{p}$ cross-sections. This approximation is based on the observation that the electron cross-sections for $1\mathrm{s} \to 3\mathrm{d}$ excitation are approximately 1/10 of $1\mathrm{s} \to 3\mathrm{p}$ at high energies (Aboudarham et al. 1992), and it is also true for 100 keV protons (Balança & Feautrier 1998). While this is not fully justifiable, it should improve accuracy of the solution.

The effect of the charge exchange has also been taken into account using the data of Balança & Feautrier (1998). On the one hand this process is efficient at energies around 25 keV, on the other hand its cross section decreases fast at higher energies. A more detailed analysis of the effect of the charge exchange and the associated Doppler shift of the line can be found in Sect. 7. Contrary to direct excitation, no approximation of the cross-sections at energies above 100 keV has been used. These cross-sections can be safely neglected due to their small magnitude.

[3] Atomic and Molecular Data Information System, `http://www-amdis.iaea.org/`

6. Impact polarization without polarized transfer

In this section, we will compare several results of atomic impact polarization obtained by Vogt et al. (2001) with our calculations performed by a similar method. We will consider the emission of radiation under the proton beam bombardment in chromospheric conditions. The local atmosphere conditions (temperature, thermal electron and proton densities, and mean radiation intensity in the hydrogen Lα, Lβ, and Hα lines) are obtained from the unpolarized radiative transfer solution. These conditions are taken at unit Hα line center optical depth. Following Vogt et al. (1997, 2001) we assume that proton beam energy distribution is given by a power law with the same spectral index δ as at the injection coronal site. The emitted radiation, which is polarized due to beam impacts, is assumed to be unaffected by radiation transfer in upper layers in this approach. Although a rough approximation, it can serve as a comparison of our calculation of collisional rates and local equilibrium, which will be used in further self-consistent solutions.

After calculation of the density matrix elements from Eq. (8) one can calculate the ratio ϵ_Q/ϵ_I of emission coefficients of the Stokes parameters Q and I. When observed at solar limb (i.e., 90 degrees from the vertical direction) and through the optically thin layer, this ratio could provide an estimation of the emergent light polarization degree. From known atomic density matrix elements, the polarization of emergent radiation reads

$$p_{90}(n \to n') = -\frac{3\vartheta^{(2)}_{n\to n'}}{2\sqrt{2}\vartheta^{(0)}_{n\to n'} - \vartheta^{(2)}_{n\to n'}}, \qquad (15)$$

with

$$\vartheta^{(k)}_{n\to n'} = \sum_{ll'jj'} (-1)^{1+j+j'}(2j+1)A_{nlj\to n'l'j'} \left\{ \begin{array}{ccc} j & j & k \\ 1 & 1 & j' \end{array} \right\} {}^{nlj}\rho^k_0. \qquad (16)$$

The quantity $A_{nlj\to n'l'j'}$ is the Einstein coefficient for spontaneous emission and the entities in the braces are the so-called $6j$ symbols. At the level of unit Hα optical depth, the beam energy cutoff is, by definition, close to zero. This cutoff has been varied in the interval 1 keV to 20 keV by Vogt et al. (2001) to find the dependence of the polarization degree. These authors show that the polarization degree can be expected as high as 2.5% for model VAL F and 0.7% for model F1 ($\delta = 4$), or 5% for model VAL F and 1.2% for model F1 ($\delta = 5$). The results of Vogt et al. (2001) contained in their Table 1 are plotted in Fig. 5.

We have repeated these calculations for the same conditions, with $E_c(\tau_{H\alpha} = 1)$ varied between 1 keV and 20 keV and total initial beam energy flux between 10^8 to 10^{11} erg s^{-1} cm^{-2}. The physical conditions of the atmosphere have been taken from Tables 2 and 3 of Vogt et al. (1997). The corresponding polarization degree for VAL F model is plotted in Fig. 6.

Although the order of both results agrees, there are differences between these solutions. The most important difference is a steeper decrease of polarization degree at higher energies. The reasons for these differences are the different cross-sections used for electron-hydrogen excitation and especially the different technique of numerical integration used for calculation of non-thermal collisional rates. While the Gauss-Laguerre quadrature has been used in Vogt's calculations, we have chosen an adaptive Simpson rule with a very fine energy grid refinement at low energies, where fast changes of cross-section data play a role (cf. Fig. 11c of Balança & Feautrier 1998)

A further step of our analysis has been the evaluation of the polarization degree in the same approximation but under local physical conditions calculated using the correct solution of the unpolarized radiation transfer (see Sect. 3). An increase of the mean radiation intensity and higher depolarization due to increased ionization degree lead to a significant decrease of the polarization degree by more than one order of magnitude (see Fig. 7). The expected polarization degree is very sensitive to $nlj \to nl \pm 1j'$ depolarizing transitions between fine structure levels of the same shell caused by background perturbers. The results of this section show that the line polarization is in fact smaller than the previously reported calculations, even if we use the not fully correct approximation (2) for the energy distribution of the beam at the Hα core-forming layer.

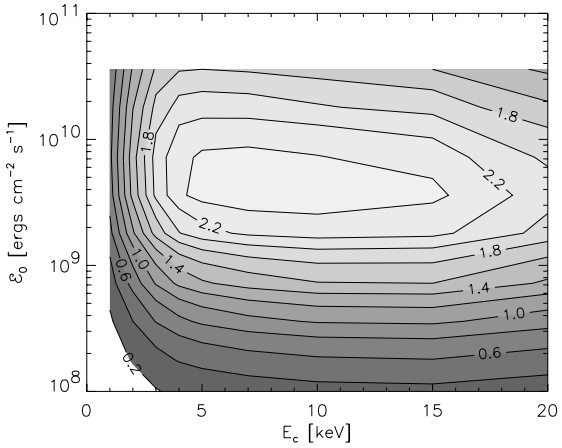

Fig. 5. Emergent polarization degree (in percent) of the on-limb observation calculated by Vogt et al. (2001) in the last scattering approximation. The horizontal axis shows the value of the local energy cut-off, and the vertical axis shows the values of the initial beam flux.

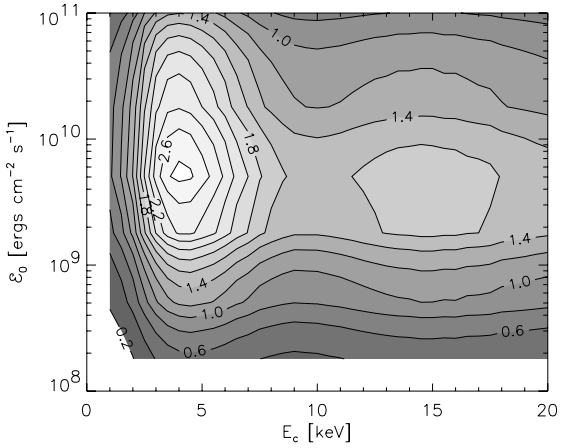

Fig. 6. Same as Fig. 5; here calculated using another numerical integration technique and different cross-section data for the electron excitation (see text for details).

7. Polarized radiation transfer solution

A self-consistent NLTE solution of the polarized transfer may provide additional information about the polarization degree of the Hα line and the effect of the proton beam. In contrast to the results of the previous section, it also provides complete emergent intensity and fractional Q/I polarization profiles. In this section, a short description of the polarized transfer solution is contained. It is beyond the scope of this paper to review the

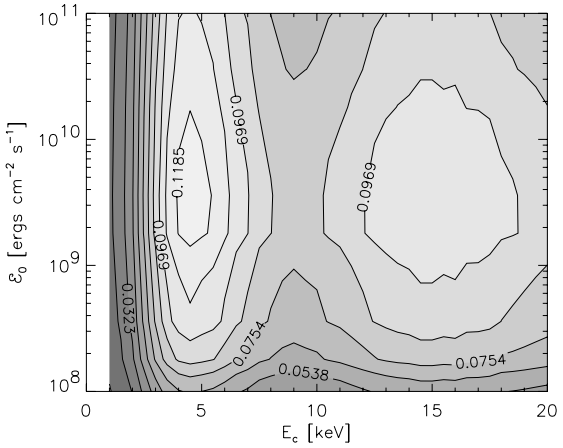

Fig. 7. Same as Fig. 6; here calculated with correct densities of the background electrons (and protons) and modified mean intensities of the radiation field.

complex problem of self-consistent modeling of the polarized transfer in hydrogen lines and thus we limit our explanation to a few notes about the method. The detailed description of this problem is a subject of other papers (Štěpán 2006, 2007, in preparation).

It is advantageous to describe the polarized radiation field by means of the so-called Stokes vector $\boldsymbol{S}(\nu, \boldsymbol{\Omega}) = (I, Q, U, V)^{\mathrm{T}}(\nu, \boldsymbol{\Omega})$, in which I is the specific intensity, Q and U correspond to the linear polarization parameters with respect to two axes, and V stands for the circular polarization. We limit our analysis to the cylindrically symmetric problem where the natural choice of the reference frame leads to a reduction of the Stokes vector to only two nonvanishing parameters, $\boldsymbol{S}(\nu, \boldsymbol{\Omega}) = (I, Q)^{\mathrm{T}}(\nu, \boldsymbol{\Omega})$, while U and V are identically zero. Stokes parameters are computed from the radiation transfer equation (RTE) formally identical to the unpolarized transfer case (all dependences on the radiation frequency ν and direction of propagation $\boldsymbol{\Omega}$ are suppressed):

$$\frac{\mathrm{d}\boldsymbol{S}}{\mathrm{d}s} = \boldsymbol{\epsilon} - (\boldsymbol{\eta} - \boldsymbol{\eta}_{\mathrm{s}})\boldsymbol{S}. \tag{17}$$

The 2-component vector $\boldsymbol{\epsilon}$ stands for the spontaneous emission in Stokes parameters, $\boldsymbol{\eta}$ is the 2×2 symmetry matrix of the absorption, and $\boldsymbol{\eta}_{\mathrm{s}}$ matrix stands for the stimulated emission. Explicit forms of these quantities can be found in Landi Degl'Innocenti (1984). For the purposes of this paper, it is only important to notice that values of these quantities can be calculated directly from the atomic density matrix coefficients ρ^k_{nlj}. In the solar chromosphere, nonlocal coupling of atomic states between different points due to radiation is strong. Therefore we have to solve the nonlinear system of RTE (17) together with ESE (8) at every point of the atmosphere. This so-called NLTE problem of the 2nd kind (Landi Degl'Innocenti 1987) can be solved numerically using efficient iterative NLTE solvers.

We have used our new multigrid technique that calculates the Stokes profiles for a given temperature and density structure of the atmosphere for an arbitrary line overlapping, and the CRD approximation. This method uses the accelerated lambda iteration technique applied to polarized radiation together with the multigrid acceleration technique (cf. Fabiani Bendicho et al. 1997), which improves the convergence rate from $O(N^{3/2})$ to $O(N)$, where N is the number of spatial discretization points in the atmosphere). The formal solver of our method is based on the short characteristics approach (Olson & Kunasz 1987) with the parabolic interpolation of the source function.

The effect of stimulated emission is taken into account as well as the continuum opacity and emissivity. In the present calculations, we have restricted our solution to the first three-principal levels of the hydrogen atom and the transfer has been solved in three spectral lines, i.e., Lα, Lβ, and Hα. A 50-point quadrature in frequency for each line and a 14-point quadrature for ray directions has been applied.

Finally, one simplification of our approach should be mentioned. While in common situations the density matrix is treated as independent of atomic velocity, this is not the case for anisotropic charge exchange interaction. In this case, there is a systematic Doppler shift in emission dependent on the direction of observations (Canfield & Chang 1985; Fang et al. 1995). This effect is dominant in the Lα and Lβ lines, while the Hα line profile is not much affected. In our approximation we do not take into account any Doppler shifts and assume charge exchange to be symmetric with respect to the center of the line. This approximation could lead to a slight overestimation of the impact polarization effect on the Hα line.

8. Results and discussion

Particular results of the Hα polarization in the approximation neglecting polarized transfer have been presented in Sect. 6. Using our multigrid method, in Sect. 7 we have solved the self-consistent NLTE transfer problem of the 2nd kind for a grid of atmospheres based on F1 and VAL F models affected by proton beams of different fluxes and energy distributions.

Figures 8 and 9 show the theoretical emergent linear polarization profiles Q/I of the Hα line for the F1 and VAL F models respectively. The intensity I-profiles (not shown) are similar to the profiles plotted in Fig. 4, although the intensity in the line core and near wings is overestimated by factor of approximately 1.3−1.5. These differences between intensity profiles are due to different collisional rates used in both calculations and because the polarized solution was restricted to three-principal levels of the hydrogen atom. However, neglecting the upper level should not affect the emergent polarization profile much. In our notation, a positive sign in Q/I plots means the tangential direction of polarization, while a negative sign is the radial one. Because of the symmetry reasons the highest fractional polarization is expected at the limb ($\mu = 0$) and the degree of polarization decreases to zero at the disk center ($\mu = 1$).

The resonance polarization of the Hα line in thermal atmosphere (no beams) shows a small tangential polarization of degree 0.01% for F1 and 0.4% for VAL F. This shows the dominant role of resonance polarization due to scattering over the impact polarization by the proton beam. The increase of tangential polarization in the F1 model with the beam flux shows the completely negligible effect of the impact polarization in comparison to other effects: the variation of the polarization is driven mainly by shifts of the optical depth scale due to higher ionization degree, which can lead to an increase of the resonance scattering effect on polarization. Another effect is the increase of radiation intensity due to non-thermal excitation in the lower chromosphere layers and an increase of the density of background colliders. All these effects compete in the formation of these small fractional polarizations. The impact polarization contributes by only a small fraction to the total polarization degree in all the studied cases, as was expected from Fig. 7.

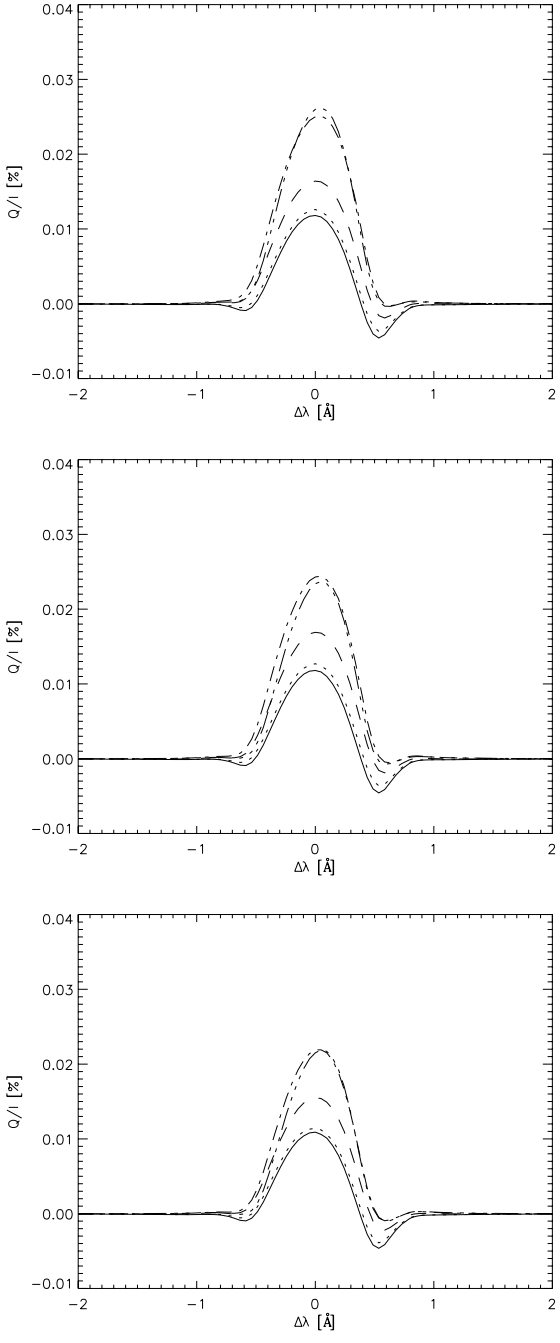

Fig. 8. Emergent fractional linear polarization Q/I profiles computed close to limb ($\mu = 0.11$) for the F1 model and different beam energy distributions: $\delta = 3$ (*upper*), $\delta = 4$ (*middle*), and $\delta = 5$ (*lower*). The different lines correspond to the same beam fluxes as in Fig. 2. All the calculations have been done for $E_c = 150$ keV.

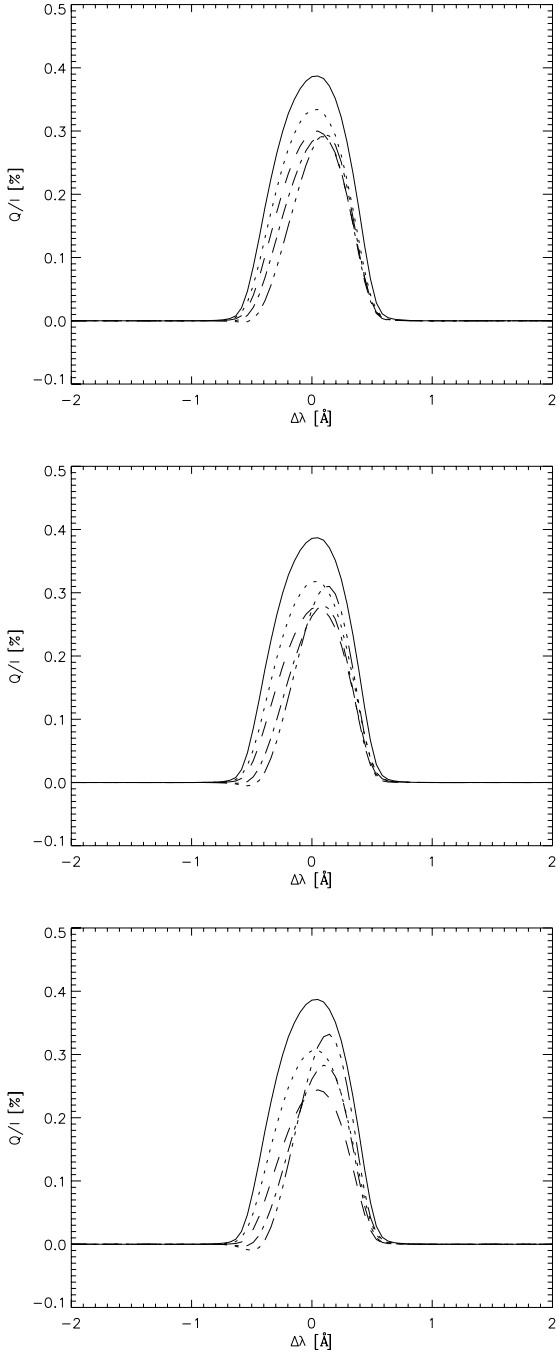

Fig. 9. Same as Fig. 8; here for the VAL F model.

Contrary to the conclusions of Vogt et al. (2001), the variation of spectral index δ does not affect the emergent polarization degree much. This is because of the negligible impact polarization effect and because the number of low energy protons in the Hα formation layers is similar across the δ values – the initial difference in energy distribution of lower energy protons is quickly lost at depths $E_N \approx E_c$. An effect that could play a role is the variation of E_c energy. The energy distribution of the beam of protons is sensitive to the chromospheric depth parametrized by E_N (see Sect. 2). One expects that a fine tuning of E_c with the energy necessary to reach the Hα-forming layers can lead to a more significant effect of impact polarization. We have calculated the dependence of the line center polarization on E_c for a wide range of cut-off energies. The results can be found in Figs. 10 and 11. It is easy to find the effect of impact polarization that emerges at cut-off energies comparable to the energy necessary to reach the Hα-forming layer. This effect is seen as a

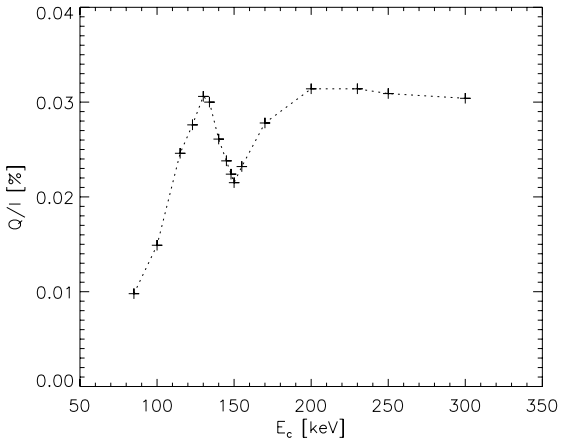

Fig. 10. Hα line center polarization as a function of a lower energy cut-off E_c at the injection site. The atmosphere model F1, beam flux $\mathcal{E}_0 = 10^{11}$ erg cm^{-2} s^{-1}, $\delta = 5$. The E_c value has been varied in the interval 85−300 keV.

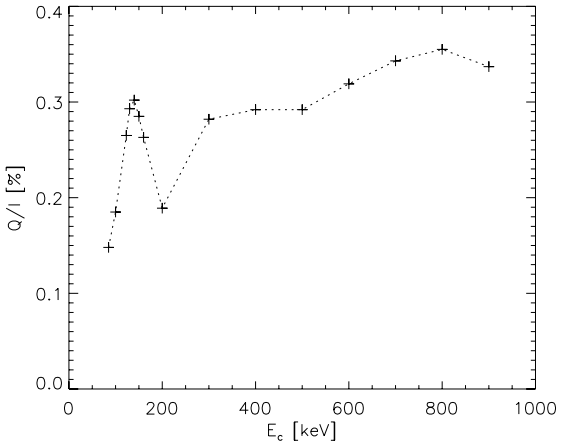

Fig. 11. Same as Fig. 10; here for the chromosphere model VAL F and the E_c energy range 85–900 keV.

decrease in the total polarization degree (i.e., increase of radial atomic polarization due to impacts that has an opposite orientation than the tangential polarization formed preferentially by scattering). In the F1 model, the thermal case of 0.01% polarization is increased as protons have enough energy to change the structure of the atmosphere at Hα formation levels. The effect of impact polarization is seen at about 150 keV when the density of protons is high enough to decrease the dominant tangential polarization. Further increase of E_c again leads to a negligible number of protons with small energies at the Hα formation layer. Similar effects can be seen in the VAL F case, where the resonance polarization scattering effect is much stronger. The total number of thermal perturbers is always lower than in the F1 case, but high enough to decrease the thermal atmosphere polarization of 0.4% even for a small energy cut-off. The impact polarization is best seen at energies around 200 keV: in this cooler model the total column mass above $\tau_{H\alpha} = 1$ is higher than in the F1 case. In any case the emergent linear polarization is low, below the stated 5% value, and it is even possible to expect a decrease of the total linear polarization due to proton impacts.

9. Conclusions

The purpose of this paper was to verify whether the anisotropic excitation of the $n = 3$ level of hydrogen caused by proton beams can lead to Hα line polarization and what degree of polarization can be expected. In our considerations, we have chosen a unidirectional vertical beam with an initial power-law energy distribution at the chromosphere injection site, which is not deflected by collisions with constituents of the chromosphere although it is decelerated. For this extremely anisotropic beam we have calculated new chromosphere conditions with a wide range of beam parameters. For all the calculated models we have found the polarization degree well below the values reported in the past. Furthermore, the theoretical polarization degree is mainly caused by resonance scattering.

The absence of impact polarization is consistent with measurements of Bianda et al. (2005), although their conclusions about the beam isotropization are not necessary for explanation of the missing polarization. In fact, a sufficient number of unidirectional low-energy protons at the Hα-forming layer cannot be achieved for beams with initial power-law distributions. Although the proton beam may significantly affect the line intensity profile, impact atomic polarization is destroyed by collisions with background electrons and protons and by the strong radiation field. The density of background perturbers is actually higher than that calculated in previous works. In addition, the beam energy distribution at the line formation layers cannot be approximated by a power-law distribution and the effect of a steep increase of fractional polarization with spectral index δ is not observed. Therefore we believe that the polarization occasionally measured (i.e., by some authors) has another source than impacts by proton beams.

Low impact polarization of the Hα line by proton beams in solar flares does not seem to be a good candidate for straightforward proton beam diagnostics, at least if most of the usual initial distributions of proton beam energies are considered. It is possible to imagine different initial energy distributions of the same energy flux with very narrow band of energies, which preferentially excite the hydrogen at low energies and in the Hα-forming layers. However, the question remains if such a distribution is physically possible and if it can lead to measurable impact polarization.

Recent spectropolarimetric measurements of an M6.3 flare performed by Xu et al. (2005b) indicate the presence of both radial and tangential polarization of the Hα line and radial polarization of the Hβ line at the edges of flare kernels. The process that is believed to play a significant role is the effect of return currents (Karlický & Hénoux 2002). Investigation of this phenomenon remains the subject of further observational and theoretical research.

Acknowledgements. We are indebted to Jana Kašparová for providing her MALI code, for her careful reading of the manuscript, and for her many useful comments. We thank Dr. C. Balança for providing us with his close-coupling data of proton-hydrogen cross-sections. We are grateful to Dr. J.-C. Hénoux and Dr. V. Bommier for clarifying discussions and Dr. E. Vogt for providing us with the radiation transfer code used in his calculations of electron and proton densities in the chromosphere. J.Š. acknowledges the support of the French government during his stay at Paris Observatory – Meudon in the frame of a co-tutelle. He also acknowledges the staff of the LERMA laboratory in Meudon and the Solar Department in Ondřejov for their support and kind hospitality. This work was partially supported by the Grant A3003203 of GA AV ČR.

References

Aboudarham, J., Berrington, K., Callaway, J., et al. 1992, A&A, 262, 302
Balança, C., & Feautrier, N. 1998, A&A, 334, 1136

Bianda, M., Benz, A. O., Stenflo, J. O., Küveler, G., & Ramelli, R. 2005, A&A, 434, 1183
Bommier, V. 1980, A&A, 87, 109
Bommier, V., & Sahal-Bréchot, S. 1982, Sol. Phys., 78, 157
Bommier, V., & Sahal-Bréchot, S. 1991, Ann. Phys. Fr., 16, 555
Bommier, V., Leroy, J. L., & Sahal-Bréchot, S. 1986a, A&A, 156, 79
Bommier, V., Leroy, J. L., & Sahal-Bréchot, S. 1986b, A&A, 156, 90
Brosius, J. W., Robinson, R. D., & Maran, S. P. 1995, ApJ, 441, 385
Brosius, J. W., & Woodgate, B. E. 1999, ApJ, 514, 430
Brown, J. C. 1971, Sol. Phys., 18, 489
Brown, J. C., Karlický, M., MacKinnon, A. L., & van den Oord, G. H. J. 1990, ApJS, 73, 343
Canfield, R. C., & Chang, C.-R. 1985, ApJ, 295, 275
Doschek, G. A., Mariska, J. T., & Sakao, T. 1996, ApJ, 459, 823
Emslie, A. G. 1978, ApJ, 224, 241
Fabiani Bendicho, P., Trujillo Bueno, J., & Auer, L. 1997, A&A, 324, 161
Fang, C., Feautrier, N., & Hénoux, J.-C. 1995, A&A, 297, 854
Fano, U. 1957, Rev. Mod. Phys., 29, 74
Frost, K. J. 1969, ApJ, 158, L159
Hénoux, J.-C., & Chambe, G. 1990, J. Quant. Spectr. Radiat. Transf., 44, 193
Hénoux, J.-C., Chambe, G., Smith, D., et al. 1990, ApJS, 73, 303
Hénoux, J.-C., Fang, C., & Gan, W. Q. 1993, A&A, 274, 923
Karlický, M., & Hénoux, J.-C. 2002, A&A, 383, 713
Kašparová, J., & Heinzel, P. 2002, A&A, 382, 688
Korchak, A. A. 1967, Soviet Astron., 11, 258
Landi Degl'Innocenti, E. 1982, Sol. Phys., 79, 291
Landi Degl'Innocenti, E. 1984, Sol. Phys., 91, 1
Landi Degl'Innocenti, E. 1987, in Numerical radiative transfer, ed. W. Kalkofen (Cambridge: Cambridge University Press), 265
Machado, M. E., Avrett, E. H., Vernazza, J. E., & Noyes, R. W. 1980, ApJ, 242, 336
Olson, G. L., & Kunasz, P. B. 1987, J. Quant. Spec. Radiat. Transf., 38, 325
Orrall, F. Q., & Zirker, J. B. 1976, ApJ, 208, 618
Sahal-Bréchot, S. 1977, ApJ, 213, 887
Sahal-Bréchot, S., Vogt, E., Thoraval, S., & Diedhiou, I. 1996, A&A, 309, 317
Štěpán, J. 2006, in proc. of the 4th Solar Polarization Workshop, ed. R. Casini, ASP Conf. Series, in press [arXiv:astro-ph/0611112]
Vernazza, J. E., Avrett, E. H., & Loeser, R. 1981, ApJS, 45, 635
Vogt, E., & Hénoux, J.-C. 1996, Sol. Phys., 164, 345
Vogt, E., Sahal-Bréchot, S., & Bommier, V. 2001, A&A, 374, 1127
Vogt, E., Sahal-Bréchot, S., & Hénoux, J.-C. 1997, A&A, 324, 1211
Xu, Z., Fang, C., & Gan, W.-Q. 2005a, Ch. J. Astron. Astrophys., 5, 519
Xu, Z., Hénoux, J.-C., Chambe, G., Karlický, M., & Fang, C. 2005b, ApJ, 631, 618
Zhao, X., Fang, C., & Hénoux, J.-C. 1998, A&A, 330, 351

Appendix G

Paper V: Hydrogen Balmer line formation in solar flares affected by return currents

A&A 472, L55–L58 (2007)
DOI: 10.1051/0004-6361:20078170

Astronomy & Astrophysics

LETTER TO THE EDITOR

Hydrogen Balmer line formation in solar flares affected by return currents

J. Štěpán[1,2], J. Kašparová[1], M. Karlický[1], and P. Heinzel[1]

[1] Astronomical Institute, Academy of Sciences of the Czech Republic, v.v.i., Fričova 298, 251 65 Ondřejov, Czech Republic
e-mail: [stepan;kasparov;karlicky;pheinzel]@asu.cas.cz
[2] LERMA, Observatoire de Paris–Meudon, CNRS UMR 8112, 5 place Jules Janssen, 92195 Meudon Cedex, France
e-mail: jiri.stepan@obspm.fr

Received 27 June 2007 / Accepted 30 July 2007

ABSTRACT

Aims. We investigate the effect of the electric return currents in solar flares on the profiles of hydrogen Balmer lines. We consider the monoenergetic approximation for the primary beam and runaway model of the neutralizing return current.
Methods. Propagation of the 10 keV electron beam from a coronal reconnection site is considered for the semiempirical chromosphere model F1. We estimate the local number density of return current using two approximations for beam energy fluxes between 4×10^{11} and 1×10^{12} erg cm^{-2} s^{-1}. Inelastic collisions of beam and return-current electrons with hydrogen are included according to their energy distributions, and the hydrogen Balmer line intensities are computed using an NLTE radiative transfer approach.
Results. In comparison to traditional NLTE models of solar flares that neglect the return-current effects, we found a significant increase emission in the Balmer line cores due to nonthermal excitation by return current. Contrary to the model without return current, the line shapes are sensitive to a beam flux. It is the result of variation in the return-current energy that is close to the hydrogen excitation thresholds and the density of return-current electrons.

Key words. Sun: flares – plasmas – line: formation – atomic processes

1. Introduction

The ongoing study of nonthermal excitation of the flaring chromospheric plasmas has been mainly concentrated on the effect of particle beams coming from the coronal reconnection site (Canfield et al. 1984; Hawley & Fisher 1994; Fang et al. 1993; Kašparová & Heinzel 2002; Štěpán et al. 2007, and references therein). However, Karlický & Hénoux (2002) and Karlický et al. (2004) recently suggested that the role of neutralizing return currents can be as important as the role of the primary beam itself, both for intensity and linear polarization profiles. Karlický et al. (2004) proposed a simple model of return current formed by the runaway electrons and compared the rates of atomic transitions due to collisions both with the thermal electrons and with the electrons of the primary beam, and due to collisions with the return current formed by the runaway electrons. They showed that the rates due to the return current would dominate the collisional processes in the atmospheric region of Balmer line formation. However, no calculations of theoretical spectral line profiles were presented.

The aim of this paper is to take a first step towards self-consistent modeling of the Balmer line formation with return-current effects taken into account. We use a semi-empirical model of the flaring atmosphere as a basis for our NLTE radiative transfer model. Then we use a standard model for electron-beam deceleration due to Coulomb collisions with the ambient atmosphere and combine it with the two different physical models of the return-current generation. We incorporate the relevant processes that enter the atomic statistical equilibrium equations and solve them with the non-local equations of radiation transfer. At the end, we discuss the results and validity of our models.

2. Electron beam and return-current propagation

We assume an electron beam that is accelerated in a coronal reconnection site and injected into the cold chromosphere along the magnetic field lines. During its propagation, the beam evolves under the influence of several processes (Karlický 1997): (a) the beam generates the return current that decelerates the beam in the return-current electric field, (b) the beam generates the plasma waves causing the quasi-linear relaxation of the beam, and (c) the beam electrons are decelerated and scattered due to collisions with the background plasma particles. In the following model, we neglect the plasma wave processes and the return current is taken in the form of runaway electrons (Rowland & Vlahos 1985; van den Oord 1990; Norman & Smith 1978). In this form, the return-current losses are strongly reduced (Rowland & Vlahos 1985; Karlický et al. 2004). Thus, only collisional losses, as described by Emslie (1978), decelerate the electron beam in our case.

Let $\Phi = n_{\rm B} v_{\rm B}$ be the particle flux of the monoenergetic beam of the energy $E_{\rm B} = m_{\rm e} v_{\rm B}^2/2$, where $n_{\rm B}$ is the density of the beam electrons, $v_{\rm B}$ their velocity, and $m_{\rm e}$ the mass of the electron. According to Norman & Smith (1978) and Karlický et al. (2004), a fraction of background electrons $\alpha = n_{\rm R}/n_{\rm e}$ forms the current that moves in the opposite direction in order to neutralize the electric current $e\Phi$ associated with the primary beam. We use $n_{\rm R}$ for the number density of the return-current electrons and

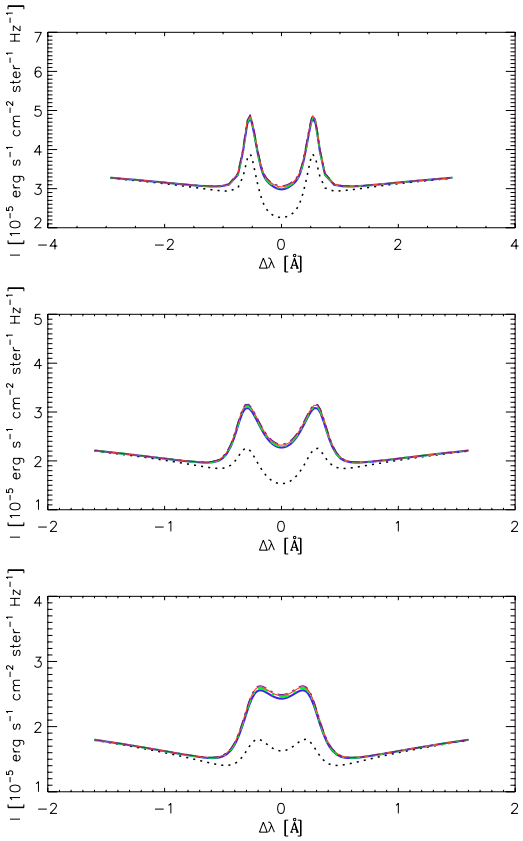

Fig. 1. From upper panel: Hα, Hβ, and Hγ disk-center line profiles for $\mathcal{F}_1 = 0$ (dotted line, black), $\mathcal{F}_1 = 4 \times 10^{11}$ (thick solid line, blue), 6×10^{11} (thick dash-dotted line, green), 8×10^{11} (thin solid line, red), and 1.0×10^{12} (thin dash-dotted line, violet) erg cm^{-2} s^{-1}. No return-current effects are taken into account. Note that nonthermal profiles almost overlap in this range of beam fluxes.

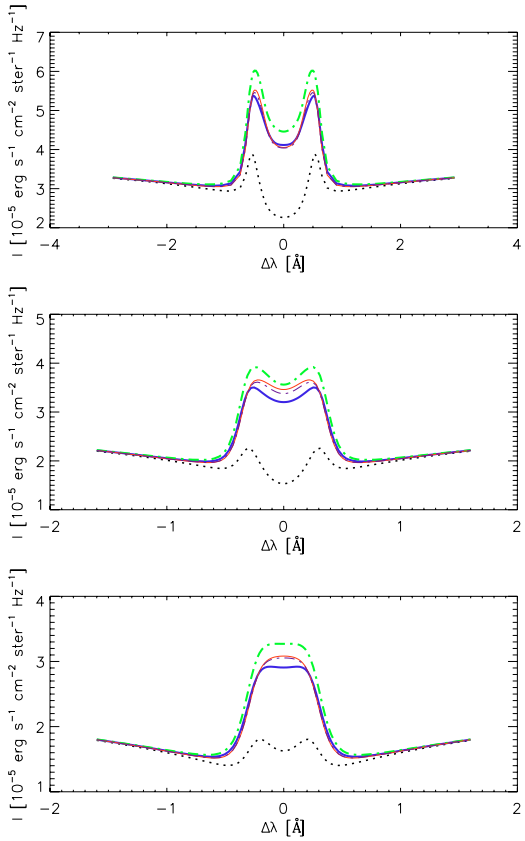

Fig. 2. Same as Fig. 1 plus including collisions with return-current electrons. The value of α is given by Eq. (2).

n_e for the number density of the background electrons. The neutralization condition can be expressed as

$$en_R v_R = e\Phi. \quad (1)$$

We assume that all the return-current electrons move with the same superthermal velocity v_R. Note that the return-current flux only depends on the total flux of the beam. For a realistic power-law distribution of the beam, the main part of the beam flux is given by electrons with energy close to the low-energy cutoff of this distribution. For these reasons and for simplicity, we consider the monoenergetic beam in our model.

We used two models for estimating n_R. First, following Norman & Smith (1978), the number of runaway electrons can be estimated as

$$\alpha = \frac{n_R}{n_e} = \frac{1}{2} \exp\left[-\frac{1}{2}\left(\sqrt{\frac{\mathcal{E}_D}{\mathcal{E}}} - \frac{\mathcal{E}}{\mathcal{E}_D}\right)^2\right], \quad (2)$$

where $\mathcal{E}/\mathcal{E}_D = n_B v_B / n_e v_{T_e}$ (see Karlický et al. 2004; Xu et al. 2005, for definition of the electric field $\mathcal{E}$ generated by the electron beam and the Dreicer electric field $\mathcal{E}_D$), and v_{T_e} stands for the thermal velocity of the background electrons. In the second model we assume that the return current is formed by a fixed relative number of background electrons everywhere in the upper chromosphere:

$$\alpha = \frac{n_R}{n_e} = \text{const.} \quad (3)$$

In this model, α is obtained by averaging the values from the previous model over the Balmer line formation layers. The resulting value for each beam flux can be found in Table 1.

The normalized energy distribution of electrons can be locally expressed in the form

$$f(E)\,\mathrm{d}E = [c_M f_M(E) + c_B \delta(E - E_B) + c_R \delta(E - E_R)]\,\mathrm{d}E, \quad (4)$$

where $E_R = m_e v_R^2/2$ is the return-current energy and c_i stands for the normalization coefficients (i.e., $c_R = n_R/(n_M + n_B + n_R)$, etc.). The index M stands for the background electrons (without the runaway ones), and they obey the Maxwell-Boltzmann energy distribution.

3. Hydrogen-electron collisions

To take the effect of the beam/return current into account, we have to calculate all the electron-hydrogen excitation rates, the rates of ionization by electron impacts, and the rates of the inverse processes. We use the data for total collisional cross-sections for the bound-bound and bound-free transitions by Janev & Smith (1993), retrieved through the GENIE database (`http://www-amdis.iaea.org/GENIE/`). We do not consider any atomic polarization or angular dependence of the collisional

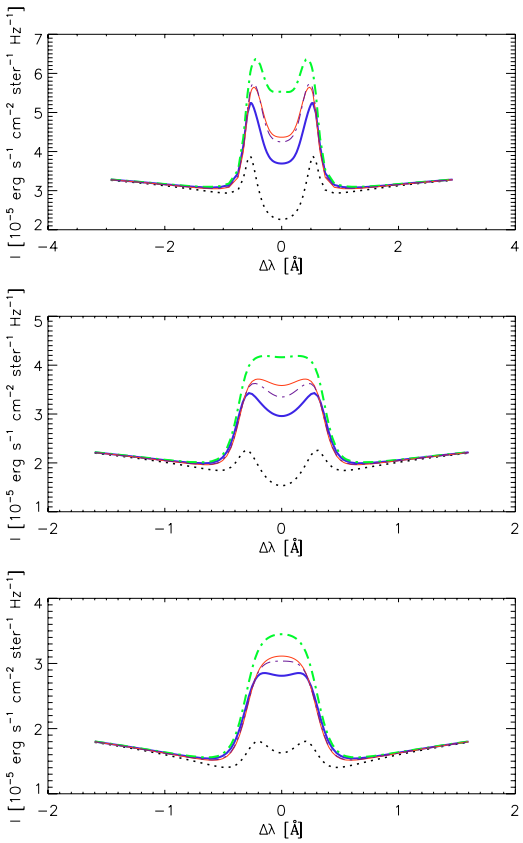

Fig. 3. Same as Fig. 1 plus including collisions with return-current electrons. The value of α is constant along whole beam trajectory.

processes in this work. The excitation or deexcitation rate of the $n \rightarrow m$ transition between the two shells can be calculated using the common formula

$$C_{nm} = n_\mathrm{e} \int_0^\infty \mathrm{d}E \, \sqrt{\frac{2E}{m_\mathrm{e}}} f(E) \sigma_{nm}(E), \tag{5}$$

where $\sigma_{nm}(E)$ is the total cross-section of $n \rightarrow m$ at impact energy E, and $f(E)$ is electron energy distribution (4). The cross-sections for deexcitation $m \rightarrow n$ ($m > n$) were calculated using the $n \rightarrow m$ cross section and the principle of detailed balance (e.g., Jefferies 1968),

$$\sigma_{mn}(E) = \frac{g_n}{g_m} \frac{E + E_{nm}}{E} \sigma_{nm}(E + E_{nm}), \tag{6}$$

where E_{nm} is the excitation threshold of the transition and $g_{n/m}$ the statistical weight of the given level.

The rates of the inverse process of ionization by an electron impact, the three-body recombination $\mathrm{e} + \mathrm{e} + \mathrm{p} \rightarrow \mathrm{H\,I} + \mathrm{e}$, must be treated separately due to the nonthermal nature of the problem. Using the arguments of detailed balance (Fowler 1955; Jefferies 1968) in the quasi-classical approximation of the electron-hydrogen collisions, one can derive a formula for the recombination rate. Let us consider the ionization of level n with the ionization energy E_n by an electron with energy E_i. Once cross-section $S_{nc}(E_i, E_a) \equiv \partial\sigma_{nc}/\partial E_a$ of the encounter after which we find the two electrons with energies E_a and $E_b = E_i - E_n - E_a$ is known, one can write the total recombination rate as

$$C_{cn} = L \int_0^\infty \mathrm{d}E_a \int_0^\infty \mathrm{d}E_b \, \frac{f(E_a) f(E_b)}{\sqrt{E_a E_b}} E_i S_{nc}(E_i, E_a), \tag{7}$$

where $L = n_\mathrm{e}^2 n^2 h^3 / 16\pi m_\mathrm{e}^2 \approx 6.97 \times 10^{-27} n_\mathrm{e}^2 n^2$ in cgs units, and h stands for the Planck constant. The expression (7) can be reduced to the well-known expression $C_{cn}^{\mathrm{Thermal}} = 2.06 \times 10^{-16} n^2 T^{-3/2} n_\mathrm{e} \exp(E_n/k_\mathrm{B}T) C_{nc}^{\mathrm{Thermal}}$ in the particular case of Maxwell-Boltzmann distribution, where T_e is the temperature of electrons and k_B the Boltzmann constant. For the cross section S_{nc} we used the approximate data of Omidvar (1965) at lower energies and the classical formula of Thomson (1912) at high energies. In our case, the electron energy distribution function given by (4) leads to 9 terms that contribute to the recombination rates. We verified numerically that, in all our models, the rates of three-body recombination involving the nonthermal electrons of the return current are more than one order of magnitude below the rates of the same processes involving the thermal electrons. Our tests show that neglecting the nonthermal three-body recombination affects the resulting profiles in a very negligible way. The three-body recombinations involving the beam electrons are completely negligible since their rates are several orders of magnitude below the thermal ones. Thus, we took only the thermal term containing $m^2 f_\mathrm{M}(E_a) f_\mathrm{M}(E_b)$ into account.

4. Results

We calculated the NLTE radiative transfer for a 5-level plus continuum hydrogen using the semiempirical 1D plane-parallel flare model F1 (Machado et al. 1980) in which the temperature structure was kept fixed; in this way, we found the differential effects on the Hα, Hβ, and Hγ lines (cf. Kašparová & Heinzel 2002). We used the preconditioned equations of statistical equilibrium (Rybicki & Hummer 1991) and solved the coupled system of NLTE equations by the accelerated lambda iteration (ALI) method. For further details, see Heinzel (1995). We found the equilibrium state for several beam fluxes with or without the return current. The initial beam fluxes chosen in our calculations were: $\mathcal{F}_1 = 4 \times 10^{11}$, 6×10^{11}, 8×10^{11}, and 1×10^{12} erg cm^{-2} s^{-1}. If the fluxes were lower, the number of runaway electrons would decrease fast and their energy would exceed the beam energy in most depths. This gives a limit for using of this simple model. Higher fluxes, on the other hand, would be unrealistic. The initial energy of beam electrons was set to $E_0 = 10$ keV.

In Fig. 1, there are first three Balmer line profiles that result from the nonthermal bombardment by the primary beam. The effects of return current were completely ignored. In this sense, these calculations are similar to the ones of Fang et al. (1993) and Kašparová & Heinzel (2002). In spite of their probably limited physical relevance, these profiles are useful for demonstrating the effects of return currents in the more appropriate models that follow. Figure 2 shows the situation where α is calculated using Eq. (2); i.e., the relative number of runaway return-current electrons is calculated at each depth in the atmosphere. Finally, in Fig. 3, there are profiles for the model with α constant along the atmosphere. In the layers of Balmer line formation, α remains approximately constant and its mean values are shown in Table 1. Comparing Fig. 1 with Figs. 2 and 3, one can see that the effect of return current is very significant: All three lines show a prominent increase emission in the line center.

Table 1. The properties of the return currents. $\mathcal{F}_1$ stands for the initial flux of the 10 keV beam, α is the mean relative number of runaway return-current electrons in the Balmer lines formation region, and E_R stands for the typical energy of the return-current electrons in these layers. Both α and E_R are average quantities which can roughly characterize the return-current properties in the region of interest.

$\mathcal{F}_1[10^{11}$ erg cm^{-2} s$^{-1}]$	α	E_R[eV]
4	0.01	100
6	0.05	14
8	0.11	6
10	0.16	3.8

In the region of Balmer line formation, the energy of the return current can be close to the excitation threshold of $n \geq 3$ levels of hydrogen, and it remains approximately constant along an extended trajectory. The beam is finally stopped on a very short path. The overall path of the beam is, however, sensitive to the initial energy of the beam. In order to model the beam propagation and line formation accurately, one has to interpolate the original F1 model of Machado et al. (1980) by a number of grid points in the layers of the Balmer line formation. Since the return-current energy and density are sensitive to the beam flux (see Table 1), the resulting variation of the nonthermal collisional rates leads to a significant variation in line profiles. For both models under consideration, a maximum emission is found for the beam flux of 6×10^{11} erg cm^{-2} s^{-1}, although the resulting profiles from these models differ slightly from each other. In contrast to the case of 4×10^{11} erg cm^{-2} s^{-1}, for which we found the least emission among the studied flux intervals, the return-current density is higher by a factor of 5. It leads to a significant increase in nonthermal excitation rates. The disagreement of the profiles at fluxes below 6×10^{11} erg cm^{-2} s^{-1} is the result of the significant dependency of α on the beam flux and atmospheric depth. The values of α at low fluxes (shown in the Table 1) are only a rough approximation for the Balmer line formation layers, and the model with α = const. seems to be less accurate than the one given by Eq. (2). On the other hand, good correspondence between the models is found for high fluxes. In this case, the variation in α is less sensitive to the beam flux and does not strongly vary with atmospheric depth. Then, the α = const. model seems to give the appropriate results. The reason the higher beam fluxes lead to a lower emission in the lines is that the energy of the return current is not sufficient to excite hydrogen atoms as can be seen in Table 1.

5. Conclusions and outlook

In this paper we used a simple model of the 10 keV electron beam propagating in the chromosphere. We used two different models of the return-current formation and calculated the differential effect on the profiles of the hydrogen Hα, Hβ, and Hγ lines of the semiempirical F1 model.

The return-current flux only depends on the total flux of the beam. For a realistic power-law distribution of the beam, the main part of the beam flux is given by electrons with energy close to the low-energy cutoff of this distribution. Therefore, for simplicity we used the monoenergetic beam in our model. Moreover, the excitation and ionization cross-sections of low-energy return-current electrons are larger than those for beam electrons, which makes the return-current effects on line core formation stronger. Taking high-energy beam electrons into account (i.e. using power-law distribution) would lead to increased emission in the line wings due to penetration of those electrons into the deeper atmospheric layers. However, the total flux of the beam in these layers is significantly lower than the initial beam flux, and the return current and corresponding effects are also strongly reduced.

Even our simple model shows that the effect of return current is very important for future study of the hydrogen lines formation since the energy of the return current can be expected to be on the order of the excitation threshold energies of upper hydrogen levels, for which the excitation cross-sections are high. Moreover, the fluxes Φ are high enough to excite a sufficient number of atoms. As shown by Karlický et al. (2004), the collisional rates from the nonthermal collisions can dominate the collisional rates in the Balmer line formation regions. The two models used in this work lead to similar results for higher energy fluxes, but the result differs for lower fluxes. The excitation threshold effects seem to play an important role for higher fluxes, but they are very likely only a consequence of the monoenergetic model we used. The difference between the two models shows the used approximations to be incompatible for lower fluxes, where the the approximation of constant α is not applicable. A detailed description of the energy distribution of the return-current electrons would lead to more realistic line intensities. This complex issue will be subject of a forthcoming paper, which will also study the impact polarization of the Balmer lines.

Acknowledgements. This work was partially supported by the grant 205/06/P135 of the Grant Agency of the Czech Republic, partially by the grant IAA300030701 of the Grant Agency of the Academy of Sciences of the Czech Republic, and partially by the project LC06014 Center for Theoretical Astrophysics.

References

Canfield, R. C., Gunkler, T. A., & Ricchiazzi, P. J. 1984, ApJ, 282, 296
Emslie, A. G. 1978, ApJ, 224, 241
Fang, C., Henoux, J. C., & Gan, W. Q. 1993, A&A, 274, 917
Fowler, R. H. 1955, Statistical mechanics (Cambridge University Press)
Hawley, S. L., & Fisher, G. H. 1994, ApJ, 426, 387
Heinzel, P. 1995, A&A, 299, 563
Janev, R. K., & Smith, J. J. 1993, in Atomic and plasma-material interaction data for fusion, 4, 1
Jefferies, J. T. 1968, Spectral line formation (A Blaisdell Book in the Pure and Applied Sciences, Waltham, Mass.: Blaisdell)
Karlický, M. 1997, Space Sci. Rev., 81, 143
Karlický, M., & Hénoux, J.-C. 2002, A&A, 383, 713
Karlický, M., Kašparová, J., & Heinzel, P. 2004, A&A, 416, L13
Kašparová, J., & Heinzel, P. 2002, A&A, 382, 688
Machado, M. E., Avrett, E. H., Vernazza, J. E., & Noyes, R. W. 1980, ApJ, 242, 336
Norman, C. A., & Smith, R. A. 1978, A&A, 68, 145
Omidvar, O. 1965, Phys. Rev., 140, A26
Rowland, H. L., & Vlahos, L. 1985, A&A, 142, 219
Rybicki, G. B., & Hummer, D. G. 1991, A&A, 245, 171
Štěpán, J., Heinzel, P., & Sahal-Bréchot, S. 2007, A&A, 465, 621
Thomson, J. J. 1912, Phil. Mag., 23, 449
van den Oord, G. H. J. 1990, A&A, 234, 496
Xu, Z., Hénoux, J.-C., Chambe, G., Karlický, M., & Fang, C. 2005, ApJ, 631, 618

Bibliography

Auer, L., Bendicho, P. F., & Trujillo Bueno, J. 1994, A&A, 292, 599

Auer, L. H. & Mihalas, D. 1969, ApJ, 158, 641

Auer, L. H. & Paletou, F. 1994, A&A, 285, 675

Avrett, E. H. & Hummer, D. G. 1965, MNRAS, 130, 295

Balança, C. & Feautrier, N. 1998, A&A, 334, 1136

Bianda, M., Benz, A. O., Stenflo, J. O., Küveler, G., & Ramelli, R. 2005, A&A, 434, 1183

Bianda, M., Stenflo, J. O., Gandorfer, A., Gisler, D., & Küveler, G. 2003, in ASPC, ed. J. Trujillo-Bueno & J. Sanchez Almeida, Vol. 307, 487

Blum, K. 1981, Density Matrix Theory and Applications (Plenum Press, New York)

Bommier, V. 1980, A&A, 87, 109

Bommier, V. 1991, Ann. Phys. Fr., 16, 599

Bommier, V. 1997a, A&A, 328, 706

Bommier, V. 1997b, A&A, 328, 726

Bommier, V. 1999, in Astrophysics and Space Science Library, Vol. 243, Polarization, ed. K. N. Nagendra & J. O. Stenflo, 43–59

Bommier, V. & Landi Degl'Innocenti, E. 1996, Sol. Phys., 164, 117

Bommier, V. & Landi Degl'Innocenti, E. Sahal-Bréchot, S. 1991, A&A, 244, 383

Bommier, V., Leroy, J. L., & Sahal-Bréchot, S. 1986, A&A, 156, 90

Bommier, V. & Sahal-Bréchot, S. 1978, A&A, 69, 57

Bommier, V. & Sahal-Bréchot, S. 1991, Ann. Phys. Fr., 16, 555

Born, M. & Wolf, E. 1999, Principles of Optics (Cambridge University Press)

Brandt, A. 1977, Math. Comp., 31, 333

Briggs, W., Henson, E. V., & McCormick, S. 2000, A multigrid tutorial: second edition (Society for Industrial and Applied Mathematics, Philadelphia)

Brink, D. M. & Satchler, G. R. 1962, Angular Momentum (Clarendon Press, Oxford)

Brown, J. C., Karlický, M., MacKinnon, A. L., & van den Oord, G. H. J. 1990, ApJS, 73, 343

Canfield, R. C. & Chang, C.-R. 1985, ApJ, 295, 275

Cannon, C. J. 1973, ApJ, 185, 621

Casini, R. & Manso Sainz, R. 2005, ApJ, 624, 1025

Chandrasekhar, S. 1960, Radiative Transfer (Dover Publications)

Cohen-Tannoudji, C. 1977, in Frontiers in laser spectroscopy, Les Houches, 1975, ed. R. Balian, S. Haroche, & S. Liberman (North-Holland, Amsterdam), 3

Cohen-Tannoudji, C., Dupont-Roc, J., & Grynberg, G. 1997, Photons and Atoms: Introduction to Quantum Electrodynamics (Wiley-Interscience)

Cohen-Tannoudji, C., Dupont-Roc, J., & Grynberg, G. 1998, Atom-Photon Interactions: Basic Processes and Applications (Wiley-Interscience)

Condon, E. & Shortley, G. 1935, The Theory of Atomic Spectra (Cambridge University Press, Cambridge)

Derouich, M., Sahal-Bréchot, S., & Barklem, P. S. 2005, A&A, 434, 779

Derouich, M., Trujillo Bueno, J., & Manso Sainz, R. 2007, A&A, 472, 269

Doschek, G. A., Mariska, J. T., & Sakao, T. 1996, ApJ, 459, 823

Emslie, A. G. 1978, ApJ, 224, 241

Fabiani Bendicho, P., Trujillo Bueno, J., & Auer, L. 1997, A&A, 324, 161

Fang, C., Henoux, J. C., & Gan, W. Q. 1993, A&A, 274, 917

Fano, U. 1957, Rev. Mod. Phys., 29, 74

Fano, U. & Racah, G. 1959, Irreducible tensorial sets (Academic Press)

Faurobert-Scholl, M. 1991, A&A, 246, 469

Faurobert-Scholl, M. 1996, Sol. Phys., 164, 79

Faurobert-Scholl, M., Frisch, H., & Nagendra, K. N. 1997, A&A, 322, 896

Frisch, H. 1999, in Astrophysics and Space Science Library, Vol. 243, Polarization, ed. K. N. Nagendra & J. O. Stenflo, 97–113

Greiner, W. 1998a, Classical Electrodynamics (Springer-Verlag, New York)

Greiner, W. 1998b, Quantum Mechanics. Special Chapters (Springer-Verlag, New York)

Hackbush, W. 1985, Multi-Grid Methods and Applications (Berlin: Springer)

Hanle, W. 1924, Z. Phys., 30, 93

Heinzel, P. 1995, A&A, 299, 563

Hénoux, J.-C. & Chambe, G. 1990, J. Quant. Spec. Radiat. Transf., 44, 193

Hénoux, J.-C., Chambe, G., Smith, D., et al. 1990, ApJS, 73, 303

Hénoux, J.-C., Fang, C., & Gan, W. Q. 1993, A&A, 274, 923

Ivanov, V. V. 1990, Soviet Astronomy, 34, 621

Jefferies, J. T. 1968, Spectral line formation (A Blaisdell Book in the Pure and Applied Sciences, Waltham, Mass.: Blaisdell, 1968)

Karlický, M. 1997, Space Sci. Rev., 81, 143

Karlický, M. 2008, personal comunication

Karlický, M. & Hénoux, J.-C. 2002, A&A, 383, 713

Karlický, M., Kašparová, J., & Heinzel, P. 2004, A&A, 416, L13

Kašparová, J. & Heinzel, P. 2002, A&A, 382, 688

Landau, L. D. & Lifshitz, E. M. 1977, Quantum Mechanics (Non-Relativistic Theory) (Oxford, England: Pergamon Press, 3rd ed.)

Landi Degl'Innocenti, E. 1983, Sol. Phys., 85, 3

Landi Degl'Innocenti, E. 1984, Sol. Phys., 91, 1

Landi Degl'Innocenti, E. 1985, Sol. Phys., 102, 1

Landi Degl'Innocenti, E. 1987, in Numerical radiative transfer, ed. W. Kalkofen (Cambridge: Cambridge University Press), 265–278

Landi Degl'Innocenti, E. & Bommier, V. 1994, A&A, 284, 865

Landi Degl'Innocenti, E., Landi Degl'Innocenti, M., & Landolfi, M. 1997, in Forum THEMIS, Science with THEMIS, proceedings of a Forum held in Paris-Meudon Observatory, 14-15 November, 1996, ed. N. Mein & S. Sahal Bréchot, 59–77

Landi Degl'Innocenti, E. & Landolfi, M. 2004, Polarization in Spectral Lines (Dordrecht: Kluwer)

Léger, L., Chevallier, L., & Paletou, F. 2007, A&A, 470, 1

Machado, M. E., Avrett, E. H., Vernazza, J. E., & Noyes, R. W. 1980, ApJ, 242, 336

Mandl, F. 1960, Introduction to Quantum Field Theory (John Wiley & Sons Inc)

Manso Sainz, R. & Trujillo Bueno, J. 1999, in Astrophysics and Space Science Library, Vol. 243, Polarization, ed. K. N. Nagendra & J. O. Stenflo, 143–156

Manso Sainz, R. & Trujillo Bueno, J. 2003a, in ASPC, Vol. 307, Solar Polarization, ed. J. Trujillo-Bueno & J. Sanchez Almeida, 251–262

Manso Sainz, R. & Trujillo Bueno, J. 2003b, Physical Review Letters, 91, 111102

Messiah, A. 1961, Quantum Mechanics (North-Holland, Amsterodam)

Mihalas, D. 1970, Stellar Atmospheres (W. H. Freeman and Company)

Mihalas, D., Auer, L. H., & Mihalas, B. R. 1978, ApJ, 220, 1001

Nagendra, K. N., Frisch, H., & Faurobert-Scholl, M. 1998, A&A, 332, 610

Norman, C. A. & Smith, R. A. 1978, A&A, 68, 145

Olson, G. L., Auer, L. H., & Buchler, J. R. 1986, Journal of Quantitative Spectroscopy and Radiative Transfer, 35, 431

Olson, G. L. & Kunasz, P. B. 1987, J. Quant. Spec. Radiat. Transf., 38, 325

Omont, A. 1977, Prog. Quantum Electronics, 5, 69

Orrall, F. Q. & Zirker, J. B. 1976, ApJ, 208, 618

Paletou, F. 1995, A&A, 302, 587

Paletou, F. & Léger, L. 2007, Journal of Quantitative Spectroscopy and Radiative Transfer, 103, 57

Press, W., Teukolsky, S., Vetterling, W., & Flannery, B. 1994, Numerical Recipes (Cambridge University Press)

Rees, D. E. 1969, Sol. Phys., 10, 268

Rees, D. E., Durrant, C. J., & Murphy, G. A. 1989, ApJ, 339, 1093

Rees, D. E. & Saliba, G. J. 1982, A&A, 115, 1

Rowland, H. L. & Vlahos, L. 1985, A&A, 142, 219

Rybicki, G. B. & Hummer, D. G. 1991, A&A, 245, 171

Rybicki, G. B. & Hummer, D. G. 1992, A&A, 262, 209

Rybicki, G. B. & Hummer, D. G. 1994, A&A, 290, 553

Sahal-Bréchot, S. 1977, ApJ, 213, 887

Sahal-Bréchot, S., Bommier, V., & Feautrier, N. 1998, A&A, 340, 579

Sahal-Bréchot, S., Vogt, E., Thoraval, S., & Diedhiou, I. 1996, A&A, 309, 317

Sánchez Almeida, J. & Trujillo Bueno, J. 1999, ApJ, 526, 1013

Scharmer, G. B. 1984, in Methods in radiative transfer, ed. W. Kalkofen, Cambridge University Press, London, 173–210

Scharmer, G. B. & Carlsson, M. 1985, Journal of Computational Physics, 59, 56

Socas-Navarro, H. & Trujillo Bueno, J. 1997, ApJ, 490, 383

Steiner, O. 1991, A&A, 242, 290

Stenflo, J. 1994, Solar Magnetic Fields (Springer)

Štěpán, J. 2006, in ASPC, Vol. 358, Solar Polarization 4, ed. R. Casini & B. W. Lites, 148–151

Štěpán, J. 2007, Memorie della Societa Astronomica Italiana, 78, 83

Štěpán, J. 2008, in Solar Polarization 5, ASPC, submitted

Štěpán, J. & Bommier, V. 2007, A&A, 468, 797

Štěpán, J., Heinzel, P., Kašparová, J., & Sahal-Bréchot, S. 2006, Cosmic Particle Acceleration, 26th meeting of the IAU, Joint Discussion 1, 16-17 August, 2006, Prague, Czech Republic, JD01, #55, 1

Štěpán, J., Heinzel, P., & Sahal-Bréchot, S. 2007a, A&A, 465, 621

Štěpán, J., Kašparová, J., Karlický, M., & Heinzel, P. 2007b, A&A, 472, L55

Stokes, G. 1852, Trans. Cambridge Phil. Soc., 9, 399

Trujillo Bueno, J. 1999, in Astrophysics and Space Science Library, Vol. 243, Solar Polarization, ed. K. N. Nagendra & J. O. Stenflo, 73–96

Trujillo Bueno, J. 2001, in ASPC, Vol. 236, Advanced Solar Polarimetry – Theory, Observation, and Instrumentation, ed. M. Sigwarth, 161–195

Trujillo Bueno, J. 2003, in ASPC, Vol. 288, Stellar Atmosphere Modeling, ed. I. Hubeny, D. Mihalas, & K. Werner, 551–582

Trujillo Bueno, J. & Fabiani Bendicho, P. 1995, ApJ, 455, 646

Trujillo Bueno, J. & Landi Degl'Innocenti, E. 1996, Sol. Phys., 164, 135

Trujillo Bueno, J. & Manso Sainz, R. 1999, ApJ, 516, 436

van den Oord, G. H. J. 1990, A&A, 234, 496

Väth, H. M. 1994, A&A, 284, 319

Vernazza, J. E., Avrett, E. H., & Loeser, R. 1981, ApJS, 45, 635

Vogt, E. & Hénoux, J.-C. 1996, Sol. Phys., 164, 345

Vogt, E., Sahal-Bréchot, S., & Bommier, V. 2001, A&A, 374, 1127

Vogt, E., Sahal-Bréchot, S., & Hénoux, J.-C. 1997, A&A, 324, 1211

von Neumann, J. 1927, Göttingen Nachriten, 245

Werner, K. 1986, A&A, 161, 177

Xu, Z., Hénoux, J.-C., Chambe, G., Karlický, M., & Fang, C. 2005, ApJ, 631, 618